Experimental and Computational Fluid Dynamics Modeling of Single-Phase and Two-Phase Shear-Thinning Flow Behavior in Pipes

by

© Abdalsalam A. I. Ihmoudah

A Dissertation submitted to the School of Graduate Studies in partial fulfillment of the requirements for the degree of

Doctor of Philosophy

Faculty of Engineering and Applied Science

Memorial University of Newfoundland

May 2024

St John's Newfoundland, Canada

ABSTRACT

The design of transport pipes for Newtonian fluids has well-established and accurate correlations for predicting most of the single- and two-phase flow measurements in both turbulent and laminar flow regions. These correlations are based on many experimental and analytical studies. In contrast, the development of correlations for non-Newtonian fluids for predicting flow pattern maps, slug flow characteristics, and pressure losses has proceeded slowly owing to the complexity and diversity of viscosity behaviour. Many methods are used to analyze non-Newtonian fluids in laminar flow; however, only limited research has been done on developing prediction methods for turbulent flow. In this thesis, we systematically study the effect of rheological parameters on non-Newtonian liquid shear-thinning behaviour (power-law and Herschel-Bulkley models) in laminar, transitional and turbulent flow in both single- and two-phase systems through experiments and using Computational Fluid Dynamics (CFD) simulations.

An extensive experimental study was conducted to investigate the effects of rheological models and their estimated parameters on the predictions of laminar, transitional, and turbulent flow based on Newtonian and shear-thinning fluid models. To achieve these goals, two non-Newtonian shear-thinning rheological models were prepared (four power-law fluids and seven Herschel-Bulkley fluids) in the Drilling Technology Laboratory using three materials: carboxymethyl cellulose, bentonite, and xanthan gum. The rheology parameters of the solutions were determined using an API-compliant rotational viscometer and mud balance. The experiments were conducted in a flow loop in a 65-m open-cycle system using test sections with internal diameters of 76.2 mm and 19.1 mm. Pressure transducers were used to provide the pressure data in all the test sections. Flow

visualization and video recordings were done using a high-speed camera to capture and compare the behaviour of two-phase Newtonian and non-Newtonian flows.

Experimental studies for single phase show that most of the correlations identified in the literature for the laminar flow in the power-law rheology model were the best fit for the pressure loss, transitional velocity, and turbulent flow. For Herschel-Bulkley fluids, pressure losses and transitional regions based on a yielded region were examined, and a new modified model was compared to the experimental results and provided a good estimation.

Experiments for two-phase flow utilized Newtonian, power-law, and Herschel-Bulkley fluids to evaluate the transition boundaries of flow pattern maps and slug flow characteristics in 76.2 mm PVC horizontal and vertical pipes. The results obtained show that the translational velocity of the slug increases with increasing concentration, while the flow behaviour index decreases and the consistency index increases for shear-thinning fluid at the same operating conditions. The plug-slug transition boundaries shift up to higher liquid velocities in shear-thinning fluids. As a result, the flow pattern map of Mandhane et al. in horizontal pipes for Newtonian fluid has been slightly adjusted to account for shear-thinning fluid based on the experimental results.

For CFD simulations, ANSYS Fluent v.19 was used to simulate single- and two-phase Newtonian and non-Newtonian fluids. The turbulent models associated with wall functions were successfully validated for Newtonian fluid in the single phase. Also, the k-ω and k-ε models give accurate results for power-law fluids with a higher flow behaviour index. For Herschel-Bulkley fluid, the percentile error was observed to increase with an increase in the yield stress. A volume of fluid mothed was selected to evaluate the influence of rheology parameters on shear-thinning fluid in a two-phase model. The study included a flow pattern map, transition boundaries, slug flow

characteristics in horizontal and upward vertical flow, and the length, velocity, and shape of Taylor bubbles in a minichannel. The CFD method was reliable for predicting gas/shear thinning in two-phase flow.

From this work, a new empirical correlation modified for the calculation of slug frequency in Newtonian and shear-thinning two-phase flow is proposed. The slug frequency and slug shape were found to be affected by changing the rheological properties of the liquid phase in horizontal and vertical pipes. With increasing concentration, a decreased flow behaviour index, and an increasing consistency index of Herschel-Bulkley fluid at the same operating conditions, we found a non-uniform and random distribution of small bubbles due to the effective viscous force of a liquid phase.

ACKNOWLEDGEMENTS

I would like to express my sincere thanks and gratitude to my supervisor Dr. Stephen D. Butt, Dr. Mohammad Azizur Rahman, and my supervisory committee members: Dr. Mohamed M. Awad for Their support, guidance, valuable suggestions throughout the work of this research have been invaluable.

Furthermore, I would like to thank Dr. Abdelsalam Abugharara and my research colleagues in Memorial University for their endless support throughout my Ph. D.

I am highly grateful to my late father, Ali Ihmoudah, who was my idol. To my mother, your endless love, prayers, and support is the light of my life.

My wife Fatma Nassir, who was there for me throughout this journey, it couldn't have been done without your support.

My kids, Bushra, Ali, Nour and Aryam, for their endless love and support. I am truly thankful for having them all in my life.

Table of Contents

List of Figures

List of Tables

Nomenclature

A	Area, (m^2)
C_0	Distribution parameter or flow coefficient, (-)
Ca	Capillary number ($\mu_L U_B/\sigma$), (-)
Ca*	Modified Capillary number ($\mu^* U_B/\sigma$), (-)
CFD	Computational fluid dynamics
C_l	Distribution parameter or flow coefficient defined by equation 3-29,
C_O	Courant number
D	Pipe diameter, (m)
D_{eff}	Effective pipe diameter (m)
D_h	Hydraulic diameter, (mm)
DTL	Drilling Technology Laboratory
f	Friction factor, (-)
f_s	Slug frequency, (1/s)
F_{SF}	Surface tension force, N/m^3
HB	Herschel-Bulkley
k	Fluid consistency coefficient, ($Pa \cdot s^n$);
L	Unit cell length, (m)
λ	Time constant, (s)
l_s	Slug unit of length, (m)
l_l	film zone of length, (m)
L_L	Slug length, (m)
l_s	Slug zone of length, (m)

$m\hat{}$	Unit normal vector
n	Flow behaviour index, (-)
P	Pressure, (Pa)
Q	Volumetric flow rate, (m^3/s)
R^2	Coefficient of determination, (-)
R	Dp/2 is the radius of the plug region, (m)
Reg	Generalized Reynolds number
Re_{ST}	Slatter modified Reynolds number, (-)
R_{MR}	Metzner and Reed Reynolds number, (-)
T	Time, (s)
u	Localized linear velocity at (r) value, (m/s)
U*	Shear velocity, (m/s)
U_B	Bubble velocity, (m/s)
U_G	Gas superficial velocity, (m/s)
U_L	Liquid superficial velocity, (m/s)
Um	Mixture superficial velocity, (m/s)
U_S	Slug Velocity, (m/s)
U_{sns}	Slug no-slip velocity, (m/s)
V_m	Mean velocity, (m/s)
V_N	Newtonian mean velocity, (m/s)
VOF	Volume of fluid
XG	Xanthan gum
YPL	Yield Power-law

α	Volume fraction, (-)
α^*	Area ratio, (-)
γ	Shear rate, (s^{-1})
δ	Controls the exponential growth of stress, (-)
ξ	Liquid film thickness, (μm)
∞	Demanding parameter (-)
Δt	Time step, (s)
Δx	Grid size, (mm)
η	Dynamic viscosity, (kg/m·s)
μ	Newtonian viscosity (Pa·s)
μ_0	Apparent viscosity (Pa·s)
μ_{eff}	Effective apparent viscosity (Pa·s)
ρ	Density of fluid (kg/m^3)
σ	Surface tension, (N/m)
τ	Shear stress (Pa)
τ_0	Yield stress, (Pa)
τ_w	Wall shear stress (Pa)
τ_y	Yield stress (Pa)
Ω	Velocity profile blunting factor
θ	Contact angle, (-)

Chapter 1: Introduction and Overview

1.1 Background

Newtonian and non-Newtonian fluids flowing in pipelines can be found in a wide range of practical and industrial applications. Newtonian fluids have well-established and accurate correlations in predicting most of the measurements of single- and two-phase flow in both turbulent and laminar flow regions. Non-Newtonian flow behaviour in laminar regions, which is related to rheological properties and pressure losses, could be predicted by integrating the constitutive rheological model. On the other hand, the prediction of pressure losses in turbulent flow remains a theoretical and practical problem [1,2]. Most of the fluids used at drilling sites are categorized as having non-Newtonian behaviour with non-linear viscosity, which makes it difficult to predict turbulent pressure losses in pipes. The mismatch between rheological models and the properties of drilling fluids can lead to serious issues during drilling operations, such as the loss of well control, reduced carrying capacity, fluid losses, and stuck pipes (Rahman [3]). Demirdal and Cunha [4], reported that the rheological parameters of non-Newtonian fluids can assist in providing a description of fluid models. Relevant parameters include yield stress, consistency index, fluid behaviour index, and density as a volumetric parameter. Such parameters are important for predicting frictional pressure loss in single-phase and flow patterns, void fraction, slug flow characteristics and pressure drop in two-phase flow; however, all these parameters can change in high and low pressure and temperature conditions, which can have a direct effect on drilling fluid rheology via the fluid's shear stress and shear rate [5-7]. In designing pipelines and drilling mud circulation for non-Newtonian fluids, pressure drop and transition limitations are among the most important technical parameters that can influence pumping energy requirements. Slug flow creates significant pressure variations, which can

disrupt process conditions and result in inaccurate instrument sensing. It also generates vibration, particularly around pipe bends and valves as well as other flow constraints. This can result in equipment damage and operational issues. The literature shows a lack of recent studies on the effect of rheological properties of shear-thinning fluid, especially Herschel–Bulkley fluid, in real flow conditions on flow measurements in a large diameter. The power-law model has been widely applied to obtain relationships between flow rate and pressure drop at a low Reynolds number in various geometries, including expanding and elastic pipes [8,9]. Several recent studies investigated various hydrodynamic problems involving shear-thinning fluids at low Reynolds numbers and clearly demonstrated a limited range of applicability of the power-law model [10-12].

In the chemical and petroleum industries, gas/shear-thinning behavior and two-phase flows are common phenomena. The characterization of two-phase flow, especially shear-thinning behavior, is of essential importance due to its appearance during the production and transportation of petroleum derivatives. There are essential hydrodynamic features in two-phase flow that should be considered in the determination of the flow pattern, void fraction, slug flow characteristics and pressure drop that imply difficulties due to the advanced flow mechanism and thus the range of parameters concerned. The majority of research thus far has examined gas-Newtonian two-phase flow, with little research focusing on shear-thinning liquids in two-phase flow [13-17]. Furthermore, there is limited understanding of the effect of the rheological parameters of shear thinning flow in two-phase flow, especially for oil and gas applications. As a result, there is a clear need for more research on two-phase Newtonian and non-Newtonian flows on an experimental, theoretical and numerical basis. Such research could assist engineers in designing safer, more efficient and more cost-effective transport and production systems. Pipeline flows characterized as two-phase gas and liquid are distributed in

different ways, giving rise to a variety of flow patterns. These patterns, which are determined by different fluid properties as well as various operating conditions, exhibit distinct flow features. The main flow patterns in horizontal pipelines are plug, slug flow (sometimes referred to as intermittent), dispersed bubble flow, wavy and annular and stratified smooth flow. Many analytical methods can be used to predict Newtonian fluids' frictional pressure loss from turbulent or laminar flows in single- or two-phase flow; however, applying these methods in non-Newtonian fluids is more difficult due to their complex characteristics. While some effective analytical strategies do exist for laminar flow in non-Newtonian fluids, models for turbulent flow tend to be less established because of the complexity of the required mathematical modeling, Chilton and Stainsby [18].

1.2 Literature Review

This section provides the literature review on the generalized Reynolds number and mathematical modelling of single-phase pressure losses for shear-thinning fluid under laminar, transitional, and turbulent flow regimes. It will also include a review of flow patterns, pressure losses, void fraction, and characteristics of slug flow two-phase gas/shear-thinning in horizontal and vertical pipes.

1.2.1 Non-Newtonian laminar, transitional, and turbulent models (single-phase)

A number of correlations have been proposed in recent decades for determining pressure losses for non-Newtonian fluids in smooth pipes. The first part of this thesis provides a comparative study of a generalized Reynolds number and pressure drop correlations in smooth pipes for all flow regimes of shear-thinning fluid.

In 1955, Metzner and Reed [19] adapted the Reynolds number to correlate the non-Newtonian pipe flow for a shear-thinning power-law model. In their formulation, the Fanning friction

factor was employed as a stability parameter. They proposed that non-Newtonian fluids occur at the limit of the laminar flow as the same Reynolds number of the Newtonian fluids in smooth pipes, which is R_{MR} = 2100 at f_N = 0.0076 [2].

In 1959, Dodge & Metzner [20] devised a critical Reynolds number for their method by applying the friction factor of power-law fluids to a generalized Reynolds number. In doing so, they found that the values of the critical Reynolds number determined by their method were in agreement with those found by Metzner and Reed.

In 1959, Torrance [21] investigated the turbulent flow of Herschel–Bulkley fluid based on the pseudoplastic model reported by Clapp [22]. In his work, Torrance assumed that the transitional flow occurs at Re = 2100. When ignoring the effect of the yield stress, Torrance derived the mean velocity for turbulent flow in smooth pipes and neglected the effect of the wall layers (viscous sub-layer and boundary layer).

Wilson and Thomas [23], followed by Thomas and Wilson [24], proposed a turbulent flow model to predict non-Newtonian flow based on velocity distribution using enhanced microscale viscosity effects. The model predicts that the wall's laminar sub-layer increases if the viscous sub-layer's size increases by the area ratio factor (α*) for both power-law fluid and Herschel–Bulkley fluid beads on shear velocity.

In 1994, Slatter [25] developed two approaches to the formulation of Reynolds numbers. In the first approach, Slatter developed a Reynolds number for the flow of Herschel–Bulkley fluid that emphasises yield stress. In the second approach, Slatter formulated a new roughness Reynolds (R_r) by considering the roughness caused by solid particles in smooth wall turbulent flow and fully developed rough-turbulent flow based on percentile passing of particle size (d_{85}).

In 2008, Hallbom [26] modified a model based on the drag reduction concept of Wilson and Thomas' [23] turbulent model in smooth wall pipe to incorporate the rheological parameters of

yield plastics. Newtonian turbulent flow constants were chosen for the modification. Hallbom used Nikuradse constants, and a yield plastic rheological model was incorporated by claiming that any rheological model with a limited shear rate or an infinite shear rate viscosity (μ_∞) could be accounted for by replacing apparent viscosity (μ') with infinite shear rate viscosity (μ_∞)

$$\frac{1}{\sqrt{f_N}} = -4.0\ log\left(\frac{1.26}{Rep\sqrt{f}_N}\right) + 4.0\log\beta \qquad (1\text{-}1)$$

Where $$\beta = \left(\frac{\mu_\infty}{\zeta}\right)\frac{e^{4.76(\alpha-10)}}{\alpha}$$

drag reduction factor β , area ratio α, and R_{ep} is the plastic Reynolds number given by:

$$R_{ep} = \frac{\rho VD}{\mu_\infty}$$

1.2.2 Two-Phase Flow Patterns

The methods available for predicting flow patterns are mostly suitable for Newtonian liquids. Many maps showing flow regimes have been used in describing flow transitions in two-phase flows. Most of the flow maps constructed are suitable for Newtonian liquids. In contrast, very little information on gas/non-Newtonian liquid flow is available. To estimate the pressure, drop and void fraction correctly, the actual flow pattern must be understood under different flow conditions and the effect of rheological parameters of non-Newtonian fluids. To date, the literature has reported dozens of experimental investigations of flow pattern maps for a two-phase gas / Newtonian fluid mixture in horizontal, vertical and inclined pipes. The Mandhane et al. [27] and Taitel and Dukler [28] flow maps for gas/Newtonian flow are the most frequently used. Research indicates that the hydrodynamics or physical properties of gas/shear-thinning

liquid two-phase flow exhibit different behaviors compared to gas-Newtonian liquid flow. However, some research findings point to liquid properties having only a slight impact on flow patterns [29-33]. Based on these conclusions, Chhabra and Richardson [34] made minor alterations to Mandhane et al.'s [27] map of horizontal flow patterns while also taking into consideration Weisman et al.'s [35] work on this map (see Figure 1.1). Gregory and Scott [36] devised a correlation that is valid to predicting slug frequency in Newtonian fluids. Based on the results of water and carbon dioxide used in a 19-mm pipe, they suggest that the slug frequency has to correlate with the Froude number. Rosehart et al. [37] published their findings on the first experimental study dealing with the effect of non-Newtonian (power-law model) characteristics. In that study, the researchers used capacitive sensors for measuring the velocity of the slug as well as the average hold-up and slug frequency. Hubbard [38, 39] and Otten and Fayed [40-41] published their experimental results, which included pressure-drop, velocity of the slug and slug frequency measurements for two-phase flows of air/non-Newtonian (Carbopol R941 solutions). Plotting the experimentally determined slug velocity against the slug no-slip velocity allowed them to determine the relationship between slug velocity and slug no-slip velocity for shear-thinning behavior. Picchi et al. [42] experimentally investigated horizontal and inclined pipes with an inner diameter of 22.8 mm for the air/power-law model in two-phase liquid flow. The model they proposed for slug flow is valid for air/power-law fluid. They also observed that flow pattern maps are affected by inclination. Bendiksen et al. [43] and Al-Kaiyem et al. [44] explored slug flow in a horizontal pipe employing medium viscosities. Bendiksen et al. [43] used oil to investigate slug bubble velocity in a 0.057-m ID horizontal pipe. They discovered that the liquid viscosity has a significant impact on the bubble shape and velocity. Al-Kaiyem et al. [44] conducted a statistical analysis of slug length and translational velocity using water as the working fluid. They discovered that the slug length

and translational velocity increase while the slug frequency decreases for a constant water velocity. Baba et al. [45] studied the slug translational velocity for highly viscous oil and gas flows in horizontal pipes. They proposed a new empirical correlation to calculate slug velocity in highly viscous two-phase flow. Other studies examined the effects of fluid properties on drift velocity, which is a component of translational velocity, as indicated in Equation (2). The most recent and significant among these researchers are Gokcal et al. [46] and Jeyachandra et al. [47], who used an inclinable facility with a diameter of 0.0508 m. Baungartner et al. [48] experimentally studied a 44.2-mm diameter horizontal pipe using carboxymethyl cellulose (CMC) power-law solutions and air. They found that the flow behavior was affected by the continuous phase.

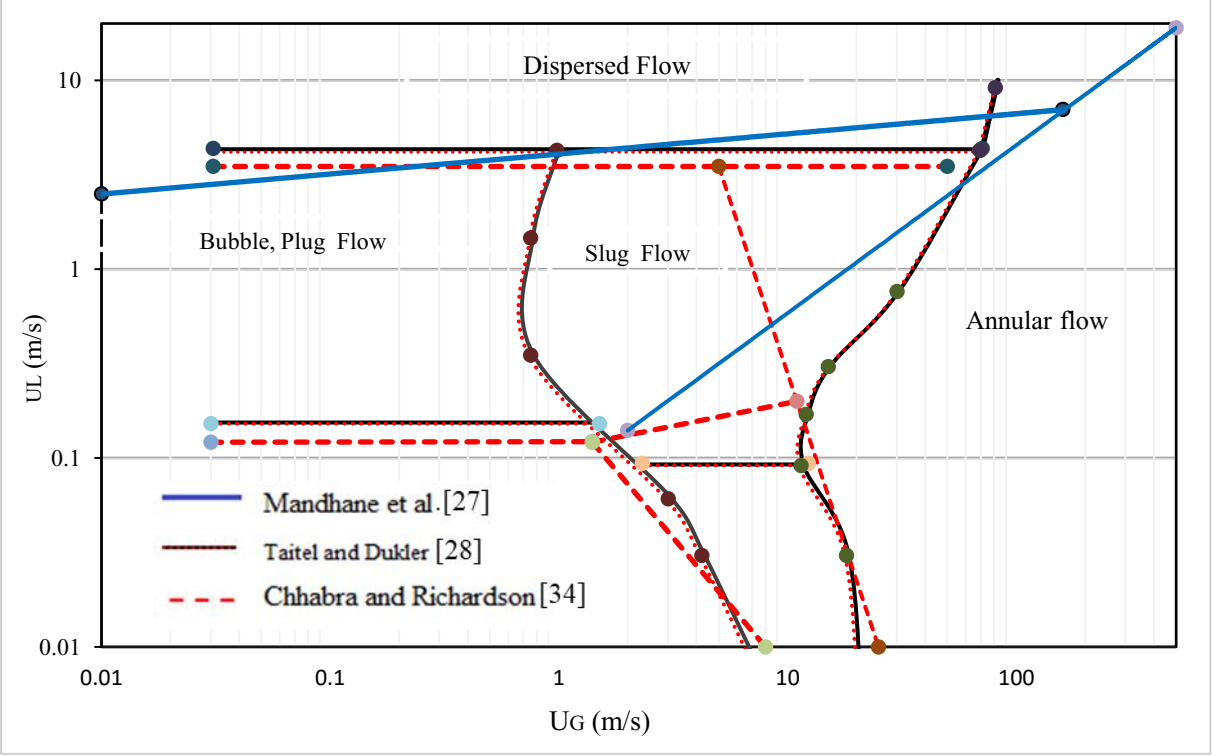

Figure 1-1. Comparison between flow regimes maps of Mandhane et al. [27], Taitel and Dukler [28], and Chhabra and Richardson [34] in Horizontal Pipes.

1.2.3 Pressure Drop Models for Gas/Non-Newtonian Fluids

To improve understanding of the flow mechanism of gas/non-Newtonian fluids, several theoretical models for predicting the pressure drop of gas/non-Newtonian (shear-thinning) fluids are reviewed. Table 1-1 summarizes the experimental data with different pipe diameters, fluid properties, and superficial velocities.

In 1989, Dziubinski and Chhabra [49] modified the dimensionless pressure drop of two-phase in horizontal flow by introducing the factor of Farooqi and Richardson [50] (J) into Lockhart and Martinelli's [51] correlation as

$$(\frac{dP}{dl})_{tp} = \left(\frac{dP}{dl}\right)_l \left(J + \frac{C_0}{X} + \frac{J}{X^2}\right) \tag{1-2}$$

Where

$$X = \sqrt{\left(\frac{dp}{dl}\right)_L / \left(\frac{dp}{dl}\right)_G} \tag{1-3}$$

and $$J = \left(\frac{u_{sl}}{u_{cl}}\right)^{1-n}$$

In 1996, Dziubinski [52] considered the flow of single-phase fluids. He proposed an empirical correlation to calculate the pressure losses of power-law (shear thinning fluid) in horizontal intermittent flow as

$$(\frac{dP}{dl})_{tp} = \left(\frac{dP}{dl}\right)_l \left(\frac{1+1.036*10^{-4}\ {Re_{TP}}^{1.235}}{1+1.036*10^{-4}\ {Re_L}^{1.235}}\right) \lambda^{1-n} \tag{1-4}$$

Taitel and Barnea [53] studied gas/Newtonian fluid slug flow. Assuming that the film does not contain any trapped gas bubbles and that both liquid and gas are incompressible, the overall pressure drop can be measured, consisting of the drop-in pressure through the liquid slugs as:

$$(\frac{dP}{dl})_{tp} = \left(\frac{dP}{dl}\right)_l + \left(\frac{dP}{dl}\right)_G \tag{1-5}$$

Table 1-1. Experimental data and limitation for gas/non-Newtonian fluids flow in horizontal pipes

References	Non-Newtonian fluid, mass concentration	Data points	Flow behavior index n	Fluid consistency coefficient K [Pa s–n]	Liquid density, q [kg/ m3]	u_{sl} [m s^{-1}]	u_{sg} [m s^{-1}]	Pipe diameter D [m]
Farooqi and Richardson, [24]	Kaolin, 13.7 %	52	0.175	4.23	1230	0.24–0.98	0–6.8	0.041
	Kaolin, 24.4 %	53	0.14	28.6	1300	0.24–0.98	0–6.6	0.041
Chhabra et al. [13]	Kaolin, 31.5 %	20	0.103	18	1265	0.28–0.79	0–2.9	0.207
	Kaolin, 36.5 %	25	0.103	48.5	1310	0.73–1.35	0–3.1	0.041–0.20
Chhabra et al. [14]	CMC, 1.25 %	59	0.58	3.2	1000	0.24–0.98	0–5.4	0.0417
	Separan AP 30, 1.5 %	56	0.28	10	1000	0.24–0.98	0–5.5	0.0417
Ruiz-Viera et al. [55]	Lubricating grease	16	0.14	610	914	0.07–0.12	0–0.8	0.025–0.03
Xu et al. [54]	CMC, 1.0 %	52	0.798	0.089	1000	0.05–1.69	0–11.7	0.02–0.06
	CMC, 2.0 %	82	0.658	0.469	1000	0.05–2.03	0–4.6	0.02–0.06
	CMC, 3.0 %	81	0.615	0.972	1000	0.05–1.70	0–2.2	0.02–0.06
Xu et al. [55]	CMC, 0.5 %	45	0.952	0.034	999	0.18–1.77	0–2.6	0.05
	CMC, 2.0 %	45	0.765	0.407	1000	0.18–1.42	0–2.6	0.05
	CMC, 2.5 %	45	0.595	1.365	1000	0.18–1.42	0–2.6	0.05
	CMC, 3.5 %	45	0.535	2.434	1000	0.18–1.06	0–2.6	0.05
Picchi et al. [43]	CMC, 1.0 %	52	0.941	0.007	998	0.05–1.4	0.1–2	0.022
	CMC, 3.0 %	82	0.872	0.061	999	0.05–1.4	0.1–2	0.022
	CMC, 6.0 %	81	0.750	0.264	1002	0.05–1.4	0.1–2	0.022

Recently, Xu et al. [54] modified Taitel and Barnea's [53] two-phase model to take power-law fluid into account by ignoring the pressure drop across the gas slug. They consider the pressure drop along with the homogeneous liquid slug. Their findings indicate that the modified two-

fluid model shows good agreement with pressure drop and drag reduction data on shear-thinning fluid (power law model) related to their experimental work [55-56].

$$(\frac{dP}{dl})_{tp} = \left(\frac{dP}{dl}\right)_{lS} = 2\frac{f_{ls}}{D}\rho_{ls}u^2{}_m\lambda \tag{1-6}$$

For non-Newtonian fluid in a smooth pipe, f_{ls} is the liquid slug factor calculated based on the liquid slug Reynolds number as:

$$f_{ls} = \frac{C}{Re_{ls}{}^{n*}} \tag{1-7}$$

Where C =0.79, n*=0.25 for turbulent flow and C=16, n*=1 for laminar flow.

And $$Re_{ls} = \frac{D^n u_m{}^{2-n}}{8^{n-1}\,k}\rho_{ls} \tag{1-8}$$

In 2006, Ruiz-Viera et al. [57] Experimentally studied air-lubricating grease two-phase flow by applying various types of geometries while considering rough as well as smooth surfaces. Additionally, they developed a two-phase pressure drop empirical model that combined sigmoidal-type equations and the power law model.

1.3 Slug Flow Characteristics

The slug flow pattern consists of a repeated cycle of a liquid slug body and liquid film region with fluctuating pressure loss (see Figure 1.2). There are two clearly defined sections or areas in a slug unit. The first area is the slug body or liquid slug area, expressed as length l_s. The second area in the slug unit is the liquid film, expressed as length l_f. This second area is comprised of liquid film (expressed as height h_f) as well as a long gas bubble. Gas from the film area of the slug unit is usually entrained at the slug's front section. Furthermore, there is typically a mixing area for length l_m. Slug unit length l_u can be written as:

$$l_u = l_f + l_s \tag{1-9}$$

Within slug bodies, the liquid slug's front velocity is denoted as U_t, the tail velocity is written as U_b, the mean liquid velocity is denoted as U_L, and the bubble velocity is designated as U_b. The intermittent slug can generate mechanical vibrations in the flow pipe with significant structural loads, jeopardizing the system's stability. As a result, understanding and predicting all parameters that affect a slug unit is of great importance.

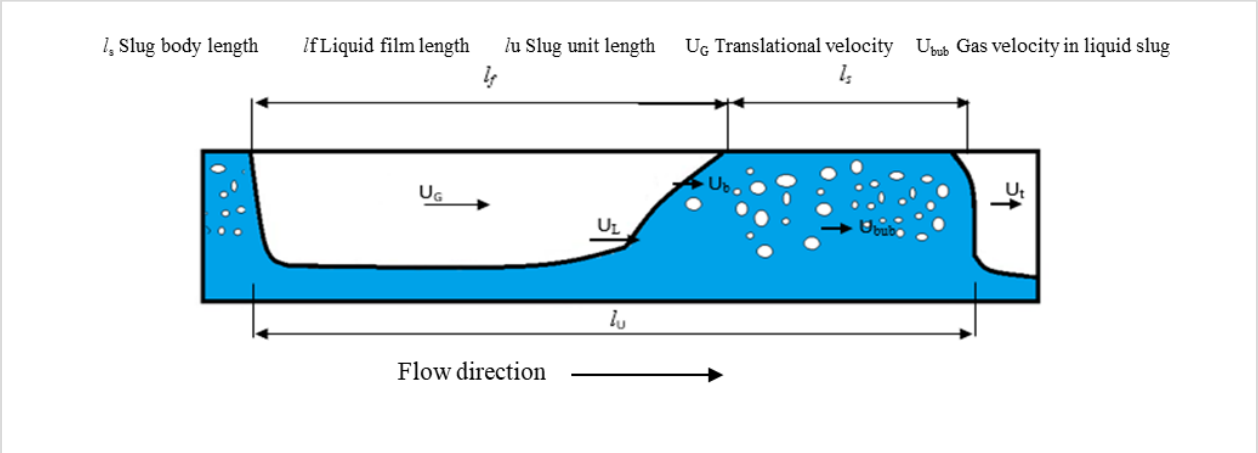

Figure 1-2. Illustration of gas-liquid slug flow.

1.2.1. Translational Velocity

Translational velocity in multiphase flows refers to the rate of speed traveled by a slug unit, which is made up of gas bubbles flowing in tandem with alternating liquid slugs in a typical slug flow pattern. Translational velocity can be calculated by multiplying the by the distribution parameter and mixture velocity. Nicklin et al. [58] were the first to study elongated bubble motion in flowing liquids. They discovered that the superimposition of the velocity in stagnant liquid and the influence of the moving liquid can be used to estimate translational velocity. The following expression was then proposed for estimating the bubble translational velocity in a vertical pipe.

$$U_s = C_0 . U_m + C_* \sqrt{gD} \quad (1\text{-}10)$$

Since the study considered a horizontal flow, the second term in Equation (1-10) is meaningless and the translational velocity in horizontal pipe is indicated as:

$$U_s = C_0 \, U_m \quad (1\text{-}11)$$

Where U_s is the translational velocity and C_0 is distribution coefficient, C_0 is assumed for air–water two-phase flow to be 1.0 for plug flow to 1.35 for fully developed turbulent flow [16-17, 21].

For non-Newtonian/air two-phase flow, Otten & Fayed [41] reported the increase of the air/Carbopol941 concentration from 0.075% to 0.2%, and the values of distribution coefficient in C_0 increased from 1.36 to 1.41, whereas, for the same concentration, Rosehart et al. [37] reported that the distribution coefficient values varied from 1.34 to 1.57. In this study, we followed the studies of Rosehart et al. and Otten & Fayed to obtain values of C_0 based on experimental results.

1.2.2. Slug Frequency

Slug frequency, f_s, can be defined as the number of slugs passing a particular point in the pipeline during a specific time. This type of frequency serves as a function for each slug unit's average translational velocity, a flow rate, and an inclination angle. Estimating the fs is required in some industrial processes and pipelines to precisely predict corrosion rates for safety and economical purposes. Gregory and Scott [36] devised a correlation that is valid to predicting slug frequency in Newtonian fluids. They suggest that the slug frequency has to be correlated with the Froude number. Where the Froude number is defined as:

$$(N_{Fr})_{slug} = \frac{U_{SL}}{gD}\left[\frac{U_s^*}{U_m} + U_m\right] \quad (1\text{-}12)$$

Gregory and Scott consider the value of U_s^* to be equal to 6 m/sec, and it is combined with the data of Hubbard, where the following equation was derived.

$$f_S = 0.0157\left[(N_{Fr})_{slug}\right]^{1.2} \quad (1\text{-}13)$$

Several authors have developed correlations for slug frequency [59-63]. The majority of the empirical models were based on the methodology of Gregory and Scott, which developed the first correlation for slug frequency.

Past research in the field of slug flow characterization has primarily concentrated on the Newtonian gas-liquid system, where there was a noticeable lack of experimental work focusing on slug frequency measurement for non-Newtonian fluid.

Rosehart et al. and Otten & Fayed dealt with slug parameter classification for air-non-Newtonian systems. They extended the Gregory and Scott for by versus Frond number.

Recently, Picchi et al. [22] extended the model of Gregory and Scott [36] as a means to predict the slug frequency of power-law fluid (shear-thinning fluid rheology).

Other recent studies in single, two-phase, and three-phase flow in pipelines and annuli [64-70] adopted a broad range of methods, including laser diagnostics, wavelet transform, probabilistic estimation, and high-speed visualization of Newtonian fluids and non-Newtonian fluids. However, these investigations ignored how the rheological properties of non-Newtonian fluids can affect slug characteristics and flow regime maps in vertical and horizontal pipes.

1.3 Computational Fluid Dynamics (CFD)

Recently, many researchers have employed computational fluid dynamics (CFD) simulation tools for examining two-phase flow hydrodynamics characteristics. However, none of these authors examined two-phase flow yield power-law fluid in pipes. Ko et al. [71] employed a

shear stress transport model for solving kinetic energy-related equations for turbulent wavy Newtonian core flow. One of the main findings was that, compared to the K-ω turbulence model, their model used gave more accurate predictions for wavelength and pressure distribution. Lo and Tomasello [72] utilized the volume of fluid approach to simulate stratified Newtonian fluid flows to demonstrate how CFD outcomes are impacted by the turbulence model. However, their findings indicate that the K-ω turbulence model gave more accurate results. Al-yaari and Abu-Sharhk [73] applied the RNG k-ε turbulence model to simulate stratified flow for horizontal pipes. Jia et al. [74] compared pressure gradients and drag reduction ratios in slug and stratified flow regime types. Additionally, they applied the 3D CFD process to determine the friction factor of the liquid wall, which they then compared to values found for empirical standard correlations. Kroes and Henkes [75] used ANSYS fluent to investigate drift velocity in elongated gas bubbles in Newtonian fluid occurring in pipelines. The researchers observed good agreement in experimental results for the analytical solution. All these studies do not consider yield power-law fluid in a two-phase flow.

Minichannel gas-liquid two-phase flow has become more and more appealing to researchers due to its enhanced feasibility in engineering and medicinal applications. Two-phase flow can be found in a variety of uses, including micro fuel cells, heat exchangers and the cooling of electronic circuitry. Earlier investigations on minichannels' gas-liquid flows primarily focused on the gas-Newtonian flow of liquid materials and employed refrigerant fluid or water for the liquid flow phase. Meanwhile, there are numerous instances of non-Newtonian fluids being applied in biological and industrial processes. Examples include waste water, polymer solutions, chemical solutions, and blood flowing through micro-vessels

Up until now, there has been little published research devoted to the flow of two-phase gas-non-Newtonian liquids with power-law behavior in a pipe with turbulent flow. For these

reasons, a series of experimental, theoretical and CFD investigations are conducted to study the behavior of gas/non-Newtonian fluids, especially yield power law behavior in a pipeline as well as to obtain and analyze new data and improve the fundamental understanding of flow regimes at a different orientation.

Recently, computational fluid dynamics (CFD) has been used by several researchers to augment and compered results of previous experiments. Lawal and Qian [76] studied two-phase flow Newtonian fluids in empty channels (0.25, 0.5, 0.75, 1, 2 and 3 mm) of a T-junction. In their numerical simulations, the researchers employed FLUENT a volume of fluid (VOF) model; they also investigated slug length for both liquids and gases under various inlet conditions. Their numerical findings indicated good agreement with previous experimental outcomes. Furthermore, they discovered that the slug lengths of liquid and gas were related to liquid and gas superficial velocity, such that increases in gas velocity resulted in an increase in the length of the gas slug from the point of constant liquid velocity onward. Conversely, when the liquid velocity increased, the length of the gas slug began to decrease, this time starting at the point of constant gas velocity. Rosengarten et al. [77] used CFD FLUENT to investigate extensional flow on contact angle and contraction affect Newtonian liquid droplet formation during the contraction phase, finding that the contact angle of the wall significantly impacted the shape and size of the droplets. Akbar, M. K., & Ghiaasiaan [78] used ANSYS FLUENT to conduct analyses on two-phase air-water flows in Taylor flow systems. They investigated bubble velocity as well as gas hold-up and length of slug in relation to liquid and gas inlet velocity. Vertical and horizontal channel orientations were simulated. The findings indicated that for both types of channel orientation, bubble speeds increased as two-phase velocity increased. Bhatelia et al. [79] used CFD to study hydrodynamic behaviors in gas- Newtonian liquid systems featuring flow capillary microchannels. In their work, the researchers modeled

the Taylor slug flow system using the VOF approach, simulating a variety of channel diameters and inlet geometries (e.g., 0.5 mm, 1 mm, and 2 mm). They also chose an equiangular microchannel at 120o (inverted Y-junction) to delve deeper into slug characteristics for different liquid and operational parameters. In other areas of their research, simulated and compared the results for 2D and 3D inverted vertical Y-junction channels, focusing on how superficial velocity and gravity impacted the contact angles and phases. They found surface tension had a notable impact on the slug. Chan et al. [80] studied the Taylor flow regime by performing numerical simulations and looking at how the shape and size of bubbles were impacted by changes in gas and liquid values. In addition to the numerical simulations, the researchers performed simulations involving alterations to inlet geometry while maintaining other parameters. They concluded that the sizes and shapes of the bubbles were strongly related to inlet dimensions. Zheng et al. [81] applied FLUENT in their study to investigate how viscous force and surface tension impacted on characteristics of a Taylor bubble. In conducting their study, they used a fine mesh to capture the liquid film around each Taylor bubble. Their results indicate that gas bubbles are naturally surrounded by the liquid film during instances of fully wetted fluids. Santos and Kawaji [82] experimentally and numerically studied the formation of Taylor slugs in a rectangular microchannel T-junction based on gas-liquid flow. They used a FLUENT volume-of-fluid (VOF) model in numerical modeling. The researchers studied the effect of flow rate on a void fraction, velocity slip and frictional pressure drop of two-phase flow.

1.3 Motivation of the Present Study

The behavior of single- and multiple-phase flow of shear-thinning compared to Newtonian behavior flow, especially in turbulent flow, is highly complicated and not well understood in

many respects due to the complex non-linear viscosity. Designing single-phase and gas/non-Newtonian pipelines requires extensive knowledge of flow behaviour, such as pressure drops, the type of flow regime that occurs in the pipe and the effect of rheological parameters of the liquid phase on slug characteristics. However, to improve the understanding of the effects of rheological parameters of the shear-thinning phase in single- and two-phase models, some research questions need to be defined.

- Is the choice of the rheological model significant to predicting the laminar, transitional, and turbulent flow of non-Newtonian fluids in pipes?
- What is the empirical transitional flow of power-law and Herschel–Bulkley fluids in single phase?
- Does the yield stress have an effect on the critical velocity of Herschel–Bulkley fluid at the same rheology parameters of power-law fluid?
- Are the rheological parameters measured in laminar flow valid in turbulent flow?
- How accurately can the pipe flow of power-law models predict the pressure drop of Herschel–Bulkley in a turbulent regime while neglecting yield stress in single- and two-phase flow?
- How do the rheology parameters of Herschel–Bulkley fluids, especially (yield stress), affect the flow regime maps and characteristics of slug flow in a horizontal and vertical flow?
- What are the important parameters that should be considered, and do they have a significant effect on pressure losses and characteristics of the slug flow of shear-thinning fluid?
- Does the Computational Fluid Dynamics (CFD) ANSYS FLUENT19 in a turbulent model have the ability to simulate single- and two-phase flow of shear-thinning fluid?

1.4 Statement of the Problem

The development of correlations for non-Newtonian fluids for the prediction of flow pattern maps, slug flow characteristics, and pressure losses in transitional and turbulent flow has proceeded at a slower pace owing to the complexity and diversity of viscosity behavior. Many methods are used to analyze non-Newtonian fluids in laminar flow. In this thesis, we systematically study the effect of rheological parameters on non-Newtonian liquid shear-thinning behavior (power-law and Herschel-Bulkley models) in laminar, transitional, and turbulent regimes in both single- and two-phase systems through experiments and the CFD method. As a result, this investigation is required to develop new prediction models. The following section describes the goal and expected outcomes.

1.5 Objectives and Research Plan

This study will present comprehensive theoretical, experimental and CFD studies of both single- and two-phase flow of Newtonian and non-Newtonian (power-law and Herschel–Bulkley fluids) through a pipeline at different orientations and diameter sizes in a laminar, transitional, and turbulent flow.

The objectives of this study are:

- To perform a comprehensive review of flow pattern maps, pressure gradient and void fraction models and characteristics of slug flow and their limitations in horizontal and vertical pipes.

- To experimentally investigate the effects of various rheology parameters on transition point (critical velocity) of non-Newtonian fluids (power-law and Herschel-Bulkley fluid) at the same operating conditions.
- To experimentally and numerically investigate the effects of various rheology parameters on the flow regime map and pressure loss of non-Newtonian fluids (power-law and yield power-law) in the same working conditions.
- To evaluate slug frequency, slug velocity correlations and their validity for gas/non-Newtonian two-phase flow (power-law and Herschel–Bulkley fluid).
- To use a high-speed camera to estimate slug flow characteristics such as slug length, slug velocity and slug frequency and the effect of rheological parameters on the shape, length, and number of slugs passing.
- To evaluate and improve the predictions of transitional region and pressure loss for Herschel-Bulkley fluid in single-phase flow.
- To develop a more reliable theoretical analysis of single-phase and multiphase flow of shear-thinning fluid in pipelines.
- To assess the ability of Computational Fluid Dynamics (CFD) ANSYS FLUENT in a turbulent model to simulate single- and two-phase flow of shear thinning fluid.

1.6 Research Scope

The first part of this research will cover laminar, transitional, and turbulent flow in a single phase of shear-thinning fluid in two flow loops with horizontal pipes (diameters of 19.1 mm and 76.2 mm) along with CFD investigations.

The second part will focus on improving the understanding of the effects of rheological parameters on shear-thinning liquids in a two-phase flow. Experimental and CFD

investigations of air/shear-thinning fluid in horizontal and vertical pipes with a diameter of 76.2 mm will be conducted.

Due to the increasing viability of using a minichannel for gas-shear-thinning two-phase flow in engineering and medical applications, this approach has become increasingly attractive to researchers and industry experts. In the third part of this research, a computational (CFD) examination of Taylor bubbles will be performed in a minichannel T-junction mixer with a hydraulic diameter of 1 mm. The investigations will consider the effect of the concentration of shear-thinning solutions and the superficial velocity of the inlet liquid phase on the length, velocity, and shape of the Taylor bubbles.

1.7 Research Methodology

To achieve the objectives, primary data were collected for Newtonian (water) and two different behaviours of non-Newtonian fluids of shear-thinning models (power-law and Herschel-Bulkley models).

Four fluids were prepared from a powder of sodium carboxymethyl cellulose (CMC), three fluids from xanthan gum (XG) powder, and four from a mixed powder of bentonite and xanthan. These different concentrations of non-Newtonian fluid were prepared in the Drilling Technology Laboratory with the addition of minute amounts of polymer powders to water. The rheology and characteristics of the solutions were determined using an 8-speed API-compliant rotational viscometer (Model 800) and a 4-scale mud balance. The CMC fluids are referred to as shear-thinning (power-law model), the XG fluids to the Herschel-Bulkley model, and the BXG mixed to shear-thinning fluid (Herschel-Bulkley model) and will be used as working fluids. Table 1-2 shows the properties of non-Newtown fluids that will be used in the experiments and simulation work.

Table 1- 2. Physical properties and rheology parameters of the test fluids at 20 "C and atmospheric pressure.

Compositions (gr/350ml)				Rheological parameters					
Symbol	Bentonite	Xanthan gum	CMC	ρ (kg/m^3)	n	K ($Pa.s^n$)	τ_y (Pa)	R^2 (HB model)	R^2 (PL model)
CMC1	-	-	2	1000	0.71	0.0601	0	-	0.991
CMC2	-	-	3	1002	0.60	0.233	0	-	0.992
CMC3	-	-	4	1005	0.57	0.405	0	-	0.999
XG-1	-	1	-	998	0.65	0.037	0.4	0.989	
XG-2	-	2	-	1003	0.56	0.131	0.7	0.993	-
XG-3	-	3	-	1006	0.43	0.353	1.33	0.997	-
BXG1	5.5	2	-	1035	0.74	0.0512	0.76	0.991	-
BXG2	5.5	3	-	1041	0.61	0.241	1.92	0.992	-
BXG4	5.5	4	-	1047	0.56	0.415	3.06	0.999	-

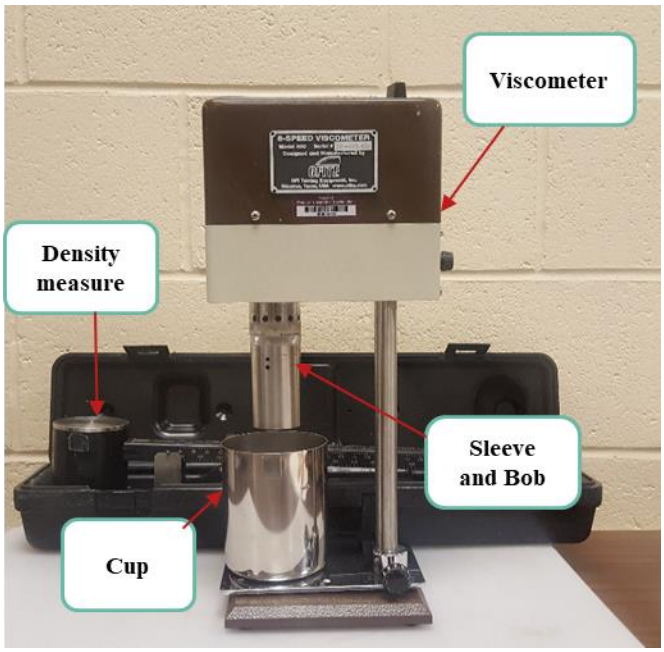

Figure 1-3. Rotational Viscometer 8-speed model and Mud density measure devices.

1.7.1 Research Instruments and Equipment

1.7.1.1 Three Inch Flow Loop.

The measurements will be performed using Newtonian and sixteen different concentrations of non-Newtonian fluid in a 3-inch flow loop. The flow loop is an open-loop re-circulating system with a total length of 65 m to ensure phase mixing and authorize flow regime patterns to develop (see Figure 1.4). The loop is built of a 76-mm diameter clear PVC pipe. A 3000-litre (792.5-gallon) reservoir tank and an inverter to control the centrifugal pump with a maximum flow rate of up to 220 GPM. An Omega FTB-730 turbine flow meter with a range of 3–400 GPM and an accuracy of ± 1% of the full scale was used to measure the volumetric flow rate of working fluids. Three Omega PX603-100G5V pressure transducers provided the pressure data in every section, and a differential pressure transmitter (0–150 psi) was used to measure high-response pressure. Two parallel Omega airflow meters with ranges of 3.5–42.5 m^3/h and 10 ~ 100 m^3/h were composited in the compressed air line. The Newtonian fluids were used as calibration fluids. Pressure transducers, sensors, and flow rate were investigated to calculate the roughness of the pipe surface based on pressure losses.

1.7.1.2 Small Diameter Flow Loop.

In the small pipe flow loop, the working fluids were pumped from the tank through a PVC pipe with a diameter of 0.0191 m and a length of 22 m. six pressure transducers (Omega PX603-100Q5V, with effective measures of 0–100 psi) were used to measure pressure losses in the test sections at different flow rates. This flow loop was used to measure pressure loss in a single phase. The experiment is schematically represented in Figure 1.5.

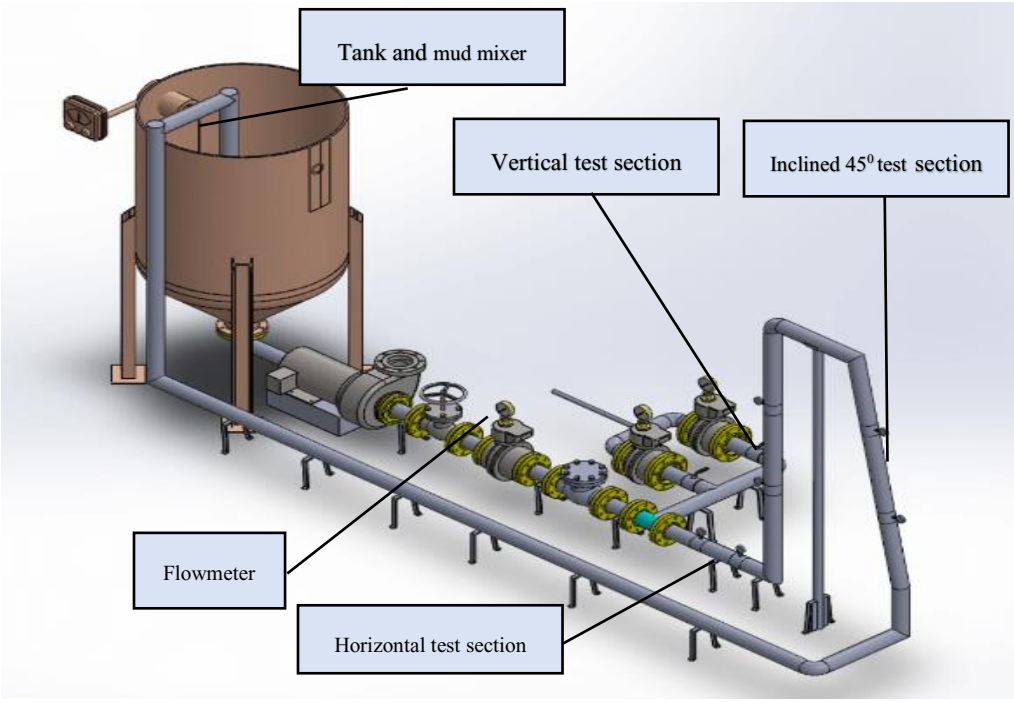

Figure 1-4. Schematic of experimental facility

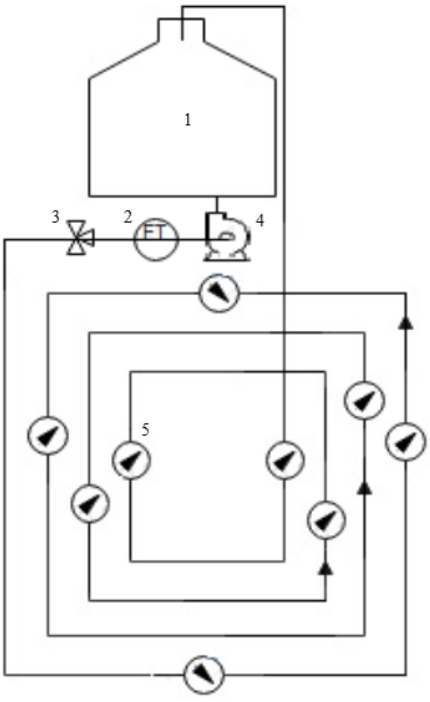

1. Mixing tank
2. Centrifugal pump
3. Relief valve
4. Turbine flow meter
5. Pressure transducer

Figure 1-5. Sketch of the experimental set-up in the small loop.

1.8 Measurement Tools and Analysis

1.8.1 Rheological Parameter Estimation for Herschel-Bulkley fluids

The usual approach for estimating the three rheological parameters for Herschel-Bulkley liquid is to complete the rheological equation.

$$\tau = \tau_0 + k\dot{\gamma}^{n} \tag{1.14}$$

where τ shear stress and, τ_y is the yield stress, k is the fluid consistency, n is fluid behavior and $\dot{\gamma}$ is the shear rate, is through non-linear regression of the viscometer data. This is usually done with a numerical package, with the sum of error squares minimized and the goodness of fit judged by the value of the correlation coefficient R2 from the linearized Eq. (1.14), as in Eq. (1.15).

$$\log(\tau - \tau_o) = \log K + n \log \dot{\gamma} \tag{1.15}$$

The first challenge was to determining the yield stress (τ_y) value at low concentrations. Klotz and Brigham [83] a trial-and-error method was used to detriment this value as:

$$n = \sum_1^6[w_i \log(\dot{\gamma}_i)] \sum_1^6[w_i \log(\tau_i - \tau_o)] - \sum_1^6 w_i \sum_1^6 [w_i \log(\dot{\gamma}_i) \log(\tau_i - \tau_o)]/$$
$$[\sum_1^6[w_i \log(\dot{\gamma}_i)]]^2 - \sum_1^6 w_i \sum_1^6 [w_i \log(\dot{\gamma}_i)]^2 \tag{1.16}$$

And

$$\log K = \frac{\sum_1^6[w_i \log(\tau_i - \tau_o)] - n \sum_1^6 [w_i \log(\dot{\gamma}_i)]}{\sum_1^6(w_i)} \tag{1.17}$$

With a guessed value of τ_0 , the value of n and k can be determined. we can then vary τ_0 until a minimum Δ is found

$$\Delta = \sum_1^6 (\tau_{\text{i data}} - \tau_{\text{i calc}})^2 \quad (1.18)$$

To make sure the results are correct, log-log scale was drawing with new value of τ_0 as in figure 1.111

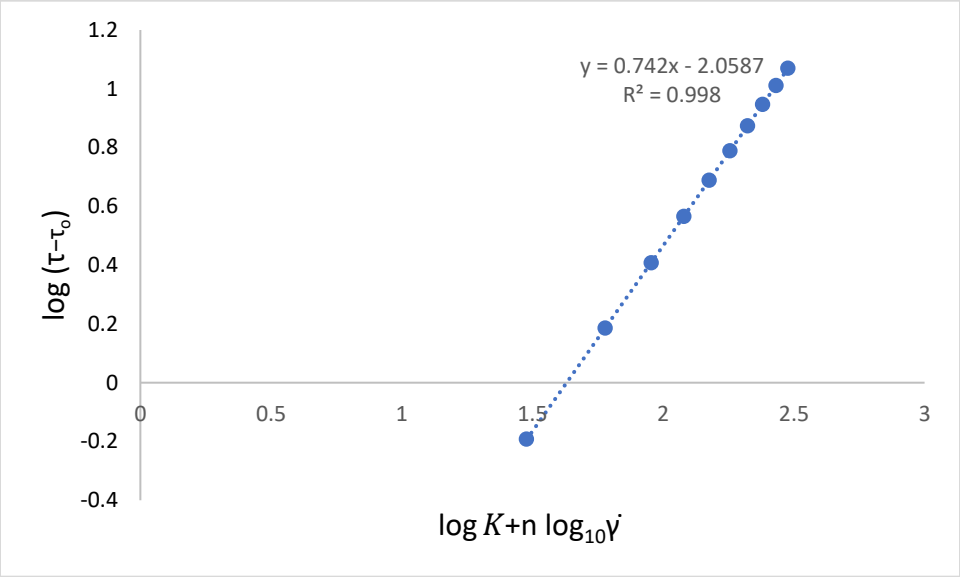

Figure 1-6. Logarithmic scale for Herschel-Bulkley liquid to calculate the rheological parameter.

Where n = 0.742 and

and K = 10^ (-2.0587) = 0.008736 Pa.sn

More information on rheological parameter estimation is found in Appendix A.

1.8.2 Uncertainty Analysis

The approach proposed by Kline and McClintock [84] was used to calculate the uncertainty in the experiment's measurements. This technique is also known as the root-sum squared (RSS) approach. The uncertainties in the primary measurements can be used to determine the uncertainty in the

results. Assuming that the experimental measurements of dependent variables were taken and the mean value of replicate measurements can be written as:

$$\boldsymbol{x_m = \frac{x_1, x_2, x_3, \ldots, x_n}{n} = \frac{\sum_{i=1}^{n} x_i}{n}} \tag{1-19}$$

in the form of a product of the primary variables raised to some power,

$$X = X_1^{a_1}, X_1^{a_1}, X_1^{a_1} \ldots . X_n^{a_n} \tag{1-20}$$

the uncertainty in the result, ΔX, is given by (Holman, 2001)

$$\left(\frac{\Delta X}{X}\right)^2 = \sum_{i=1}^{n} \left(\frac{a_i \Delta x_i}{x_i}\right)^2 \tag{1-21}$$

1.8.2.1 Uncertainty in Wall Shear Stress

friction pressure was measured using the pressure transducers with an accuracy of 0.1% of full scale. Wall shear stress was calculated from pressure drop as:

$$\tau_w = \frac{\mathrm{D}\Delta P}{4L} \tag{1-22}$$

The errors in wall shear stress are calculated from Eq. (3.7), and were estimated to vary between 2.3 and 6.4 %.

$$\left(\frac{\Delta \tau_w}{\tau_w}\right)^2 = \left(\frac{\Delta D}{XD}\right)^2 + \left(\frac{\Delta(\Delta P)}{\Delta P}\right)^2 + \left(-\frac{\Delta L}{L}\right)^2 \tag{1-23}$$

Before performing shear-thinning fluid testing in the pipe loops, the instrumentation and data acquisition were validated by comparing the water test results with the Colebrook-White equation. Then, the pipe roughness ε from the water pipe testing was determined by optimizing the value for ε in the Colebrook-White equation to produce the best fit of the water test.

1.8.3 Flow Patterns

In order to assess the current flow regime transition boundaries and to investigate the effects of the rheological models of the shear-thinning fluids and their estimated parameters on the

predictions of flow regime prediction, flow visualization studies are performed in horizontal and upward vertical pipes. Videos are acquired at a location of L/D = 262 in horizontal pipe and h = 4.5 m in vertical pipe (Figure 1-6). The videos are captured by the high-speed video camera at different resolutions depending on the flow regime. Then, the videos are classified into conventional flow regimes in horizontal flow, namely: dispersed bubble, plug, and slug flows.

Figure 1-7. Test setup showing image acquisition equipment. (a) Data acquisition system in a horizontal pipe. (b) In Vertical pipe

In the vertical position, only slug flow was considered. Due to the limitations of the experimental loop, stratified, stratified wavy, and annular flows are not investigated. The superficial liquid (U_L) velocity is in the range of 0.36–6.5 m/s, while the superficial gas (U_g) velocity is in the range of 0.18–3.62 m/s. In total, videos of 215 and 256 flow conditions were taken to span all the flow regimes considered above.

1.8.4 Slug flow Characteristics

The measurement began by calibration stage, which computed the pixel to real distance ratio in order to receive data related to the real dimension. For calibration, a meter gauge with a length of 1.5 m was employed. The calibration methods began by selecting two places on a frame and then determining the true distance between these two points using a meter.

The translational velocity of the slug *U*s, was calculated by computing the time required for the slug unit to travel between two points along the pipe, which are denoted by x_1, x_2. Each slug unit's translational velocity was calculated by dividing the distance between two predefined points by the time required for the slug unit to travel between these two sites. The required travelling time (T_{time}) was obtained by dividing the number of frames (N_F) by the frame (F_f) frequency, which ranged from 0.001 to 0.003s^{-1}.

$$U_S = \frac{X_2 - X_1}{T_{Time}} \tag{1-24}$$

Where

$$F_{Time} = \frac{N_F}{F_f}$$

Slug frequency f_s was obtained from the video that was taken by setting a point at section 262D and then recording the number of slugs that passed through this part and the arrival time for each slug. The time intervals Δt between each pair of consecutive slugs were then estimated, and the slug frequency was calculated as:

$$f_S = \frac{1}{N}\sum_{n=1}^{n}\frac{1}{\Delta t} \tag{1-25}$$

Slug length, L_S, was obtained simply by calculating the slug velocity and the time difference between the slug nose (t_{nose}) and tail (t_{tail}) that travelled along section 262D. The slug length can be calculated as:

$$L_S = U_S(t_{tail} - t_{nose}) \tag{1-26}$$

1.8.5 Simulation and Statistical Analysis

All geometries were developed using design modular and ICEM meshing techniques. Computational simulation was performed using Ansys Fluent 19.1. Transient simulation was carried out using Compute Canada, Graham, and Beluga on the ACENET supercomputer. For statistical analysis, Design Expert and RStudio were utilized.

1.9 Organization of the Thesis

The thesis is written in manuscript format. One published journal article, one article under review and two conference manuscript are included in the thesis. A co-authorship statement is provided at the beginning of all chapters. Overall organization of the thesis is shown in Figure 1-2 and the brief overview of each chapter is below.

Chapter 1 of thesis describes the motivations and objectives of the research. This chapter also includes a brief review of the related previous studies.

Chapter 2 presents experimental and computational fluid dynamics model (CFD) to investigate the effects of rheological models of shear-thinning fluids and their estimated parameters on the predictions of laminar, transitional, and turbulent flow.

Chapter 3 describes the experimental work and CFD volume of fluid (VOF) method studies in a horizontal pipe to investigate the effects of the rheological parameters of the shear-thinning fluid on flow regime transition boundaries. The chapter also includes a visualization of slug flow characteristics.

Chapter 4 presents an experimental and numerical investigation of the influence of rheological properties of non-Newtonians fluids in two-phase flow (gas/shear-thinning fluid) on slug characteristics in an upward vertical flow.

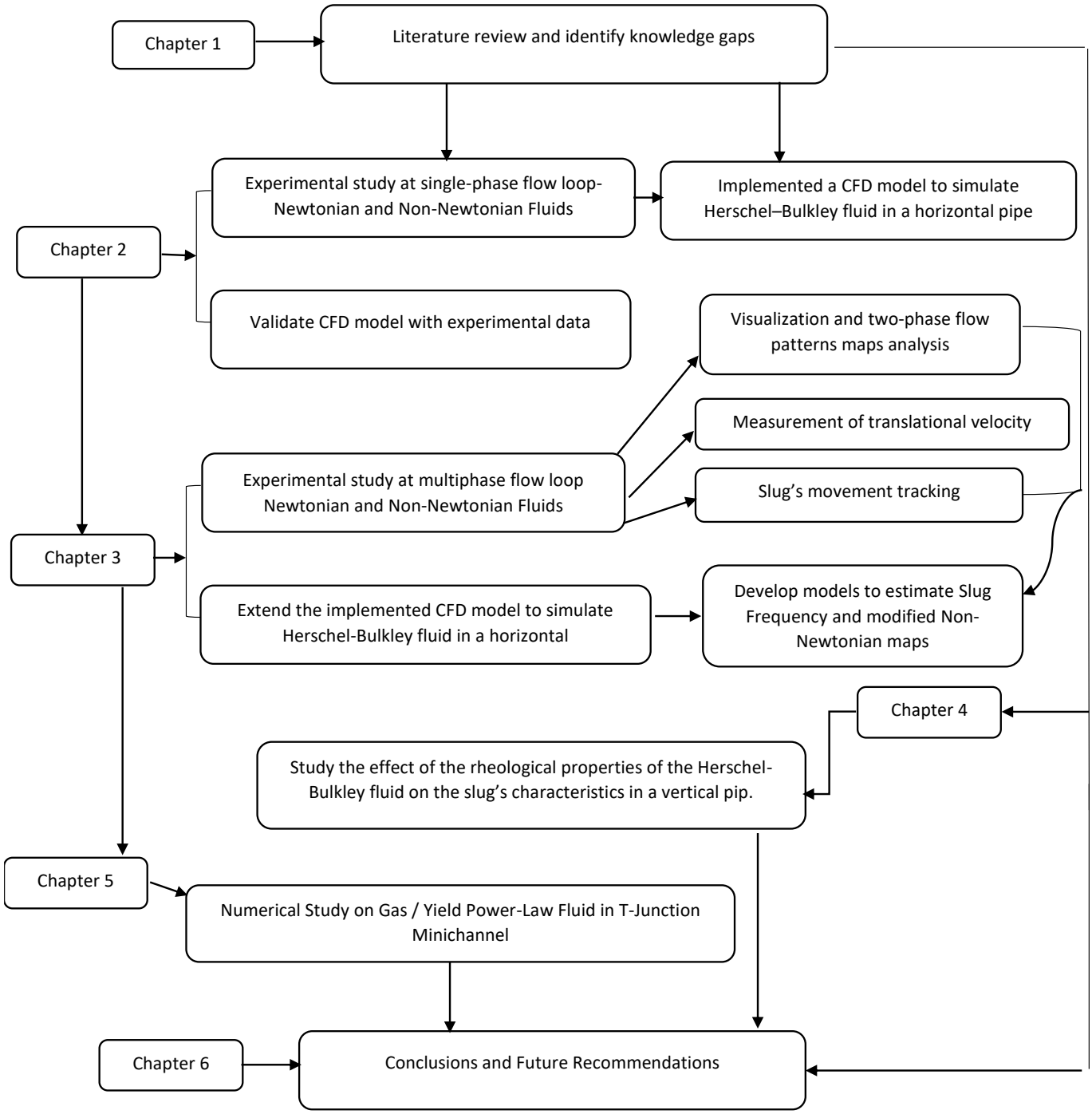

Figure 1-8. Organization of the thesis

Chapter 5 reports computational fluid dynamics (CFD) study on gas/shear-thinning fluid (Herschel–Bulkley model) in T-junction minichannel. This chapter also discusses The effective concentration of the xanthan gum solutions and superficial velocity of the inlet liquid phase on the length, velocity, and shape of the Taylor.

Chapter 6 provides the outcomes of the study and the probable scopes of future investigation

Appendices This section includes supplementary materials and some calculations used in research work.

Appendix A: Shows the methods used to determine the rheological parameters of non-Newtonian fluids for power-law and Herschel-Bulkley models.

Appendix B: Experimental and Numerical Investigation of Gas/Yield Power-Law Fluids in a Horizontal Pipe.

Appendix C: A user defined function (UDF) to implement the Herschel-Bulkley-Papanastasiou model

Appendix D: Includes some images from the experimental work.

1.10 References

1. El-Nahhas, K.; Mostafa, N.H. Prediction of non-Newtonian turbulent flow behaviour by a Newtonian approach. In Proceedings of the 10th International Water Technology Conference, IWTC10, Alexandria, Egypt, 23–25 March 2006; pp. 479–490.
2. Chhabra, R.P.; Richardson, J.F.; Flow, N.N. *Applied Rheology: Engineering Applications*; Butterworth-Heinemann: Oxford, UK, 2008.

3. Rahman, K.M. Analysis of Drilling Fluid Rheology & Pressure Drop Modelling to Improve Drilling Efficiency. Master's Thesis, Schulich School of Engineering, University of *Calgary*, Calgary, AB, Canada, 2018.
4. Demirdal, B.; Cunha, J.C. Olefin-based synthetic-drilling-fluids volumetric behaviour under downhole conditions. *SPE Drill. Complet.* **2009**, *24*, 239–248.
5. Garvin, T.R.; Moore, P.L. A Rheometer for Evaluating Drilling Fluids at Elevated Temperatures. In Proceedings of the SPE 3062 Presented at the Fall Meeting of the Society of Petroleum Engineers of AIME, Houston, TX, USA, 4–7 October 1970.
6. Minton, R.C.; Bern, P.A. Field Measurement and Analysis of Circulating System Pressure Drops with Low-Toxicity Oil-Based Drilling Fluids. In Proceedings of the SPE 17242 Presented at the SPE/IADC Drilling Conference, Dallas, TX, USA, 28 February–2 March 1988.
7. De Wolfe, R.C.; Coffin, G.B.; Byrd, R.V. Effects of Temperature and Pressure on Rheology of Less Toxic Oil Muds. In Proceedings of the SPE 11892 Presented at Offshore Europe, Aberdeen, UK, 6–9 September 1983.
8. American Petroleum Institute. *Recommended Practice on the Rheology and Hydraulics of Oil Well Drilling Fluids. API RP 13D*, 3rd ed.; American Petroleum Institute: Washington, DC, USA, 1995.
9. Pinho, F.T.; Oliveira, P.J.; Miranda, J.P. Pressure losses in the laminar flow of shear-thinning power-law fluids across a sudden axisymmetric expansion. Int. J. Heat Fluid Flow 2003, 24, 747–761.
10. Anand, V.; David Jr, J.; Christov, I.C. Non-Newtonian fluid–structure interactions: Static response of a microchannel due to internal flow of a power-law fluid. J. Non-Newton. Fluid Mech. 2019, 264, 62–72.

11. Moukhtari, F.E.; Lecampion, B. A semi-infinite hydraulic fracture driven by a shear-thinning fluid. J. Fluid Mech. 2018, 838, 573–605.
12. Picchi, D.; ullmann, A.; Brauner, N.; Poesio, P. Motion of a confined bubble in a shear-thinning liquid. J. Fluid Mech. 2021, 918, A7.
13. Chhabra, R. P., Farooqi, S. I., Richardson, J. F., & Wardle, A. P. (1983). Co-current flow of air and shear thinning suspensions in pipes of large diameter. Chem. Eng. Res. Des.(United Kingdom), 61(1).
14. Chhabra, R. P., Richardson, J. F. (1986). The co-current horizontal and vertical upward flow of gas and non- Newtonian liquid. Encyclopedia of Fluid Mechanics, 3, 563-609.
15. Dziubinski, M. (1995). A General Correlation for 2-Phase Pressure-Drop in Intermittent Flow of Gas and Non- Newtonian Liquid-Mixtures in a Pipe. Chemical engineering research and design, 73(5), 528-534.
16. Oliver, D. R., Hoon, A. Y. (1968). 2-phase non-Newtonian flow heat transfer. Transactions of the Institution of Chemical Engineers and the Chemical Engineer, 46(4), T116.
17. Srivastava, R. P. S., Narasimhamurthy, G. S. R. (1981). Void Fraction and Flow Pattern during Two-Phase Flow of Pseudoplastic Fluids. The Chemical Engineering Journal, 21(2), 165-176.
18. Chilton, R. A., & Stainsby, R. (1998). Pressure loss equations for laminar and turbulent non-Newtonian pipe flow. Journal of hydraulic engineering, 124(5), 522-529.
19. Metzner, A.B.; Reed, J.C. Flow of non-Newtonian fluids—Correlation of the laminar, transition, and turbulent-flow regions. AIChE J. 1955, 1, 434–440.
20. Dodge, D.W.; Metzner, A.B. Turbulent flow of non-Newtonian systems. AIChE J. 1959, 5, 189–204.

21. Torrance, B. Friction factors for turbulent non-Newtonian fluid flow in circular pipes. S. Afr. Mech. Eng. 1963, 13, 89–91.
22. Clapp, R.M. Turbulent heat transfer in pseudoplastic non-Newtonian fluids. In International Developments of Heat Transfer Part III; The American Society of Mechanical Engineers: New York, NY, USA, 1961,pp 652–661.
23. Wilson, K.C.; Thomas, A.D. A new analysis of the turbulent flow of non-Newtonian fluids. Can. J. Chem. Eng. 1985, 63, 539–546.
24. Thomas, A.D.; Wilson, K.C. New analysis of non-Newtonian turbulent flowndashyield-power-law fluids. Can. J. Chem. Eng. 1987, 65, 335–338.
25. Slatter, P.T. Transitional and Turbulent Flow of Non-Newtonian Slurries. Unpublished Ph.D. Dissertation, University of Cape Town, Cape Town, South Africa 1994.
26. Hallbom, D. J. (2008). Pipe flow of homogeneous slurry (Doctoral dissertation, University of British Columbia).
27. Mandhane, J. M., Gregory, G. A., Aziz, K. (1974). A flow pattern map for gas-liquid flow in horizontal pipes. International Journal of Multiphase Flow, 1(4), 537-553.
28. Taitel, Y., & Barnea, D. (1990). Two-phase slug flow. In Advances in heat transfer (Vol. 20, pp. 83-132). Elsevier.
29. Chhabra, R. P., Richardson, J. F. (1986). The co-current horizontal and vertical upward flow of gas and non- Newtonian liquid. Encyclopedia of Fluid Mechanics, 3, 563-609.
30. Dziubinski, M. (1995). A General Correlation for 2-Phase Pressure-Drop in Intermittent Flow of Gas and Non- Newtonian Liquid-Mixtures in a Pipe. Chemical engineering research and design, 73(5), 528-534.
31. Oliver, D. R., Hoon, A. Y. (1968). 2-phase non-Newtonian flow heat transfer. Transactions of the Institution of Chemical Engineers and the Chemical Engineer, 46(4), T116.

32. Srivastava, R. P. S., Narasimhamurty, G. S. R. (1973). Hydrodynamics of non-Newtonian two-phase flow in pipes. Chemical Engineering Science, 28(2), 553-558.
33. Srivastava, R. P. S., Narasimhamurthy, G. S. R. (1981). Void Fraction and Flow Pattern during Two-Phase Flow of Pseudoplastic Fluids. The Chemical Engineering Journal, 21(2), 165-176.
34. Chhabra, R. P., Richardson, J. F. (1984). Prediction of flow pattern for the co-current flow of gas and non-Newtonian liquid in horizontal pipes. The Canadian Journal of Chemical Engineering, 62(4), 449-454.
35. Weisman, J., Duncan, D. G. J. C. T., Gibson, J., Crawford, T. (1979). Effects of fluid properties and pipe diameter on two-phase flow patterns in horizontal lines. International Journal of Multiphase Flow, 5(6), 437-462.
36. Gregory, G.A.; Scott, D.S. Correlation of liquid slug velocity and frequency in horizontal concurrent gas-liquidslug flow. AIChE J. 1969, 15, 933–935.
37. Rosehart, R. G., Rhodes, E., & Scott, D. S. (1975). Studies of gas→ liquid (non-Newtonian) slug flow: void fraction meter, void fraction and slug characteristics. The Chemical Engineering Journal, 10(1), 57-64.
38. Hubbard, M.G. An Analysis of Horizontal Gas-Liquid Slug Flow; University of Houston: Houston, TX, USA, 1965.
39. Hubbard, M.G.; Dukler, A.E. The characterization of flow regimes for horizontal two-phase flow. Proc. Heat Transf. Fluid 1966, 1996, 100–121.
40. Otten, L., & Fayed, A. S. (1976). Pressure drop and drag reduction in two-phase non-Newtonian slug flow. The Canadian Journal of Chemical Engineering, 54(1-2), 111-114.
41. Otten, L.; Fayed, A.S. Slug velocity and slug frequency measurements in concurrent air-non-Newtonian slug flow. Trans. Inst. Chem. Eng. 1977, 55, 64–67.

42. Picchi, D., Manerba, Y., Correra, S., Margarone, M., Poesio, P. (2015). Gas/shear-thinning liquid flows through pipes: Modeling and experiments. International Journal of Multiphase Flow, 73, 217-226.
43. Bendiksen, K.H.; Langsholt, M.; Liu, L. An experimental investigation of the motion of long bubbles in high viscosity slug flow in horizontal pipes. Int. J. MULtiph. Flow 2018, 104, 60–73.
44. Al-kayiem, H.H.; Mohmmed, A.O.; Al-hashimy, Z.I.; Time, R.W. Statistical assessment of experimental observation on the slug body length and slug translational velocity in a horizontal pipe. Int. J. Heat Mass Transf. 2017, 105, 252–260.
45. Baba, Y. D., Archibong-Eso, A., Aliyu, A. M., Fajemidupe, O. T., Ribeiro, J. X., Lao, L., & Yeung, H. (2019). Slug translational velocity for highly viscous oil and gas flows in horizontal pipes. Fluids, 4(3), 170.
46. Gokcal, B. E_ects of High Oil Viscosity on Oil/Gas Flow Behavior in Horizontal Pipes. Master's Thesis, University of Tulsa, Tulsa, OK, USA, 2006.
47. Jeyachandra, B.C.; Gokcal, B.; Al-Sarkhi, A.; Serica, C.; Sharma, A.K. Drift-Velocity Closure Relationships for Slug Two-Phase High-Viscosity Oil Flow in Pipes. Soc. Pet. Eng. 2012, 17, 593–601.
48. Baungartner, R., J., Loureiro, G., Freire, A. (2017). Horizontal Pipe Slug Flow of Air/Shear-thinning Fluid Experiments and Modelling. Multiphase Flow Journeys, 4, 2017-0053. March 27, 2017.
49. Dziubinski, M., Chhabra, R., 1989. Predicting two-phase pressure drop for the flow of gas/non-Newtonian liquid mixtures in horizontal pipes. Int.J. Engng Fluid Mechanics 2.1, 63-78.
50. Farooqi, S.I., Heywood, N.I., Richardson, J.F., 1980. Drag reduction by air injection for highly shear-thinning suspensions in horizontal pipe flow. Trans. IChemE 58, 16–27.

51. Lockhart, R. W., Martinelli, R. C. (1949). Proposed correlation of data for isothermal two-phase, two-component flow in pipes. Chem. Eng. Prog, 45(1), 39-48.
52. Dziubinski, M. (1995). A General Correlation for 2-Phase Pressure-Drop in Intermittent Flow of Gas and Non-Newtonian Liquid-Mixtures in a Pipe. Chemical engineering research & design, 73(5), 528-534.
53. Taitel, Y., & Barnea, D. (1990). Two-phase slug flow. In Advances in heat transfer (Vol. 20, pp. 83-132). Elsevier.
54. Xu, J. Y., Gao, M. C., & Zhang, J. (2014). Pressure Drop Models for Gas/Non-Newtonian Power-Law Fluids Flow in Horizontal Pipes. Chemical Engineering & Technology, 37(4), 717-722.
55. Xu, J. Y., Wu, Y. X., Shi, Z. H., Lao, L. Y., & Li, D. H. (2007). Studies on two-phase co-current air/non-Newtonian shear-thinning fluid flows in inclined smooth pipes. International journal of Multiphase flow, 33(9), 948-969.
56. Xu, J. Y., Wu, Y. X., Li, H., Guo, J., & Chang, Y. (2009). Study of drag reduction by gas injection for power-law fluid flow in horizontal stratified and slug flow regimes. Chemical Engineering Journal, 147(2-3), 235-244
57. Ruiz-Viera, M. J., Delgado, M. A., Franco, J. M., Sánchez, M. C., Gallegos, C. (2006). On the drag reduction for the two-phase horizontal pipe flow of highly viscous non-Newtonian liquid/air mixtures: Case of lubricating grease. International Journal of Multiphase Flow, 32(2), 232-247.
58. Nicklin, D. J. (1962). Two-phase flow in vertical tubes, Trans. Inst. Chem. Engr., 40(1), 61-68. 1965.
59. Woods, B. D., Fan, Z., & Hanratty, T. J. (2006). Frequency and development of slugs in a horizontal pipe at largeliquid flows. International Journal of Multiphase Flow, 32(8), 902-925.

60. Gokcal, B., Al-Sarkhi, A., Sarica, C., & Alsafran, E. M. (2009, January). Prediction of slug frequency for high viscosity oils in horizontal pipes. In SPE Annual Technical Conference and Exhibition. Society of Petroleum Engineers.
61. Azzi, A., Al-Attiyah, A., Qi, L., Cheema, W., & Azzopardi, B. J. (2010). Gas–liquid two-phase flow division at a micro-T-junction. Chemical Engineering Science, 65(13), 3986-3993.
62. Abdulkadir, M., Hernandez-Perez, V., Lowndes, I. S., Azzopardi, B. J., & Sam-Mbomah, E. (2016). Experimental study of the hydrodynamic behaviour of slug flow in a horizontal pipe. Chemical Engineering Science, 156, 147-161.
63. Baba, Y. D., Archibong, A. E., Aliyu, A. M., & Ameen, A. I. (2017). Slug frequency in high viscosity oil-gas two-phase flow: Experiment and prediction. Flow Measurement and Instrumentation, 54, 109-123.
64. Rahman, M.A., Adane, K.F., and Sanders, R.S., An improved method for applying the lockhart-martinelli correlation to three-phase gas-liquid-solid horizontal pipeline flows. Canadian Journal of Chemical Engineering, 2013. 91(8): p. 1372-1382.
65. Amin, A., Imtiaz, S., Rahman, A., and Khan, F., Nonlinear model predictive control of a Hammerstein Weiner model based experimental managed pressure drilling setup. ISA Transactions, 2019. 88: p. 225-232.
66. Manikonda, K., Hasan, A.R., Kaldirim, O., Rahmani, N., and Rahman, M.A. Estimating Swelling in Oil-Based Mud due to Gas Kick Dissolution. in ASME 2020 39th International Conference on Ocean, Offshore and Arctic Engineering. 2020a.
67. Manikonda, K., Hasan, A.R., Barooah, A., Rahmani, N.H., El-Naas, M., Sleiti, A.K., and Rahman, M.A. A Mechanistic Gas Kick Model to Simulate Gas in A Riser with Water and Synthetic-Based Drilling Fluid. in Abu Dhabi International Petroleum Exhibition & Conference. 2020b.

68. Zahid, A.A., ur Rehman, S.R., Rushd, S., Hasan, A., and Rahman, M.A., Experimental investigation of multiphase flow behavior in drilling annuli using high speed visualization technique. Frontiers in Energy, 2020. 14(3): p. 635-643.
69. Qureshi, M.F., Ali, M.H., Ferroudji, H., Rasul, G., Khan, M.S., Rahman, M.A., Hasan, R., and Hassan, I., Measuring solid cuttings transport in Newtonian fluid across horizontal annulus using electrical resistance tomography (ERT). Flow Measurement and Instrumentation, 2021. 77: p. 101841.
70. Huque, M.M., Imtiaz, S., Zendehboudi, S., Butt, S., Rahman, M.A., and Maheshwari, P., Experimental Study of Cuttings Transport with Non-Newtonian Fluid in an Inclined Well Using Visualization and Electrical Resistance Tomography Techniques. SPE Drilling & Completion, 2021: p. 1-18.
71. Ko, T., Choi, H. G., Bai, R., Joseph, D. D. (2002). Finite element method simulation of turbulent wavy core-annULar flows using a k–ω turbulence model method. International Journal of Multiphase Flow, 28(7), 1205-1222
72. Lo, S., Tomasello, A. (2010). Recent progress in CFD modeling of multiphase flow in horizontal and near-horizontal pipes. In 7th North American Conference on Multiphase Technology. BHR Group.
73. Al-Yaari, M. A., Abu-Sharkh, B. F. (2011). CFD prediction of stratified oil-water flow in a horizontal pipe. Asian Transactions on Engineering, 1(5), 68-75.
74. Jia, N., Gourma, M., Thompson, C. P. (2011). Non-Newtonian mulita-phase flows: On drag reduction, pressure drop and liquid wall friction factor. Chemical engineering science, 66(20), 4742-4756.
75. Kroes, R. F., Henkes, R. A. W. M. (2014). CFD for the motion of elongated gas bubbles in viscous liquid. In 9th North American Conference on Multiphase Technology. BHR Group.

76. Qian, D., & Lawal, A. (2006). Numerical study on gas and liquid slugs for Taylor flow in a T-junction microchannel. *Chemical Engineering Science*, *61*(23), 7609-7625.

77. Rosengarten, G., Harvie, D. J. E., & Cooper-White, J. (2006). Contact angle effects on microdroplet deformation using CFD. *Applied Mathematical Modelling*, *30*(10), 1033-1042.

78. Akbar, M. K., & Ghiaasiaan, S. M. (2006). Simulation of Taylor flow in capillaries based on the volume-of-fluid technique. *Industrial & engineering chemistry research*, *45*(15), 5396-5403.

79. Bhatelia, T., Utikar, R., Pareek, V., & Tade, M. (2009). Hydrodynamics of slug flow in capillary microchannels. *University Journal of Engineering and Technology*, *1*, 1-9.

80. Chen, Y., Kulenovic, R., & Mertz, R. (2007, January). Numerical study on the formation of Taylor bubbles in capillary tubes. In *ASME 2007 5th International Conference on Nanochannels, Microchannels, and Minichannels* (pp. 939-946). American Society of Mechanical Engineers.

81. Zheng, D., He, X., & Che, D. (2007). CFD simulations of hydrodynamic characteristics in a gas-liquid vertical upward slug flow. *International Journal of Heat and Mass Transfer*, *50*(21-22), 4151-4165.

82. Santos, R. M., & Kawaji, M. (2010). Numerical modeling and experimental investigation of gas-liquid slug formation in a microchannel T-junction. International Journal of Multiphase Flow, 36(4), 314-323.

83. Klotz, James A., and William E. Brigham. "To determine Herschel-Bulkley coefficients." Journal of Petroleum Technology 50, no. 11 (1998): 80-81.

Chapter 2: Experimental and Numerical Analysis of the Effect of Rheological Models on Measurements of Shear-Thinning Fluid Flow in Smooth Pipes

Abdalsalam Ihmoudah [1, 2], Abdelsalam Abugharara [1, 3], Mohammad Azizur Rahman[4] and Stephen Butt[1]

[1]Memorial University of Newfoundland, St. Johns,

[2]Wadi Alshatti University, Alshatti, Libya

[3]Sebha University, Sebha, Libya

[4]Texas A&M University at Qatar

This chapter is based on the objectives defined in Section 1.5 and has been published in Energies 2023, 16, 3478. Section of Petroleum Engineering, https://doi.org/10.3390/en16083478.

Co-authorship Statement

Abdalsalam Ihmoudah is the first author of this manuscript, along with co-authors Dr. Abdelsalam Abugharara, Dr. Mohammad Azizur Rahman, and Dr. Stephen Butt. I proposed the idea and concept, conducted a literature review, and prepared the fluid samples with the assistance of Dr. Abugharara. I collected and analyzed the experimental data and numerical simulation. Dr. Aziz and Dr. Butt evaluated the methodology and reviewed the manuscript. I wrote the original manuscript, and Dr. Abugharara, Dr. Aziz, and Dr. Butt reviewed the manuscript and provided feedback.

Abstract

The aim of this research is to investigate the effects of rheological models of shear-thinning fluids and their estimated parameters on the predictions of laminar, transitional, and turbulent flow. The

investigation was carried out through experimental and computational fluid dynamics (CFD) studies in horizontal pipes (diameters of 19.1 mm and 76.2 mm). Six turbulent models using Reynolds averaged Navier–Stokes equations in CFD_ANSYS Fluent 19.0 were examined in a 3D simulation followed by comparison studies between numerical and experimental results. Regarding results of laminar regions in power-law rheology models, Metzner and Reed presented the best fit for the pressure loss and transitional velocity. For the turbulent region, correlations observed by Wilson and Thomas as well as Dodge and Matzner had good agreement with the experimental results. For Herschel–Bulkley fluids, pressure losses and transitional regions based on a yielded region were examined and compared to the experimental results and the modified Slatter Reynolds number, where the results provided good estimation. For both pipe diameters, the Slatter model was the best fit for pressure losses of Herschel–Bulkley fluids in the turbulent regime. Furthermore, when comparing k-omega and k-epsilon turbulence models to the power-law behaviour, numerical studies delivered the most accurate results with fluids that have a higher behaviour index. However, the error percentage significantly increased at a higher shear rate in the Herschel–Bulkley fluids with a greater yield stress effect. Moreover, the modified Herschel–Bulkley viscosity function by Papanastasiou was implemented in the current CFD study. This function was numerically stabilized, devoid of discontinuity at a low strain rate, and more effective in transitional regions.

Keywords: shear-thinning fluids; laminar flow; transitional velocities; turbulent flow; computational fluid dynamics (CFD)

2.1 Introduction

Non-Newtonian fluids flowing in pipelines can be found in a wide range of practical and industrial applications. Non-Newtonian flow behaviour in the laminar region, which is related to rheological

properties and pressure losses, could be predicted by integrating the constitutive rheological model. On the other hand, the prediction of pressure losses in turbulent flow remains one of the most theoretical and practical problems [1,2]. Most of the fluids used at drilling sites are categorized as having non-Newtonian behaviour with non-linear viscosity, which makes it difficult to predict turbulent pressure losses in pipes. The mismatch between the rheological models and the properties of drilling fluids can lead to serious issues during drilling operations, such as loss of well control, reduced carrying capacity, fluid losses, and stuck pipes [3]. Rheological parameters of non-Newtonian fluids can assist in providing a description of fluid models. Those relevant parameters include yield stress, consistency index, fluid behaviour index, and density as a volumetric parameter [4]. Such parameters are important for predicting frictional pressure loss; however, all these parameters could change in conditions of high and low pressure and temperature, which could have a direct effect on drilling fluid rheology via the fluid's shear stress and shear rate [5–9]. In designing pipelines and drilling mud circulation for non-Newtonian fluids, pressure drops and transient limitations are among the most important technical parameters that could influence pumping energy requirements. Pressure drops could occur due to internal fluid friction as well as friction between the fluid and the pipe wall. Literature shows that there is a lack of recent studies that report the effect of rheological properties of shear-thinning fluid, especially Herschel–Bulkley fluid, in real flow conditions on flow measurements in pipes. The power-law model has been widely applied to obtain relationships between flow rate and pressure drop at a low Reynolds number in various geometries, including expanding and elastic pipes [10,11]. Several recent studies investigated various hydrodynamic problems involving shear-thinning fluids at low Reynolds numbers and clearly demonstrated a limited range of applicability for power-law model [12,13].

The aim of this study is to experimentally and numerically investigate the effect of the choice of the rheological model on predicting pipe flow characteristics for a laminar, transitional, and turbulent flow. This study also evaluates the ability of computational fluid dynamics (CFD) in the turbulent model of ANSYS Fluent 19 to simulate non-Newtonian fluids with various rheological behaviours. The experimental data of this work were obtained for two shear-thinning rheological models (power-law and Herschel–Bulkley fluids) that were prepared and used in this study. Moreover, the performance of three tested materials, including carboxymethyl cellulose (CMC), bentonite, and Xanthan gum, were fitted to the laminar flow data and evaluated based on the nonlinear fits' root-mean square error (RMSE) [14,15].

2.2 Background and Theory

2.2.1 Rheological Models

There is no direct proportionality between shear stress and shear rate in non-Newtonian fluids. Therefore, in order to describe the rheological behaviour of non-Newtonian shear-thinning fluids, different flow models are used. Equations (2.1) and (2.2) present the power-law and the Herschel–Bulkley models used in this study [2,16].

2.2.2 The Power-Law Model

For a power-law fluid, a relationship between shear stress and shear rate is described in the form of the following:

$$\tau = k\dot{\gamma}^{n} \tag{2.1}$$

Where τ is the shear stress, k is the fluid's consistency coefficient, $\gamma^{\cdot}$ is the shear rate, and n is the flow behaviour index. If n > 1, the fluid exhibits shear-thickening properties, and if n < 1, the fluid shows shear-thinning behaviour.

2.2.3 Herschel–Bulkley Model

The Herschel–Bulkley model combines Bingham and power-law fluid properties as difinded in eq (2.2) . When n < 1, the Herschel–Bulkley model is considered as a shear-thinning fluid model [2,17–19].

$$\tau = \tau_y + k\gamma^{\cdot n} \qquad (\tau > \tau y) \tag{2.2}$$

where τ is the shear stress, k is the fluid consistency coefficient, $\gamma^{\cdot}$ is the shear rate, τ_y is the yield stress, and n is the flow behaviour index.

2.2.4 Laminar and Transitional Flow Models

The Rabinowitsch–Mooney relationship is derived for shear stress at the pipe's wall (τw) in relation to the liquid volumetric flow rate (Q/s). The volumetric flow rate and the shear stress are expressed in Equation (2.3) [2].

$$Q = \frac{\pi R^3}{\tau_w^3}\int_0^{\tau_w} \tau_{rz}^2 f(\tau_{rz}) d\tau_{rz} \tag{2.3}$$

Shear-thinning fluids can be formulated by integrating and substituting the rheological parameters in Equation (2.3) and then written in terms of 8V/D against τ_w as in Equations (2.4) and (2.5).

Power-law fluid:

$$\frac{8V}{D} = 4\left(\frac{\tau_w}{K}\right)^{\frac{1}{n}}\left(\frac{n}{3n+1}\right) \tag{2.4}$$

Herschel–Bulkley:

$$\frac{8V}{D} = \frac{4}{{\tau_w}^3}\left(\tau_w - \tau_y\right)^{(n+1)/n}\left(\frac{1}{K}\right)^{1/n}\left[\frac{n{\tau_w}^2}{n+1} - \frac{2n^2\tau_y(\tau_w-\tau_y)}{(n+1)(2n+1)} - \frac{2n^2(\tau_w-\tau_y)^2}{(n+1)(3n+1)}\right] \tag{2.5}$$

For non-Newtonian transition criteria analysis, the present work uses the approach of Metzner and Reed [20] as the power-law fluid method and Slatter [21] as the Herschel–Bulkley fluid approach. Details on these techniques are provided in the following sections.

Metzner and Reed [20] adapted the Reynolds number to correlate the non-Newtonian pipe flow for a time-independent power-law fluid. In their formulation, the Fanning friction factor was employed as a stability parameter. They proposed that non-Newtonian fluids occur at the limit of the laminar flow as the same Reynolds number of the Newtonian fluids in smooth pipes, which is R_{MR} = 2100 at f_N = 0.0076 [2], as in Equations (2.6) and (2.7).

$$\tau_w = K`\left(\frac{8V}{D}\right)^n \tag{2.6}$$

$$R_{MR} = \frac{8\rho v^2}{K`\left(\frac{8V}{D}\right)^n} \qquad K = K`\left(\frac{3n+1}{4n}\right)^n \tag{2.7}$$

The friction factor for the laminar flow was then determined by Metzner and Reed in the same approach as for the Newtonian fluids.

$$f = \frac{16}{R_{MR}} \tag{2.8}$$

2.2.5 Current Study Test Model

For the correlation of the laminar flow data, the generalized Reynolds number was developed in this study from the Reynolds number proposed by Slatter [21] by considering the effect of the pipe diameter and the effect of the apparent viscosity. In Herschel–Bulkley fluids, the velocity distribution is discrete into yielded and unyielded regions [2]. As illustrated in Figure 2-1, in the middle of the pipe ($0 \leq D/2 \leq Dp/2$), an unsheared plug-like core was flowing, where the m-agnitude of the shear stress was less than that of the yield stress. *Dp/2* is the radius of the plug region and depends upon the wall shear stress and the yield stress as follows:

$$D_P/2 = D/2\ \frac{\tau_y}{\tau_w} \tag{2.9}$$

where *Dp/2* is the radius of the plug region, *D* is the pipe diameter, τ_y is the yield stress, and τ_w is the wall shear stress obtained from the laminar flow using Equation (2.5).

In this study, the modified Reynolds number is based on the fluid density (ρ), the superficial velocity (v), the effect of the pipe diameter D_{eff}, and the effect of apparent viscosity (μ_{eff}) as in Equation (2.10) [2]

$$R_{eM} = \frac{\rho v D_{eff}}{\mu_{eff}} \tag{2.10}$$

where D_{eff} is the effect diameter of the pipe as expressed below:

$$D_{eff} = D - D_p \tag{2.11}$$

The effect of apparent viscosity is presented in Equation (2.12).

$$\mu_{eff} = \tau_y \left(\frac{8V}{D_{eff}}\right)^{-1} + K\left(\frac{8V}{D_{eff}}\right)^{n-1} \tag{2.12}$$

where τ_y is yield stress, D_{eff} is the effect diameter (which can be calculated form Equation (2.11)), K is the consistency coefficient, and n is the flow index.

The fact that when the shear stress is less than the yield stress, as in the unsheared core region, the material will behave as a solid is implicit in the definition of yield stress. Under laminar flow conditions, most models ignore the presence of the unsheared solid plug concentric alignment with the pipe axis due to the presence of yield stress [21]. The pressure drop values measured on the measuring section during flow are sufficient to determine the fluid's rheological properties, K [22].

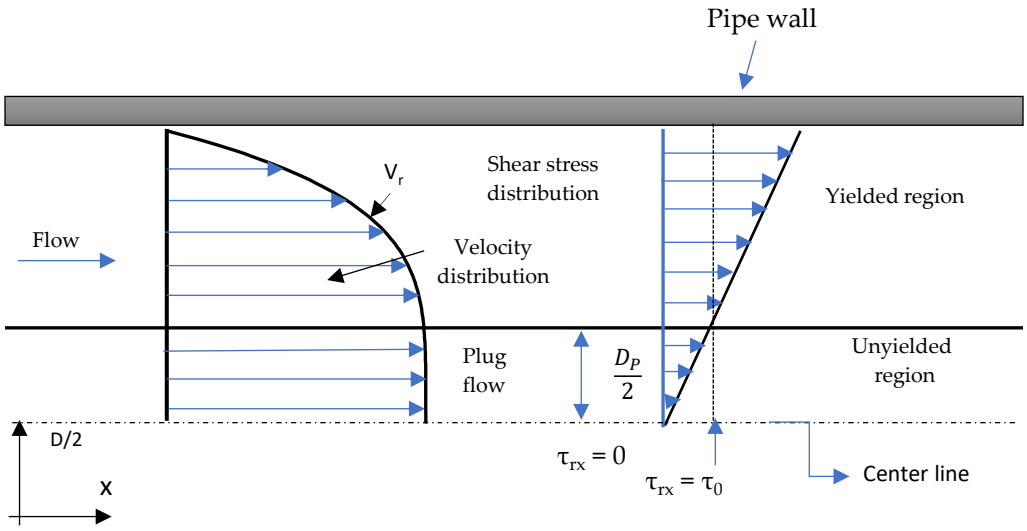

Figure 2-1.Velocity distribution in fully developed laminar flow for Herschel–Bulkley fluid in a circular pipe

Slatter [21] proposed a modified Reynolds number (Re_{ST}) that represented yield power-law-type fluid flow, with an emphasis on yield stress. In this formulation, the modified Reynolds number assumes that viscous and inertial forces can be calculated only by the material section undergoing shearing. Laminar flow was taken at $Re_{ST} = 2100$.

$$R_{eST} = \frac{8\rho {v_{ann}}^2}{\tau_y + K\left(\frac{8v_{ann}}{D_{shear}}\right)^n} \tag{2.13}$$

$$v_{ann} = \frac{Q - Q_{plug}}{\pi(R^2 - {R^2}_{plug})} \tag{2.14}$$

$$Q_{plug} = V_{plug} * \pi {D^2}_{plug} \tag{2.15}$$

$$V_{plug} = \frac{nR}{(n+1)}\left(\frac{\tau_y}{k}\right)^{\frac{1}{n}}(1 - \emptyset)^{(n+1)/n} \tag{2.16}$$

Where

$$\emptyset = \frac{D_{plug}}{D}\frac{\tau_0}{\tau_y} \tag{2.17}$$

$$D_{plug} = 2\, R_{Pulg} \tag{2.18}$$

$$D_{shear} = D - D_{plug} = 2(R^2 - {R^2}_{plug}) \tag{2.19}$$

In later work on Herschel–Bulkley fluid transition, Slatter [23] demonstrated the Re_{ST} as being highly reliable compared to other Reynolds numbers in predicting transitional velocity for different pipe sizes. In particULar, for small pipe diameters (D < 25 mm), Slatter [23] reported that every method agreed with the experimental data except the intersection approach reported by Hedström [24]. Vlasak and Chara [25] tested the prediction accuracy of the Slatter [21] model for kaolin slurry turbulent flow and had good results. The researchers discovered that the findings were very similar to those discovered by Wilson and Thomas [26].

2.2.6. Turbulent Flow Models

A number of different models have been developed for predicting the pressure gradient of shear-thinning turbulent pipe flow. The accuracy, applicability, and limitation of these correlations have been examined. Such correlations considered in this work were proposed by Dodge and Metzner [27], Torrance [28], Yoo [29], Wilson and Thomas [26], and Slatter [21].

Dodge and Metzner [27] devised a critical Reynolds number for their method by applying the friction factor of power-law fluids to a generalized Reynolds number. In so doing, they found that the values of the critical Reynolds number that were determined by their method were in agreement with those determined by Metzner and Reed [20].

$$\frac{1}{\sqrt{f}} = \frac{4.0}{n^{0.75}} log\left(R_{MR} f^{\left(1-\frac{n}{2}\right)}\right) - \frac{0.4}{n^{1.2}} \tag{2.20}$$

However, because the experimental results presented that the critical Reynolds number falls in the range of $2{,}900 \leq R_{MR} \leq 36{,}000$ and the flow behaviour index is in the range of $0.36 \leq n \leq 1$, these limits should not be exceeded when applying Equation (20) [30]. Moreover, based on experimental results of shear-thinning fluid, Equation (20) could also be applied to Herschel–Bulkley fluids, Casson fluids, and Bingham plastic if K0 and n0 are determined from the curve of the laminar τ_w vs. 8V/D at the turbulent flow for the value of τ_w [3,20].

Torrance [28] investigated the turbulent flow of Herschel–Bulkley fluid based on the pseudoplastic model reported by Clapp [31]. In his work, Torrance assumed that the transitional flow occurs at Re = 2100. When ignoring the effect of the yield stress, Torrance derived the mean velocity for turbulent flow in smooth pipes as follows:

$$R_{Torr} = \frac{8\rho v^2}{K\left(\frac{8V}{D}\right)^n} = R_{MR} \tag{2.21}$$

$$\frac{V}{U_*} = \frac{3.8}{n} + \frac{2.78}{n} \ln\left(1 - \frac{\tau_0}{\tau_w}\right) + \frac{2.78}{n} + \ln\left(\frac{{U_*}^{2-n} \rho R^n}{K}\right) - 4.17 \tag{2.22}$$

$$U_* = \sqrt{\tau_w}/\rho \tag{2.23}$$

On the other hand, El-Nahhas et al. [1] concluded that the Slatter [21] model that predicts the turbulent flow of Herschel–Bulkley fluid is better than the Torrance model [28], which ignores the impact of the yield stress.

Yoo's [29] experimental results for power-law fluid presented that the critical Reynolds number falls in the limits of $5000 \leq R_{MR} \leq 30{,}000$. These limits should not be exceeded when using Equation (2.24) [30].

$$f = 0.079n^{0.675}\left({R_{MR}}^{-0.25)}\right) \tag{2.24}$$

Wilson and Thomas [26], followed by Thomas and Wilson [32], proposed a turbulent flow model to predict non-Newtonian flow based on the velocity distribution using enhanced microscale viscosity effects. The model predicts that the wall's laminar sub-layer increases if the viscous sub-layer size increases by the area ratio factor (α*), as indicated in Equation (2.25).

$$\frac{V}{U_*} = \frac{V_N}{U_*} + 11.6(\alpha^* - 1) - 2.5\ln\alpha^* - \Omega \tag{2.25}$$

where U_* is the shear velocity given by Equation (2.23), and VN is the Newtonian mean velocity for smooth pipe flow as provided below:

$$V_N = U_*\left[2.5\ln\frac{\rho D}{\mu_e} + 1.75\right] \tag{2.26}$$

$$\Omega = 2.5\ln(1 - \frac{\tau_0}{\tau_w}) + 2.5\frac{\tau_0}{\tau_w}(1 - 0.5\frac{\tau_0}{\tau_w}) \tag{2.27}$$

For Herschel–Bulkley fluid, α^* is expressed as follows:

$$\alpha^* = 2(1 + \frac{\tau_0}{\tau_w}n)/(1 + n) \tag{2.28}$$

whereas for power-law fluid, α^* is expressed as follows:

$$\alpha^* = 2(\frac{1}{1+n}) \tag{2.29}$$

Generally, the ratio (α*) represents a combination of expected Newtonian rheogram and non-Newtonian areas occurring near a wall's shear stress. For each different rheological model (power-law and Herschel–Bulkley fluid), the (α*) first needs to be estimated in order to formulate the velocity distribution of a turbulent model.

Slatter [21] developed an approach for the turbulent flow of Herschel–Bulkley fluid. In his approach, Slatter emphasizes the effect of yield stress based on the effect of particle roughness combined with the Newtonian approach. He formulated a new roughness Reynolds (R_r) by considering the roughness caused by solid particles in smooth wall turbulent flow and fully developed rough-turbulent flow based on percentile passing of particle size (d_{85}) as expressed below:

If $R_r < 3.32$, then smooth wall turbulent flow exists, and the mean velocity is given by:

$$\mathrm{V} = U_*[2.5\ln(R/d_{85}) + 2.5\ln \mathrm{R}_r + 1.75\ ] \tag{2.30}$$

Where $$R_r = \frac{8\rho {v_*}^2}{\tau_y + K(8v_*/d_{85})^n} \tag{2.31}$$

If $R_r > 3.32$, then fully developed rough wall turbulent flow exists, and the mean velocity is given by:

$$\mathrm{V} = U_*[2.5\ln(R/d_{85}) + 4.75\ ] \tag{2.32}$$

In other experiments, Slatter et al. [33] used Equation (2.31) in Bingham plastic, Hershel–Bulkley fluids, and power-law fluids. These researchers found that the correlation was most applicable to Herschel–Bulkley rheology with an average error of only 18%. In contrast, the power-law model gave an average error of 35%, which was similar to that which resulted from the models of Torrance [28] and Wilson and Thomas [26]. The Bingham plastic fluid model gave errors of about 20%. To date, the Dodge and Metzner [27] correlations are widely applied and quoted in relation to non-Newtonian fluid (power-law fluid) technology (e.g., Skelland [34]; Steffe [35]; Van den Heever [36]; and Chabra and Richardson [2]).

2.3 Computational Fluid Dynamics (CFD) and Shear-Thinning Fluids

As computational resources are further developed, the analysis of certain industrial flows is increasingly being made by numerical computations using equations of Reynolds averaged Navier–Stokes (RANS). RANS models for shear-thinning fluids, on the other hand, have yet to gain traction in the CFD community as a result of the effect of non-linear viscosity [37–39]. The experimental facilities required to conduct these studies could be costly, whereas CFD allows for a wide range of configurations and superficial velocities. Researchers have recently proposed using a combination of turbulence models (i.e., zero, one, and two equations) for predicting homogenous flow. For instance, Stainsby and Chilton [40] developed a hybrid model suitable for application implementing Herschel–Bulkley fluids. In order to explain their observations, the authors combined a modified rheological model with the Launder–Sharma k-ε turbulence model, comparing predictions using high yield stress fluid measurement.

Several numerical studies on non-Newtonian fluid flows in pipelines have been conducted since the development of CFD to compare experimental results and theoretical modelling [41,42]. Most

of those studies were related to power-law fluids. In related work to find the apparent viscosity, Bartosik [43] and Bartosik et al. [44] combined a modified turbulence damping function in Launder and Sharma's k-ε turbulence model [45] with Wilson and Thomas's hypotheses, thus adapting them to the Bingham rheological model. In so doing, the researchers used the measurements to compare pressure drop predictions for different rheological parameters. The results showed good agreement between the measurements and predictions. Other studies investigated whether the experimental data matched the predicted velocity distribution, with the results confirming satisfactory prediction accuracy [46]. Cayeux and Leulseged [47] developed a general solution for modelling the viscous pressure loss in a pipe under a thixotropic rheological model, and they applied this generic solution to configurations where the diameters change. It was observed that the choice of rheological behaviour should be guided by the actual fluid response, especially in the turbulent flow regime. Recently, methods for estimating fluid rheological properties based on pressure loss measurements were developed by Magnon and Cayeux [48].

2.4 Experimental Work

Experimental data for this study were collected using two flow loops of diameters 19.1 and 76.2 mm in a laboratory at Memorial University of Newfoundland (MUN), Canada. The setup in which the experiments were carried out is depicted schematically in Figure 2-2. The large pipe flow loop (Figure 2a) was a clear PVC open-loop re-circulating pipe with a diameter of 0.0762 m and a total length of 65 m. The flow loop included a 3000 L (792.5 gallons) fluid reservoir and a variable-frequency controlled pump with a maximum flow rate of 450 gallons per minute (GPM). An Omega turbine flow meter with an accuracy of ± 1% of the full scale and a range of 3~450 GPM was used to measure the flow rate of working fluids. Three PX603-100G5V (0–100 Psi) Omega pressure transducers provided the pressure data in the test sections, and pressure taps positioned

2.5 m from each other were utilized. In the small pipe flow loop (Figure 2b), the working fluids were pumped from the tank through a PVC pipe with a diameter of 0.0191 m and a length of 22 m. Six pressure transducers (Omega PX603-100Q5V, with effective measures of 0–100 psi) were used to measure pressure losses in the test sections at different flow rates.

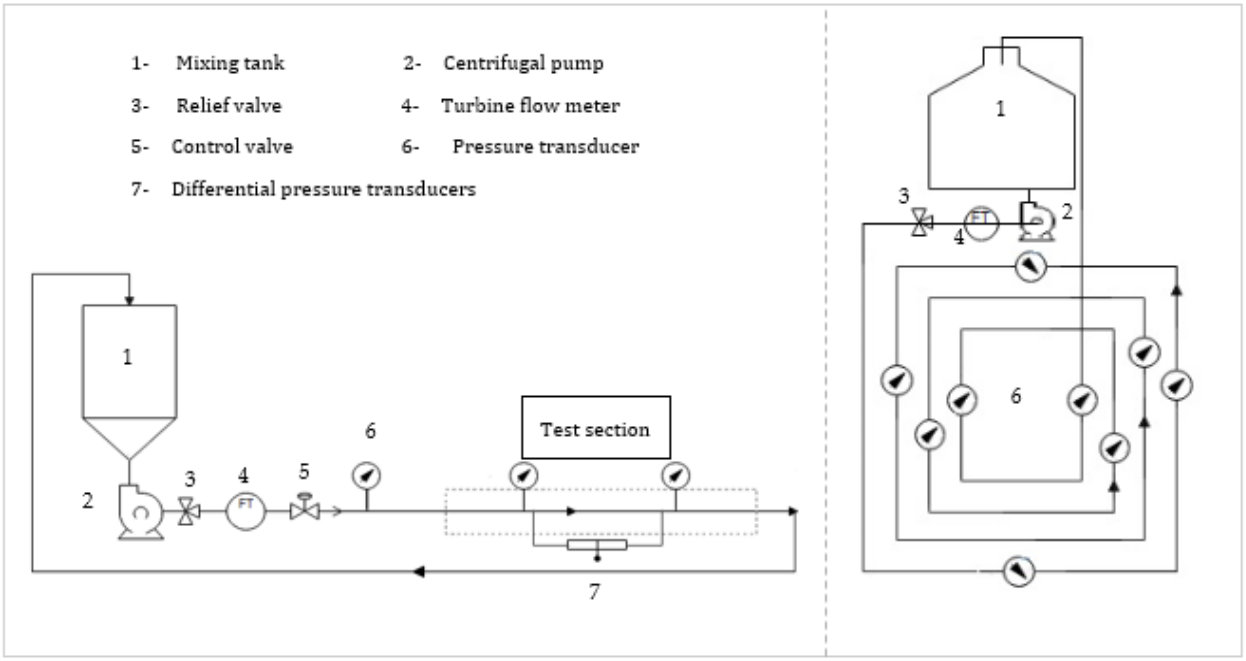

(a) (b)

Figure 2-2. Experimental setup components and flow loops system: (a) clear PVC open-loop re-circulating pipe with a diameter of 0.0762 m and a total length of 65 m. (b) PVC pipe with a diameter of 0.0191 m and a length of 22 m

2.4.1 Characterization of Test Fluids

To achieve the stated goals, six polymer-based fluids were prepared in the Drilling Technology Laboratory (DTL) at MUN and tested in this study. However, one case that was experimentally adopted by Slatter [21] was considered in this study with a higher yield shear effect for Herschel–Bulkley fluid and compared to the CFD-ANSYS study.

The base fluid for each of these fluids was water. The non-Newtonian fluids tested were shear-thinning fluids (power-law and Herschel–Bulkley fluids). The rheological measurements of the fluids were determined by using an 8-speed API-compliant rotational viscometer (Model 800) and mud balance scale three times during the experiment at the same circulation temperatures. The relationships between shear rates varied between 5.11 and 1022.04 s^{-1}, and shear stress was between 0 and 23 Pa, as shown in Figure 2-3. The parameters of the shear-thinning rheological fluids (n, K and τ_y) were obtained by fitting a -curve to the rheology (shear stress vs. shear rate graph) from the rotational viscometer data. We used an accurate method to determine the parameters of power-law fluid and three parameters of the Herschel–Bulkley fluid from 8-speed viscometer data following to procedure of Klotz and Brigham [14] and Kelessidis and Maglione [15]. The rheological parameters for each drilling fluid are listed in Section 4.8. When comparing different drilling fluids, the Herschel–Bulkley model with dimensionless shear rates is preferable to the traditional way of writing this model [49].

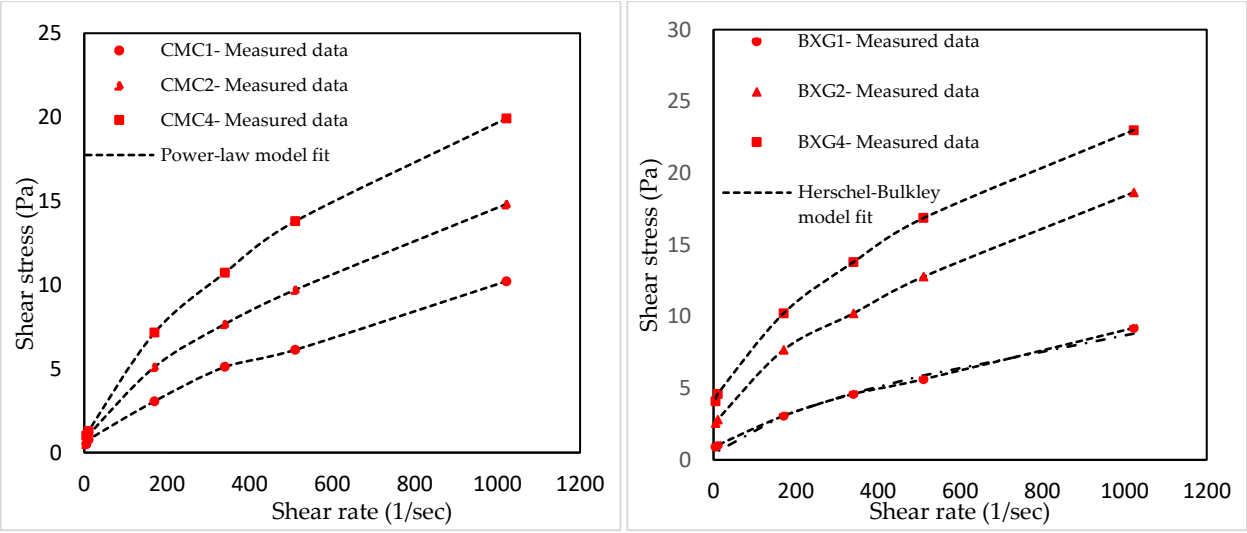

(a) (b)

Figure 2-3. Shear stress vs. shear rate curves for non-Newtonian models. (a) Rheological curves of power-law model fit. (b) Rheological curves of Herschel–Bulkley model fit.

2.5 Numerical Procedure

In this work, six turbulence models for Newtonian and non-Newtonian fluids in two pipe diameters of 19.1 mm and 76.2 mm were evaluated by comparing the wall shear stress τ_w obtained from CFD ANSYS Fluent 19.0 with our experimental results. Compute Canada ACENET supercomputers were used for all simulations to solve CFD ANSYS Fluent code. For single-phase models, the turbulence models of Reynolds averaged Navier–Stokes (RANS) can be expressed as follows [50].

2.5.1 Turbulence Modelling

The present study considered a turbulent regime since experimental critical velocity and modified Reynolds numbers for power-law and Herschel–Bulkley fluids are in the range of turbulent flow. Many models have been developed in CFD codes ANSYS Fluent 19 commercials, such as k-ε models, large eddy simulation (LES), and k-ω models. In this study k-ε and k-ω approaches were used, and the classification of Reynolds averaged Navier–Stokes (RANS) was selected to solve two transport equation models are shown below [50]:

k-ε Models

$$\frac{\partial}{\partial t}(\rho k) + \frac{\partial}{\partial x_i}(\rho k u_i) = \frac{\partial}{\partial x_i}\left[\mu_{eff}\alpha_k \frac{\partial k}{\partial x_j}\right] + G_k + G_b - \rho\varepsilon \tag{2.33}$$

$$\frac{\partial}{\partial t}(\rho \varepsilon) + \frac{\partial}{\partial x_i}(\rho \epsilon u_i) = \frac{\partial}{\partial x_i}\left[\mu_{eff}\alpha_{k\varepsilon} \frac{\partial k}{\partial x_j}\right] + G_\varepsilon + G_b + \frac{\varepsilon}{k}\left(c_{1\varepsilon}G_k + {}_{3\varepsilon}c_b\rho - \varepsilon c_{2\epsilon\rho}\right) \tag{2.34}$$

where k and ε represent turbulence kinetic energy, G_b and G_k are turbulent kinetic energy generated from buoyancy and mean velocity gradient, $c_{1\varepsilon}$, $c_{2\varepsilon}$, and $c_{3\varepsilon}$ are constants, and μ_{eff} is the effective viscosity.

k-ω Models,

The k and ω transport equation can be written as:

$$\frac{\partial}{\partial t}(\rho k) + \frac{\partial}{\partial x_i}(\rho k u_i) = \frac{\partial}{\partial x_i}\left[(\Gamma_k + \frac{\partial k}{\partial x_j}\right] + G_k - Y_k + S_K \tag{2.35}$$

$$\frac{\partial}{\partial t}(\rho\omega) + \frac{\partial}{\partial x_i}(\rho\omega u_i) = \frac{\partial}{\partial x_i}\left[(\Gamma_\omega \frac{\partial \omega}{\partial x_j}\right] + G_\varepsilon - Y_\omega + S_\varepsilon \quad (2.36)$$

Where

$$\Gamma_k = \mu_t + \frac{\mu_t}{\rho_k} \ , \Gamma_\omega = \mu_t + \frac{\mu_t}{\rho_\omega}$$

where ω is the specific dissipation rate, Γ_k and Γ_ω are the effective diffusivity of k and ω, S_ω is the source term, and Y_ω is the dissipation of ω.

2.5.2 Modified Herschel–Bulkley–Papanastasiou Viscosity Model

There is a singularity issue associated with the classical Herschel–Bulkley viscosity model at an evanescence shear rate, especially in translucent regions. To alleviate this, Papanastasiou [51] suggested using an exponential regularization for Equation (2-2) by involving a parameter that not only modulates exponential stress growth but also includes time dimensions. Figure 2-4 depicts the relationship of shear stress and shear rate using Papanastasiou's proposed model as well as the effect of the added exponent for Herschel–Bulkley BXG4 fluid. Papanastasiou's model was later adopted as the Herschel–Bulkley–Papanastasiou model.

$$\tau = K\dot{\gamma}^n + \tau_Y\,[1 - \exp(-\delta\dot{\gamma})] \quad (2.37)$$

The Papanastasiou-modified Herschel–Bulkley viscosity function is not available in general-purpose codes of ANSYS Fluent 19. A new viscosity function was implemented in the current CFD study. This modified viscosity function is numerically stabilized and devoid of discontinuity at a vanishing shear rate.

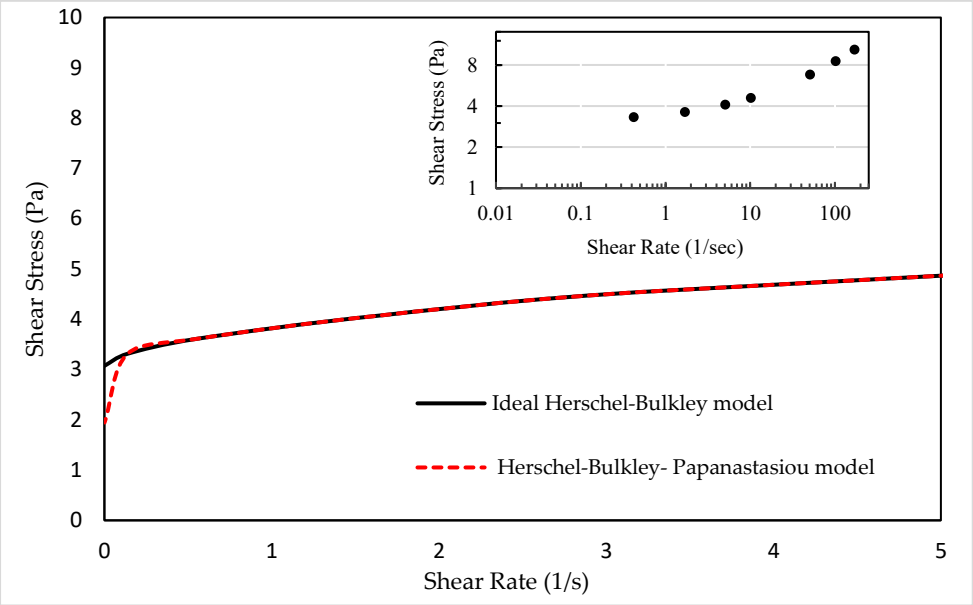

Figure 2-4. Shear stress vs. shear rate for BXG4 fluid according to the exponential model proposed by Papanastasiou [51].

2.5.3 Solver and Numerics

CFD ANSYS Fluent [34], which employs a finite-volume method, was used to solve the RANS Equations (2-33) and (2-35). A second-order upwind scheme was used to ensure numerical stability during spatial discretization. The SIMPLE scheme was used for pressure–velocity coupling, and the QUICK scheme was used to discretize momentum equations. These schemes were chosen because of their ability to solve momentum and mass conservation equations with reasonable stability and convergence. The RANS models, k-ε and k-ω, were used with the standard model constants, which can be further explored in the ANSYS Fluent 19 guide [50].

2.5.4 Mesh Size and Grid Study

Mesh size and quality play an important role in CFD studies. Due to the simple geometry of the pipe, a structured hexagonal mesh was used in this simulation. A mesh independence study was

performed for all geometric conditions to determine the best number of mesh sizes that gives an acceptable result within a given accuracy and minimum computer operating requirements.

As shown in Figure 2-5, a 3D computational grid for simulating fluid flow in two different diameters of horizontal pipes were generated and meshed using ICEM meshing techniques. The inlet for both pipes had a specified velocity and turbulence intensity, while the outlet had an outflow condition with mass flow balance. The walls of the pipes were modelled using the specified spear approach. The cells in the pipe wall increase in height towards the center. This pattern is commonly used with wall functions when simulating turbulent boundary layers [45,49]. Each grid follows the same pattern from the wall to half of the radius, after which the cells were more uniformly arranged into an O-grid. In order to avoid being within the fully laminar or turbulent regimes for the Newtonian standard wall function in the k-ε model, y^+ must be within the range of 30 to 300 [52]. To ascertain the grid convergence for non-Newtonian fluids, the height of the first grid point y+ was stabilized at 1.2 in the k-ω model as a correspondence to the increase in the Reynolds number. In the k-ε model with scalable wall functions, the first grid height was $y^+ \geq 11.3$ and placed gradually further from the wall as the Reynolds number value increased.

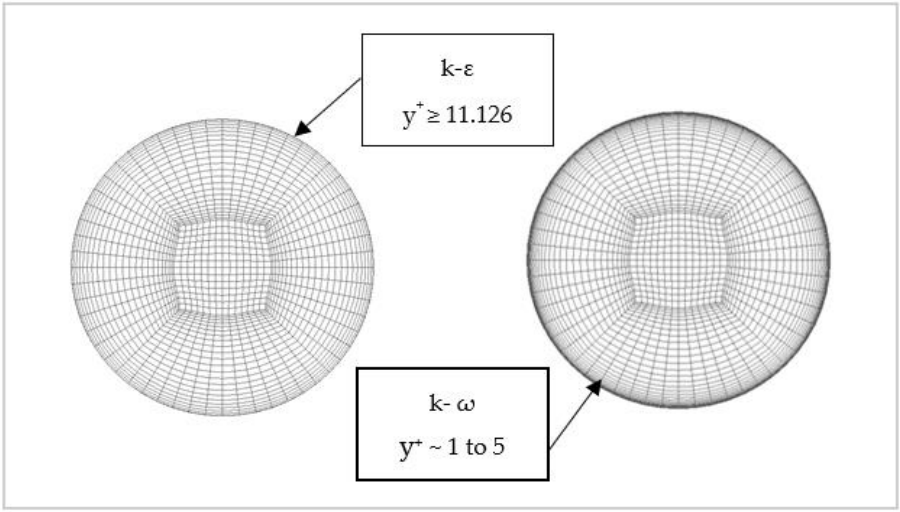

Figure 2-5. The grid structure in the computational domain.

Table 2-1. Mesh properties.

Statistics		Newtonian system		Newtonian system	
	Pipe diameter	k-ε models	k- ω models	k-ε models	k- ω models
Number of elements	76.2 mm	2,680,564	3,206,386	3,826,891	4,874,284
	19.1 mm	1,763,592	2,153,491	2,617,330	2,771,148
Average orthogonality	76.2 mm	0.9912	0.9953	0.9959	0.9975
	19.1 mm	0.9923	0.9966	0.9971	0.9985
Average skewness	76.2 mm	0.0806	0.0585	0.0261	0.0154
	19.1 mm	0.0641	0.0511	0.0193	0.0106

The grid independence analysis for Newtonian and non-Newtonian geometric conditions are shown in Figure 2-6. Water and shear-thinning fluid (BXG4) with a velocity of 2.205 m/s was used to check the grid study for the horizontal pipe, and the corresponding pressure drop was estimated. Only two cases were plotted for illustration, and they are shown in Figure 2-6. The approximate number of elements for a Newtonian and non-Newtonian system (power-law and Herschel–Bulkley fluids) that are required to free the simulation from mesh size dependency are reported in Table 2-1. A high orthogonal quality and low skewness ensured a decent mesh quality. The residual convergence criteria were set at 10^{-5} for continuity and 10^{-4} for other residuals. Compute Canada supercomputer servers (Graham and Cedar) were used for all simulations.

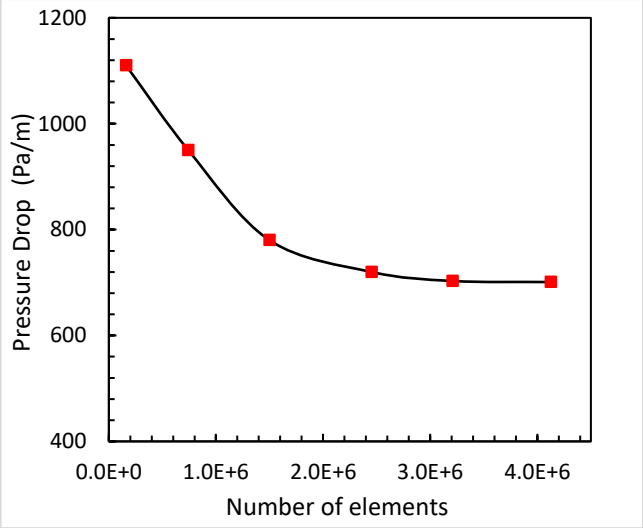

(a)

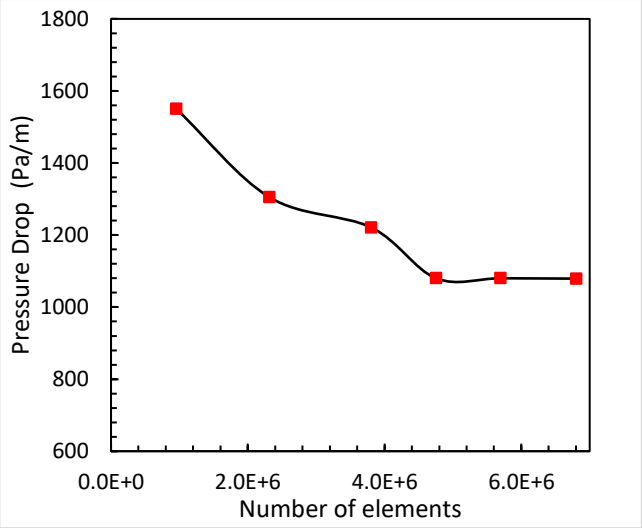

(b)

Figure 2-6. Grid independence study for Newtonian and shear-thinning fluids. (a) Water in pipe diameter 76.2 mm for k-ω models. (b) BXG4 (Herschel–Bulkley fluid) in pipe diameter 76.2 mm for k-ω models.

2.6. Error Calculation

In order to compare predicted data E_{pred} or CFD numerical results with experimental data E_{exp}, the commonly used mean absolute relative error was implemented based on the literature recommendations [53–56] as follows:

$$\text{MARE } \% = \frac{1}{n}\sum_{i=1}^{n}|x_i| \tag{2-38}$$

$$\text{Where} \qquad x_i = \left[\frac{E_{Pred} - E_{exp}}{E_{exp}}\right] \times 100 \tag{2-39}$$

E_{Pred} is predicted data or CFD numerical data, E_{exp} is experiment data, and n is the number of data points. A smaller value of MARE % indicates a better model.

2.7 Results and Discussion

2.7.1 Rheological Parameter Estimation

The results of the laminar flow and the rheological model fits are shown in Figure 2-3. The laminar data were experimentally determined using an 8-speed API-compliant rotational viscometer (Model 800) for all types of working fluids. The samples were collected from the flow loop after 25 min of circulation. The stability of the rheological model was verified three times during each experiment. The values of the rheological parameters were achieved by the coefficient of determination R^2 for each tested fluid. Each fluid was described by fitting its rheological models to the experimental laminar data.

By ranking them according to the coefficient of determination, R^2 values indicated that the power-law and Herschel–Bulkley rheological models gave the best fits to the CMC, bentonite, and xanthan gum mixture. Table 2-2 shows the laminar data. FBXG1 and CMC1 are the same fluids, but they differ in ranking prediction. When the temperature of the fluid is 20 °C, the rheological model predicted by power-law was $R^2 \sim 0.985$, and the model predicted for Herschel–Bulkley was ($R^2 \sim 0.991$). The power-law model was fitted to FBXG1 fluid to study the influence of the selected rheological model on the predicted pressure loss.

Table 2-2. The curve-fitted parameters for shear-thinning fluid models are based on the rotational viscometer (Model 800), and KERS09 fluid came from experimental work provided by Slatter [21].

Symbol	Compositions (gr/350ml)			ρ (kg/m3)	Rheological parameters				
	Bentonite	Xanthan gum	CMC		n	K (Pa.sn)	τ_y (Pa)	R^2 (YPL model)	R^2 (PL model)
BXG1	5.5	2	0	1010	0.74	0.0512	0.76	0.991	-
BXG2	5.5	3	0	1015	0.61	0.241	1.92	0.992	-
BXG4	5.5	4	0	1025	0.56	0.415	3.06	0.999	-
CMC1	-	-	2	1000	0.72	0.0601	0	-	0.992
CMC2	-	-	3	1002	0.60	0.233	0	-	0.994
CMC4	-	-	4	1005	0.57	0.405	0	-	0.999
FBXG1	5.5	2	0	1010	0.53	0.221	0	-	0.985
KERS09	Kaolin			1131	0.838	0.0162	10.7	Slatter [21] *	

2.7.2 Laminar Flow

Figure 2-7 presents the experimental data of Herschel–Bulkley fluids in laminar flow. Figure 2-7a shows collated data in a log–log scale where the fluid viscosity obtained from the viscometer readings was depicted by the black solid curve. The dashed line represents the viscosity values calculated by the modified Equation (2-12) while disregarding the flow regime (laminar flow was assumed).

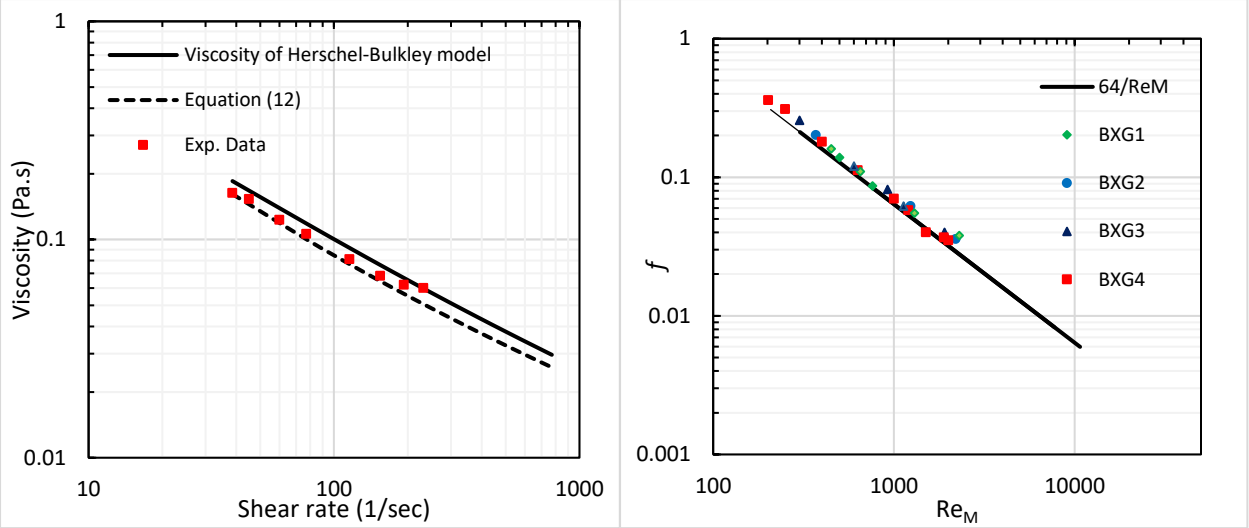

(a) (b)

Figure 2-7. Comparison of the predicted and experimental data for Herschel–Bulkley fluids in pipe diameter 76.2 mm. (a) Estimated and experimental viscosity vs. Herschel–Bulkley viscosity for polymer solutions BXG4. (b) Laminar data of Herschel–Bulkley fluids (BXG1)

The modified equation provided a reasonable estimation of fluid viscosity for the laminar regions that matches the experimental results based on the Herschel–Bulkley rheological model. Additionally, it was noted that the calculated viscosity matched the modified laminar Herschel–Bulkley viscosity model until a certain point where a mismatch became apparent at transitional and turbulent flow regimes.

Figure 2-7b illustrates the laminar flow experimental data for four Herschel–Bulkley fluids (BXG1, BXG2, BXG3, and BXG4), which showed better values for the high yield effect in terms of error percentage than that of the calculated results.

2.7.3 Transitional Velocity Predictions

Critical velocity V_c or transitional velocity predictions were made for the Metzner and Reed method [20], the method with a modified Reynolds number by Slatter [21], and our modified

method. These predictions were compared to the experimental critical velocity for each rheological model to evaluate the effect of changing the rheological parameters, to validate our improved method, and to evaluate the transitional velocity of Herschel–Bulkley fluids. The average percentage error of prediction models was compared to the experimental results. The experimental critical velocities versus the prediction for CMC1; high-concentration CMC4 for the power-law model; and BXG1, BXG2, and BXG4 for the Herschel–Bulkley model are shown in Table 2-3. The Metzner and Reed [20] method was found to be in good agreement with the experimental results when using power-law fluids, with an overpredicting of critical velocity by an average error of 6.4% in both diameters. The average error was found to decrease with an increased concentration of CMC by 4.6%. Slatter [21] predicted the transitional velocity of Herschel–Bulkley fluids to be most accurate when the effect of yield stress is small with an average under prediction of 5.1%. At higher yield stress fluid, errors increased by 7.6%. The developed method that considered the effective inner diameter of the pipe and yield region of Herschel–Bulkley fluid was compared to the experimental data. This model gives an average overprediction of the transitional velocity of 5.5% at minor effect yield stress. Using BXG4 fluid with high dominated yield stress resulted in an average of 6.1%. This model provides a reasonable estimate of fluid viscosity up to transitional regions and matches the calculation of the Herschel–Bulkley fluid exceptionally well.

2.7.4 Turbulent Flow Predictions

The experimental results from each pipe were compared to the turbulent prediction models of Slatter [21], Wilson and Thomas [26], and Dodge and Metzner [27] and presented on plots of shear stress τ_w against 8V/D in both laminar and turbulent conditions. The average absolute error was used to estimate and rank turbulent flow predictions to the experimental values.

Table 2-3. Transitional velocity model evaluation.

Diameter (mm)	Power law fluids - Metzner and Reed				Herschel-Bulkley fluids - Slatter					
	Exp. Critical velocity (m/s)	CMC1	Exp. Critical velocity (m/s)	CMC4	Exp. Critical velocity (m/s)	BXG1	Exp. Critical velocity (m/s)	BXG2	Exp. Critical velocity (m/s)	BXG4
19.1 mm	1.19	1.21 7.5%	2.15	2.28 6.1%	1.04	0.96 -5.7%	1.65	1.55 -7.8%	*2.22*	2.03 -8.5%
76.2 mm	0.56	0.59 5.3%	1.24	1.28 3.2%	0.7	0.67 -4.2%	1.01	0.96 -5.2%	1.63	1.52 -6.7%
Average		6.4%		4.6%		-5.1%		-6.5%		-7.6%
Developed model results										
19.1 mm					1.04	1.11 6.7%	1.65	1.74 5.4%	2.22	2.42 7.2%
76.2 mm					0.7	0.73 4.2%	1.01	1.04 2.4%	1.63	1.71 4.9%
Average						5.5%		4.2%		6.1%

The experimental results and prediction models in Ø19.1 and Ø76.2 mm diameters for power-law FBXG1 and Herschel–Bulkley fluid BXG1 are shown in Figure 2-8. Using the power-law model for FBXG1, the Dodge and Metzner [23] method gave accurate predictions for a small diameter with an average error of 2.6%. For a large diameter, it gave an underprediction by a mean absolute relative error of 2.5% (Figure 2-8a). With an increase in pipe diameter, the mean absolute relative

error increased by 3.32%. However, the Wilson and Thomas [22] method gave overpredicted turbulent experimental data with a mean absolute relative error of 4.15% in a small diameter. It gave an underprediction at a 76.2 mm diameter by a mean absolute relative error of 5.86% when choosing power-law behaviour for FBXG1 fluid (Figure 2-8b). The experimental turbulent flow data points were compared to the theoretical prediction made by Slatter's [21] model when choosing Herschel–Bulkley behaviour for BXG1 fluid. The evaluated turbulent flow model gave an overprediction in the small loop with a mean absolute relative error of 7.7%, and it was an underestimate of experimental results with a mean absolute relative error of 2.9% in a 76.2 mm diameter flow loop. The Slatter model considered his adoptive concept of the affected boundary layer from particle roughness in a turbulent model. The choice of rheological model has a minimal effect on the estimation of pressure gradients when the fluid has the same rheological curve and low dominated yield stress.

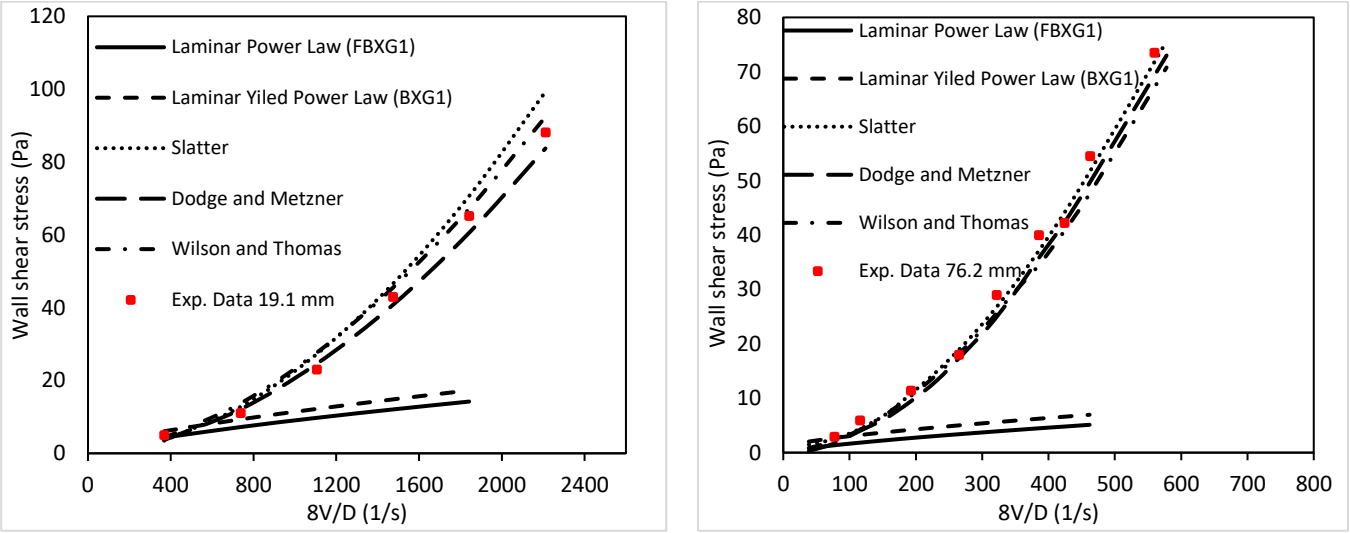

(**a**) (**b**)

Figure 2 8. Comparison between predictions and experimental data of turbulent flow for low-concentrated FBXG1, BXG1 power-law fluids, and BXG1 Herschel–Bulkley fluids: (a) pipe diameter 19.1 mm, (b) pipe diameter 76.2 mm.

Figure 2-9 shows the experimental results and the predicted flow for the CMC4 power-law fluid. The Wilson and Thomas [26] method generated acceptable accuracy results for both small and large pipe sizes by a mean absolute relative error of 6.3% and 4.4%, respectively, especially for the high shear stress range. Dodge and Metzner [27] issued similar predictions for this fluid when using either small or large pipe diameters with a mean absolute relative error of 5.7–3.8% each across two pipe sizes, mainly at lower shear stress ranges. Estimations were also conducted by Yoo [29] on the correlation of turbulent flow for power-law fluids. Results obtained by Yoo in both diameters showed underprediction in terms of mean absolute relative error by 12 and 14%, respectively, which matched the shape of the experimental data at a lower shear stress range. Yoo's model was unsuccessful in predicting, and it exhibited the greatest variability and deviation from the experimental results. Binxin Wu [57] made similar observations.

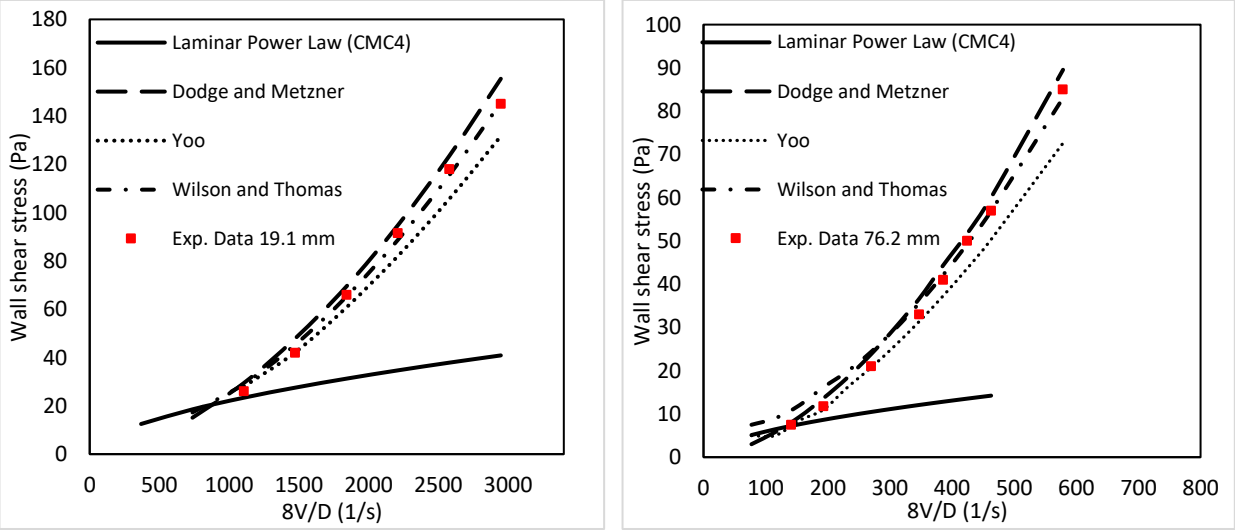

(a) (b)

Figure 2-9. Comparison between predictions and experimental data of turbulent flow for high-concentrated CMC4 power-law fluid: (a) pipe diameter 19.1 mm, (b) pipe diameter 76.2 mm.

The theoretical predictions were compared to the experimental results of turbulent flow behaviour for Herschel–Bulkley fluids in Figures 2-10 and 2-11 with two different rheology parameters in small and large pipe flow loops. When using the Herschel–Bulkley model, flow results for the BXG2 fluid are shown in Figure 2-10 for a pipe diameter of 19.1 mm (a) and a pipe diameter of 76.2 mm (b). Within the low effect of yield shear, the Slatter [21] method provided good estimates, while the accuracy increased with the increase in pipe diameter with a mean absolute relative error of 8.8% in Figure 2-10a and of 5.1% in Figure 2-10b.

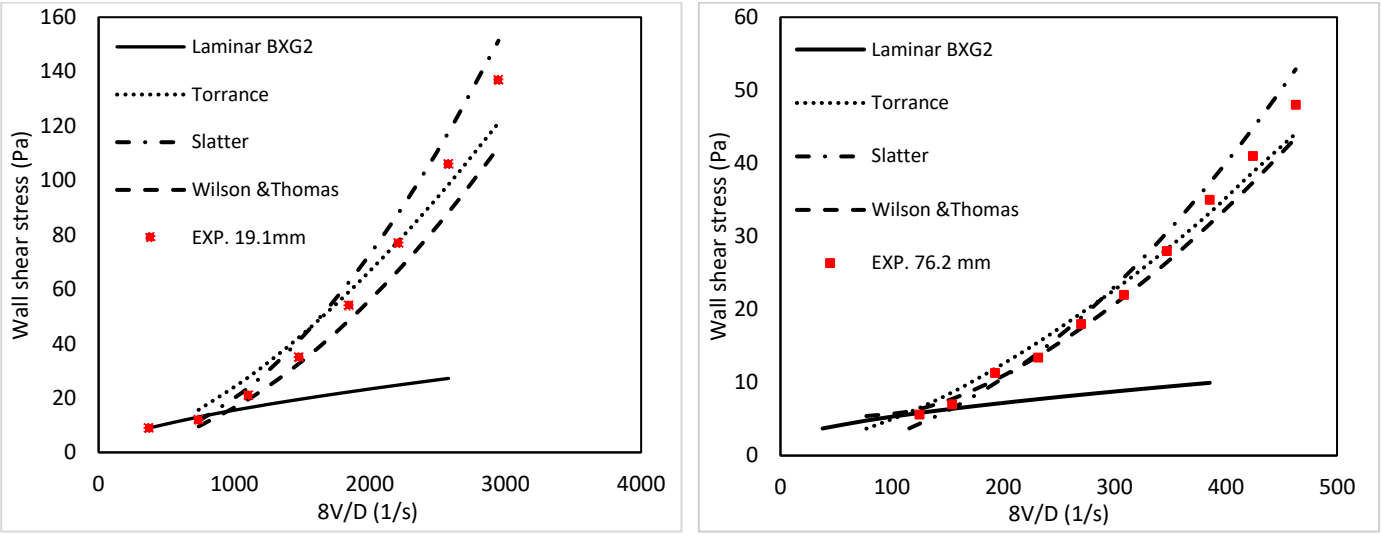

(a) (b)

Figure 2-10. Comparison between predictions and experimental data of turbulent flow for BXG2 Herschel–Bulkley fluids: (a) pipe diameter 19.1 mm, (b) pipe diameter 76.2 mm.

The Wilson and Thomas [26] method gave underpredictions in both diameters: Ø19.1 mm and Ø76.2 mm. The error decreased as the pipe diameter increased, which followed the shape of the experimental data at a lower shear stress range with a mean absolute relative error of 11.2 and 8.7%, respectively, when using the Herschel–Bulkley model. The Torrance [28] method overpredicted at low turbulent shear stress for both small and larger pipe diameters, while it

underpredicted at high effects of shear stress, and errors varied from 10.7% in a small diameter pipe to 8.6% in a large diameter pipe.

Regarding increased rheological parameters and the higher presence of yield stress, high-concentrated BXG4 experimental results and predictions are shown in Figure 2-11. The Wilson and Thomas [26] method resulted in an average underprediction of 8.9% in a small diameter pipe, which decreased as diameter increased with a mean absolute error of 7.3%.

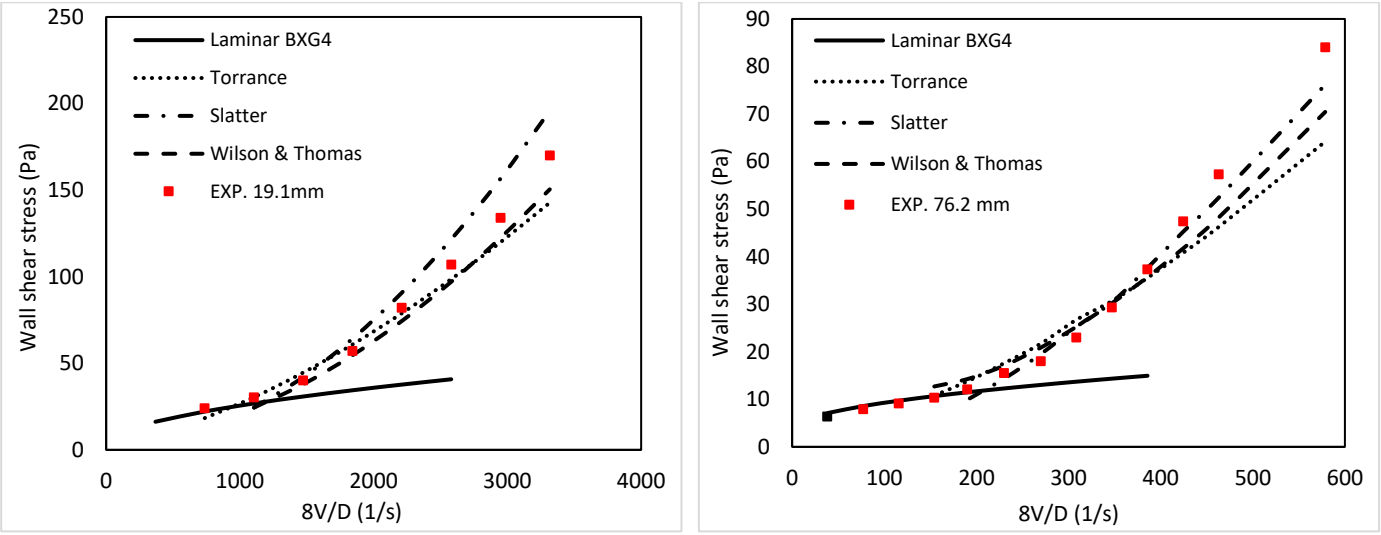

(a) (b)

Figure 2-11. Comparison between predicted and experimental data of turbulent flow for BXG4 Herschel–Bulkley fluids: (a) pipe diameter 19.1 mm, (b) pipe diameter 76.2 mm.

The Torrance [28] model gave overpredicted experimental turbulent data at low shear stress and an underprediction at high shear with an average mean absolute relative error of 11.1% in the small diameter pipe. In contrast, the average error increased in a 76.2 mm diameter pipe by a mean absolute relative error of 13.5% due to the neglect of the effective yield shear rate. As shown in Figure 2-11, the Slatter [21] method generated acceptable accuracy results for both pipe sizes. This approach gave an overestimate in the small loop with a mean absolute relative error of 10.1% and

an overestimate in the experimental results with a mean absolute relative error of 4.9% in a 76.2 mm diameter pipe.

2.7.5 Investigation of ANSYS Fluent Turbulence Models

The aim of this numerical study based on varying flow conditions was to assess the ability of CFD ANSYS Fluent in a turbulent model to simulate shear-thinning fluids, especially Herschel–Bulkley fluids, with the effect of yield stress. It also aimed to determine the effect of the selected rheological model on transport process efficiency by comparing the experimental pressure gradient to the CFD results.

2.7.6 Validation of Simulation Model

Calibration tests with water were performed prior to the beginning of shear-thinning fluid procedures to evaluate pressure loss. The experimental results were then compared to CFD ANSYS Fluent to assess the ability of those models to simulate Newtonian fluid (water) flows in two horizontal pipe sizes with a different wall function approach.

Two horizontal pipes of diameters 19.1 mm and 76.2 mm and a length of 8 m were used to examine six turbulence models for solving two transport equations that include three k-ε models (standard, RNG, and realizable k-ε) and three k-ω models (standard, BSL, and SST k-ω). A fine mesh was used to achieve mesh resolution near the pipe wall. Scalable wall functions were set for the k-ε models with y+ > 11.225 and y+ ~ 1 to 5 for the k-ω models to be able to resolve the viscous sublayer and buffer layer.

Table 2-4 shows ΔP_{CFD} and the error indicator δ at two flow rates of water in a pipe with a diameter of 19.1 mm and two flow rates in a pipe with a diameter of 76.2 mm compared to our experimental

results. In comparison to the collected experimental data, the CFD model replicated with good agreement, resulting in errors that varied from 2.2% to 9.3% and were larger for the small-diameter pipe. For turbulent Newtonian fluids, most of the RANS models coupled with the wall function approach successfully evaluated the pressure drop.

Table 2-4. Comparison between experimental results and CFD-predicted pressure gradient.

		Large-Diameter Pipe				Small-Diameter Pipe			
		Q = 100 L/min		**Q = 1000 L/min**		**Q = 15 L/min**		**Q = 60 L/min**	
		ΔP_{CFD} (Pa/m)	**δ (%)**	**ΔP_{CFD} (Pa/m)**	**δ (%)**	**ΔP_{CFD} (Pa/m)**	**δ (%)**	**ΔP_{CFD} (Pa/m)**	**δ (%)**
k–ε	Standard	21.7	3.1	1349.2	3.7	520.4	−5.2	6152.9	−3.1
	RNG	21.8	3.3	1381.0	6.1	519.1	−5.4	6151.5	−3.2
	Realizable	20.6	-2.6	1384.0	6.4	497.5	−9.4	5936.6	−6.5
k–ω	Standard	22.1	4.8	1369.0	5.2	591.7	7.7	6752.2	6.3
	BSL	22.3	5.5	1396.0	7.3	600.2	9.3	6763.6	6.5
	SST	21.6	2.2	1335.0	2.6	570.4	3.9	6498.5	2.3

2.7.7 Evaluation of Turbulence Models for Shear-Thinning Fluids

CFD ANSYS Fluent simulations were performed in a steady-state regime. A second-order upwind approach was applied to maintain numerical stability. The RANS models k–ε and k–ω were used with the standard model constants. More details are given in [51].

The comparison between the experimentally measured pressure gradient and the numerically predicted pressure gradient by CFD for power-law fluids (FBXG1 and CMC1) in different flow conditions are presented in Figure 2-12a for Ø19.1 mm and Figure 2-12b for Ø76.2 mm. Overall, this comparison demonstrated that all models could predict the pressure gradient in pipelines accurately at a low effect of viscosity. Both k-ω and k-ε gave high-precision underestimations by 5.8% to overestimations by 6.6% with an error margin of 15%, where all the measured points were within the indicated margin.

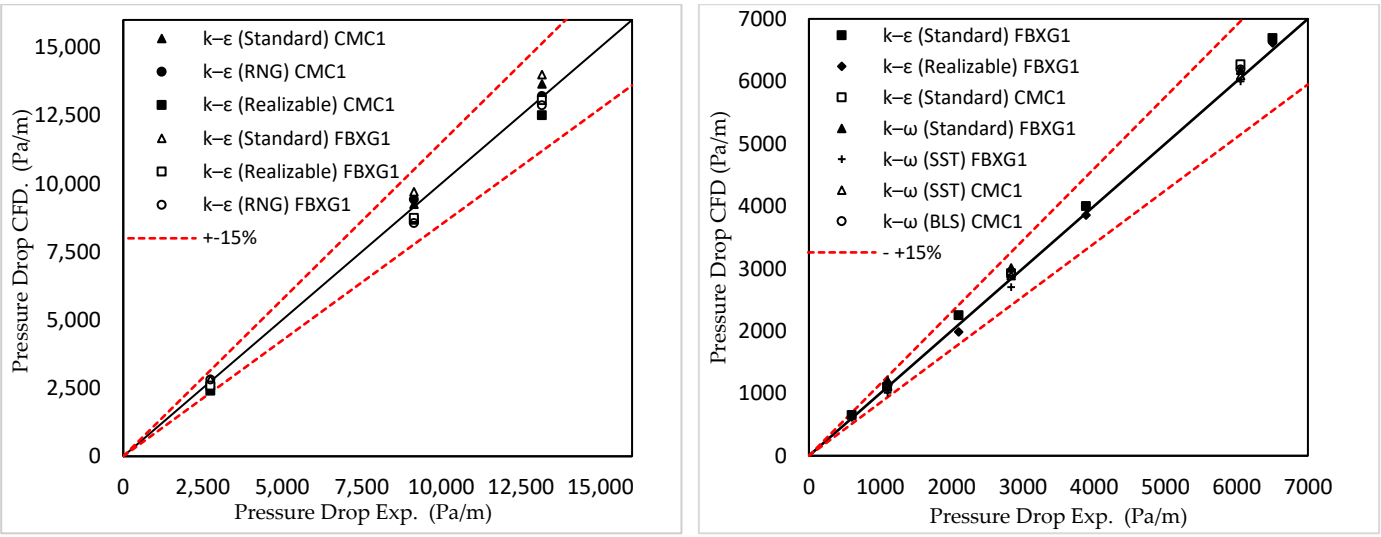

(a) (b)

Figure 2-12. Comparison of frictional pressure drop obtained from CFD model vs. experimental data. (a) FBXG1 and CMC1 power-law fluids pipe diameter 19.1 mm. (b) FBXG1 and CMC1 power-law fluids pipe diameter 76.2 mm.

As a response to increasing CMC concentration, n decreased, and k (rheological parameters) and viscosity of shear-thinning fluids increased. The experimental results and results from CFD predictions for power-law CMC4 fluid are shown in Figure 2-13. The comparison of CFD models showed that the k-ω and k-ε models were consistently overestimated in the small diameter (Figure 2-13a). The comparison also showed that the k-ω models had better results and standard deviation than the k-ε models. Furthermore, all models predicted the experimental results of CMC4 fluid with an error margin of less than 15%. The majority of data points were above 6.2% error, and the mean absolute error was determined at 6.9% to 13.5% for all models.

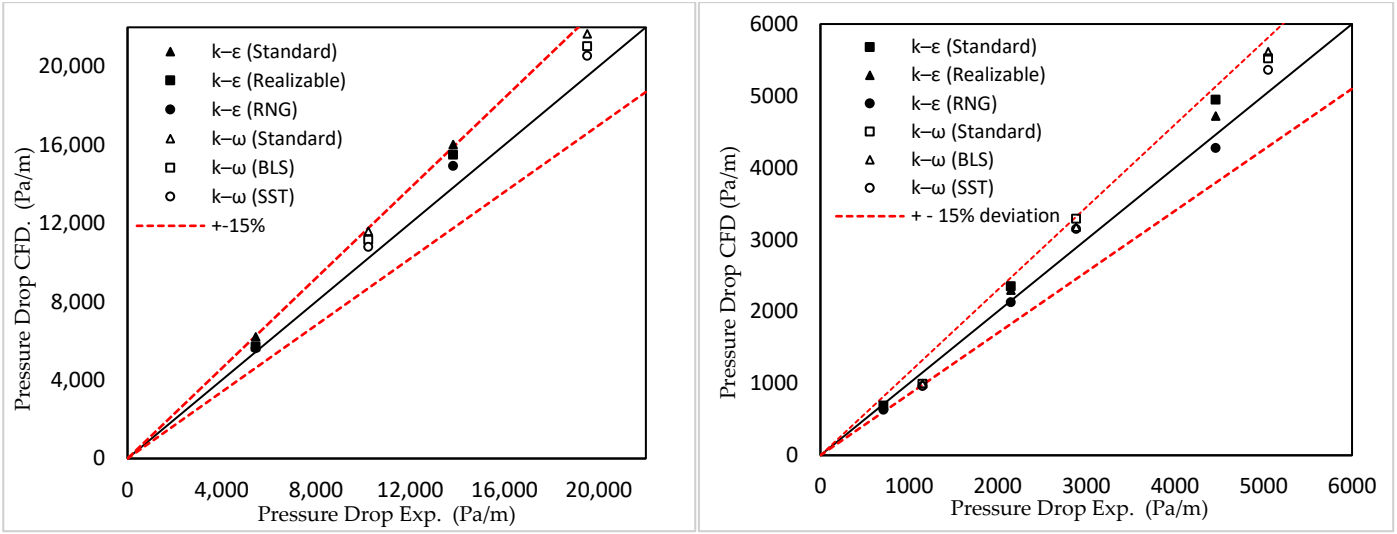

(a) (b)

Figure 2-13. Comparison of frictional pressure drops obtained from CFD model vs. experimental data. (a) CMC4 power-law fluid pipe diameter 19.1 mm. (b) CMC4 power-law fluids pipe diameter 76.2 mm.

To investigate the effects of different yield stress values, simulations of shear-thinning Herschel–Bulkley fluids through two different pipe sizes were performed and presented in Figure 2-14. The Herschel–Bulkley fluid (BXG2) with a low effect of yield stress (1.92 Pa) in a pipe diameter of 19.1 mm is shown in Figure 2-14a, and BXG4 with a mild impact of yield stress (3.06 Pa) in a pipe diameter of 76.2 mm is shown in Figure 2-14b.

The comparison showed overprediction of the CFD results in Figure 14a for all k-ω models and k-ε models, especially at high flow rates. The k-ε renormalization group (RNG) and SST k-ω gave a better average absolute relative error than other models by 18.3% and 16.1%, respectively.

Figure 2-14b shows results for decreasing n, increasing k, and greater presence of yield stress (rheological parameters) of the highly concentrated BXG4 fluid CFD model compared with the experimental data. In comparison with three k-ω and three k-ε models, when the concentration and the pipe diameter increased, the mean absolute relative error increased. The k–ε (standard) gave an average absolute relative error of 25.1%, while k–ε (realizable) and k–ε (RNG) were overpredicted by 33.2% and 38.3%, respectively. The standard k-ε turbulence model did not count the drag reduction impact and could deliver unsatisfactory results and predictions in near-wall zones, where viscosity changed rapidly with distance from the pipe wall [58,59]. The k–ω (standard) and k–ω (BLS) were also overrated by 27.2% and 26.3%, respectively. The SST k-ω model had a low average absolute relative error of 20.1% when using BXG4 fluid. When compared to other models, the SST k-ω model performed better in the near-wall region. Such performance was important to consider, as shown in the next section.

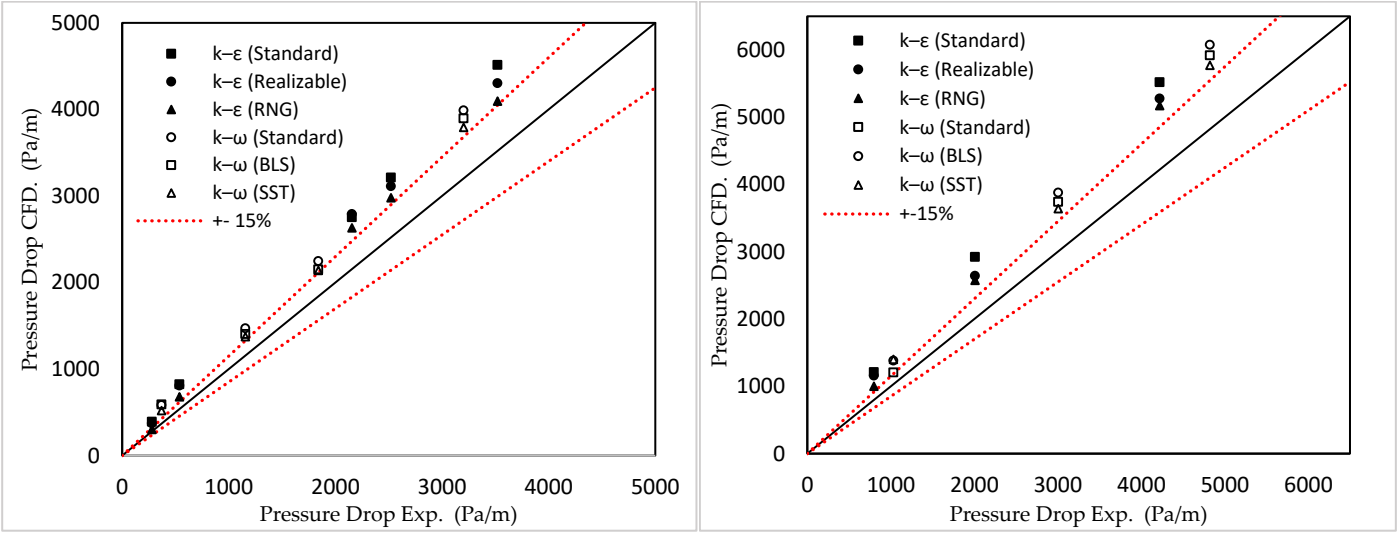

(a) (b)

Figure 2-14. Comparison of frictional pressure drop obtained from CFD model vs. experimental data for Herschel–Bulkley fluids. (a) BXG2 fluid in pipe diameter 19.1 mm. (b) BXG4 fluid in pipe diameter 76.2 mm.

2.7.8 Modified Viscosity Model

To show the obtained differences between the numerical predictions using the modified Papanastasiou [51] model and the standard Herschel–Bulkley viscosity model, the results obtained in two cases are shown in Figure 15.

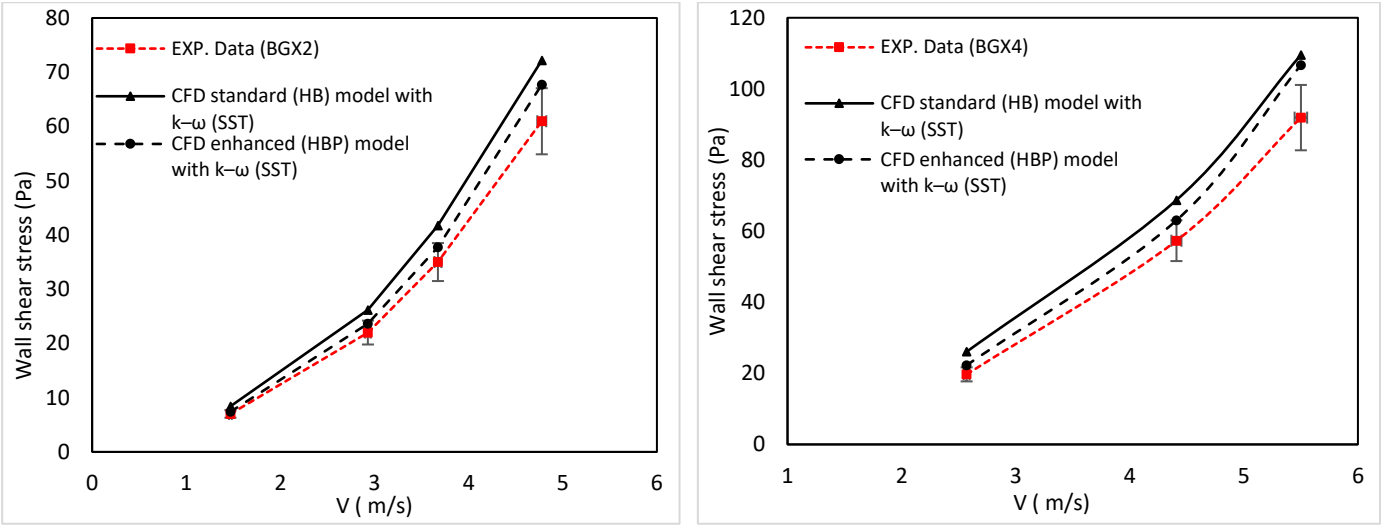

(a) (b)

Figure 2-15. Comparison of pressure drop between experimental data and simulation results for standard and modified Herschel-Bulkley viscosity models: (a) BXG2 fluid in pipe diameter 19.1 mm, (b) BXG4 fluid in pipe diameter 76.2 mm.

The Papanastasiou-modified Herschel–Bulkley viscosity equation is not available in the library of CFD codes in ANSYS Fluent 19. A turbulence model was implemented using user-defined functions (UDFs). Papanastasiou's modified viscosity equation was applied in the current CFD study. This modified viscosity function was shown to be numerically stabilized and devoid of

discontinuity at a vanishing shear rate. Figure 2-15 shows a comparison between experimental data and measured CFD data for different yield stress values at the same pipe diameter. Figure 2-15a depicts a comparison between the experimental results of BXG2 Herschel–Bulkley fluid with a small effect of yield stress in the 76.2 mm pipe diameter and CFD-predicted results both by the standard Herschel–Bulkley viscosity model and by the modified Herschel–Bulkley–Papanastasiou viscosity model.

As observed in Figure 2-15a, the average absolute relative error decreased to 12.5% when using the SST k-ω model, especially in the transitional region. Moreover, the modified Herschel–Bulkley–Papanastasiou viscosity model gave better results in the transitional region. With increasing viscosity and yield stress effects (BXG4 fluid) (Figure 2-15b) the modified Herschel–Bulkley–Papanastasiou model CFD results showed an overprediction with an average absolute relative error within 16.1% when applying the SST k-ω model. The results from CFD data using the modified viscosity were better than those from CFD data using the normal Herschel–Bulkley viscosity model, which gave an average absolute relative error of 20.1%.

To investigate the effect of high yield stress of Herschel–Bulkley fluid, Figure 2-16 represents a KERS09 fluid, which had a very high yield stress effect, τ_y = 10.9 Pa. When using the standard Herschel–Bulkley viscosity model, the average absolute relative error was 30–57% in all k–ε and k–ω models. While using the Herschel–Bulkley–Papanastasiou viscosity model, the results of the SST k-ω model could reproduce the experimental results by an average absolute relative error of 22.3%. As shown in Figure 16, the regularization parameter δ in the rheological Herschel–Bulkley–Papanastasiou model was more effective in the transitional region, where R_{eST} = 2628 to 4069.

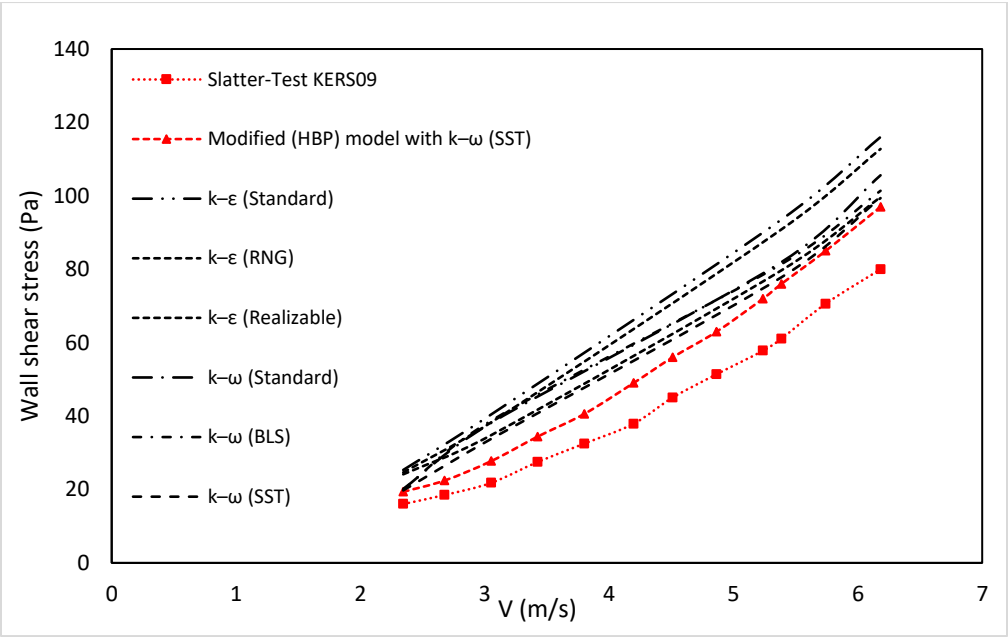

Figure 2-16. Comparison of frictional pressure drop obtained from CFD model vs. experimental data for KERS09 Herschel–Bulkley law fluids.

2.8 Conclusions

This research helps to understand the properties of shear-thinning fluids in the engineering process through investigating their flow behaviour. The investigation was conducted experimentally and numerically using two different pipe diameters. The experimental data on the rheology and the pressure drop were the source for the collected experimental data, where two flow loops with smooth pipes were used to generate the data. The main conclusions of this study are summarized as follows:

- ❑ The characteristics of the shear-thinning fluid flow including translational velocity and friction pressure gradient loss were measured using twelve explicit equations;
- ❑ All models were statistically compared with the experimental results;

- In power-law rheology models, Wilson and Thomas [26] and Dodge and Matzner [27] models were discovered to be the best-fit models to the experimental results up to 45,000 R_{MR}. However, beyond this limit, the Wilson–Thomas model results were significantly different from that of the Dodge and Metzner [27] model;
- For Herschel–Bulkley fluids, the modified Reynolds number Slatter model [21] was found to be the most accurate in predicting the critical velocity compared to the experimental results of this research and the modified model;
- For laminar and transitional regions, Equation (12), which considered the effect of the plug region, provided a good agreement with the viscosity of the Herschel–Bulkley fluid;
- The Herschel–Bulkley rheological model occasionally described the drilling fluid viscosity for low values of the shear rate;
- The Slatter [21] model was found to be most accurate in predicting the critical velocity and pressure losses through all pipe sizes and across all flow regimes;
- Predictions in turbulent pipe flow of Herschel–Bulkley fluid are superior with a specific rheological model. Using a different model could have a significant impact on predictions, particularly when the yield stress is high;
- Most turbulent models in CFD, which were associated with wall functions, were successfully validated for Newtonian fluid turbulent flows;
- When comparing numerical (ANSYS Fluent) k-ω models to the power-law fluid, more accurate results were observed with fluids that have a higher behaviour index. On the other hand, k-ε was observed to work better with fluids that have a value of behaviour index greater than 0.54;

- When comparing numerical results of the Herschel–Bulkley fluid against the experimental results of this study, the percentile error was observed to increase with an increase in the yield stress (τ_y);
- User-defined functions were implemented in the current ANSYS Fluent 19, where the modified viscosity function resulted in the best fit at the low shear rates experimentally and produced more stable and discontinuity-free results at vanishing shear rates numerically.

Author Contributions: Conceptualization, A.I.; methodology, A.I., A.A., M.A.R. and S.B.; investigation, experimental, and numerical simulations, A.I.; Writing—original draft, A.I.; Writing—reviewing and editing, A.I. and A.A. All authors have read and agreed to the published version of the manuscript.

Funding: This research received no external funding.

Data Availability Statement: Some data are not publicly available but can be provided upon request.

Conflicts of Interest: The authors declare no conflicts of interest.

Nomenclature

A = area (m^2);

D = pipe diameter (m);

D_{eff} = effect pipe diameter (m);

f = friction factor (-);

k = fluid consistency coefficient (Pa $\cdot s^n$);

n = flow behaviour index (-);

Q = volumetric flow rate (m^3/s);

R = Dp/2 is the radius of the plug region (m);

Re_{ST} = Slatter Reynolds number (-);

R_{MR} = Metzner and Reed Reynolds number (-);

U^* = shear velocity (m/s);

u = localized linear velocity at (r) value (m/s);

V = mean velocity (m/s);

V_N = Newtonian mean velocity (m/s);

α^* = area ratio (-);

γ= shear rate (s^{-1});

$\mu 0$ = apparent viscosity (Pa $\cdot$ s);

μ = Newtonian viscosity (Pa $\cdot$ s);

μ_{eff} = effect apparent viscosity (Pa $\cdot$ s);

ρ = density of fluid (kg/m^3);

τ = shear stress (Pa);

τ_w = wall shear stress (Pa);

τ_y = yield stress (Pa);

δ = Controls the exponential growth of stress, (-)

Ω = velocity profile blunting factor

2.9 References

1. El-Nahhas, K.; Mostafa, N.H. Prediction of non-Newtonian turbulent flow behaviour by a Newtonian approach. In Proceedings of the 10th International Water Technology Conference, IWTC10, Alexandria, Egypt, 23–25 March 2006; pp. 479–490.
2. Chhabra, R.P.; Richardson, J.F.; Flow, N.N. Applied Rheology: Engineering Applications; Butterworth-Heinemann: Oxford, UK, 2008.
3. Rahman, K.M. Analysis of Drilling Fluid Rheology & Pressure Drop Modelling to Improve Drilling Efficiency. Master's Thesis, Schulich School of Engineering, University of Calgary, Calgary, AB, Canada, 2018.
4. Demirdal, B.; Cunha, J.C. Olefin-based synthetic-drilling-fluids volumetric behaviour under downhole conditions. SPE Drill. Complet. 2009, 24, 239–248.
5. Garvin, T.R.; Moore, P.L. A Rheometer for Evaluating Drilling Fluids at Elevated Temperatures. In Proceedings of the SPE 3062 Presented at the Fall Meeting of the Society of Petroleum Engineers of AIME, Houston, TX, USA, 4–7 October 1970.
6. Minton, R.C.; Bern, P.A. Field Measurement and Analysis of Circulating System Pressure Drops with Low-Toxicity Oil-Based Drilling Fluids. In Proceedings of the SPE 17242 Presented at the SPE/IADC Drilling Conference, Dallas, TX, USA, 28 February–2 March 1988.

7. De Wolfe, R.C.; Coffin, G.B.; Byrd, R.V. Effects of Temperature and Pressure on Rheology of Less Toxic Oil Muds. In Proceedings of the SPE 11892 Presented at Offshore Europe, Aberdeen, UK, 6–9 September 1983.
8. American Petroleum Institute. Recommended Practice on the Rheology and Hydraulics of Oil Well Drilling Fluids. API RP 13D, 3rd ed.; American Petroleum Institute: Washington, DC, USA, 1995.
9. Jim, F.; Young, S.; De Stefano, G.; Lee, J.; Guo, Q. Nanotechnology for oilfield applications-hype or reality. In SPE International Oilfield Nanotechnology Conference and Exhibition; One Petro: Richardson, TX, USA, 2012.
10. Pinho, F.T.; Oliveira, P.J.; Miranda, J.P. Pressure losses in the laminar flow of shear-thinning power-law fluids across a sudden axisymmetric expansion. Int. J. Heat Fluid Flow 2003, 24, 747–761.
11. Anand, V.; David Jr, J.; Christov, I.C. Non-Newtonian fluid–structure interactions: Static response of a microchannel due to internal flow of a power-law fluid. J. Non-Newton. Fluid Mech. 2019, 264, 62–72.
12. Moukhtari, F.E.; Lecampion, B. A semi-infinite hydraulic fracture driven by a shear-thinning fluid. J. Fluid Mech. 2018, 838, 573–605.
13. Picchi, D.; ULlmann, A.; Brauner, N.; Poesio, P. Motion of a confined bubble in a shear-thinning liquid. J. Fluid Mech. 2021, 918, A7.
14. Klotz, J.A.; Brigham, W.E. To determine Herschel-Bulkley coefficients. J. Pet. Technol. 1998, 50, 80–81.
15. Kelessidis, V.C.; ; Maglione, R. Modelling rheological behaviour of bentonite suspensions as Casson and Robertson-Stiff fluids using Newtonian and true shear rates in Couette viscometry. Powder Technol. 2006, 168, 134–147.

16. Whorlow, R.W. Rheological Techniques; E. Horwood: *Bristol, UK*, 1980; ISBN 0470267364, ISBN 9780470267363.
17. Herschel, W.H.; Bulkley, R. Measurement of consistency as applied to rubber-benzene solutions. Proc. ASTM Part II 1926, 26, 621–629
18. Saramito, P. A new elastoviscoplastic model based on the Herschel–Bulkley viscoplastic model. J. Non-Newton. Fluid Mech. 2009, 158, 154–161.
19. Amoo, L.M.; Layi Fagbenle, R. Overview of non-Newtonian boundary layer flows and heat transfer. In Applications of Heat, Mass and Fluid Boundary Layers; Woodland Publishing: Salt Lake City, UT, USA, 2020; ISBN 9780128179499.
20. Metzner, A.B.; Reed, J.C. Flow of non-Newtonian fluids—Correlation of the laminar, transition, and turbulent-flow regions. AIChE J. 1955, 1, 434–440.
21. Slatter, P.T. Transitional and Turbulent Flow of Non-Newtonian Slurries. Unpublished Ph.D. Dissertation, University of Cape Town, Cape Town, South Africa 1994.
22. Kaczmarczyk, K.; Kruk, J.; Ptaszek, P.; Ptaszek, A. Pressure Drop Method as a Useful Tool for Detecting Rheological Properties of Non-Newtonian Fluids during Flow. Appl. Sci. 2021, 11, 6583.
23. Slatter, P.T. The role of the yield stress on the laminar/turbulent transition. In Proceedings of the 9th International Conference on Transport and Sedimentation of Solid Particles, Cracow, Poland, 2–5 September 1997; pp. 2–5.
24. Hedström, B.O.A. Flow of plastic materials in pipes. Ind. Eng. Chem. 1952, 44, 652–656.
25. Vlasak, P.; Chara, Z. Laminar and turbulent flow experiments with yield-power-law slurries. Powder Technol. 1999, 104, 200–206.
26. Wilson, K.C.; Thomas, A.D. A new analysis of the turbulent flow of non-Newtonian fluids. Can. J. Chem. Eng. 1985, 63, 539–546.

27. Dodge, D.W.; Metzner, A.B. Turbulent flow of non-Newtonian systems. AIChE J. 1959, 5, 189–204.
28. Torrance, B. Friction factors for turbulent non-Newtonian fluid flow in circular pipes. S. Afr. Mech. Eng. 1963, 13, 89–91.
29. Yoo, S.S. Heat Transfer and Friction Factors for Non-Newtonian Fluids in Turbulent Pipe Flow; University of Illinois at Chicago: Chicago, IL, USA, 1974.
30. Brown, N.P.; Heywood, N.I. Slurry Handling: Design of Solid-Liquid Systems; Elsevier Science: London, UK, 1991.
31. Clapp, R.M. Turbulent heat transfer in pseudoplastic non-Newtonian fluids. In International Developments of Heat Transfer Part III; The American Society of Mechanical Engineers: New York, NY, USA, 1961,pp 652–661.
32. Thomas, A.D.; Wilson, K.C. New analysis of non-Newtonian turbulent flowndashyield-power-law fluids. Can. J. Chem. Eng. 1987, 65, 335–338.
33. Slatter, P.T.; Petersen, F.W.; Moodie, L. Rheological characterisation of mineral slurries using balanced beam tube viscometry. J. South. Afr. Inst. Min. Metall. 1998, 98, 165–170.
34. Skelland, A.H.P. Non-Newtonian Flow and Heat Transfer (Book on Quantitative Relationships for Non-Newtonian Systems, Considering Classification and Fluid Behaviour of Materials with Anomalous Flow Properties); John Wiley and Sons, Inc.: New York, NY, USA, 1967; 469p.
35. Steffe, J.F. Rheological Methods in Food Process Engineering; Freeman Press: Dallas, TX, USA, 1996.
36. Van den Heever, E. Rheological Model Influence on Pipe Flow Predictions for Homogeneous Non-Newtonian Fluids. Master's Thesis, Cape Peninsula University of Technology, Cape Town, South Africa, 2013.

37. Lovato, S.; Keetels, G.H.; Toxopeus, S.L.; Settels, J.W. An eddy-viscosity model for turbulent flows of Herschel–Bulkley fluids. J. Non-Newton. Fluid Mech. 2022, 301, 104729.
38. Gavrilov, A.A.; Rudyak, V.Y. Reynolds-averaged modeling of turbulent flows of power-law fluids. J. Non-Newton. Fluid Mech. 2016, 227, 45–55.
39. Gavrilov, A.A.; Rudyak, V.Y. Direct numerical simulation of the turbulent flows of power-law fluids in a circULar pipe. Thermophys. Aeromechanics 2016, 23, 473–486.
40. Stainsby, R.; Chilton, R.A. Prediction of pressure losses in turbulent non-Newtonian flows: Development and application of a hybrid theological model. In Bhr Group Conference Series Publication; Mechanical Engineering Publications Limited, 1996; Volume 20, pp. 21–40.
41. Singh, R.; Ahmed, R.; Karami, H.; Nasser, M.; Hussein, I. CFD analysis of turbulent flow of power-law fluid in a partially blocked eccentric annulus. Energies 2021, 14, 731.
42. Ihmoudah, A.; Rahman, M.A.; Butt, S.D. CFD and experimental studies of yield power-law fluids in turbulent pipe flow. In International Conference on Offshore Mechanics and Arctic Engineering. Am. Soc. Mech. Eng. 2018, 51296, V008T11A012.
43. Bartosik, A. Modification of k-ε model for slurry flow with the yield stress. In Proceedings of the 10th International Conference Numerical Methods in Laminar and Turbulent Flow, Swansea, UK, 28 July–1 August 1997; pp. 265–274.
44. Bartosik, A.S.; Hill, K.B.; Shook, C.A. Numerical Modelling of Turbulent Bingham Flow. In Proceedings of the 9th International Conference Transport and Sedimentation of Solid Particles, Cracow, Poland, 2–5 September 1997; Agricultural University of Wroclaw: Wroclaw, Poland, 2002; Part 1, pp. 69–81.

45. Launder, B.E.; Sharma, B.I. Application of the energy-dissipation model of turbulence to the calculation of flow near a spinning disc. Lett. Heat Mass Transf. 1974, 1, 131–137.
46. Bartosik, A.S. Influence of Rheological Parameters on Predictions of Bingham Slurry Flow. In Proceedings of the 11th International Conference Transport and Sedimentation of Solid Particles, Ghent, Belgium, 9–12 September 2002; Agricultural Academy of Wrocław: Wrocław, Poland, 2002; Volume 438, pp. 143–150.
47. Cayeux, E.; Leulseged, A. The effect of thixotropy on pressure losses in a pipe. Energies 2020, 13, 6165.
48. Magnon, E.; Cayeux, E. Precise method to estimate the Herschel-Bulkley parameters from pipe rheometer measurements. Fluids 2021, 6, 157.
49. Saasen, A.; Ytrehus, J.D. Viscosity models for drilling fluids—Herschel-Bulkley parameters and their use. Energies 2020, 13, 5271.
50. ANSYS FLUENT Theory Guide 15.0; ANSYS, Inc.: Canonsburg, PA, USA, 2013. Available online: http://www.ansys.com (accessed on 5 March 2023).
51. Papanastasiou, T.C. Flows of materials with yield. J. Rheol. 1987, 31, 385–404.
52. Genić, S.; Arandjelović, I.; Kolendić, P.; Jarić, M.; Budimir, N.; Genić, V. A review of explicit approximations of Colebrook's equation. FME Trans. 2011, 39, 67–71.
53. García, F.; García, J.M.; García, R.; Joseph, D. Friction factor improved correlations for laminar and turbulent gas–liquid flow in horizontal pipelines. Int. J. MULtiph. Flow 2007, 33, 1320–1336.
54. García, F.; García, R. ; Padrino, J.C.; Mata, C.; Trallero, J.; Joseph, D. Power-law and composite power-law friction factor correlations for laminar and turbulent gas– liquid flow in horizontal pipelines. Int. J. Multiph. Flow 2003, 29, 1605–1624.

55. Ouyang, L. Single Phase and Multiphase Fluid Flow in Horizontal Wells. Ph.D. Dissertation, Dept. of Petro Eng., School of Earth Sciences, Stanford University, Stanford, CA, USA, 1998; 248p.
56. Xiao, J. J., Shonham, O., and J. P. Brill. "A Comprehensive Mechanistic Model for Two-Phase Flow in Pipelines." Paper presented at the SPE Annual Technical Conference and Exhibition, New Orleans, Louisiana, September 1990. doi: https://doi.org/10.2118/20631-MS
57. Wu, B. Computational fluid dynamics investigation of turbulence models for non-Newtonian fluid flow in anaerobic digesters. Environ. Sci. Technol. 2010, 44, 8989–8995.
58. Mathur, A.; He, S. Performance and implementation of the Launder–Sharma low-Reynolds number turbulence model. Comput. Fluids 2013, 79, 134–139.
59. Versteeg, H.K.; Malalasekera, W. An Introduction to Computational Fluid Dynamics: The Finite Volume Method; Pearson Education: London, UK, 2007.

Chapter 3: Systematic Investigation of Newtonian and non-Newtonian Shear-Thinning Fluid Two-Phase Flows in Horizontal Pipe

Abdalsalam Ihmoudah[1, 2,*], Abdelsalam Abugharara[1, 3], Mohammad Azizur Rahman[4] and Stephen Butt[1]

[1] Faculty of Engineering & Applied Science, Memorial University of Newfoundland, St. Johns, NL, Canada

[2] Wadi Alshatti University, Libya

[3] Sebha University, Sebha, Libya

[4] Petroleum Engineering, Texas A&M University at Qatar, Doha 23874, Qatar

*Correspondence: aai117@mun.ca

This chapter is based on the objectives defined in Section 1.5 and was submitted to the Journal of Dynamics by the Multidisciplinary Digital Publishing Institute (MDPI) on October 2023, and is currently under review. This article is a new build and improvement based on recommendations and discussions of the version of the conference contribution: Experimental and Numerical Investigation of Gas/Yield Power-Law Fluids in a Horizontal Pipe, Paper OMAE2019-95219 presented at the ASME 2019 38th International Conference on Ocean, Offshore, and Arctic Engineering, 9–14 June, Glasgow, UK, attached in Appendix B.

Co-authorship Statement

Abdalsalam Ihmoudah is the first author of this manuscript, along with co-authors Dr. Abdelsalam Abugharara, Dr. Mohammad Azizur Rahman, and Dr. Stephen Butt. I proposed the idea and concept, conducted the literature review, and prepared the fluid samples. I collected and analyzed the experimental data and numerical simulation. Dr. Abdelsalam Abugharara, technical support, and manuscript review Dr. Azizur and Dr. Butt evaluated the methodology and reviewed the manuscript. The manuscript preparation was mainly contributed by Abdelsalam Ihmoudah, with revision assistance provided by all other coauthors.

Abstract

Two-phase flow of gas/ non-Newtonian fluids in pipes is widely used and can be found in a wide range of industrial applications. For a deeper understanding of the effects of gas dynamics on rheological parameters of non-Newtonian liquids in two-phase flow, experimental and computational fluid dynamics investigations have been conducted. The air/Newtonian and air/non-Newtonian shear-thinning fluids in two-phase flow were evaluated in a horizontal pipe. Two shear-thinning rheological models (power-law and Herschel–Bulkley fluids) were used as working fluids. The experiments were conducted in a flow loop of a 65-m open-cycle system. The horizontal test section had a diameter of 3 inches (0.0762 m). The numerical calculations were conducted using a volume of fluid model in ANSYS Fluent version 19 for tracking the flow regime and transition boundaries of flow pattern maps. Slug flow characteristics were observed and recorded by a high-speed digital camera under various operating conditions. The slug velocity and slug frequency were experimentally investigated, and the results were compared with reported data in the published research. The effects of rheological properties on flow regime transitions were observed with increasing concentrations of the shear-thinning phase. The results showed that the bubbles were observed to be concentrated more near the top pipe wall as a result of the increased rheological characteristics. The effect of liquid superficial velocity on slug translational velocity at low air superficial velocity was relatively high. A new empirical correlation for the calculation of slug frequency in Newtonian and shear-thinning of power-law and Herschel–Bulkley fluids in two-phase flow is proposed. Validation of the new correlations to experimental results revealed improved prediction performance.

3.1 Introduction

Two-phase flows of gas/shear-thinning are typical phenomena within the petroleum and chemical industries and some of the fluid mechanics categories. The characterization of shear-thinning fluid is especially important in relation to two-phase flow during both the processing and transportation phases of petroleum products for process enhancement and safety improvement. In two-phase flows, hydrodynamic characteristics such as flow pattern, void fraction, pressure drop, and slug flow are required to be considered in relation to parameter range and advanced flow mechanisms. To date, relevant research has mainly investigated gas-Newtonian two-phase flow, whereas only little research has been conducted on shear-thinning liquids of two-phase flows [1-6]. Moreover, the effect of the rheological parameters in two-phase shear-thinning flow in oil and gas applications still needs more investigate.

Considering the above, there is an obvious necessity for theoretical, experimental, and numerical research that focuses on two-phase Newtonian and non-Newtonian flows. The results of this research direction could help scientists and engineers design production and transportation systems that are not only cheaper, efficient, and reliable, but also safer.

Two-phase gas and liquid pipeline flows have various distribution and flow patterns. The patterns, which have easily recognizable features, are generally determined by operating conditions and the fluid's characteristics. In horizontal pipelines, most of the flow patterns are dispersed bubble, (plug and slug sometimes referred to as intermittent flow), stratified smooth, wavy, and annular flow. Several flow maps have been designed to predict the flow patterns for gas/Newtonian, such as Mandhane et al. [7] and Taitel and Dukler [8] which are the most frequently used.

In gas/shear-thinning liquid two-phase flows, the physical properties (i.e., hydrodynamics) show behaviors that differ from gas-Newtonian liquid flow, despite some researchers finding that liquid properties have very little effect on flow patterns [9-13]. Based on these results, Chhabra and Richardson [14] adjusted Mandhane et al.'s [7] of horizontal flow patterns while also taking into consideration Weisman et al.'s [15] work on this map. In other research, Gregory and Scott [16] developed a correlation that is valid to predicting slug frequency in Newtonian fluids. Based on the use of carbon dioxide and water in a 19-mm-diameter pipe, Gregory and Scott suggest that the slug frequency has to correlate to the Froude number. Rosehart et al. [17] published their findings on the first experimental study dealing with the effect of non-Newtonian (power-law model) characteristics. In that study, the researchers used capacitive sensors for measuring the velocity of the slug as well as the average hold-up and slug frequency. The published experimental results of Hubbard [18], Hubbard and Dukler [19], and Otten and Fayed [20-21] included the pressure-drop, the velocity of the slug and the measurement slug frequency for two-phase flow of air/non-Newtonian (Carbopol R941 solutions). Plotting the experimentally determined slug velocity versus the slug no-slip velocity allowed them to determine the relationship between the slug and slug no-slip velocities for shear-thinning behavior. Picchi et al. [22] experimentally investigated horizontal and inclined pipes with an inner diameter of 22.8 mm for the air/power-law model in two-phase flow. The model they proposed for slug flow is valid for air/power-law fluid. They also observed that flow pattern maps are affected by inclination. Bendiksen et al. [23] and Al-Kaiyem et al. [24] explored slug flow in a horizontal pipe while employing medium viscosities. Bendiksen et al. used oil to investigate slug bubble velocity in a 0.057-m ID horizontal pipe. They discovered that the liquid viscosity has a significant impact on the bubble shape and velocity. Al-Kaiyem et al. conducted a statistical analysis on the slug translational velocity and the slug length using water as a working fluid. They discovered that the translational velocity and slug length increase while the

slug frequency decreases for a constant water velocity. The effect of translational velocity of the highly viscous oil / gas flow was studied by Baba et al. [25] in horizontal pipes. They proposed an empirical correlation to calculate the highly viscous oil slug velocity in two-phase flow. Other studies examined the effect of the fluid physical properties on the drift velocity that is a component of the slug translational velocity, as emphasized in Eq. (2). The most recent and significant among these researchers are Gokcal et al. [26] and Jeyachandra et al. [27], who used an inclinable facility with a diameter of 0.0508 m. Baungartner et al. [28] experimentally studied a 44.2-mm diameter horizontal pipe using carboxymethyl cellulose (CMC) power-law solutions and air. They found that the flow behavior was affected by the continuous phase. Farooqi and Richardson [29] studied pressure loss and void fraction predictions for air/non-Newtonian liquid, modifying Lockhart and Martinelli's [30] model in predicting the averages of void fractions. As well, they studied intermittent regimes' drag reductions. Dziubinski [31] then updated the drag ratio for two-phase pressure drops occurring in air/non-Newtonian fluid intermittent flows. Meanwhile, Ruiz-Viera et al. [32] conducted experiments on air lubricating grease for two-phase flow using different geometries and surface smoothness. The same researchers also proposed an empirical model for two-phase pressure drop in power-law fluid. Xu et al. [33] examined power-law fluids using 20, 40, and 60 mm diameter pipes at different angles of inclination as well as three different CMC solution concentrations. Based on their results for liquid phase properties and inclination, the researchers developed a model to describe shear-thinning pressure drop. Other recent two-phase flow studies [34-38] adopted a broad range of methods, including laser diagnostics, wavelet transform, probabilistic estimation, and high-speed visualization of Newtonian fluids. However, these investigations ignored how rheological properties of non-Newtonian fluids can affect slug characteristics and flow regime in vertical and horizontal pipes.

Although researchers have recently increased their use of computational fluid dynamics (CFD) simulation tools to investigate two-phase flow hydrodynamic characteristics, few have yet to investigate two-phase flow shear-thinning of Herschel-Bulkley model. Ko et al. [39] applied a shear stress transport model in kinetic energy-related equations when they investigated turbulent wavy Newtonian core flows. They discovered that their approach resulted in wavelength and pressure distribution predictions with greater accuracy than those resulting from the K-ω turbulence model. Lo and Tomasello [40] employed a fluid volume method when simulating stratified Newtonian fluid flows, aiming to determine whether the turbulence models affects CFD outcomes. Unlike [39], Lo and Tomasello found the K-ω turbulence model to be more accurate. The RNG k-ε turbulence model was used by Al-yaari and Abu-Sharhk [41] when they simulated horizontal pipe stratified flow, while different types of slug and stratified flow regimes were used by Jia et al. [42] to test and compare drag reduction rations and pressure gradients. The latter researchers also utilized a three-dimensional (3D) version of CFD to calculate the liquid wall friction factor, afterwards comparing it with empirical standard correlation values. Kroes and Henkes [43] applied Ansys Fluent when studying elongated gas bubble drift velocity in pipelines using Newtonian fluid flows, finding good agreement in their experimental results. However, none of these studies looked at two-phase flows of Herschel-Bulkley fluids. Sanderse et al. [44] tracked elongated bubbles in a channel by applying CFD Fluent in a two-phase model. Ihmoudah et al. [45] studied numerically how rheological parameters can impact air/yield power-law two-phase flows. Using a 2D microchannel Herschel-Bulkley model simulation, the researchers aimed to predict drift velocity and pressure variations for bubbles in a channel. They then validated the simulation results with 2D or 3D CFD inviscid flow solution. However, as with the earlier studies mentioned above, the yield stress effect of Herschel-Bulkley fluid in two-phase flows was ignored.

Aiming to fill this research gap, the present study experimentally investigates how rheology parameters of shear-thinning (Herschel-Bulkley and power-law fluid) affect slug flow and flow pattern maps in horizontal pipes. The study also applies the volume of fluid (VOF) method in CFD_ANSYS Fluent 19.0 to examine liquid and gas interfaces in a 3D model. A re-circulating polyvinyl chloride (PVC) open loop measuring 65 m in length and 0.0762 m in diameter is used to perform the experiments, testing air and four shear-thinning working fluids (i.e., power-law and Herschel-Bulkley fluids). The primary objective is to assess transitional boundaries of flow regimes and to study how shear-thinning rheological model fluids, along with their estimated parameters, affect flow regime predictions in a horizontal pipe using CFD and flow visualization. The results of this work will contribute to a better understanding of efficient design for transporting pipelines, accurately predicting slug flow that induces vibrations, and enhancing reverse mud circulation in the pressurized drilling of oil and gas wells.

3.2 Laminar Region and Transitional Limitations

Metzner and Reed [46] modified a Reynolds number to correlate shear-thinning (power-law model). They proposed that the non-Newtonian fluids have nearly the same Reynolds number as Newtonian fluids in smooth pipes at the laminar flow as per Eq. 3-1.

$$R_{MR} = \frac{8\rho v^2}{K\left(\frac{8V}{D}\right)^n} \tag{3-1}$$

For Herschel-Bulkley fluid, the generalized Reynolds number used was based on the experiments of Ihmoudah et al. [47]. This model considered the effect of pipe diameter on the apparent viscosity, where the laminar flow was taken at Reg =2100. The generalized Reynolds number for Herschel-Bulkley fluid can be expressed as:

$$R_{eg} = \frac{\rho V D_{eff}}{\tau_y \left(\frac{8V}{D_{eff}}\right)^{-1} + K\left(\frac{8V}{D_{eff}}\right)^{n-1}} \tag{3-2}$$

Where $$D_{eff} = D - D_p \tag{3-3}$$

$$D_p = \frac{\tau_y}{\tau_w} \tag{3-4}$$

For laminar flow, shear-thinning fluids could be formulated by incorporating the rheological parameter model in the Rabinowitsch-Mooney relation and written in terms of 8V/D relative to τ_w. Where τ_w in Eq.3-4 can be calculated using Eq. (3-5).

For the Herschel-Bulkley model [48-49].

$$\frac{8V}{D} = \frac{4}{{\tau_w}^3}\left(\tau_w - \tau_y\right)^{\frac{n+1}{n}}\left(\frac{1}{K}\right)^{1/n}\left[\frac{n{\tau_w}^2}{n+1} - \frac{2n^2\tau_{y(\tau_w-\tau_y)}}{(n+1)(2n+1)} - \frac{2n^2\left(\tau_w-\tau_y\right)^2}{(n+1)(3n+1)}\right] \tag{3-5}$$

3.3. Materials and Methods

3.1 Experimental Setup

Figure 3-1 presents the setup used in the experimental study. As shown in the figure, an air tank with a regulating valve channels a compressor air pump to maintain stable pressure. The non-Newtonian liquid phase is moved from the liquid phase tank by the centrifugal pump, which then circulates the non-Newtonian liquid phase through the whole system. The rotary pump's speed is controlled and maintained by an inverter that regulates the power by changing frequencies. During the experiment, gas can be injected into the pipe via a T-junction located 20 m before the test section. The volumetric flow rates for gas and liquids can be regulated and measured

independently. In order to ensure the independent regulation and measurement of volumetric flow rates of all phases, two Omega meters are utilized as part of the test installation. One of the meters is an FLR 6715D, a DN 15 pipe flow meter measuring 3.3 m^3/h to 2.50 m^3/h, and the other is an FLR 6750D, which is a DN 25 pipe flow meter measuring 9 m^3/h to 85 m^3/h. The working liquid phase is measured using an Omega FTB-730 turbine flow meter in the range of 0.7 m^3/h and 89.87 m^3/h. It has an accuracy of around ±1.1% at full scale. The setup also includes Omega PX603-100Q5V differential and absolute pressure transducers at 0–100 Psi, which provide data on liquid and gas pressure. Additionally, four T-type sensor thermo-coupling Omega TC-(*)-NPT series devices are used for measuring fluid temperature, and high-speed cameras are positioned L/D=262 from the mixing tee to evaluate slug flow and ensure that flow rates of all the phases are independently regulated. After entering the test section, the fluid mixture moves back to the primary storage tank. Gravitational effects are used to separate the phases.

3.3.2 Fluid Rheology Estimation

In the Drilling Technology Laboratory, two shear-thinning rheological models comprising Herschel-Bulkley and power-law fluids are prepared using bentonite, carboxymethyl cellulose (CMC), and xanthan gum. The solutions' rheology parameters are determined with a 4-scale mud balance and an 8-speed API-compliant Model 800 rotational viscometer. Table 3.1 presents a list of the CMC liquids that indicate shear-thinning of the power-law model. These are described using two parameters, as follows [50].

$$\tau = k\dot{\gamma}^{\,n} \tag{3-6}$$

Where τ denotes the shear stress, k indicates the fluid consistency coefficient, $\dot{\gamma}$ represents the shear rate, and n stands for the flow behavior index. In cases where $n > 1$, the fluid has shear-thickening behavior; in cases where $n < 1$, the fluid has shear-thinning properties

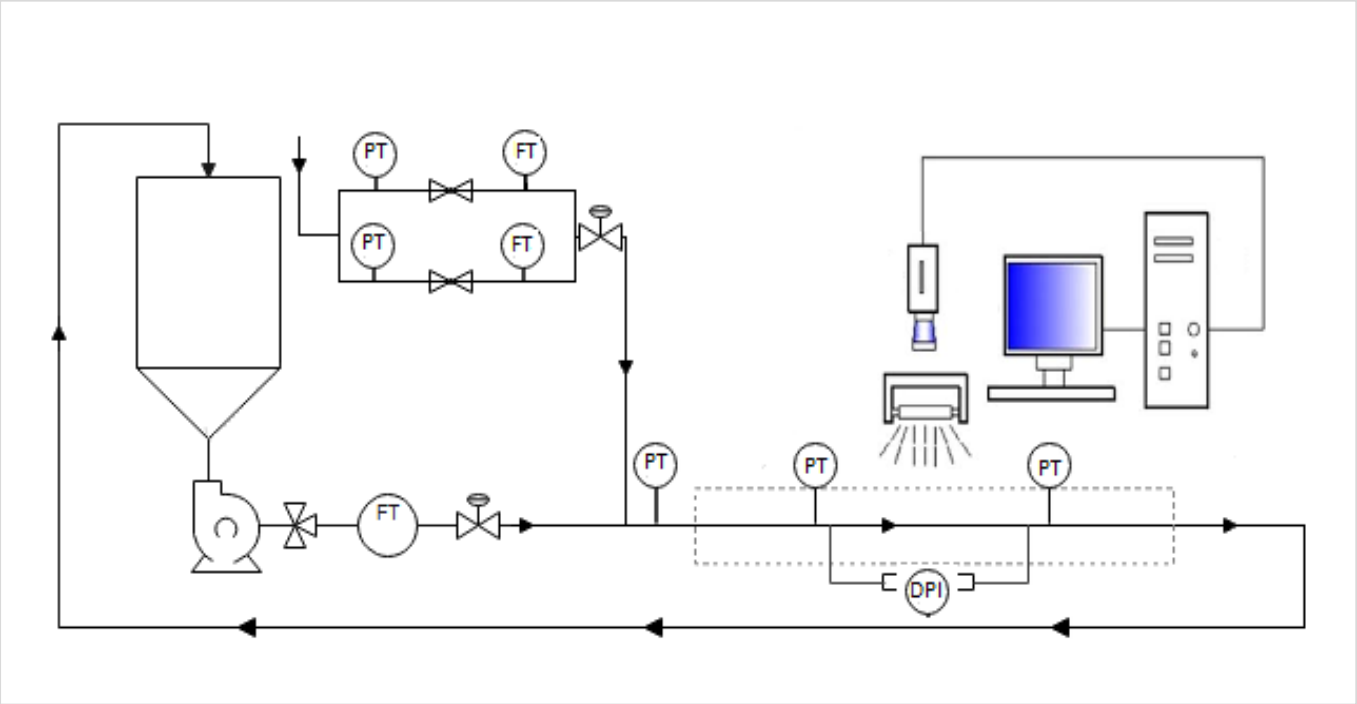

Figure 3-1. The experimental setup diagram.

To calculate the bentonite/xanthan gum solution's fluid rheology, Herschel and Bulkley's [51] nonlinear three parameters are used. In cases where n < 1, the Herschel-Bulkley model should be considered a shear-thinning fluid model [49, 51] and is expressed as:

$$\tau = \tau_y + k\,\dot{\gamma}^{\,n} \tag{3-7}$$

Where τ denotes the shear stress, τ_y indicates the yield stress, k represents the fluid consistency coefficient, and $\dot{\gamma}$ stands for the shear rate. The flow behavior index is designated by n.

Furthermore, because the fluid type is defined by the rheological behavior of the non-Newtonian liquid's apparent viscosity and the shear rate, shear-thinning occurs when there is a decrease in the apparent viscosity and an increase in the shear rate. Conversely, shear-thickening occurs when there is an increase in the apparent viscosity along with an increase in the shear rate. Figure 3-2 illustrates this process [49].

Table 3-1: Physical properties of test fluids at 20°C.

	Rheological parameters						
Symbol	ρ (kg/m3)	Surface tension σ (N/m)	n	K (Pa.sn)	τy (Pa)	R^2 (HB model)	R^2 (PL model)
Water	998.1	0.0712	1	0.001	-	-	-
CMC1	1000.3	0.072	0.71	0.0601	-	-	0.991
CMC4	1003.1	0.0746	0.57	0.405	-	-	0.995
BXG2	1041	0.0737	0.61	0.241	1.92	0.992	-
BXG4	1047	0.0764	0.56	0.415	3.06	0.997	-

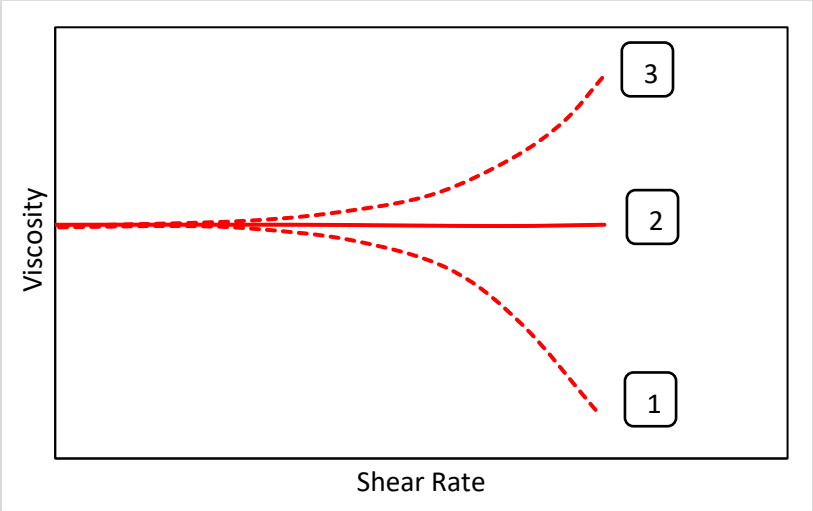

Figure 3-2. Viscosity vs. shear rate: (1) Shear-thinning, (2) Newtonian, and (3) Shear-thickening.

3.3.3 Experimental Procedure

The present study uses water along with four non-Newtonian shear-thinning rheological models for liquid phases (Herschel-Bulkley and power-law fluids). Further, to maintain critical transition conditions for the study's three flow regimes, the regimes' transition boundary limitations for liquid and gas velocities in a horizontal pipe are chosen from Mandhane et al.'s [7] flow pattern map. Each experiment has a 25 min waiting time for stabilizing readings prior to recording the video, and a total of four slugs are deemed sufficient to calculate slug flow characteristics for each case. The tests are repeated to ensure results consistency. Via the inverter frequency changes noted in the previously section, a liquid solution (U_L) is introduced into the system at low speed. Gas (U_G) is also introduced at low speed. The flow rates of the introduced U_L and U_G are increased following the recorded data's observations. Using these operational conditions, the same procedure is repeated for the other solutions. Throughout the experimental procedures, a high-speed digital camera is used to record flow patterns. The captured images are later analyzed in slow-motion.

3.4. Simulation Setup and Procedure

The simulations in this study are conducted as 3D transient flows in a horizontal pipe. As shown in Figure 3-3, the domain is built and meshed using ANSYS Fluent 19 and comprises a horizontal section with a 76.2 mm inner diameter. The test fluids and gas are injected into the horizontal pipe via a T-junction, with both non-Newtonian and Newtonian liquids entering from a horizontal direction while gas is introduced from a vertical one (Figure3-3a). The grid convergence of the non-Newtonian fluids is estimated by calculating the initial grid point y+ height in the k-model and scaling wall functions. This is then stabilized at 1.2 with increases in the Reynolds number.

Figure 3-3b shows a 3D schematic of a pipe and layers next to a wall. Ten layers near the wall-adjacent pipe are used to illustrate the bubble shape and the film thinness. A convergence criterion (also known as a time step) of 10^{-5} is utilized in order to maintain the Courant number (CLF) $\leq$ 0.25. For pressure-velocity coupling, a SIMPLE scheme is applied to the setup; for volume fraction, Geo-Reconstruct is applied; and for the momentum equation, second-order upwind is applied [52].

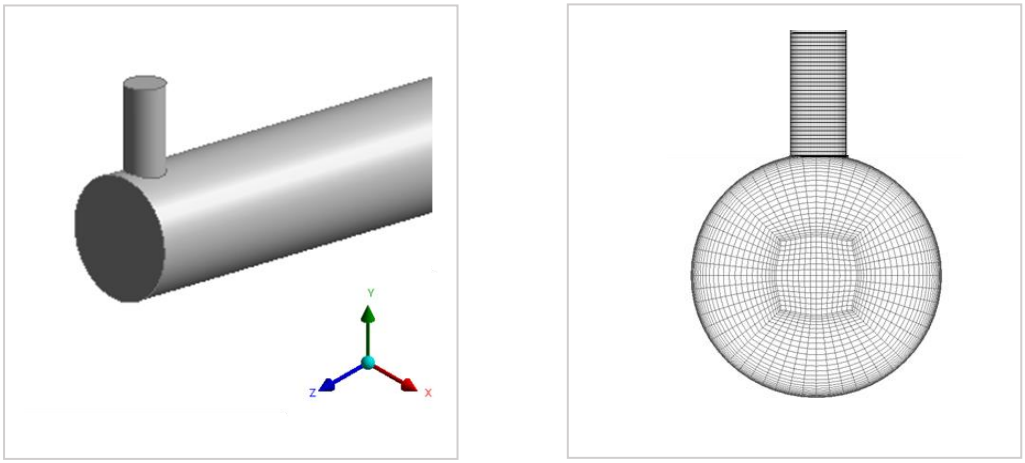

(a) (b)

Figure 3-3. Geometry generation and mesh form (a) The pipe 3D geometry (b) Mesh distribution in the pipe geometry

3.4.1 VOF Model in ANSYS Fluent

In ANSYS Fluent, the VOF model with a surface-tracking mechanism is applied. This model tracks the liquid/gas interface by determining changes in volume fraction rates of each fluid within the computational domain. Note that the fluid motion for each domain point is governed by the continuity and momentum equations as [52].

The equation of continuity:

$$\frac{\partial \rho}{\partial t} + \nabla.\left(\rho\, \vec{U}\right) = 0 \tag{3.8}$$

Where ρ, t and U are density, time, and velocity, respectively.

The equation of momentum:

$$\frac{\partial(\rho \vec{U})}{\partial \mathrm{t}} + \nabla.\left(\rho \vec{U}\vec{U}\right) = -\nabla P + \nabla.\bar{\bar{\tau}} + F_{ST} \tag{3.9}$$

$$\bar{\bar{\tau}} = \eta(\nabla \vec{U} + \nabla \vec{U}^{T}) \tag{3.10}$$

Where $\vec{U}$ is the velocity vector, P is the pressure, ρ is the volume-averaged density, η is the dynamic viscosity, F_{SF} is the surface tension force, and $\bar{\bar{\tau}}$ is the shear stress.

The mixture density and viscosity given by the continuity equation in each cell are as follows:

$$\rho = a_2\rho_2 + (1 - a_2)\rho_1 \tag{3.11}$$

$$\eta = a_2\rho\eta_2 + (1 - a_2)\eta_1 \tag{3.12}$$

The continuity equation for each αq is considered as follows:

$$\frac{\partial a_q}{\partial x}\left(U_q.\Delta\right) = S_{\alpha q} \tag{3.13}$$

Where q is a liquid or gas phase. The tracking of the interfaces between the liquid phase and the gas phase can be calculated by solving the continuity equation of one of the phases as follows.

$$\sum_{q=1}^{n} \alpha_q = 1 \tag{3.14}$$

For a two-phase model, the void fraction takes the following three cases.

$\alpha_q = 0$ if the cell is empty of fluid.

$\alpha_q = 1$ if the cell is full of fluid.

$0 < \alpha q < 1$ interface between the two fluids.

The surface tension force can be expressed as:

$$F_{SF} = \sigma \left[\frac{[k_n \rho \nabla \alpha_1]}{\frac{1}{2}(\rho_1 + \rho_2)} \right] \tag{3.15}$$

Where σ is the surface tension and k_n is the radius of curvature.

$$k_n = \nabla . \hat{m} = \frac{1}{|m|} \left[\left(\frac{m}{|m|} . \nabla \right) |m| - (\nabla . m) \right] \tag{3.16}$$

Where $\hat{m} = \frac{m}{|m|}$ and $m = \nabla \alpha_q$

In the VOF model, the wall adhesion angle with the surface tension is:

$$\hat{m} = \hat{m}_w \cos \theta_w + \hat{t}_w \sin \theta_w \tag{3.17}$$

Where $\hat{m}_w$ and $\hat{t}_w$ are vectors normal and tangential to the wall, respectively.

3.4.2. Turbulent Model

In this investigation, a turbulent regime is measured since the Reynolds numbers of the gas and Newtonian non- Newtonian liquids phase are in the range of the turbulent flow. Several models have been developed in ANSYS FLUENT 19 such as κ-ω and κ-ϵ models and large eddy simulation (LES). In this study, the SST κ-ω approach as classification of Reynolds-averaged

Navier-Stokes (RANS) is selected to solve two transport equations according to Ihmoudah et al.'s recommendations [47]. It is worth noting that the Herschel-Bulkley-Papanastasiou modified viscosity equation is not included in the Ansys Fluent 19 CFD code library [53]. Therefore, a turbulence model that utilizes user-defined functions (UDF) is employed in this study, along with a modified viscosity equation written by Papanastasiou. The k-ω transport equation can be expressed as [52]:

$$\frac{\partial}{\partial t}(\rho k) + \frac{\partial}{\partial x_i}(\rho k u_i) = \frac{\partial}{\partial x_i}\left[(\Gamma_k + \frac{\partial k}{\partial x_j}\right] + G_k - Y_k + S_K \tag{3.18}$$

$$\frac{\partial}{\partial t}(\rho \omega) + \frac{\partial}{\partial x_i}(\rho \omega u_i) = \frac{\partial}{\partial x_i}\left[(\Gamma_\omega \frac{\partial \omega}{\partial x_j}\right] + G_\varepsilon - Y_\omega + S_\varepsilon \tag{3.19}$$

Where $\Gamma_k = \mu_t + \frac{\mu_t}{\rho_k}$, $\Gamma_\omega = \mu_t + \frac{\mu_t}{\rho_\omega}$

The turbulent viscosity is computed by ε *and* k as follows:

$$\mu_t = \rho c_\mu \frac{k}{\varepsilon} \tag{3.20}$$

3.4.3 Shear-Thinning Phase

For shear-thinning fluids, the shear stress can be written in terms of viscosity as:

$$\tau_{ij} = \mu\left(\frac{\partial u_i}{\partial x_j} + \frac{\partial u_j}{\partial x_j}\right) \tag{3.21}$$

The Herschel-Bulkley viscosity function modified by Papanastasiou is not available under the ANSYS Fluent 19 General Purpose Codes. Instead, a new viscous function is implemented using

UDFs in this CFD study. Ihmoudah et al. [47] found the new viscous function more numerically stabilized.

$$\tau = K\dot{\gamma}^{n} + \tau_{Y}\left[1 - \exp(-\delta\dot{\gamma})\right] \tag{3.22}$$

Where μ is the viscosity, k is the consistency coefficient (Pa s^n), $\dot{\gamma}$ is the shear rate (s^{-1}), n is the power-law index, and δ is the regularization parameter Papanastasiou [53].

3.5 Boundary Condition and Simulation Setup

The inlet superficial velocities and the mass flux of the gas and liquid were calculated using the following equations (see Field and Hrnjak [54]):

$$\mathrm{U_G} = \frac{G_x}{\rho_g} \tag{3.23}$$

$$\mathrm{U_L} = \frac{G\,(1-x)}{\rho_l} \tag{3.24}$$

$$G = \frac{\dot{m}_g + \dot{m}_l}{A} \tag{3.25}$$

$$x = \frac{\dot{m}_g}{\dot{m}_g + \dot{m}_l} \tag{3.26}$$

Where G is the mass flux and ρ_l and ρ_g represent the density of liquid phase and gas, respectively. $\dot{m}_l$ and $\dot{m}_g$represent the mass flowrate for liquid phase and gas, respectively. x is the flow quality. A is the pipe cross-section area. The subscripts 'U_G' and 'U_L' represent superficial gas and superficial liquid velocities, respectively. The inlet air and liquid (Newtonian and non-Newtonian) superficial velocities were calculated using Equations 23 to 26.

3.6 Measurement Technique and Analysis

6.1 Two-phase Flow Visualization

The methods available for predicting flow patterns are mostly suitable for Newtonian liquids. In contrast, very little information for gas/non-Newtonian liquid flow is available. Thus, in this work, the maps of the existing flow pattern were extended to include the shear-thinning fluids. We follow the flow pattern classification given by Taitel & Dukler [8], Mandhane et al. [7] and Chhabra and Richardson [6].

To assess the current flow regime transition boundaries and investigate the effects of the rheological models of the shear-thinning fluids and their estimated parameters on the flow regime prediction, flow visualization studies are performed in a horizontal pipe. Videos are acquired at the location of L/D=262 in a pipe diameter of 0.0762 m. The videos are captured by a high-speed video camera with different resolutions depending on the flow regime. Then, the videos are classified into conventional flow regimes in a horizontal flow and categorized as dispersed bubble, plug, and slug flows. The current study excluded the investigation of stratified, stratified wavy, and annular flows. The superficial liquid velocity (U_L) is in the range of 0.36–6.5 m/s, while the superficial gas velocity (U_G) is in the range of 0.18–3.62 m/s. In total, 215 videos and 255 flow conditions were taken to span all the flow regimes considered above in a horizontal pipe.

3.6.1 Translational Velocity Measurement

Translational velocity in multiphase flows refers to the rate of speed traveled by a slug unit consisting of gas bubbles flowing in tandem with alternating liquid slugs as typical pattern of a slug flow. The translational velocity can be calculated by multiplying the mixture velocity and the

distribution parameter. Nicklin et al. [55] were the first to study the motion of elongated bubble in flowing liquids. They discovered that the super-imposition velocity in stagnant liquid phase and the effect of the moving liquid are used to estimate the translational velocity. The following expression was then proposed by Nicklin et al. [55] to estimate the pipe's vertical bubble translational velocity.

$$U_s = C_0.U_m + C_* \sqrt{gD} \tag{3.27}$$

Since the study considered a horizontal flow, the 2nd term in Eq. (3-27) is ignored leading to the translational velocity in horizontal pipes to be [25]:

$$U_s = C_0\, U_m \tag{3.28}$$

Where U_s is the translational velocity and C_0 is a constant. Theoretically, C_0 is assumed for air–water two-phase flow to be 1.0 for plug flow to 1.35 for fully developed turbulent flow [16-17, 21]. Using the idealized slag liquid and gas phase mass balances, continuity considerations, and Eq (3-29) can lead to obtaining the correlation between slag velocity and the slug no-slip velocity [21].

$$U_s = C_1 U_{sns} \tag{3.29}$$

Where U_{sns} slug no-slip velocity is defined as the sum of the gas and liquid superficial velocities:

$$U_{sns} = U_{\mathrm{L}} + U_g \tag{3.30}$$

For the non-Newtonian/air two-phase model, Otten and Fayed [21] reported the air/Carbopol941 concentration increase from 0.075% to 0.2%, and the values of C_1 increased from 1.36 to 1.41. Although, for the same concentration used by Otten and Fayed [21], Rosehart et al. [17] reported the variation of C1 values between 1.34 and 1.57, in this study, we followed the studies of Rosehart et al. [17] and Otten and Fayed [21] to obtain values of C_1 based on experimental results.

3.6.3 Slug Frequency

Slug frequency f_s is defined as the number of slugs passing through point in the pipeline at a specified time. This frequency is a function of the average translational velocity, flow rate, and inclination angle of each slug unit. In various industrial processes and pipelines, estimating the fs is needed to accurately estimate corrosion rates for safety and economic reasons. Gregory and Scott [16] developed a reliable correlation for forecasting slug frequency of carbon dioxide and water in a 19-mm-diameter pipe. They suggest that the slug frequency has to be correlated with the Froude number. Where the equation that follows was created:

$$(\mathrm{N_{Fr}})_{\mathrm{slug}} = \frac{\mathrm{U_{SL}}}{\mathrm{gD}}\left[\frac{{U_s}^*}{\mathrm{U_m}} + \mathrm{U_m}\right] \tag{3.31}$$

Gregory and Scott consider the value of ${U_s}^*$ to be equal to 6 m/sec, and it is combined with the data of Hubbard, where the following equation was derived.

$$\mathrm{f_S} = 0.0157\left[(\mathrm{N_{Fr}})_{\mathrm{slug}}\right]^{1.2} \tag{3.32}$$

Gregory and Scott also defined the correlation of a slug frequency based on carbon dioxide and water used in a 19 mm pipe diameter as:

$$\mathrm{f_S} = 0.0226\left[\frac{\mathrm{U_{SL}}}{\mathrm{gD}}\left(\frac{19.75}{\mathrm{U_m}} + \mathrm{U_m}\right)\right]^{1.2} \tag{3.32}$$

Where U_L is the velocity of superficial liquid and U_m is the mixture velocity of gas and liquid. As a result, the slug frequency and the Froude number can be combined for the superficial fluid velocity.

Several authors have developed correlations for slug frequency [56-61]. Most empirical models were based on Gregory and Scott's [16] methodology, which created the first correlation for slug frequency. Past research in the field of slug flow characterization has primarily concentrated on the Newtonian gas-liquid system, where there was a noticeable lack of experimental work focusing on slug frequency measurement for non-Newtonian fluid.

Rosehart et al. [17] and Otten and Fayed [21] dealt with slug parameter classification for air-non-Newtonian systems. They extended the Gregory and Scott [16] versus Frond number as:

$$f_S = \mathrm{P}_1\left[\left(\mathrm{N}_{Fr}\right)_{slug}\right]^{\mathrm{P}_2} \tag{3.34}$$

The results obtained for P_1 and P_2 are discussed later in the next sections.

Recently, Picchi et al. [22] extended the model of Gregory and Scott [16] as a means to predict the slug frequency of power-law fluid (shear-thinning fluid rheology) as:

$$f_s = 0.0448\left[\frac{U_{SL}}{gD}\left(\frac{32.2014}{U_m}+U_m\right)\right]^{0.88}\left(\frac{Re_p}{Re_w}\right)^{0.07}(n)^{-2.85} \tag{3.35}$$

Where f_S donated the slug frequency, $U_m$is the mixture velocity, n is the flow behavior index, U_{SL} is the liquid velocity, g is the gravity, D is the pipe diameter, Re_p is the non-Newtonian fluid power-law model Reynolds number and Re_w is the Newtonian liquid Reynolds number.

In this study, flow visualization and the recording of videos were achieved using an Olympus high-speed video camera with 1280x1024 pixels and full resolution recording to 1,000 fps to a maximum of 150,000 fps record speed. I-SPEED Control Software Suite 2.0 was used for tracking slug characteristics along a horizontal pipe.

3.7 Results and Discussion

3.7.1 Grid Independence and Model Validation

The quality and mesh size of the grid have a considerable influence on the ANSYS Fluent simulation results. To assess the correctness of our numerical simulation findings, the results of the model created in ANSYS Fluent 19 as a gas-water and non-Newtonian two-phase flow are verified to our experimental results. Table 3.2 shows the approximate number of elements required for a Newtonian and non-Newtonian system to liberate the simulation from mesh size dependency. Figure 3-4 shows a comparison of and numerical simulation by using the VOF method and experimental results. The effect of mesh size on simulation results was examined under the operation conditions at slug no-slip velocity, $Usns$ = 2.2(m/s) to ensure all flows are in the turbulent region. Moreover, the elements number increased from $1.1x10^5$ to $6.9x10^6$. This study used $5.7x10^6$ elements and a grid size of 0.0045 as indicated in Figure 3-4, depending on the computing time and accuracy of. Transient simulation was carried out using Compute Canada, Graham, and Beluga on the ACENET supercomputer.

Table 3-2. Mesh properties utilized in this study

		Skewness			Orthogonal Quality	
	Elements	Min	Max	Avg.	Min	Max	Avg.
Newtonian System	3,760,632	0.03495	0.065138	0.049024	0.9013	0.9941	0.9812
non-Newtonian System	5,735,251	0.0325	0.1436	0.0755	0.8384	0.9919	0.9796

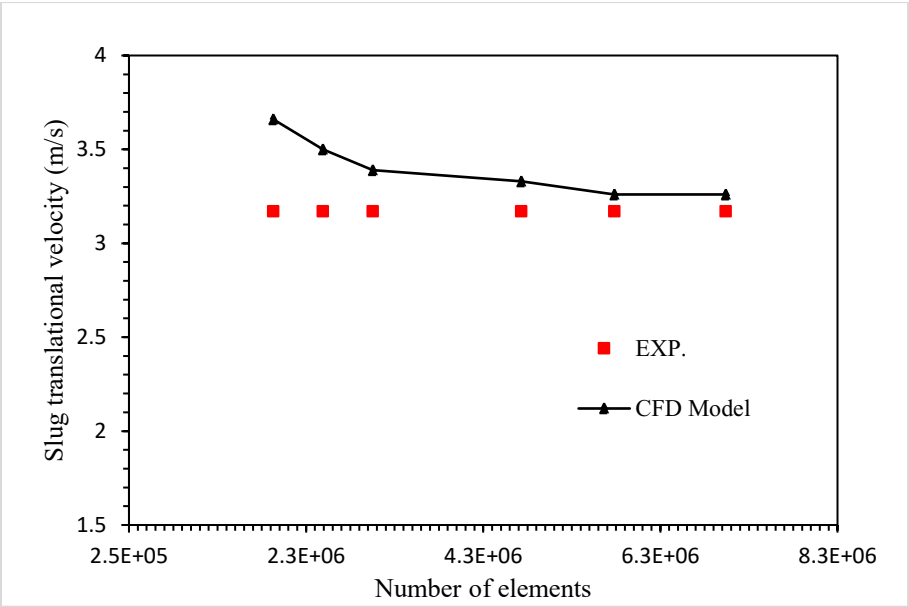

Figure 3-4. Mesh independence test for air- water two-phase flow at slug no-slip velocity, $Usns$ = 2.2(m/s).

3.7.2 Flow Pattern Maps

The experimental flow pattern maps obtained through visual observations are presented in this section. We distinguish three types of flow patterns: dispersed bubble, plug, and slug. There was no inclusion of stratified or annular flow due to the limitations of the experimental facilities. We use the classification of flow patterns proposed by Taitel and Dukler [8] and Mandhane et al. [7] for Newtonian flow and Chhabra and Richardson [6] for non-Newtonian flow in this study.

Figure 3-5 displays high-speed pictures of typical plug and slug flows of water and two shear-thinning fluids (CMC4 and BXG4). There are various discrepancies between gas-Newtonian liquid and gas/shear-thinning liquid flows at the same boundary condition flow pattern. For instance, there are less clearly scattered bubbles in a liquid plug or slug for gas/shear-thinning flow than there are in a liquid plug or slug for Newtonian flow, especially for higher-concentration BXG4 solutions.

The same conduct was noted by Xu et al. [33] and Picchi et al. [22] for shear-thinning (power-law fluid). The detected shape for the slug nose and tail was affected by rheological parameters of the shear-thinning fluid as displayed in Figure 3-5. The results were obtained at t = 42 s, while the flow field had stabilized. It can be observed that the plug flow reduces in size and increases in number with an increase in concentration, which agrees with the experimental results. Furthermore, the additional dimension values of the bubble nose, wake zone, and liquid film in simulations are nearly identical to those in experiments, proving the ability of VOF method in ANSYS Fluent to simulate non-Newtonian fluid.

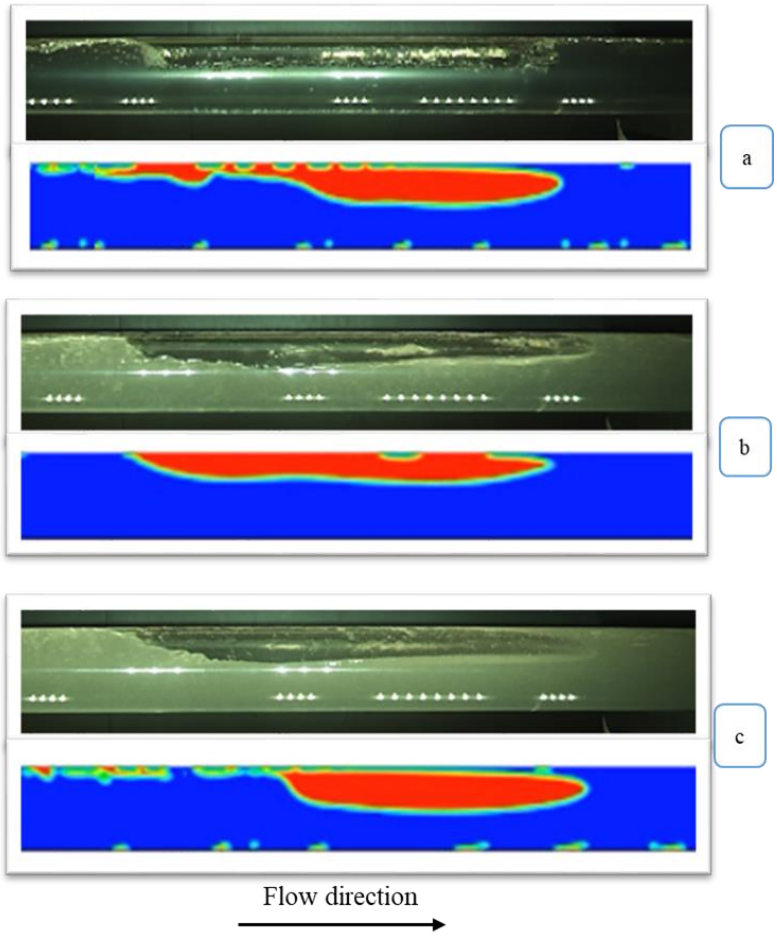

Figure 3-5. Visual observation obtained from the experiment compared to VOF results of the plug flow during two-phase flow in a horizontal pipe (a) air-water (b) air-CMC4 (c) air-BXG4.

3.7.2.1 Flow Regime Transition Boundaries of Gas/ Newtonian liquid

Figure 3-6 shows the experimental flow pattern maps obtained in a horizontal flow for gas/Newtonian liquid. When comparing these flow regime maps to those of Mandhane et al. [7] and Taitel and Dukler [7], which used water and superficial air velocity, most experimental points fall within the boundaries denoted by Taitel and Dukler's [8] flow map regime. However, compared to the flow map of Taitel and Dukler [8], Mandhane et al. [7] show a more accurate projection of the dispersed bubbles flow at high water velocities.

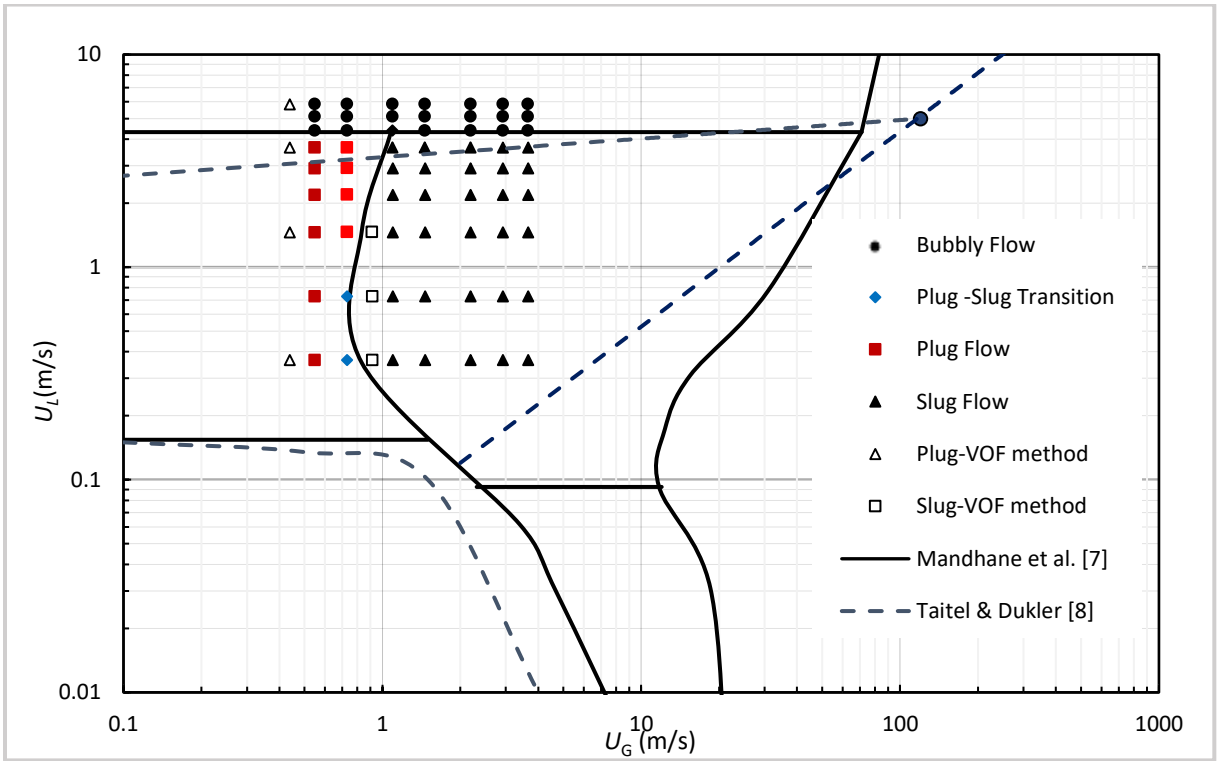

Figure 3-6. Comparison of experimental flow regime transition boundaries to Mandhane et al. [7] and Taitel & Dukler's [7] flow maps in a horizontal air-water two-phase flow

3.7.2 Flow Regime Transition Boundaries Gas/Shear-Thinning Liquid

Flow visualization studies in a 76.2-mm diameter horizontal pipe are performed to assess the current flow regime transition boundaries and to investigate the effects of the rheological properties

of shear-thinning fluids on the flow regime prediction. Chhabra and Richardson [6] created a flow pattern map in a horizontal pipe for the gas/shear-thinning fluid through minor modifications based on Weisman et al.'s [15] work on the horizontal flow pattern map of Mandhane et al. [7]

Figure 3-7 shows the experimental flow pattern maps obtained for the air-CMC1 shear-thinning fluid (power-law model) along with the flow regime boundaries suggested by Chhabra & Richardson [6], Mandhane et al. [7] and Taitel and Dukler [8]. The flow map of Chhabra & Richardson almost matches the experimental flow regime transition from plug or slug flow to dispersed bubbly flow for this experiment. The regime transition from plug to slug flow was not considered in this map. When compared with Mandhane et al. [7], no transition case notice.

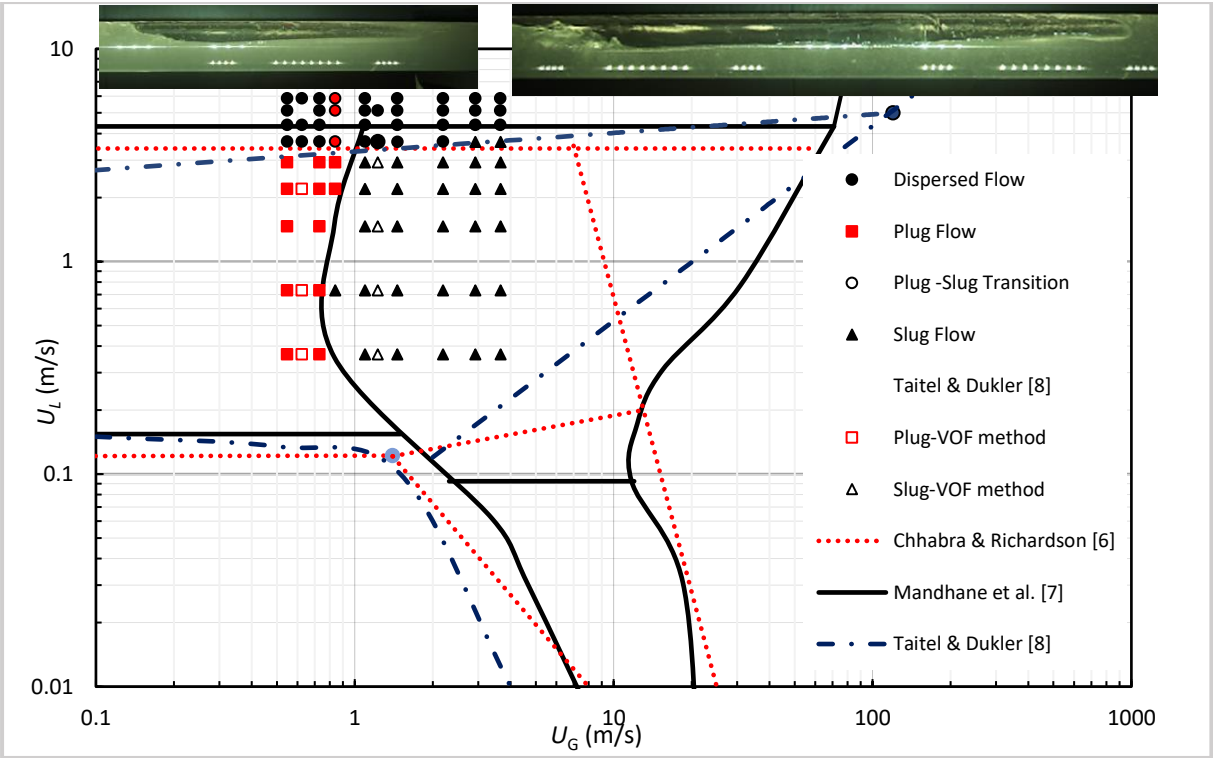

Figure 3-7. Comparison of experimental flow regime transition boundaries to Mandhane et al. [7], Taitel & Dukler [8] and Chhabra and Richardson's [6] flow maps in horizontal air-CMC1 two-phase flow.

Figure 3-8 shows the experimental flow pattern map for highly concentrated CMC4 power-law fluid along with the flow regime boundaries suggested by Chhabra & Richardson [6], Mandhane et al. [7] and Taitel and Dukler [8].

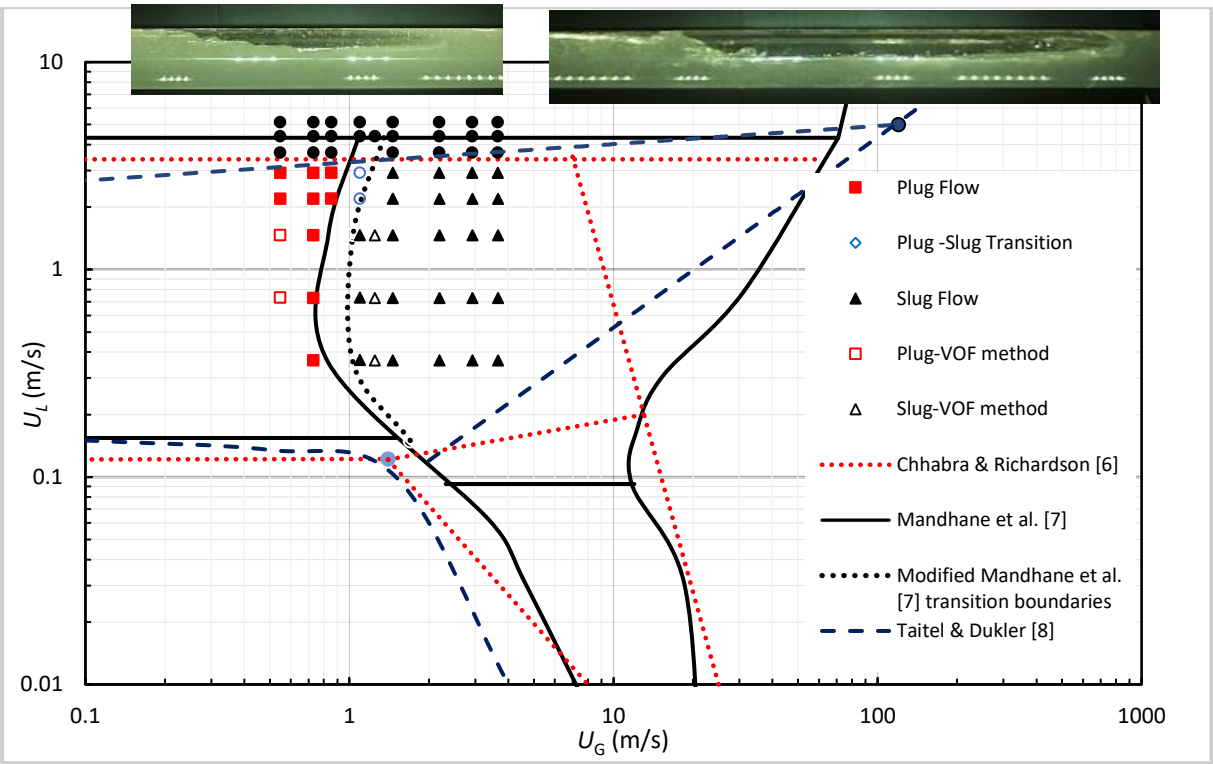

Figure 3-8. Comparison of experimental flow regime transition boundaries to Mandhane et al. [7], Taitel & Dukler [8] and Chhabra and Richardson's [6] flow maps in horizontal air-CMC4 two-phase flow.

Within increasing CMC concentration and decreasing n and increasing k (rheological parameters), the transition from dispersed bubbly to plug or slug flow keeping fixed and still matches with the Chhabra & Richardson [6] flow map. Two cases indicate the transition from slug to plug flow. With the increase of CMC concentration, the superficial velocity of the liquid provided by the centrifugal pump was decreased. The existence region of the plug and slug flow regimes was compared to the experimental data and to the flow regime map of Mandhane et al. [7]. For air-CMC4 power-law fluid, the modified predicted boundary considered the effect of viscosity power-

law fluid agrees very well with the transition boundary from plug to slug flow in the experimental maps.

The effect of yield stress of Herschel-Bulkley fluids on the flow pattern map is presented in Figures 3-9 and 3-10. Two flow patterns were observed for a low effect of yield stress (1.92 Pa) and a mild impact of yield stress (3.06 Pa). The comparison experimental flow pattern map for the air-BXG2 (Herschel-Bulkley fluid) along with the flow regime boundaries suggested by Chhabra & Richardson [6], Mandhane et al. [7] and Taitel and Dukler [8] are shown in Figure 3-9.

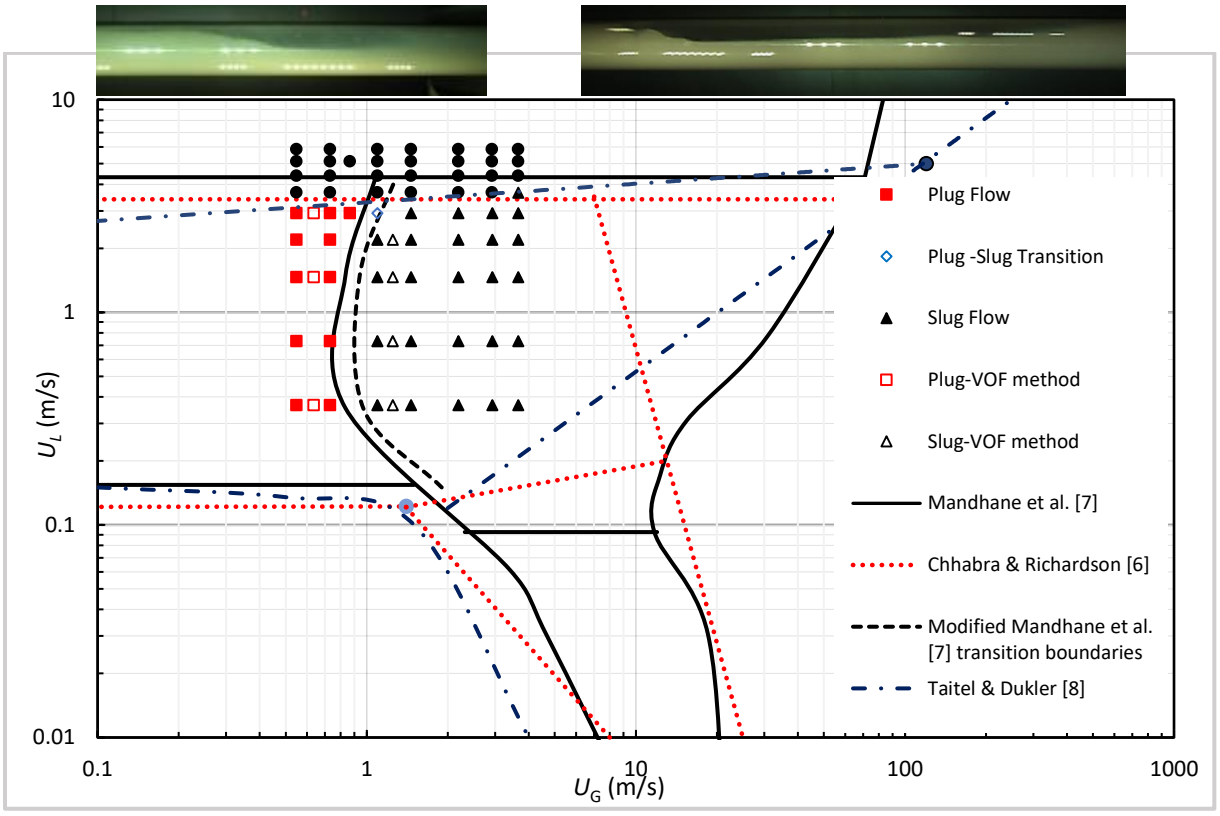

Figure 3-9. Comparison of experimental flow regime transition boundaries to Mandhane et al. [7], Taitel & Dukler [8] and Chhabra and Richardson's [6] flow maps in horizontal air-BXG2 two-phase flow.

We observe that the flow pattern distribution was similar to the regime boundaries of bubble flow to plug and slug flow reported by Chhabra & Richardson [6]. However, there are two transition

boundaries noticed for plug and slug flow transition to Mandhane et al.'s [7] map flow. By considering the effect of diameter and yield stress applied to modify the X* value between plug and slug flow in the boundaries of Mandhane et al. [7], the flow map for the air- BXG2 Herschel-Bulkley fluid can be seen in Table 3-2. The transition line of the regions plug and slug flow patterns moves to the lower right due to the increase of solution mass fraction.

To expand the application of their map to further gas-liquid systems, Mandhane et al. proposed the scalability parameters shown below:

$$X = \left(\frac{\rho_G}{1.21}\right)^{0.3} * Y \tag{3-35}$$

$$Y = \left(\frac{\rho_L}{1000}\right)^{0.25} * \left(\frac{\mu_L}{0.001}\right)^{0.2} * \left(\frac{0.0728}{\sigma}\right)^{0.25} \tag{3-36}$$

The applicability of new transition boundary from plug to slug were based on experimental work to update Mandhane et al. flow map, we proposed the following scaling parameters in Table 3-3:

Table 3-3. Coordinates for transition boundaries of proposed flow pattern map (Mandhane et al. [8])

Transition boundary	Physical property correction. Multiply equation of transition boundary by
Plug and slug to dispersed bubble	Y
Stratified and plug to slug and wavy	X
Plug to slug	X*

Where X^* for Herschel-Bulkley fluid is:

$$X^* = \left(\frac{\rho_G}{1.21}\right)^{0.3} * Y * \left(\frac{D_{eff}}{D_{SC}}\right)^{0.12} \quad (3\text{-}37)$$

Where $D_P = D\,\frac{\tau_y}{\tau_w}$ τ_w obtaining it from Eq (3-5)

And $D_{eff} = D - D_p$

While decreasing n and increasing k and yield stress τ_y values of rheological parameters, the high concentrated BXG4 experimental results and predictions are shown in Figure 3-10.

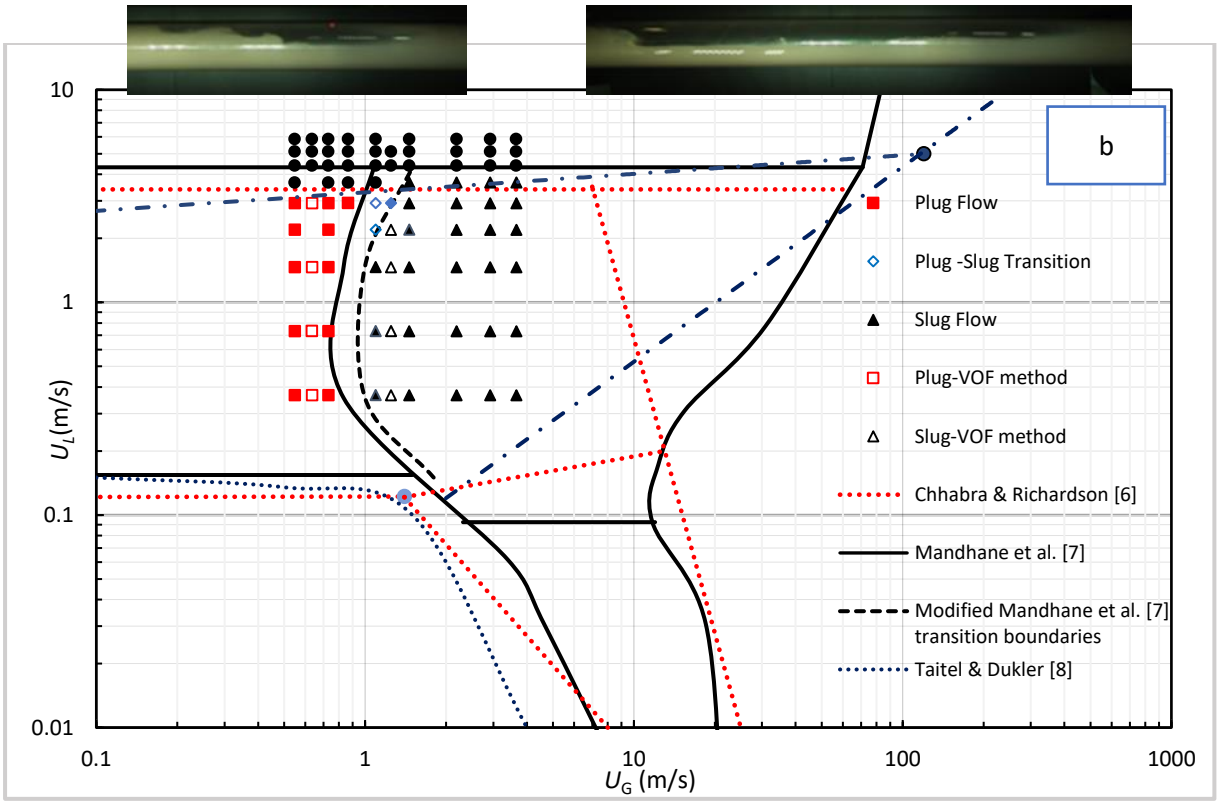

Figure 3-10. Comparison of experimental flow regime transition boundaries to Mandhane et al. [7], Taitel & Dukler [8] and Chhabra and Richardson's [6] flow maps in horizontal air-BXG4 two-phase flow.

As shown in Figure 3-10, the flow pattern changes in the transition region from the slug flow into the plug flow. In experimental observations, the plug flow was observed while it was still in the

range of the superficial liquid velocity of BXG4 and the superficial gas velocity of 0.3-1.0 m/s. Moreover, the slug flow pattern was observed when the gas phase was gaining more kinetic energy due to an increase in the superficial gas velocity. It is worth noting that the range of shear thinning viscosity fluids was examined and showed that the intermittent range of plug flow and slug flow dominated the flow map and was even magnified as the viscosity of the liquid increased in accordance with the previous findings [15, 17, 45, and 49]. Such an increase in this study may be due to the increase in wall shear in the pipe as a result of viscosity effects.

In the current study, newly derived regime transition boundaries (plug to slug) are shown alongside the flow regime boundaries proposed by Chhabra and Richardson [6] between bubble to plug and slug. The new transition boundaries were found to typically agree with experimental observations.

3.7.3 Slug Flow Characteristics

In this work, the measurements of slug flow characteristics such as slug velocities and slug frequency were achieved by visualization and recorded videos using a high-speed-video-camera. Experiments were performed to characterize slug translational velocity of air/shear-thinning fluid in a two-phase model.

3.7.4 Slug Translational Velocity

The slug translational velocity of shear-thinning liquids flowing through horizontal pipe was experimentally tested utilizing a high-speed camera and compression, with empirical correlations found in the literature reports in Table 3-4. Generally, ‘slug translational velocity’ refers to the interface velocity between liquid slugs and the gas pocket. The velocity at this interface is typically the greatest for slug units occurring in the horizontal flow.

To obtain the values of the distribution parameter C_1 in Eq. 28, the experimental data were plotted for slug velocity versus no-slip velocity. A flow visualization study was performed using a high-speed camera for a total of 180 flow conditions presented in Figures 11 and 12.

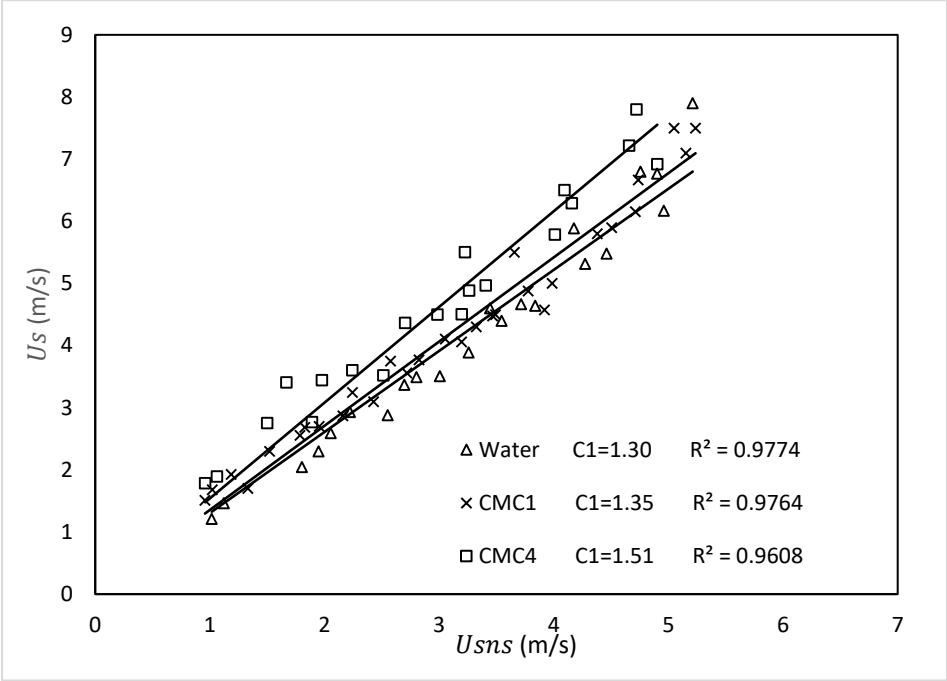

Figure 3-11. Measured slug velocity versus no-slip velocity for the flow of air-water and two air/power-law solutions.

Slug translational velocities were determined visually by recording videos for a slug nose time to travel from a benchmark at the position of L/D = 262. The average of five velocity readings replay for each condition. Variations between those readings were generally less than 2.1%.

To obtain the values of C_1, a linear least-squares fit of the data to Eq. 3-28 was performed. Figure 3-11 displays the results, the statistical data, and the experimental linear correlation coefficient R^2 values of the measured slug velocity versus no-slip velocity for the flow of water and two air/power

law solutions. It is noticed that R^2 always equals to one, which implies that the slug velocity and the no-slip velocity are perfectly correlated.

The value of C_1 obtained for the air-water two-phase flow 1.30 is in excellent agreement with that of the values reported in the literature by [16-17, 20]. For the shear thinning fluid, the values of C_1 for power-law fluids (CMC1 and CMC4) agree very well with the results reported by Picchi et al. [17,22] at almost the same rheological parameters. See Table 3-4.

Figure 3-12 represents a typical plot of two air/shear-thinning (BXG2 and BXG4 Herschel-Bulkley fluids). The recorded slug translational velocity increases as the slug no-slip velocity increases, and the slope of the graph was determined to be 1.55-1.72. The resultant slope indicates the flow coefficient C_1 as expressed in translational velocity in Eq. 3-28. The investigation also reveals that the value of C_1 increases as the liquid phase deviates more from Newtonian behavior.

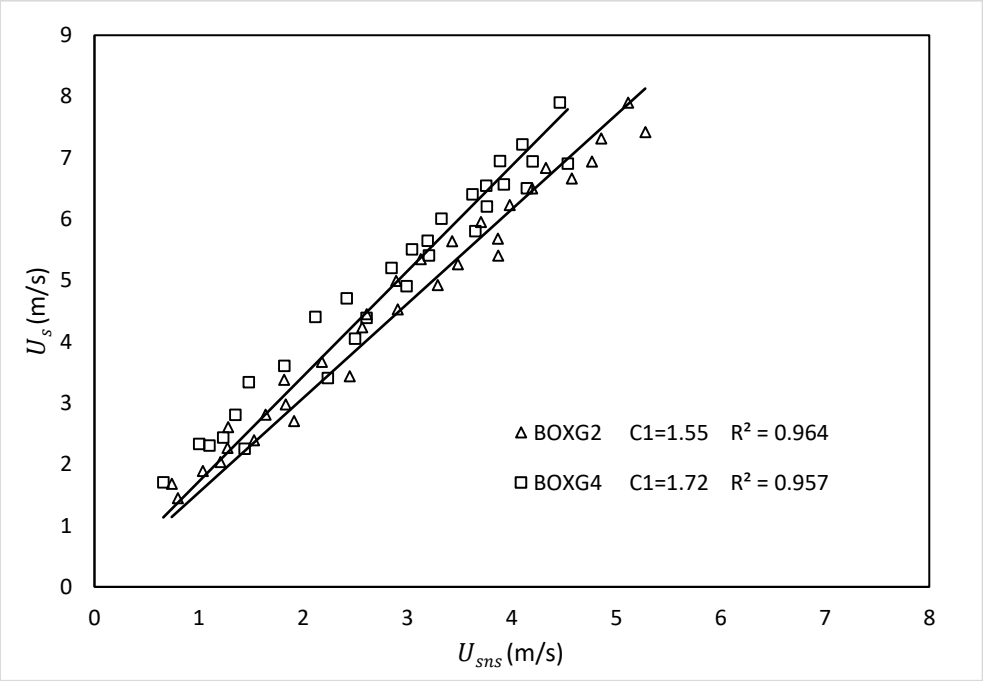

Figure 3-12. Measured slug velocity versus no-slip velocity for the flow of two air/Herschel-Bulkley solutions.

Table 3-4. Slug frequency correlation and values of C_1 for Newtonian and shear-thinning solutions systems.

Authors	Developed Correlations	Diameter of pipe	Working fluids	Rheological Model	Rheological parameters					
					n	K (Pa.sn)	τγ (Pa)	C1	β_1	β_2
Gregory and Scott [16]	$f_S = \beta_1 \left[\left(N_{Fr} \right)_{slug} \right]^{\beta_2}$	-	Water	Newtonian	1.00	0.001	-		0.0157	1.2
Rosehart et al. [17]	$f_S = \beta_1 \left[\left(N_{Fr} \right)_{slug} \right]^{\beta_2}$	0.0254	Water	Newtonian	0.71	0.0601	-	1.25	0.0163	0.13
			CMC7H3S	Power-law	0.56-0.7	1.5-0.15	-	1.57	0.048	0.98
			Polyhal1295	Power-law	0.38-0.44	0.8-0.1	-	1.54	0.025	1.0
			Carbopol941	Herschel-Bulkley	0.40-0.54	1-0.2	0.05-3	1.34	0.054	1.0
Otten and Fayed [21]	$f_S = \beta_1 \left[\left(N_{Fr} \right)_{slug} \right]^{\beta_2}$	0.0254	Water	Newtonian	1.00	0.001	-	1.24	0.02	1.13
			Carbopol942	Herschel-Bulkley	0.63	0.19	0.42	1.36	0.056	0.96
					0.63	0.25	0.68	1.34	0.079	0.89
					0.56	0.85	1.80	1.41	0.103	0.88
Picchi et al. [22]	$f_s = \beta_1 \left[\left(N_{Fr} \right)_{slug} \right]^{\beta_2} \left(\frac{Re_p}{Re_w} \right)^{0.07} (n)^{-2.85}$	0.0228	CMC-1	Power-law	0.94	0.007	-	1.08	0.0173	0.88
			CMC-2		0.87	0.061	-	1.73	0.0173	0.88
			CMC-3		0.75	0.264	-	1.52	0.0173	0.88
Current study	$f_S = \beta_1 \left[\left(N_{Fr} \right)_{slug} \right]^{\beta_2}$	0.0762	Water	Newtonian	1.00	0.001	-	1.30	0.0157	1.2
	$f_s = \beta_1 \left[\left(N_{Fr} \right)_{slug} \right]^{\beta_2} \left[\frac{D_S}{D_{Ex}} \right]^{0.12} \left[\frac{R_{NR}}{Re_w} \right]^{0.11}$		CMC1	Power-law	0.71	0.0601	-	1.35	$\left[\frac{0.0226}{n} \right]^n$	$n^{0.2}$
			CMC4		0.57	0.405	-	1.51	$\left[\frac{0.0226}{n} \right]^n$	$n^{0.2}$
	$f_s = \beta_1 \left[\left(N_{Fr} \right)_{slug} \right]^{\beta_2} \left[\frac{D_S}{D_{Ex}} \right]^{0.12} \left[\frac{Re_g}{Re_w} \right]^{0.11}$		BXG2	Herschel-Bulkley	0.61	0.241	1.92	1.55	$\left[\frac{0.0226}{n} \right]^n$	$n^{0.2}$
			BXG4		0.56	0.415	3.06	1.72	$\left[\frac{0.0226}{n} \right]^n$	$n^{0.2}$

The values of C_1 for shear-thinning (Herschel-Bulkley fluid) does not match very well with Rosehart et al. [11] and Otten and Fayed 's [15] findings for shear-thinning (Herschel-Bulkley) systems, which are the only data for Herschel-Bulkley at this time. It is believed that the differences in the solution preparation and the rheological properties are the reasons behind the lack of agreement. Previous research has shown that the distribution parameter C_1 for low-viscosity liquids ranges from 1.0 to 1.35. However, Wallis [62] noted that the value of C_1 can be greater than 2 for fully developed laminar flow, despite the fact that his work stated that the exact behavior was to be determined.

3.7.5 Slug Frequency

The obtained experimental frequency results at x = 262D were compared to empirical correlations suggested by Gregory and Scott [16] for air-water, Picchi et al. [22] for power-law fluid and Rosehart et al. [11] and Otten and Fayed [15] for Herschel-Bulkley fluids. The slug frequency obtained from experimental results for air- water two-phase flow was compared against Gregory and Scott's correlations as shown in Figure 3-13. Gregory and Scott's model introduced the slug frequency as a function of Froude number, as follows:

$$f_S = 0.0157\left[\left(\mathrm{N}_{Fr}\right)_{slug}\right]^{1.2} \tag{3-38}$$

As can be seen in Figure 3-13, the points represent the measured experimental values, while the solid curves represent the theoretical model results. The dashed curves also represent Gregory and Scott's model for different slug velocities. The current experimental results showed a similar trend as Gregory and Scott's correlation. However, this trend shows that the predicted frequency in the current work is lower than that of Gregory and Scott's correlation where the superficial velocities of the water varied from 0.36 to 2.19 m/s. Because Gregory and Scott measured the slug frequencies

in a 19.05-mm pipe for a carbon dioxide/water system, the modified model in Eq.3-39 used in this study considered the effect of the pipe diameter. This modified model was chosen since it yielded the lowest standard deviation for all experimental data points. The same conduct was noted by when used a big pipe diameter Zabaras. [63].

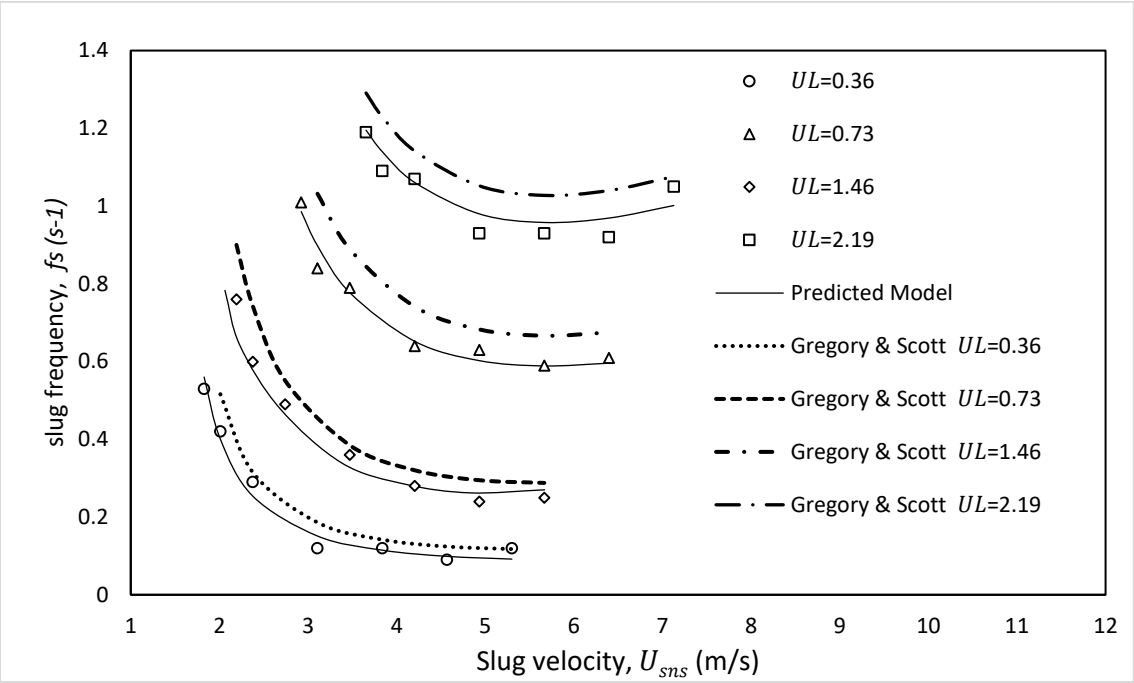

Figure 3-13. Measured slug velocity versus slug velocity for the flow of two air/water two-phas flow.

The parameter ∞ was determined by demanding that the average error for subsets be zero and the average absolute error for all data to be as small as possible. The following is the final correlation form and value ∞ =0.12:

$$f_S = 0.0226\left[\frac{U_{SL}}{gD}\left(\frac{19.75}{U_m} + U_m\right)\right]^{1.2} * \left[\frac{D_S}{D_{Ex}}\right]^{\infty} \quad (3\text{-}39)$$

The effect of slug velocity on slug frequency, where the slug frequency is calculated using Eq.3.39 are depicts in Figure 3-13 for four liquid flow rates. The slug frequency initially decreases to a

minimum value at a slug velocity of 4 to 6 m/s and then increases. When comparing the measured slug frequencies with the empirical equation proposed by Gregory and Scott [16] and our modified model in this study, an examination of these figures reveals that the predicted values of Gregory and Scott have the greatest affinity to the experimental results at a low slug velocity. However, when the slug velocity increases, the mean absolute relative error increases of 2.8–11.2%, respectively. A comparison of the prediction of Eq.3.39 with experimental data is also shown in Figure 3-13. Therefore, the new model was modified based on those results.

The experimental data and predictions of slug frequency for shear-thinning fluid (power-law and Herschel-Bulkley model) are shown in Figure 14 and 15, respectively.

Figure 14 shows the comparison between the measured and predicted frequency for the air-CMC1 solution systems by Eq.3.40 and Picchi et al [22]. We also modified the correlation of Picchi et al. [22] for the shear-thinning fluid (power-law model). The new structure of this correlation respected the flow behavior index (*n*) and the ratio between the Newtonian and non-Newtonian Reynolds numbers. The extended relationship yields are represented as follows:

$$f_S = \beta_1 [N_{\text{Froude}}]_{slug}^{\beta_2} \left[\frac{D_S}{D_{Ex}}\right]^{0.11} \left[\frac{Re_N}{Re_w}\right]^{0.11} \tag{3-40}$$

$$\text{Where} \qquad \beta_1 = \left[\frac{0.0157}{n}\right]^n$$

$$\text{and} \qquad \beta_2 = n^{0.2}$$

β_1 is the correlation coefficient, β_2 is the correlation exponent, $(\frac{D_S}{D_{Ex}})$ is the diameter corrected, Rew is the water Reynolds number, and R_{eN} is the Reynolds number for a power-law fluid

considering superficial conditions. Moreover, despite the fact that the implication of the term fluid behavior n in Eq.3-40 is unconventional, it allows for better agreement with experimental results for different shear-thinning fluid behavior values. The first attempt was by Rosehart et al. [17] and Otten and Fayed [21] to propose a correlation for the slug frequency that is valid for gas/non-Newtonian fluids. The frequencies are correlated using the relation of Gregory and Scott [16], which uses different values of the β_1 and β_2 for each non-Newtonian fluid that are summarized in Table 3-4.

Figure 3-14 illustrates the obtained experimental slug frequency as a function of slug velocity for shear-thinning fluid (CMC1). It was observed that the trend was similar to what Picchi et al. [22] obtained for the same fluid behavior. However, the frequency was with mean absolute relative error higher by 5.3–13.4%, relatively with the increase of liquid velocity when compared to the correlation of Picchi et al. [22].

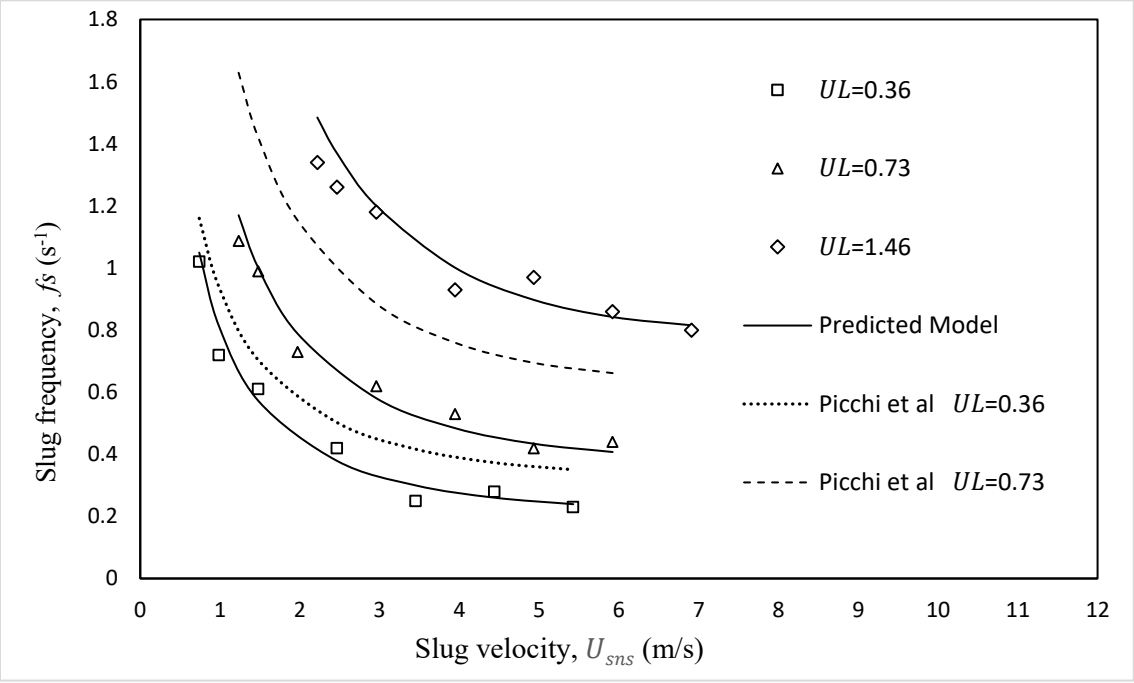

Figure 3-14. Measured slug velocity versus slug velocity for the flow of two air/ CMC1 power-law fluid.

Figure 3-15 depicts the effect of the flow rheology parameters of an air-CMC4 solution flow. The points represent the measured experimental values, while the solid curves represent the theoretical model results. The dashed curves also represent the model of Picchi et al. [22] for different slug velocities. With more effect of rheology parameters, the theoretical curves' deviation from the experimental results grows. As shown in Figure 3-15, the majority of the experimental data is within the 12% deviation range, indicating a reasonably good agreement between the theoretical model and the experimental results. The proposed theoretical model has also been validated with the available data. The aim is to propose a correlation that is valid for all rheology parameters (power-law and Herschel-Bulkley fluids) and to deliver a reasonable agreement.

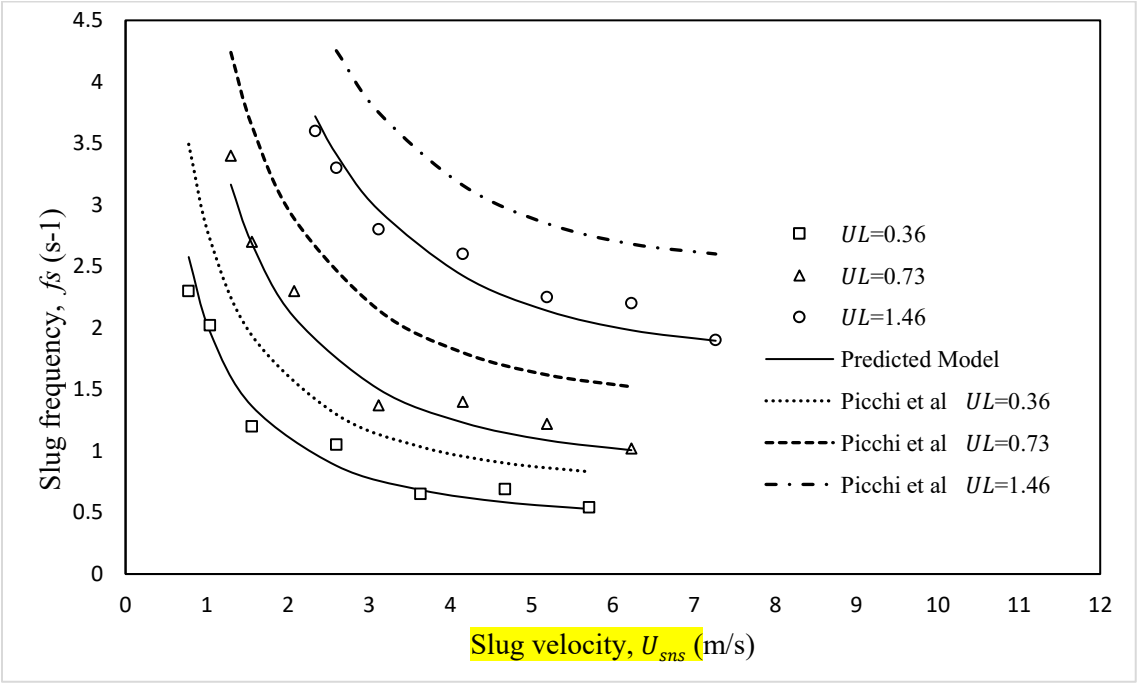

Figure 3-15. Measured slug velocity versus slug velocity for the flow of two air/ CMC4 power-law fluid.

To investigate the effects of different yield stress values on slug frequency, shear-thinning Herschel-Bulkley fluids through a horizontal pipe was performed experimentally. The Herschel-

Bulkley fluid (BXG2) with low effect of yield stress (1.92 Pa) and BXG4 fluid with a mild impact of yield stress (3.06 Pa) are shown in Figure 3-16 and Figure 3-17, respectively.

Figure 3-16 depicts the experimental results and the estimated slug frequency for BXG2 Herschel-Bulkley fluid. For all examinations, the slug frequency reduces with the increase of the slug velocity and was discovered to be less than approximately 5 to 7 m/s. In all cases studied, a constant slug frequency value was observed for higher slug velocities. It was observed that the slug frequency reduces with the increase of the no-slip velocity. However, the curves' patterns did not ensure or indicate whether the slug velocity would increase or not as a result of the limit of the experimental setup that produced a maximum slug velocity of 8 m/s. This is in contrast to the results previously discussed for the air/water due to the effect of viscosity differences.

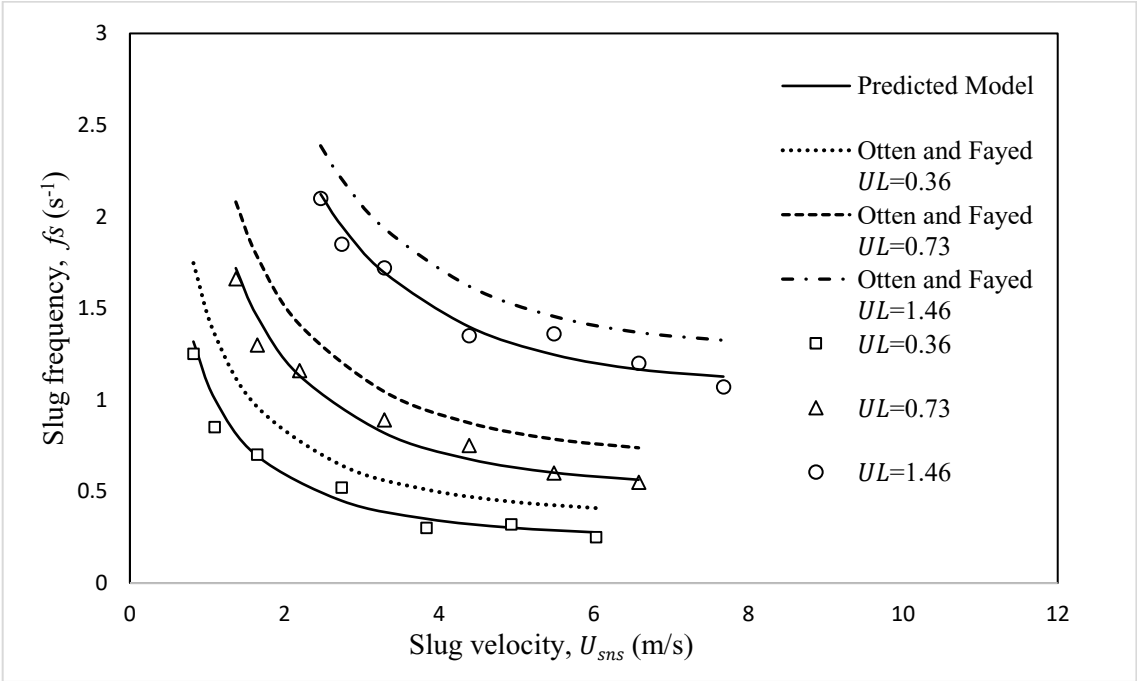

Figure 3-16. Measured slug velocity versus slug velocity for the flow of two air/ BXG2 Herschel-Bulkley fluid.

The extended relationship yields are represented as follows:

$$f_S = \beta_1 [N_{\text{Froude}}]_{slug}^{\beta_2} \left[\frac{D_S}{D_{Ex}}\right]^{0.11} \left[\frac{Re_g}{Re_w}\right]^{0.11} \quad (41)$$

Where $\beta_1 = \left[\frac{0.0157}{n}\right]^n$

and $\beta_2 = n^{0.2}$

Where R_{eg} is the Reynolds number for Herschel-Bulkley fluid considering superficial conditions in Eq. 2. Moreover, despite the fact that the implication of the fluid behavior n in Eq.3-41 is unconventional, it allows for better agreement with experimental results for different shear-thinning Herschel-Bulkley model. Figure 3-17 shows the observations of the increased effects of the rheological parameters and the higher presence of yield stress of the air and highly concentrated BXG4 experimental results and predictions.

The results of the present study observed a similar experimental trend as Otten and Fayed [15] for the air/Carbopol 941 solution system. The Carbopol 941 solutions exhibit non-Newtonian flow properties of the Herschel-Bulkley model. However, this trend shows that the frequency predicted in the present work tends to be lower than that in Otten and Fayed's work. The lack of agreement is most likely due to a difference in rheological properties caused by differences in the solution preparation.

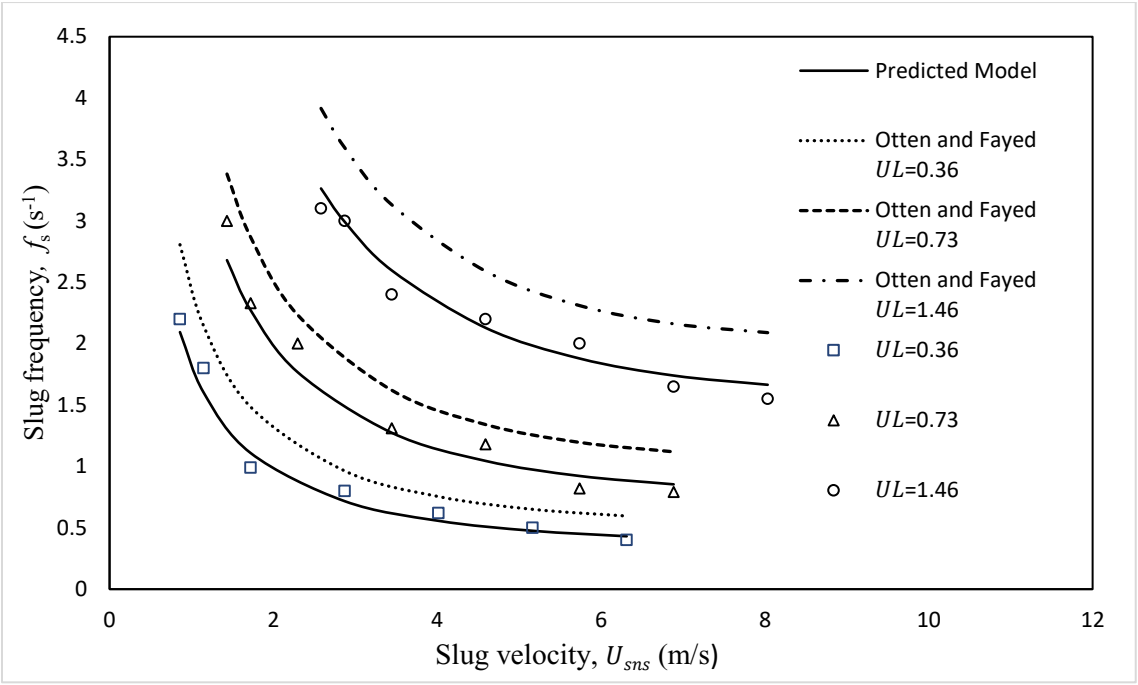

Figure 3-17. Measured slug velocity versus slug velocity for the flow of two air/ BXG4 Herschel-Bulkley fluid.

Figure 3-17 shows that up to 7 m/s, the slug frequency was decreasing with the increase of slug velocity for all tested superficial liquid velocities. As a result of the greater effect of yield stress at lower superficial liquid velocities, the slug frequency rise rises sharply, whereas at higher liquid velocities, the slug frequency decreases. As the liquid velocity increases, more energy is needed by the air to propel the viscous fluid. The model for the shear-thinning Herschel-Bulkley fluid was modified and used in this study based on our experimental results. The modifications we made also considered the observations of Rosehart [17] and Otten and Fayed [21] and the correlations of Gregory & Scott [16].

3.8 Conclusions

In the present work, experimental and CFD studies were conducted for the purpose of investigating the effect of the rheological parameters of flow regime maps for air/Newtonian and air/shear

thinning fluids on the transition boundaries in a two-phase model. The slug flow characteristics such as slug translational velocities and slug frequency were captured by visual observations. The experiments were achieved in a 3-inch PVC horizontal pipe to study the flow characteristics of water and four different shear-thinning solutions. The VOF model in ANSYS Fluent 19 was implemented for detecting flow regimes and investigating the influence of the rheological parameters on the flow pattern maps.

This work evaluated the flow regime maps reported by previous researchers, and modifications have been performed based on the findings of this experimental work. Meanwhile, the developed transition boundaries of the maps were compared with our experimental results and previous published studies. For the air- water flow, most of the experimental testing points reported by Mandhane et al and Taitel and Dukler fall within the boundaries of the corresponding flow maps.

The rheological parameters' effect on the transition boundaries of the flow regime transitions were observed. The plug to slug transition was observed to shift right and pass the line of Mandhane [7] at higher liquid and gas velocities. For flow regime transition boundaries, air-CMC1 and air-CMC4 power-law fluids, Chhabra & Richardson [6] was almost matching the experimental flow regime transition in the interval of dispersed bubbly flow to plug or slug flow. However, the transition from plug to slug flow was not considered in the regime map of Chhabra & Richardson [6]. When compared with the flow map of Mandhane et al. [7], No cases of transition were observed from plug to slug flow for air-CMC1 with a low concentration. Moreover, one case of transition was observed to begin earlier from plug to slug flow for air-CMC4. The predicted boundary of Mandhane et al. [7] flow map that considered the effect of the viscosity power-law fluid agreed well with the experimental maps of the transition boundary from plug to slug flow. The effect of yield stress of Herschel-Bulkley fluids on the flow pattern maps were also observed for two cases

with a low effect (1.92 Pa) and a mild impact of yield stress (3.06 Pa). The effect of viscosity and yield stress applied to the modified X value between plug and slug flow in the boundaries of Mandhane et al.'s [7] flow map for the air-BXG2 and BXG4 Herschel-Bulkley fluids were considered. The transition line of the regions' plug and slug flow patterns were found to shift to the right due to increases in the solution mass fraction. The modified predicted boundary to the Mandhane et al. [7] flow map that considered the effect of solid plug (diameter affect) of Herschel-Bulkley fluid is well agreed with the transition boundary from plug to slug flow with the experimental maps. The number of bubbles in the liquid plug-slug flow increases with the increasing concentration of shear-thinning working fluids, which are produced by the shear between the liquid film and the gas slug. Due to the viscosity and relative motion, the bubbles conglomerate and travel beneath the large bubble. Also, the experimental results show that the slug velocity increases with increased concentrations and the no-slip velocity at the same operating conditions. The slug translational velocity was developed from experimental results for water and two shear-thinning models. A statistical evaluation of the existing correlations against experimental results showed that the developed model had better predictions for the shear-thinning fluid. The correlations developed in this work require further testing on a broader range of data sets to be more reliable. The more data used to generate it, the greater its predictive power over a broader range of conditions, fluid rheology, and pipe sizes. As a result, our measurements were obtained using one pipe diameter.

Author Contributions: Conceptualization, A.I.; methodology, A.I., A.A., M.A.R. and S.B.; investigation, experimental, and numerical simulations, A.I.; Writing—original draft, A.I.; Writing—reviewing and editing, A.I. and A.A. proofreading, A.I, A.A.; supervision, M.A.R. and S.B. All authors have read and agreed to the published version of the manuscript.

Funding: This research received no external funding.

Conflicts of Interest: The authors declare no conflicts of interest.

3.9 References

1. Chhabra, R. P., Richardson, J. F. (1986). The co-current horizontal and vertical upward flow of gas and non- Newtonian liquid. Encyclopedia of Fluid Mechanics, 3, 563-609.
2. Dziubinski, M. (1995). A General Correlation for 2-Phase Pressure-Drop in Intermittent Flow of Gas and Non- Newtonian Liquid-Mixtures in a Pipe. Chemical engineering research and design, 73(5), 528-534.
3. Oliver, D. R., Hoon, A. Y. (1968). 2-phase non-Newtonian flow heat transfer. Transactions of the Institution of Chemical Engineers and the Chemical Engineer, 46(4), T116.
4. Astarita, G., & Apuzzo, G. (1965). Motion of gas bubbles in non-Newtonian liquids. AIChE Journal, 11(5), 815-820..
5. Hassager, O. (1979). Negative wake behind bubbles in non-Newtonian liquids. Nature, 279(5712), 402-403. Chhabra, R. P., Richardson, J. F. (1984). Prediction of flow pattern for the co-current flow of gas and non-Newtonian liquid in horizontal pipes. The Canadian Journal of Chemical Engineering, 62(4), 449-454.
6. Chhabra, R. P., Richardson, J. F. (1984). Prediction of flow pattern for the co-current flow of gas and non-Newtonian liquid in horizontal pipes. The Canadian Journal of Chemical Engineering, 62(4), 449-454.
7. Mandhane, J. M., Gregory, G. A., Aziz, K. (1974). A flow pattern map for gas-liquid flow in horizontal pipes. International Journal of MULtiphase Flow, 1(4), 537-553.

8. Taitel, Y., & Dukler, A. E. (1976). A model for predicting flow regime transitions in horizontal and near horizontal gas-liquid flow. AIChE journal, 22(1), 47-55.
9. Chhabra, R. P., Richardson, J. F. (1986). The co-current horizontal and vertical upward flow of gas and non- Newtonian liquid. Encyclopedia of Fluid Mechanics, 3, 563-609.
10. Dziubinski, M. (1995). A General Correlation for 2-Phase Pressure-Drop in Intermittent Flow of Gas and Non- Newtonian Liquid-Mixtures in a Pipe. Chemical engineering research and design, 73(5), 528-534.
11. Oliver, D. R., Hoon, A. Y. (1968). 2-phase non-Newtonian flow heat transfer. Transactions of the Institution of Chemical Engineers and the Chemical Engineer, 46(4), T116.
12. Srivastava, R. P. S., Narasimhamurty, G. S. R. (1973). Hydrodynamics of non-Newtonian two-phase flow in pipes. Chemical Engineering Science, 28(2), 553-558.
13. Srivastava, R. P. S., Narasimhamurthy, G. S. R. (1981). Void Fraction and Flow Pattern during Two-Phase Flow of Pseudoplastic Fluids. The Chemical Engineering Journal, 21(2), 165-176.
14. Chhabra, R. P., Richardson, J. F. (1984). Prediction of flow pattern for the co-current flow of gas and non-Newtonian liquid in horizontal pipes. The Canadian Journal of Chemical Engineering, 62(4), 449-454.
15. Weisman, J., Duncan, D. G. J. C. T., Gibson, J., Crawford, T. (1979). Effects of fluid properties and pipe diameter on two-phase flow patterns in horizontal lines. International Journal of Multiphase Flow, 5(6), 437-462.
16. Gregory, G.A.; Scott, D.S. Correlation of liquid slug velocity and frequency in horizontal concurrent gas-liquidslug flow. AIChE J. 1969, 15, 933–935.

17. Rosehart, R. G., Rhodes, E., & Scott, D. S. (1975). Studies of gas→ liquid (non-Newtonian) slug flow: void fraction meter, void fraction and slug characteristics. The Chemical Engineering Journal, 10(1), 57-64.
18. Hubbard, M.G. An Analysis of Horizontal Gas-Liquid Slug Flow; University of Houston: Houston, TX, USA, 1965.
19. Hubbard, M.G.; Dukler, A.E. The characterization of flow regimes for horizontal two-phase flow. Proc. Heat Transf. Fluid 1966, 1996, 100–121.
20. Otten, L., & Fayed, A. S. (1976). Pressure drop and drag reduction in two-phase non-Newtonian slug flow. The Canadian Journal of Chemical Engineering, 54(1-2), 111-114.
21. Otten, L.; Fayed, A.S. Slug velocity and slug frequency measurements in concurrent air-non-Newtonian slug flow. Trans. Inst. Chem. Eng. 1977, 55, 64–67.
22. Picchi, D., Manerba, Y., Correra, S., Margarone, M., Poesio, P. (2015). Gas/shear-thinning liquid flows through pipes: Modeling and experiments. International Journal of MULtiphase Flow, 73, 217-226.
23. Bendiksen, K.H.; Langsholt, M.; Liu, L. An experimental investigation of the motion of long bubbles in high viscosity slug flow in horizontal pipes. Int. J. Multiphase. Flow 2018, 104, 60–73.
24. Al-kayiem, H.H.; Mohmmed, A.O.; Al-hashimy, Z.I.; Time, R.W. Statistical assessment of experimental observation on the slug body length and slug translational velocity in a horizontal pipe. Int. J. Heat Mass Transf. 2017, 105, 252–260.
25. Baba, Y. D., Archibong-Eso, A., Aliyu, A. M., Fajemidupe, O. T., Ribeiro, J. X., Lao, L., & Yeung, H. (2019). Slug translational velocity for highly viscous oil and gas flows in horizontal pipes. Fluids, 4(3), 170.

26. Gokcal, B. E_ects of High Oil Viscosity on Oil/Gas Flow Behavior in Horizontal Pipes. Master's Thesis, University of Tulsa, Tulsa, OK, USA, 2006.
27. Jeyachandra, B.C.; Gokcal, B.; Al-Sarkhi, A.; Serica, C.; Sharma, A.K. Drift-Velocity Closure Relationships for Slug Two-Phase High-Viscosity Oil Flow in Pipes. Soc. Pet. Eng. 2012, 17, 593–601.
28. Baungartner, R., J., Loureiro, G., Freire, A. (2017). Horizontal Pipe Slug Flow of Air/Shear-thinning Fluid Experiments and Modelling. Multiphase Flow Journeys, 4, 2017-0053. March 27, 2017.
29. Farooqi, S.I., Heywood, N.I., Richardson, J.F., 1980. Drag reduction by air injection for highly shear-thinning suspensions in horizontal pipe flow. Trans. IChemE 58, 16–27.
30. Lockhart, R. W., Martinelli, R. C. (1949). Proposed correlation of data for isothermal two-phase, two-component flow in pipes. Chem. Eng. Prog, 45(1), 39-48.
31. Dziubinski, M. (1996). A general correlation for two-phase pressure drop in intermittent flow of gas and non-Newtonian liquid mixtures in a pipe. International Journal of Multiphase Flow, 22(S1), 101-101.
32. Ruiz-Viera, M. J., Delgado, M. A., Franco, J. M., Sánchez, M. C., Gallegos, C. (2006). On the drag reduction for the two-phase horizontal pipe flow of highly viscous non-Newtonian liquid/air mixtures: Case of lubricating grease. International Journal of Multiphase Flow, 32(2), 232-247.
33. Xu, J. Y., Wu, Y. X., Shi, Z. H., Lao, L. Y., Li, D. H. (2007). Studies on two-phase co-current air/non-Newtonian shear-thinning fluid flows in inclined smooth pipes. International Journal of Multiphase Flow, 33(9), 948-969.

34. Rahman, M. A., Heidrick, T., & Fleck, B. A. (2009, January). Characterizing the two-phase, air/liquid spray profile using a phase-doppler-particle-analyzer. In IOP Journal of Physics–conference series (Vol. 147, pp. 1-15).
35. Barooah, A., Khan, M. S., Khaled, M. S., Rahman, M. A., Hassan, I., Hasan, R., & Hascakir, B. (2022). Investigation of cutting transport in horizontal/deviated annulus using visualization and pressure drop techniques for two-phase slurry flow. Journal of Natural Gas Science and Engineering, 100, 104460.
36. Morshed, M.; Khan, M.S.; Rahman, M.A.; Imtiaz, S. Flow Regime, Slug Frequency and Wavelet Analysis of Air/Newtonian and Air/non-Newtonian Two-Phase Flow. Appl. Sci. 2020, 10, 3272. https://doi.org/10.3390/app10093272
37. Manikonda, K., Islam, R., Obi, C. E., Hasan, A. R., Sleiti, A. K., Abdelrazeq, M. W., ... & Rahman, M. A. (2022, February). Horizontal Two-Phase Flow Regime Identification with Machine Learning Classification Models. In International Petroleum Technology Conference (p. D011S021R002). IPTC.
38. Zahid, A. A., Ur Rehman, S. R., Rushd, S., Hasan, A., & Rahman, M. A. (2020). Experimental investigation of multiphase flow behavior in drilling annuli using high speed visualization technique. Frontiers in Energy, 14, 635-643.
39. Ko, T., Choi, H. G., Bai, R., Joseph, D. D. (2002). Finite element method simulation of turbulent wavy core-annULar flows using a k–ω turbulence model method. International Journal of Multiphase Flow, 28(7), 1205-1222
40. Lo, S., Tomasello, A. (2010). Recent progress in CFD modeling of multiphase flow in horizontal and near-horizontal pipes. In 7th North American Conference on Multiphase Technology. BHR Group.

41. Al-Yaari, M. A., Abu-Sharkh, B. F. (2011). CFD prediction of stratified oil-water flow in a horizontal pipe. Asian Transactions on Engineering, 1(5), 68-75.
42. Jia, N., Gourma, M., Thompson, C. P. (2011). Non-Newtonian mulita-phase flows: On drag reduction, pressure drop and liquid wall friction factor. Chemical engineering science, 66(20), 4742-4756.
43. Kroes, R. F., Henkes, R. A. W. M. (2014). CFD for the motion of elongated gas bubbles in viscous liquid. In 9th North American Conference on Multiphase Technology. BHR Group.
44. Sanderse, B., Haspels, M., Henkes, R. A. W. M. (2015). Simulation of Elongated Bubbles in a Channel Using the Two-Fluid Model. Journal of Dispersion Science and Technology, 36(10), 1407-1418.
45. Ihmoudah, A., Awad, M. M., Rahman, M. A., & Butt, S. D. (2019, June). Experimental and Numerical Investigation of Gas-Yield Power-Law Fluids in a Horizontal Pipe. In International Conference on Offshore Mechanics and Arctic Engineering (Vol. 58875, p. V008T11A013). American Society of Mechanical Engineers.
46. Metzner, A. B., & Reed, J. C. (1955). Flow of non-Newtonian fluids—correlation of the laminar, transition, and turbulent-flow regions. Aiche journal, 1(4), 434-440.
47. Ihmoudah, A., Abugharara, A., Rahman, M. A., & Butt, S. (2023). Experimental and Numerical Analysis of the Effect of Rheological Models on Measurements of Shear-Thinning Fluid Flow in Smooth Pipes. Energies, 16(8), 3478.
48. Heywood, N. I., and Cheng, D. C.-H. (1984). “Comparison of methods for predicting headloss in turbulent pipe-flow of non-Newtonian fluids”. Trans. Inst. Meas. Control, 6(1), 33–45.
49. Chhabra, R. P., and Richardson, J. F. (2008). Non-Newtonian flow in the process industries, 2nd Ed., Butterworth-Heinemann, Oxford, U.K.

50. Ostwald, W. (1925). Ueber die geschwindigkeitsfunktion der viskosität disperser systeme. i. Kolloid-Zeitschrift, 36(2), 99-117.
51. Herschel, W.H.; Bulkley, R. Measurement of consistency as applied to rubber-benzene solutions. Proc. ASTM Part II 1926, 26,621–629.
52. ANSYS FLUENT Theory Guide 15.0; ANSYS, Inc.: Canonsburg, PA, USA, 2013. Available online: http://www.ansys.com (accessed on 5 March 2023).
53. Papanastasiou, T.C. Flows of materials with yield. J. Rheol. 1987, 31, 385–404
54. Field, B. S., & Hrnjak, P. S. (2007). Two-phase pressure drop and flow regime of refrigerants and refrigerant-oil mixtures in small channels. Air Conditioning and Refrigeration Center. College of Engineering. University of Illinois at Urbana-Champaign.
55. Nicklin, D. J. (1962). Two-phase flow in vertical tubes, Trans. Inst. Chem. Engr., 40(1), 61-68. 1965.
56. Bird, R.B., Armstrong, R.C. and Hassager, O., Dynamics of Polymeric Liquids, Vol. 1, Fluid Dynamics, 2nd edn. Wiley, New York (1987).
57. Woods, B. D., Fan, Z., & Hanratty, T. J. (2006). Frequency and development of slugs in a horizontal pipe at largeliquid flows. International Journal of Multiphase Flow, 32(8), 902-925.
58. Gokcal, B., Al-Sarkhi, A., Sarica, C., & Alsafran, E. M. (2009, January). Prediction of slug frequency for high viscosity oils in horizontal pipes. In SPE Annual Technical Conference and Exhibition. Society of Petroleum Engineers.
59. Azzi, A., Al-Attiyah, A., Qi, L., Cheema, W., & Azzopardi, B. J. (2010). Gas–liquid two-phase flow division at a micro-T-junction. Chemical Engineering Science, 65(13), 3986-3993.

60. Abdulkadir, M., Hernandez-Perez, V., Lowndes, I. S., Azzopardi, B. J., & Sam-Mbomah, E. (2016). Experimental study of the hydrodynamic behaviour of slug flow in a horizontal pipe. Chemical Engineering Science, 156, 147-161.
61. Baba, Y. D., Archibong, A. E., Aliyu, A. M., & Ameen, A. I. (2017). Slug frequency in high viscosity oil-gas two-phase flow: Experiment and prediction. Flow Measurement and Instrumentation, 54, 109-123.
62. Wallis, G.B. One-Dimensional Two-Phase Flow; American Institute of Chemical Engineers: New York, NY, USA, 1969.
63. Zabaras, G. J. (2000). Prediction of slug frequency for gas/liquid flows. SPE journal, 5(03), 252-258.

Chapter 4: Effect of Rheological Properties of Yield Pseudoplastic Fluids on Slugs Characteristics in an Upward Vertical Pipe: Experiments and Modeling

Abdalsalam Ihmoudah[1], Mohamed M. Awad[2], Mohammad Azizur Rahman[3] and Stephen Butt[1]

[1]Memorial University of Newfoundland.

[2]Mansoura University, Egypt

[3]Texas A&M University at Qatar, Doha, Qatar

This chapter is based on the objectives defined in Section 1.3.1 and was presented at ASME 2020, the 39th International Conference on Ocean, Offshore, and Arctic Engineering (OMAE-2020), held in Fort Lauderdale, FL, USA, June 28–July 3, 2020.

Co-authorship Statement

Abdalsalam Ihmoudah is the first author of this manuscript, along with co-authors Dr. Mohamed Awad, Dr. Mohammad Azizur Rahman, and Dr. Stephen Butt. I proposed the idea and concept, conducted a literature review, and prepared the fluid samples. I collected and analyzed the numerical simulation results. Dr. Awad, Dr. Aziz, and Dr. Butt evaluated the methodology and reviewed the manuscript. Manuscript preparation is mainly contributed by Abdelsalam Ihmoudah, with revision assistance provided by all other coauthors.

ABSTRACT

Two-phase flow of gas/yield Pseudoplastic fluids can be found in different industrial applications like the chemical processes, oil industry, and petroleum transport in pipelines. In this study, experimental and numerical investigation of the influence of Rheological properties of non-

Newtonians fluids in two-phase flow (gas/yield Pseudoplastic fluids) on slug characteristics in an upward vertical flow were performed. Different concentrations of Xanthan gum solutions (0.05%, 0.10%, and 0.15%, by w/w), which are referred to as non-Newtonian, yield Pseudoplastic behavior used as the working liquids and air as a gas. The experiments were conducted in an open-loop re-circulating system has a total length of 65 m to ensure phase mixing and authorize flow regime patterns to develop. The vertical pipe has a diameter of 76.3 mm. API-compliant 8-speed rotational viscometer model 800 was used to measure the rheological properties of non-Newtonian fluids. Flow visualization and recording videos were achieved by a high-speed camera to a comparison between behavior of Newtonian and non-Newtonian fluids in the two-phase model. Pressure transducers used to measure high-response pressure. Computational fluid dynamics software (ANSYS fluent 2019 R3) was used for the numerical investigation. The volume of fluid (VOF) model has been chosen for tracking immiscible fluids. The CFD simulation results were compared to the experimental data. The slug behavior and shape were noticed to be affected by changing the rheological properties of the liquid phase. With increasing XG concentration at the same operations conditions, we found that non-uniform and random distribution of small bubbles due to the effective viscous force of a liquid phase.

4.1 Introduction

Multiphase flows can be found in a variety of industrial applications, including in the oil and gas (O&G) industry. Nowadays, multiphase flow is being employed in upstream petroleum processing [1]. Among two-phase types of flows, precisely the slug flow is the most frequently used. In general terms, upward slug flow can be described as intermittent multiphase flow patterns that feature elongated bullet-shaped bubbles in sequence, trailed by liquid deposits underneath the bubble [2]. Slug flow's hydrodynamics can be quite complex as a result of numerous factors, the main ones

being fluids properties or the rheologies, flow intermittency, pipe orientation, geometry dependence, and the presence of Taylor bubbles. These factors and others may lead to systemic instability [2]. However, slug flow is well known for its characteristics of irregularity, randomness, and intermittency, properties that are caused in large part by the flow's unbalanced character, as well as the length of the liquid slugs and elongated bubbles. Also contributing to slug flow properties is how many slugs pass by a certain point in a pipe within a specific time duration [3] Another characteristic of multiphase flow is the presence of non-Newtonian fluids, in particular, shear-thinning fluids. Examples of non-Newtonian fluids include slurries, gelled oils, drilling muds, fracturing fluid, and waxy crude oils [1, 3]. The literature contains several studies that focus on non-Newtonian fluids. In one of the earliest, Chhabra and Richardson [4] carried out experiments work to explore the characteristics of gas/non-Newtonian liquid fluid flows. Their focus was on how these flows performed within horizontal pipelines. In their study, the researchers also sourced data from the literature, proposing a modified Newtonian version of Mandhane et al.'s [5] correlation related to transitions in flow patterns. Rosehart et al. [6] also carried out an investigation on gas-liquid (non-Newtonian) slug flow. In their work, they used three diverse polymer solutions in different concentrations and applied the power-law model for determining slug properties (e.g., slug velocity and frequency) and void fractions. In [7], Otten and Fayed continued along the same research path as Rosehart et al. [6] carried out an investigation on gas-liquid (non-Newtonian) slug flow. In their work, they used three polymer solutions of the power-law model to determining slug properties in a horizontal pipe. Otten and Fayed [7] conducted experiments with polymers to determine drag reduction and pressure drop in gas-liquid slug flow. Khatib and Richardson [8] used air-Kaolin suspension holdups in water, analyzing their data in accordance with the approach used in Zuber and Findlay's [9] study. Chandraker et al. [10] investigated how gas/non-Newtonian two-phase flows performed under enhancements to the gas-

liquid mixing process and proposed several correlations for holdup predictions related to systemic dynamic and physical variables. In [11] and based on their experimental work on the holdup factor in gas/non-Newtonian liquid mixtures for horizontal and vertical pipeline flows, Das et al. suggested a range of correlations for predicting holdup within slug flow patterns. Meanwhile, Dziubinski [12] introduced a semi-theoretical approach to experimental data correlation for single- or two-phase gas and non-Newtonian flows, and Xu et al. [13] experimentally and theoretically examined two-phase air/non-Newtonian shear-thinning fluid flows within smooth pipes. In recent work, the researchers focused on how liquid properties affect aspects such as pressure drop, void fraction, and flow patterns. More Recent Picchi et al. [14] studied air/shear-thinning liquid systems for horizontal and inclined pipelines, while Heywood and Charles [15] investigated holdup and pressure drop in stratified gas/non-Newtonian liquid flows, using the power-law model adopted by Ostwald-deWaele [15]. In their work, Bishop and Deshpande [16] applied the Heywood-Charles model, finding it mostly invalid when used in determining a two-phase drag reduction for stratified flow. Picchi et al. [17] investigated gas/non-Newtonian power-law fluid stratified pipe flow. Ihmoudah et al. [18] numerically investigated the effect of yield power-law of non-Newtonian fluids parameters on pressure drop in a horizontal pipe. Ratkovich et al. [19] employed a Computational Fluid Dynamics (CFD) model in order to determine how Newtonian fluid slug flow impacted surface shear stress for vertical tubular membranes. Also relying on CFD, Taha and Cui [20] used a commercial package (fluent) for examining Taylor bubbles occurring in vertical pipelines, focusing in particular on flowing as well as stagnant liquids. The researchers' findings on velocity, shape and distribution of the slugs agreed well with findings from the literature [20]. Finally, Ratkovich et al. [21] used CFD as well, investigating two-phase slug flows of Newtonian and non-Newtonian liquids within vertical pipeline environments to determine void fraction. These researchers applied the two-phase CFD model in Star CCM+ and also included the VOF (volume

of fluid) model. Ihmoudah et al. [22] investigated experimentally and numerically (CFD) the effect of yield power-law of non-Newtonian fluids parameters on slug flow in a horizontal pipe.

The present work will investigate the validity of using computational fluid dynamics (CFD) ANSYS fluent software in a two-phase model to examine the effect of the rheology parameters non-Newtonian in for turbulent model on slug's characteristics in an upward vertical pipe. Water and three non-Newtonian were referred to yield pseudoplastic fluids that will apply as working fluids and air as gas to evaluate the accuracy of the simulation results. The results of the developed model in ANSYS Fluent 2019R3 will be validating to experimental results for two-phase flow air-Newtonian fluid. Flow visualization and recording videos will be achieved by using a High-speed camera and pressure transducers to analyze pressure fluctuations for both Newtonian and non-Newtonian fluids.

4.2 Material and Procedure

4.2.1 Fluid Rheology

There are different rheological models that can be used in describing the rheological behavior for non-Newtonian fluids depends on the non-linear relation between shear rate and shear stress. The pseudoplastic or power-law model or shear-thinning fluid has two parameters to describe the behavior of the liquid. As shown in Figure 4-1, the shear stress and shear rate relationship of the fluid passes through the origin with a power-law shape. Eq. (4.2) describes the behavior of a power-law fluid [23].

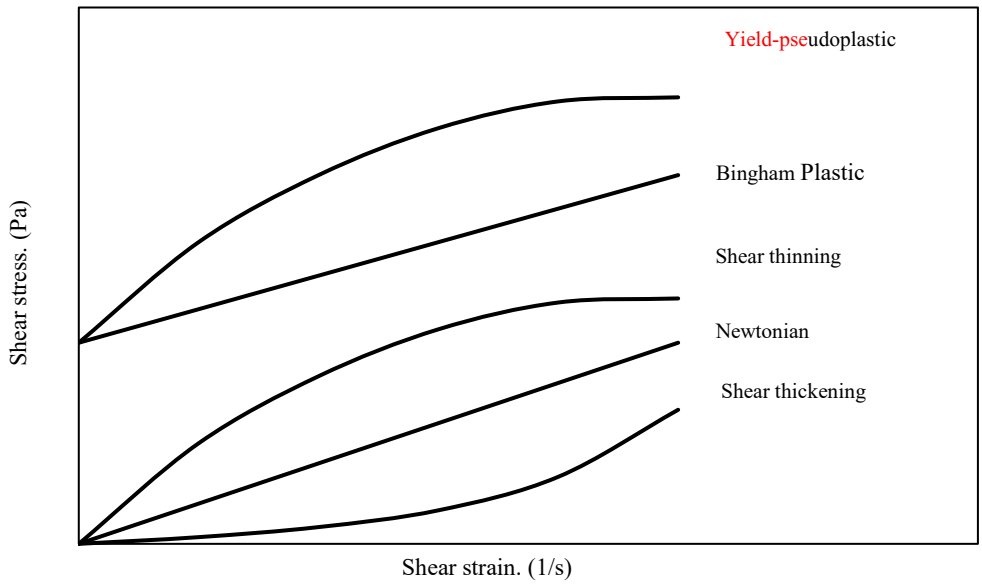

Figure 4-1. Shear stress vs. shear strain rate for different types of non-Newtonian fluids

$$\tau = k\,\gamma^{n} \tag{4.1}$$

Herschel and Bulkley or pseudoplastic or yield power-law fluid have three parameters to describe the behavior of the fluid [25].

$$\tau = \tau o + k\,\gamma^{n} \qquad (\tau > \tau o) \tag{4.2}$$

As can see in Figure 1, these types of fluids exhibit yield stress, requiring minimum stress to initiate flow. “Yield-Power Law Model More Accurately Predicts Mud Rheology" [25]

Material and Procedure

4.2.2 Fluid Preparation

In this study, water is represented as the Newtonian liquid phase, and three solutions of Xanthan gum (XG) served as non-Newtonian phases. The non-Newtonian phases have three separate

concentrations according to weight (XG-1, XG-2, and XG-3) prepared and tested in the Drilling Technology Laboratory (DTL) by the addition of polymer powders (dried) to water. An 8-speed API-compliant rotational viscometer (Model 800) used to measure the XG solutions' rheology and characteristics, details are shown in table 4-1. The liquids display behavior of the yield pseudoplastic shear thinning model.

Determine the Critical velocity of non-Newtonian fluids. Slatter [26] modified Reynolds number to determine the criterion of yield-pseudoplastic or Herschel–Bulkley behaver fluid transition from laminar to turbulent as:

$$R_{eg} = \frac{8\rho {v_{ann}}^2}{\tau_y + K\left(\frac{8v_{ann}}{D_{shear}}\right)^n} \quad \text{Laminar at } R_{eg} \leq 2100 \tag{4.3}$$

Where

$$v_{ann} = \frac{Q - Q_{Plug}}{\pi(r - r_{Pulg})} R$$

$$r_{Pulg} = \frac{\tau_y}{\tau_0} R$$

$$D_{shear} = D - D_{plug}$$

$$D_{plug} = 2\, r_{Pulg}$$

$$Q = \pi n r^3 \left(\frac{\tau_w}{k}\right)^{\frac{1}{n}} (1-\zeta)^{n+1/n} \left(\frac{(1-\zeta)^2}{3n+1} + \frac{2\zeta(1-\zeta)}{2n+1} + \frac{\zeta^2}{n+1}\right) \tag{4.4}$$

Table 4-1. Non-Newtonian fluid properties at different concentrations,

Symbol	Con. % (g/0.350L)	τ_y (Pa)	K (Pa.s^n)	n	ρ (kg/m^3)
XG-1	0.017	0.4	0.037	0.65	1000
XG-2	0.035	0.7	0.131	0.56	1002
XG-3	0.052	1.33	0.353	0.43	1005

4.3 Experimental Unit

The measurements were performed using air and three different concentrations of non-Newtonian fluid in a 3-in flow loop at the Memorial University of Newfoundland. The flow loop is an open-loop re-circulating system has a total length of 65 m to ensure phase mixing and authorize flow regime patterns to develop Figure 2. The loop is built of a 76 mm diameter clear PVC pipe. A 3000-liter (792.5 gallons) reservoir tank and an inverter to control the centrifugal pump with the maximum flow rate up to 220 GPM. Omega FTB-730 turbine flow meter with a range of 3 ~ 400 GPM and with an accuracy of ± 1% of the full scale was used to measure the volumetric flow rate of working fluids. Five Omega PX603-100G5V pressure transducers provided the pressure data, with every section had two pressure transducers to measure high-response pressure. Two parallel Omega air flow meters with ranges of 0.5~42.5 m³/h and 10~100 m³/h were composite in the compressed airline. Steel platform with 5 m to permits comfortable access to the vertical test section. A high-speed camera was located 56 L/D from the nearest elbow in the vertical section to obtain bubble velocities, frequencies of passage and change in a bubble shape. To evaluate the effect flow rates of air-water and air/non-Newtonian fluids on slug characteristics. Four cases were

established according to the limitation of the experiment's unit. The sum of differential pressure, the frictional pressure, and the momentum pressure difference as:

$$\Delta P_T = \Delta P_D + \Delta P_F + \Delta P_M \tag{4.5}$$

For each experiment, the differential pressure data were collected from two points of the ascending pipe. Based on these measurements, the mean void fraction α was obtained from Bernoulli's principle of energy balance. [27]

$$\alpha_g = 1 - \frac{\Delta P_D}{\rho_l g h} + \frac{2C_f v^2}{gD} \tag{4.6}$$

For the gas/non-Newtonian fluids flow, the liquid void fraction is determined as [13]:

$$\alpha_g = \frac{1}{1+3.166*10^{-5}\, Re_{tp}{}^{1.225}} \tag{4.7}$$

4.4 Numerical Modeling

The volume of fluid VOF model in AYSAS Fluent was adopted to track the interface between the gas and liquid by defined the changing in the volume fractions of fluid in the computational domain [28]. The two-phase model is governed by equations of continuity and momentum as:

Equation of continuity:

$$\frac{\partial \rho}{\partial t} + \nabla.\left(\rho\, \vec{U}\right) = 0 \tag{4.8}$$

The equation of Momentum:

$$\frac{\partial(\rho \vec{U})}{\partial \mathrm{t}} + \nabla.\left(\rho \vec{U}\vec{U}\right) = -\nabla P + \nabla.\bar{\bar{\tau}} + \rho g + F_{ST} \tag{4.9}$$

The mixture density and viscosity of the contents of each call are as follows:

$$\rho = a_2\rho_2 + (1 - a_2)\rho_1 \tag{4.10}$$

$$\eta = a_2\rho\eta_2 + (1 - a_2)\eta_1 \tag{4.11}$$

4.4.1 Turbulence model

The turbulent model considers since the Reynolds numbers and modified Reynolds numbers for non-Newtonian fluid were in the range of turbulent flow. Several models have been developed in CFD software ANSYS FLUENT commercials such as $\kappa-\epsilon$ model, large eddy simulation (LES) and $\kappa-\omega$ model. In this study applied Reynolds-averaged Navier-Stokes (RANS) selected to solving two transport equation model are shown as:

$$\frac{\partial}{\partial t}(\rho k) + \frac{\partial}{\partial x_i}(\rho k u_i) = \frac{\partial}{\partial x_i}\left[\mu_{\text{eff}}\alpha_k \frac{\partial k}{\partial x_j}\right] + G_k + G_b - \rho\varepsilon \tag{4.12}$$

$$(\rho\varepsilon) + \frac{\partial}{\partial x_i}(\rho\epsilon u_i) = \frac{\partial}{\partial x_i}\left[\mu_{\text{eff}}\alpha_{k\varepsilon} \frac{\partial k}{\partial x_j}\right] + G_\varepsilon + G_b + \frac{\varepsilon}{k}\left(c_{1\varepsilon}G_k + {}_{3\varepsilon}c_b\rho - \varepsilon c_{2\epsilon\rho}\right) \tag{4.13}$$

Where

$$\mu_t = \rho c_\mu \frac{k}{\varepsilon} \tag{4.14}$$

For Non-Newtonian liquids, shear stress terms, τ_{ij}, can be formulated as:

$$\tau_{ij} = \mu\left(\frac{\partial u_i}{\partial x_j} + \frac{\partial u_j}{\partial x_j}\right) \tag{4.15}$$

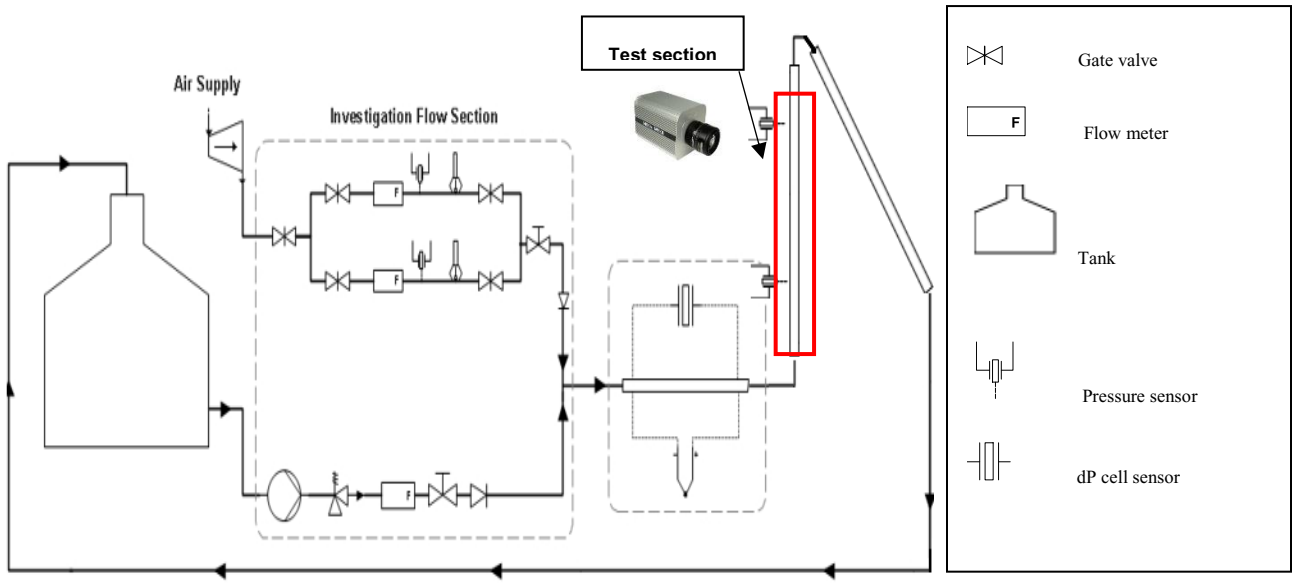

Figure 4-2. Schematic diagram of the experimental set-up.

The viscosity of non-Newtonian yield pseudoplastic expressed as:

$$\mu = \frac{\tau_0}{(\lambda\dot{\gamma})} + k(\lambda\dot{\gamma})^{n-1} \tag{4.16}$$

Where k, n, and τ_0 yield pseudoplastic model parameters were added to the ANSYS software's to viscous panel.

4.4.2 Geometry and Mesh

The simulations wear carried out as 3D transient flow through a horizontal-to-vertical upward. The horizontal, vertical lengths and diameter are 1.5 m, 5.5 m, and 0.0762 m, respectively, as shown in figure 1.3. The gas was introduced into the pipe through a T- junction with a diameter of 0.0254 m. ANSAY fluent 2019R3 software [28] was employed for geometry and meshing. Furthermore, tetrahedron meshing comprising 395323 nodes and 871386 tetrahedral elements has been used for generating the unstructured network. The thickness of the initial layer determines the inflation across the seven layers.

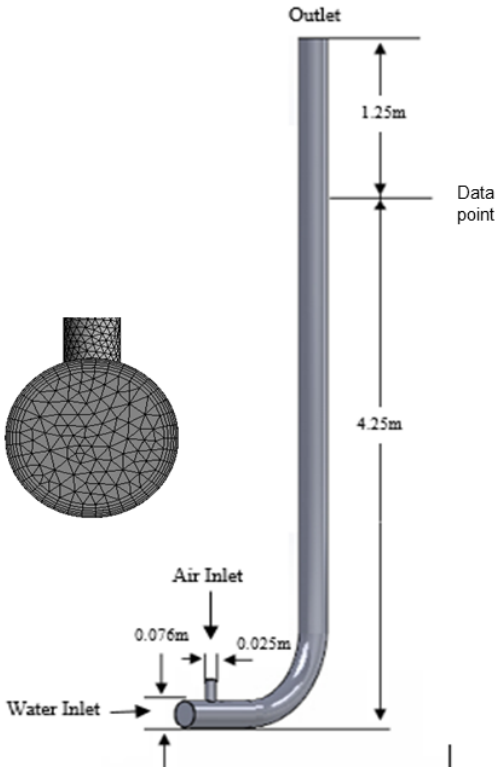

Figure 4- 3. Pipe geometry and mesh

4.4.3 Simulation Procedure

The simulation cases were considering for Newtonian and non-Newtonian fluids in the two-phase flow model. In this set-up, the air was working as a gas, while water and three non-Newtonian fluids working as liquids. The gas enters in a vertical direction and working fluids in a horizontal direction at different flow rates. Based on pressure-based, under the VOF model, the transient simulations were carried out. The convergence criterion or time step from 10^{-4} to10^{-6} has been employed to maintain the Courant number (CLF) below 0.25. A SIMPLE scheme for pressure-velocity coupling, a second-order upwind scheme for momentum equation, and Geo-Reconstruct for void fraction discretization. The flow time of simulations reached out at least 20 s.

4.5 Results and Discussion

Experiment results were collected with the experimental unit, as detailed in Figure 4-2. In all cases, differential and absolute pressure transducers obtained pressure values for both liquids and gas at different flow rates. In computational fluid dynamics (CFD), the grid size strongly related to the quality and mesh size of the grid size. To evaluate the sincerity of the simulation results, the results of the developed model in ANSYS Fluent 2019R3 were validated to the experimental results for two-phase flow air-Newtonian fluid as shown in Figure 4.4. When the inlet air flow rate is constant, the differential pressure increases with increasing water flow rate. By using Eq. (4-5), the average of void fraction air-water determined based on two absolute pressure sensors located on a vertical pipe 1.5 m after the elbow and at the highest 4.5 m and compared to simulation results. The values void fraction of non-Newtonian fluids was calculated based on Eq. (4.6).

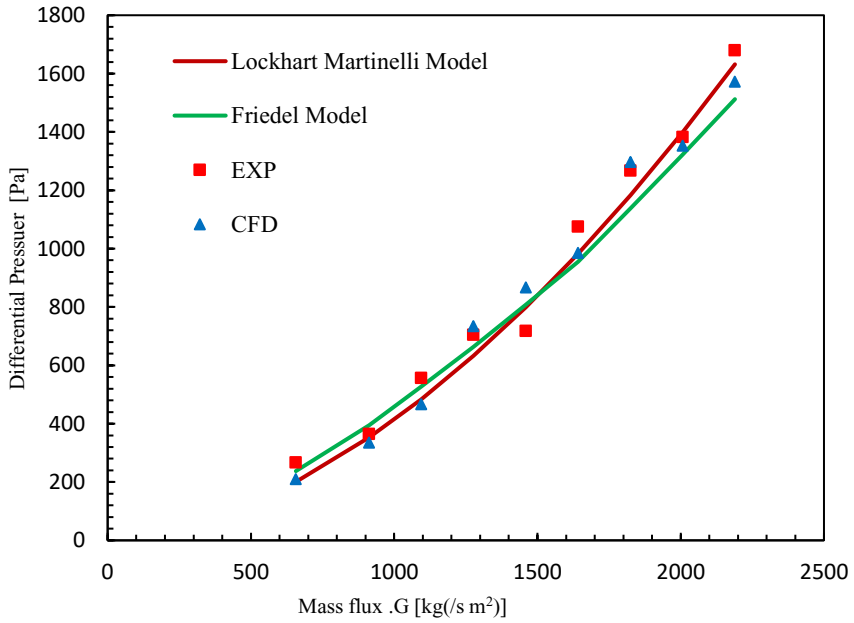

Figure 4- 4. Compaction two-phase (Newtonian fluid) pressure drops models to experimental and CFD results.

Calculating the difference between correlations and experimental results and numerical measurements for volume fraction at a measured point, the average errors of simulation of cases 1, 2, 3, and 4 resulted in 8.5%, 11.51%, 14.2% and 17.34%, respectively. The average errors increased with increasing rheology parameters due to increasing XG concentrations and wall shear stress. The values of the critical velocity of the laminar-turbulent transition condition of yield-pseudoplastic non-Newtonian fluids calculated based on Slatter modified Reynolds number Eq. [4-3] reported in table 2. Three different concentrations of XG solutions were used for continuous liquid phases that present characteristics of yield pseudoplastic fluid to obtain a deeper understanding of the effect rheological parameters of a non-Newtonian fluid phase. The simulations were conducted a plane a 4.25 m of the experimental unite. The analyzed values are following in these sections.

Table 4-2.Values of Critical velocity of yield pseudoplastic fluids

Fluid	$R_{yp\ (-)}$	Critical velocity(m/s)
XG-1	2100	0.46
XG-2	2100	0.51
XG-3	2100	0.59

The simulations were conducted a plane a 4.25 m of the experimental unite. The analyzed values are following in these sections.

4.5.1 Flow Visualization

Flow visualization and recording videos achieved by using Mega Speed MS55K - High-speed camera with a full resolution of 1280x1024 and speed 2000fps. Phantom camera control (PCC)

software was used to tracking slug characteristics in a vertical pipe. Figures 4-5 to 4-8 (a) shows a visualization of volume fraction contour by ANSYS and video images development at the same working fluids and gas superficial velocities for both Newtonian and non-Newtonians fluids. The experimental and numerical simulation was done by a kept flow rate of liquids at 0.00305 m^3/s and maintaining the flow rates of gas constant at 0.00053 m^3/s. we can notice as the concentration of the XG phases increases, slug-bubble transition gradually evolves into slug flow, as shown in Figure 4.8 a. In addition, increasing XG concentrations cause an increasing number of small bubbles due to the dominated viscous force over the surface tension force. In Figures 4-7 and 4-8 (a), the shape of slugs changed to a bullet-shaped with increasing XG concentrations due to the influence of the higher wall share force of the liquid phases.

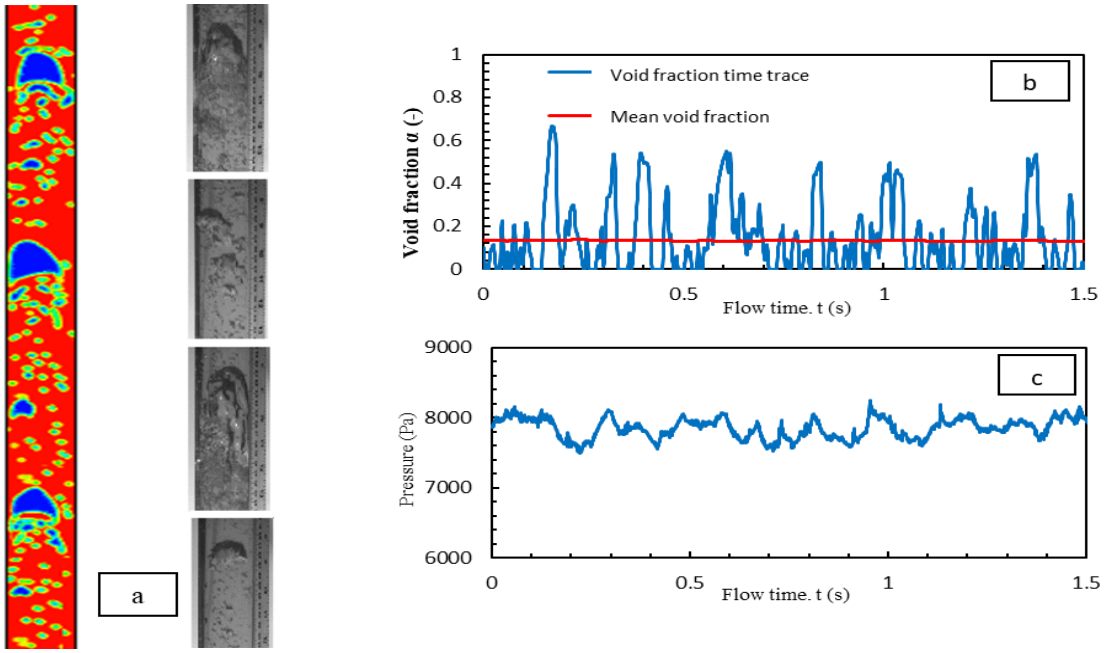

Figure 4-5. Experimental image and simulated counter void fractions (a), Simulated of void fractions time trace and Average void fraction(b), Simulated of pressure fluctuations (c) for gas-water two-phase flow, U_{SL}=0.65 and U_{SG}=0.65.

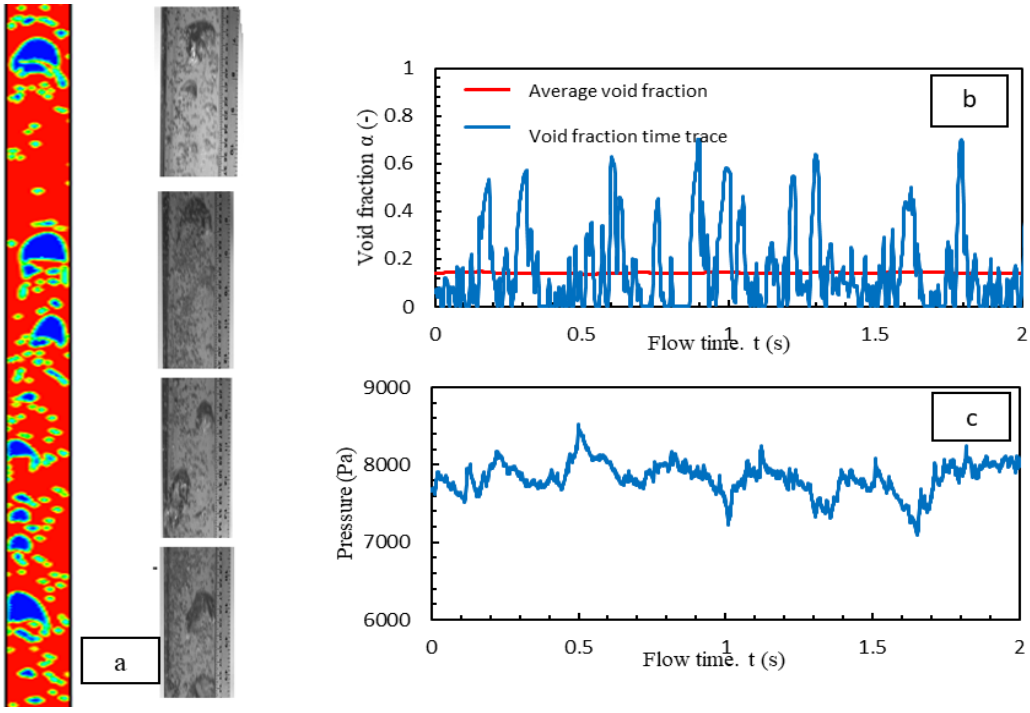

Figure 4-6. Experimental image and simulated counter void fractions (a), Simulated of void fractions time trace and Average void fraction(b), Simulated of pressure fluctuations (c) for gas-XG1 two-phase flow, U_{SL}=0.65 and U_{SG}=0.65.

4.5.2 Time-averaged Volume Fraction and Pressure Fluctuations

The time-domain void fraction, pressure fluctuations, and void fraction time trace data were obtained from simulations at a cross-sectional plane created at 4.25m height of the pipe, as shown in Figures 5 to 8 (b,c). The average void fraction also obtained from a vertical plane along the pipe. Figures 4-5 (b) show different traces of the average void measured at the plane and void fraction time trace at test section location with 0.65 m/s water, superficial velocity and 0.50 m/s gas superficial velocity compared to pressure fluctuations at the same location Figures 4-5 (c). The recurrence plot of slug-bubble transition flow is shown in Figure 4-5(b) instability the single of void fraction time trace due to change in size and shape of the bubbles.

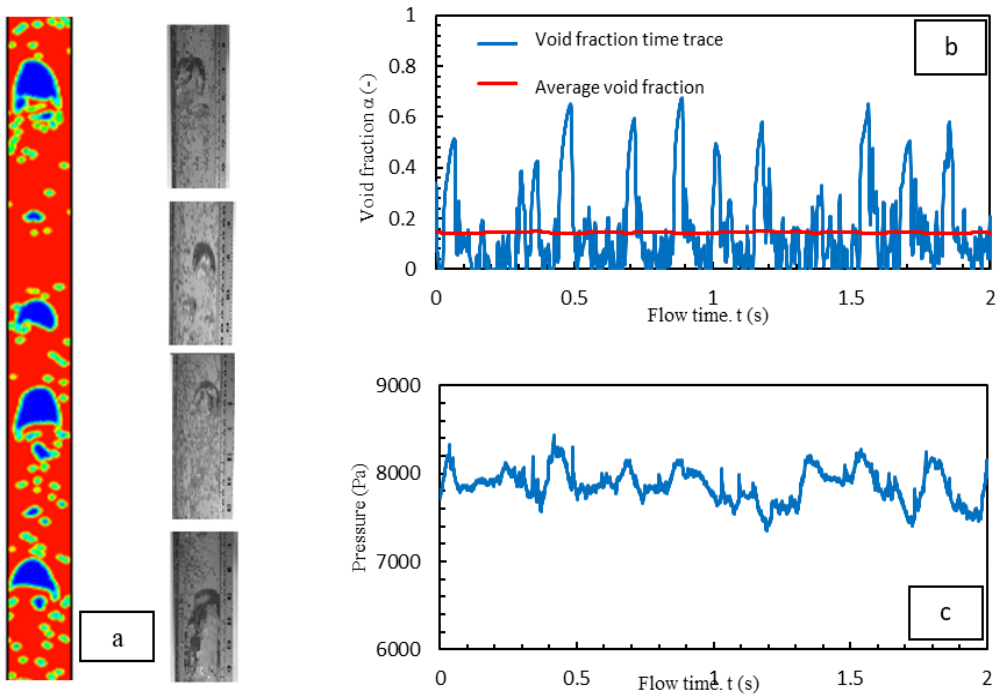

Figure 4-7. Experimental image and simulated counter void fractions (a), Simulated of void fractions time trace and Average void fraction(b), Simulated of pressure fluctuations (c) for gas-water two-phase flow, U_{SL}=0.65 and U_{SG}=0.65.

We observed with increasing XG concentration, and the chaotic pattern decreases, as we can notice in Figures 4-7 and 4-8 (b). Due to the increasing amount and size of bubbles. The pressure fluctuation signals of water and three of non-Newtonian fluids with different rheology parameters at the test section are shown in Figure 4-5 to 4-8 (c). In slug-bubble transition flow, the high-pressure signal indicates that liquid and the low-pressure signal indicate that slug passes through the measurement section.

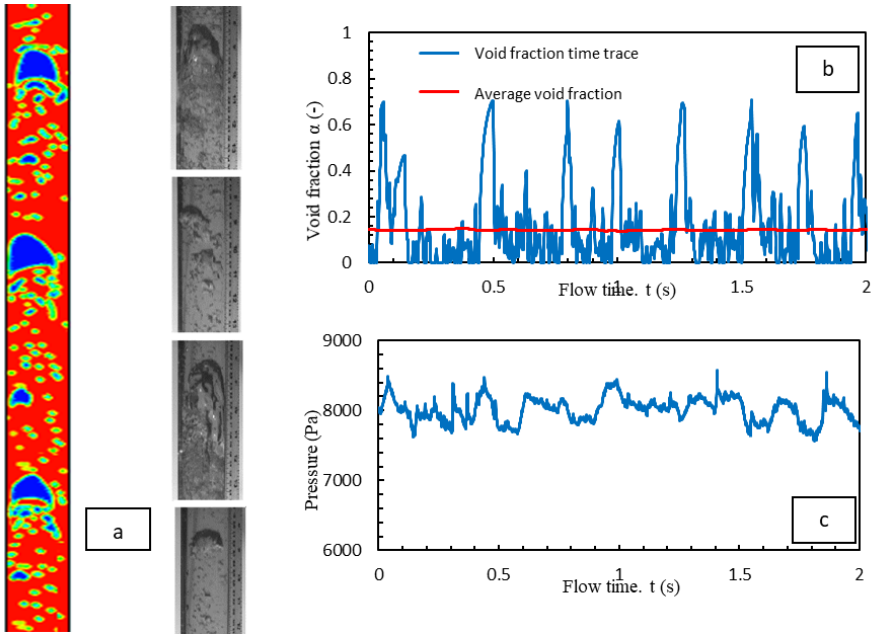

Figure 4-8. Experimental image and simulated counter void fractions (a), Simulated of void fractions time trace and Average void fraction(b), Simulated of pressure fluctuations (c) for gas-XG2 two-phase flow, U_{SL}=0.65 and U_{SG}=0.65.

The pressure signal fluctuation of slug-bubble transition flow is concentrated in a middle range, reflecting the non-uniform and random and distribution of dependent on size the bubbles. When the flow pattern changes from slug-bubble transition to the slug flow with increase XG concentration, as shown in Figure 4-8 (c) due to the effect of rheology parameters of working fluids.

4.6 Conclusion

In this study, experimental and numerical investigation of the influence of the rheological properties of non-Newtonians fluids in two-phase flow (gas/yield Pseudoplastic fluids) on slug characteristics in an upward vertical flow with different concentrations of Xanthan gum solutions. The experiments were conducted in an open-loop re-circulating system has a total length of 65 m to ensure phase mixing and authorize flow regime patterns to develop. Water and three

concentrations of XG 0.017%, 0.035%, and 0.052% (g/0.350ml), which are referred to as non-Newtonian, yield Pseudoplastic behavior used as the working liquids and air as a gas. A high-speed camera to observe the effect of the behavior non-Newtonian fluids in the two-phase model and pressure transducers used to measure high-response pressure. A volume of fluid (VOF) model in ANSYS Fluent 2019 R was selected to evaluate the influence of rheology parameters characteristics on slug flow in non-Newtonian two-phase flow in turbulent model. The empirical correlations reported in the literature and experimental results were compared to simulation results. We observed that the slug-bubble transition flow was affected by changing the rheology parameters of the non-Newtonian phase. With increasing XG concentration at the same operations conditions, we found that non-uniform and random distribution of small bubbles with an increase in slug size due to the effective viscous force of a liquid phase. The shape of slug changed to bullet shape in higher concentration due to the influence higher shear force of the liquid phase. Gas /non-Newtonian fluid slug flows, which can be found in many industrial processes, cause loss to equipment over time. Thus, it needs to evaluate for successful design. Based on this study, it can be concluded that computational fluid dynamics are a useful technique and had acceptable reliability to the prediction gas /non-Newtonian fluid in two-phase flow.

References

[1] R. D. Kaminsky and S. Flow, “Predicting Single-Please and Two-Phase Non-Newtonian Flow Beliavior in Pipes,” vol. 120, no. March 1998, 2016.

[2] J. D. P. Araújo, J. M. Miranda, and J. B. L. M. Campos, “CFD Study of the Hydrodynamics of Slug Flow Systems: Interaction between Consecutive Taylor Bubbles,” Int. J. Chem. React. Eng., vol. 13, no. 4, pp. 541–549, 2015.

[3] D. Barnea and Y. Taitel, “A model for slug length distribution in gas-liquid slug flow,” Int. J. Multiphase. Flow, vol. 19, no. 5, pp. 829–838, 1993

[4] Chhabra, R.P., Richardson, J.F., 1984. Prediction of flow patterns for concurrent flow of gas and non-newtonian liquid in horizontal pipes. Can. J. Chem. Eng. 62, 449–454.

[5] Mandhane, J.M., Gregory, G.A., Aziz, K., 1974. A flow pattern map for gas–liquid flow in horizontal pipes. Int. J. Multiphase Flow 1, 537–553.

[6] Rosehart RG, Rhodes E, Scott DS (1975) Studies of gas-liquid (non-Newtonian) slug flow: void fraction meter, void fraction, and slug characteristics. Chem Eng J 10(1):57–64

[7] Otten L, Fayed AS (1976) Pressure drop and drag reduction in two-phase non-Newtonian slug flow. Can J Chem Eng 54:111–114

[8] Khatib, Z. and J. F. Richardson, “Vertical Concurrent Flow of Air And Shear Thinning Suspensions of Kaolin” Chem. Eng. Res. Dev. 62, 139-154 (1984).

[9] Zuber, V. and J. A. Findlay, “Average Volumetric Concentrations in Two-Phase Flow Systems” Trans. ASME (C). J. Heat Trans. 87, 453-467 (1965).

[10] Chandraker, S. K., M. N. Biswas, and A. K. Mitra, “Two-Phase Gas-Non-Newtonian Liquid Flow in Vertical Pipe With

Improved Gas Dispersion”, paper E2, 2nd Int. Conf. MULti-phase Flow, London (1985), pp. 197-213.

[11] Das SK, Biswas MN, Mitra AK (1992) Holdup for two-phase flow of gas-non-Newtonian liquid mixtures in horizontal and vertical pipes. Can J Chem Eng 70(3):431–437

[12] Dziubinski M (1996) A general correlation for two-phase pressure drop in intermittent flow of gas and non-Newtonian liquid mixtures in a pipe. Int J Multiphase Flow 22:101

[13] Xu J, Wu Y, Shi Z, Lao L, Li D (2007) Studies on two-phase concurrent air/non-Newtonian shear-thinning fluid flows in inclined smooth pipes. Int J Multiphase Flow 33(9):948–969

[14] Picchi D, Manerba Y, Correra S, Margarone M, Poesio P (2015)Gas/shear-thinning liquid flows through pipes: modeling and experiments. Int J Multiphase Flow 73:217–226

[15] Heywood NI, Charles ME (1979) the stratified flow of gas and non-Newtonian liquid in horizontal pipes. Int J Multiphase Flow 5:341–352.

[16] Bishop AA, Deshande SD (1986) Non- Newtonian liquid- air stratified flow through horizontal tubes-ii. Int J Multiphase Flow 12(6):977–996

[17] Picchi D, Correra S, Poesio P (2014) Flow pattern transition, pressure gradient, hold-up predictions in gas/non-Newtonian power law fluid stratified flow. Int J Multiphase Flow 63:105–115

[18] Ihmoudah, A., Rahman, M. A., & Butt, S. D. (2018). CFD and Experimental Studies of Yield Power-Law Fluids in Turbulent Pipe Flow. In ASME 2018 37th International Conference on Ocean, Offshore and Arctic Engineering. American Society of Mechanical Engineers Digital Collection.

[19] Ratkovich, N., Chan, C.C.V., Berube, P.R., Nopens, I., 2009. Experimental study and CFD modelling of a two-phase slug flow for an airlift tubular membrane. Chem. Eng. Sci. 64 (16), 3576–3584.

[20] Taha, T., Cui, Z.F., 2006. CFD modelling of slug flow in vertical tubes. Chem. Eng. Sci. 61 (2), 676–687.

[21] Ratkovich, N., Majumder, S. K., & Bentzen, T. R. (2013). Empirical correlations and CFD simulations of vertical two-phase gas–liquid (Newtonian and non-Newtonian) slug flow compared against experimental data of void fraction. Chemical Engineering Research and Design, 91(6), 988-998

[22] Ihmoudah, A., Awad, M. M., Rahman, M. A., & Butt, S. D. Experimental and Numerical Investigation of Gas-Yield Power-Law Fluids in a Horizontal Pipe. In ASME 2019 38th International Conference on Ocean, Offshore and Arctic Engineering. American Society of Mechanical Engineers Digital Collection.

[23] Bourgoyne, A. T., Millheim, K. K., Chenevert, M. E., & Young, F. S. (1991). Applied drilling engineering (Vol. 2, pp. 137-144). Richardson, TX: Society of Petroleum Engineers.

[24] Herschel, V. W. H. (1926). Consistency of Measurements Rubber-Benzene Solutions. Kolloid-Zeit., 39, 291-300.

[25] Hemphill T, Campos W and Pilehvari A: "Yield-Power Law Model More Accurately Predicts Mud Rheology," Oil & Gas Journal 91, no. 34 (August 23, 1993): 45–50.

[26] Slatter, P. T. (1995). Transitional and turbulent flow of non-Newtonian slurries in pipes (Doctoral dissertation, University of Cape Town).

[27] Jia, J., Babatunde, A., & Wang, M. (2015). Void fraction measurement of gas–liquid two-phase flow from differential pressure. Flow Measurement and Instrumentation, 41, 75-80.

[28] Fluent, A. ANSYS Fluent 17.0 User's Guide; 2017.

Chapter 5: Numerical Study on Gas / Yield Power-Law Fluid in T-Junction Minichannel

Abdalsalam Ihmoudah[1], Mohamed M. Awad[2], Mohammad Azizur Rahman[3] and Stephen Butt[1]

[1]Memorial University of Newfoundland.

[2]Mansoura University, Egypt

[3]Texas A&M University at Qatar, Doha, Qatar

This chapter is based on the objectives defined in Section 1.4 and was presented at the ASME 2019 17th International Conference on Nanochannels, Microchannels, and Minichannels (ICNMM 2019) held June 23–26, 2019 in St. John's, NL, Canada

Co-authorship Statement

Abdalsalam Ihmoudah is the first author of this manuscript, along with co-authors Dr. Mohamed Awad, Dr. Mohammad Azizur Rahman, and Dr. Stephen Butt. I proposed the idea and concept, conducted a literature review, and prepared the fluid samples. I collected and analyzed the numerical simulation results. Dr. Awad, Dr. Aziz, and Dr. Butt evaluated the methodology and reviewed the manuscript. Manuscript preparation is mainly contributed by Abdalsalam Ihmoudah, with revision assistance provided by all other coauthors.

ABSTRACT

In this study, a computational examination of Taylor bubbles was performed for gas/non-Newtonian fluid two-phase flows developed in a minichannel T-junction mixer with a hydraulic diameter of 1 mm. The investigations employed three separate aqueous xanthan gum solutions at

concentrations of 0.05, 0.1 and 0.15 w/w, which are referred to as non-Newtonian (yield power-law) fluids. The effective concentration of the xanthan gum solutions and superficial velocity of the inlet liquid phase on the length, velocity, and shape of the Taylor bubbles was studied using the ANSYS FLUENT 19 software package. The simulation results show an increase in bubble velocity with increasing film thickness, particularly in solutions of higher viscosity XG-0.15%. Furthermore, bubble lengths decreased as the xanthan gum concentrations increased, but bubble shapes underwent alterations when the concentrations increased. Another interesting result of the tests shows that when the liquid inlet velocity increases, bubble lengths decrease during lower liquid superficial velocity, whereas during higher velocities, they change only slightly after increases in concentration. Finally, with increasing XG concentration, the liquid film thickness around the bubble increased. The results show good agreement with correlations after modifying a capillary number (Ca*) for non-Newtonian liquids in all cases.

5.1 Introduction

The increased viability of using minichannel gas-liquid two-phase flow in engineering and medical applications has made this approach increasingly attractive to researchers and industry experts. Two-phase flow can be found in a variety of uses, including micro fuel cells, heat exchangers and the cooling of electronic circuitry. Earlier investigations on minichannels' gas-liquid flows primarily focused on the gas-Newtonian flow of liquid materials and employed refrigerant fluid or water for the liquid flow phase. Meanwhile, there are numerous instances of non-Newtonian fluids being applied in biological and industrial processes. Examples include waste water, polymer solutions, chemical solutions, and blood flowing through micro-vessels.

Recently, computational fluid dynamics (CFD) has been used by several researchers to augment and validate previous experiments. Lawal and Qian [1] studied two-phase flow Newtonian fluids in empty channels (0.25, 0.5, 0.75, 1, 2 and 3 mm) of a T-junction. In their numerical simulations, the researchers employed FLUENT, a commercial CFD package, which tracked the interface using a volume of fluid (VOF) model; they also investigated slug length for both liquids and gases under various inlet conditions. Their numerical findings indicated good agreement with previous experimental outcomes. Furthermore, Lawal and Qian [1] discovered that the slug lengths of liquid and gas were related to liquid and gas superficial velocity, such that increases in gas velocity resulted in an increase in the length of the gas slug from the point of constant liquid velocity onward. Conversely, when the liquid velocity increased, the length of the gas slug began to decrease, this time starting at the point of constant gas velocity. Lawal and Qian [1] express this dependency in a bubble velocity equation. In other research, Taha and Cui [2] studied Taylor bubble motion for conventional channels. In their investigations, they used the CFD volume of fluid (VOF) approach, succeeding in capturing the motion of an individual gas bubble. Taylor bubbles are characterized as having spherical noses but differently shaped tails. The tail shapes likely play a role in the variations in velocity. They noted that increases in velocity of the bubble led to an increase in the liquid film. The increased velocities gradually resulted in a merging of the liquid slug in a mixing zone. Rosengarten et al. [3] used CFD FLUENT to investigate how contact angle and contraction affect liquid droplet formation during the contraction phase, finding that the contact angle of the wall significantly impacted the shape and size of the droplets. Salman et al. [4] studied the formation of the Taylor bubble in 1 mm ID vertical minichannel experimentally. They found that the process of bubble generation has three distinct stages: 1) the bubble expands; 2) the bubble contracts, and 3) the bubble undergoes necking. Size and shape of the bubble are determined by stages 1 and 2. Bubble shape and size depend on the first two stages, so various bubble sizes

and shapes occurred in various sizes and orientations of channels. Additionally, Ghiaasiaan and Akbar [5] used ANSYS FLUENT to conduct analyses on two-phase air-water flows in Taylor flow systems. They investigated bubble velocity as well as gas hold-up and length of slug in relation to liquid and gas inlet velocity. Vertical and horizontal channel orientations were simulated. The findings indicated that for both types of channel orientation, bubble speeds increased as two-phase velocity increased. Bhatelia et al. [6] used CFD to study hydrodynamic behaviors in gas-liquid systems featuring flow capillary microchannels. In their work, the researchers modeled the Taylor slug flow system using the VOF approach, simulating a variety of channel diameters and inlet geometries (e.g., 0.5 mm, 1 mm, and 2 mm). They also chose an equiangular microchannel at 120^{o} (inverted Y-junction) to delve deeper into slug characteristics for different liquid and operational parameters. In other areas of their research, simulated and compared the results for 2D and 3D inverted vertical Y-junction channels, focusing on how superficial velocity and gravity impacted the contact angles and phases. They found surface tension had a notable impact on the slug. Chen and Guo [7] used the volume of fluid (VOF) method in ANSYS FLUENT to investigate Taylor bubble flow within a conventional channel. They have observed that liquid slug length and bubble are dependent on superficial velocity and pipe orientation. They also mentioned at a lower capillary number, the flow dominated by surface tension and at a higher capillary number, the shear force being dominant over surface tension and the creation of small slugs. Chan et al. [8] studied the Taylor flow regime by performing numerical simulations and looking at how the shape and size of bubbles were impacted by changes in gas and liquid values. In addition to the numerical simulations, the researchers performed simulations involving alterations to inlet geometry while maintaining other parameters. They concluded that the sizes and shapes of the bubbles were strongly related to inlet dimensions. Zheng et al. [9] applied FLUENT in their study to investigate how viscous force and surface tension impacted on characteristics of a Taylor bubble. In

conducting their study, they used a fine mesh to capture the liquid film around each Taylor bubble. Their results indicate that gas bubbles are naturally surrounded by the liquid film during instances of fully wetted fluids. Santos and Kawaji [10] experimentally and numerically investigated gas-liquid two-phase flow in a square microchannel. 3D modeling was performed in (CFD) FLUENT. They found that the velocity slip depends on gas slug coverage in the cross-sectional area. They also found that numerical modeling requires improvements to the treat line slip and contact angle. Santos and Kawaji [11] experimentally and numerically studied the formation of Taylor slugs in a rectangular microchannel T-junction based on gas-liquid flow. They used a FLUENT volume-of-fluid (VOF) model in numerical modeling. The researchers studied the effect of flow rate on a void fraction, velocity slip and frictional pressure drop of two-phase flow.

Recently, few numerical and experimental studies non-Newtonian Taylor bubble in minichannel are performed. Mansour et al. [12] studied the formation of bubbles occurring in a rectangular microchannel, using polyacrylamide aqueous solutions in their experiments. The researchers studied bubble velocity and length, frictional pressure drop, and length of liquid slugs in the non-Newtonian fluid, comparing these features with measurements of the same elements in a Newtonian system. In a similar study, Mahjoob et al. [13] numerically analyzed laminar non-Newtonian flows in rectangular micro channels, testing how alterations (e.g., changes in aspect ratio and height/width from 1 to 5) to the power law non-Newtonian fluid. The researchers discovered that the flow regime affected by change rheological properties of the non-Newtonian fluid in a vertical rectangular microchannel. Also, they found that the geometrical of the channel and cross-section case can affect on the flow pattern transition. Yang et al. [14] experimentally investigated two-phase nitrogen/non-Newtonian fluid for three separately sized and shaped micro channels measuring D_h= 2.5, 2.886 and 0.866 mm, respectively. The researchers studied flow and

pattern-transition maps to determine the existence of various nitrogen/non-Newtonian fluids. Their findings indicated the presence of three distinct flow patterns (annular, churn, and slug) in the non-Newtonian fluids. Also, they noted some novel flow patterns that appeared to be related to both the shape/size of the microchannel cross section and the properties of non-Newtonian liquids. The researchers' also noted variations were appearing in their flow transition maps, which they attributed to the unique characteristics of non-Newtonian fluids. Fu et al. [15] studied the generation of nitrogen bubbles occurring within non-Newtonian fluids for square micro-channels of two separate sizes (i.e., 400x400 μm & 600x600 μm). The researchers employed polyacrylamide aqueous solution concentrations (at 0.25, 0.5, 0.75 and 1 w_t %) in their experiments in order to gauge how non-Newtonian behavior affects flow patterns. As well, they altered the volume flow rates for liquid and gas in the range 0.17-23.33 mm3/s and 2.57-135.78 mm^3/s respectively, four flow patterns generated (missile bubble, intermittent, annular, and slug bubble) as a result of changes in operational conditions. They surmised from their results that bubble size could be determined through alterations to liquid/gas volume flow rate ratios up to the point of critical ratio, where microchannel width exceeds that of gas bubbles. More recently Sontti and Atta [16] Investigated Taylor bubble behavior in Newtonian and non-Newtonian carboxymethyl cellulose (CMC) power law behavior through a co-flow microchannel. They studied the effective surface tension, apparent viscosity on the bubble length, film thickness, a velocity of a bubble. They found in all cases the bubble length decreases with increasing Ca and U_L/U_G ratio.

Up until now, there has been very little published research's devoted to the flow of two-phase gas-non-Newtonian liquids especially, yield power-law model in minichannel. What is available focuses mainly on power law shear thinning fluid. Given this gap in the research, In the present work, a computational fluid dynamics (CFD) model is used to simulate three different

concentrations of Xanthan gum solutions are referred to as non-Newtonian (yield power-law) shear thinning with consider viscoelastic effects to explore how different rheology parameters effect in slug length, bubble length, bubble velocity, bubble shape and film thickness in minichannel.

5.2 Characteristics of Non-Newtonian Liquids

In this study, the Newtonian liquid phase is represented by water and solutions of xanthan gum (XG). The non-Newtonian phases have three separate concentrations according to weight, (XG-0.05%, XG-0.10%, and XG3-0.15%) prepared and are tested in the Drilling Technology Laboratory (DTL) through the addition of minute amounts of polymer powders (dried). This combination is then carefully mixed to avoid lump formation. Next, the solution densities are determined by used the 4-scale mud balance, and an 8-speed API-compliant rotational viscometer (Model 800) is utilized as a means to gauge the xanthan solutions' rheology and characteristics, as shown in Figure 5-1.

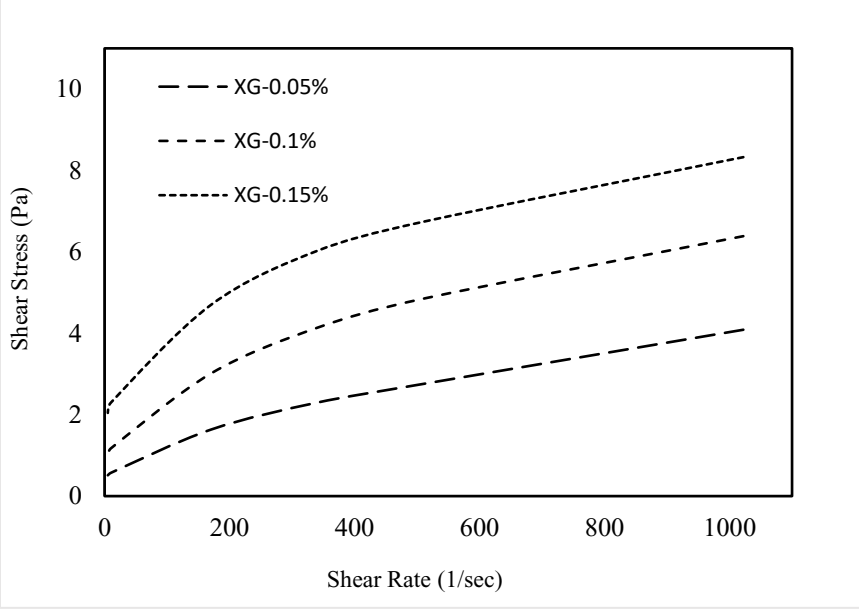

Figure 5- 1. Rheology measurements of xanthan gum solutions.

As can be seen, the liquids display behavior that is similar to that in the yield power-law shear thinning model.

$$\tau = \tau o + k\,\gamma^{n} \qquad (\tau > \tau o) \tag{5.1}$$

Where

τ_0= yield stress.

k = consistency index.

n = fluid behavior index.

The Surface tension and air–XG contact angle of the different XG concentration are measured. The properties of test liquids are listed in Table 5-1. The relationship between shear rate and non-Newtonian liquid apparent viscosity determines the fluid type. Hence, if the increased shear rate decreases viscosity, it is called "shear-thinning," whereas if viscosity increases along with the shear rate, it is called "shear-thickening," as illustrated in Figure 5-2. See Ihmoudah et al. [17] for more details.

Table 5- 1. Rheological properties of non-Newtonian YPL at different concentration.

Symbol	Con. % (g/0.350L)	τ_y (Pa)	K (Pa.s^n)	n	ρ (kg/m^3)
XG-1	0.017	0.4	0.037	0.65	1000
XG-2	0.035	0.7	0.131	0.56	1002
XG-3	0.052	1.33	0.353	0.43	1005

5.3 Numerical Methodology

In the present study, a 2D T-junction minichannel was built and meshed in ANSYS FLUENT 19. The domain has a hydraulic diameter D_h of 1 mm. The minichannel reactor includes a horizontal reaction zone (measuring 60 D in length) as well as a vertical inlet mixing zone. The reaction zone length enables the mixing of the two fluids to be readily captured and the subsequent flow easily observed. Figure 3 shows the schematic of minichannel and layers near the wall. In this set-up, 8 layers near the minichannel wall have been utilized in order to capture both shapes of the bubbles and film thickness zone in the study area. The grid was formulated and built by applying a growth function using these properties. The initial grid has 1μ as a distance, and y^+ expresses the non-dimensional wall distance in wall-bound flow regarding the fineness or coarseness of the applied mesh.

In this set-up, three non-Newtonian fluids, as well as water, serve as liquids, while air serves as gas. The liquid materials enter the mixing zone via two separate inlets in the T-junction, with fluids proceeding in an upward direction and gas proceeding downwards in the channel direction. The flow's numerical solution is derived from a commercially available CFD package. The pressure-based solver is utilized in every case, and the phase-coupled SIMPLE algorithm accomplishes the pressure-velocity coupling. Note that, for the whole simulation, convergence parameters of 10^{-4} to10^{-5} are required.

Volume of fluid (VOF) model in Fluent has been selected. In this approach, a single of conservation equation set has been used to solve for immiscible liquids (i.e., unable to form a homogenous mixture when combined), applying the following VOF governing equations that are used in multiphase flows [15]. The VOF strategy employed in this study can determine changing

rates of volume fractions for individual types of fluid found in the computational cells. Moreover, for every control volume, the volume fraction for the phases combined equate to unity as the model dictates that each phase must share the entirety of the physical properties and variables. Physical properties can thus be denoted here as volume-averaged values since the phase's volume fraction can be known for every cell. Furthermore, based on both volume-averaged properties and volume fraction values, one or the other of the phases can be detected in cells [18]. In two-phase systems, when volume fraction (α) for a secondary phase has been identified, and the phases can be denoted through subscripts, the viscosity and density levels assigned to each cell can be expressed using an αq continuity equation, as expressed in the following:

The equation of continuity:

$$\frac{\partial \rho}{\partial t} + \nabla . \left(\rho \, \vec{U} \right) = 0 \tag{5.2}$$

Where, t, *U* and ρ are time, velocity, and density, respectively.

The equation of Momentum:

$$\frac{\partial (\rho \vec{U})}{\partial \mathrm{t}} + \nabla . \left(\rho \vec{U} \vec{U} \right) = -\nabla P + \nabla . \bar{\bar{\tau}} + F_{ST} \tag{5.3}$$

Where p, ρ, τ, η and F_{SF} are pressure, density, shear stress, dynamic viscosity, and volumetric surface tension force, respectively.

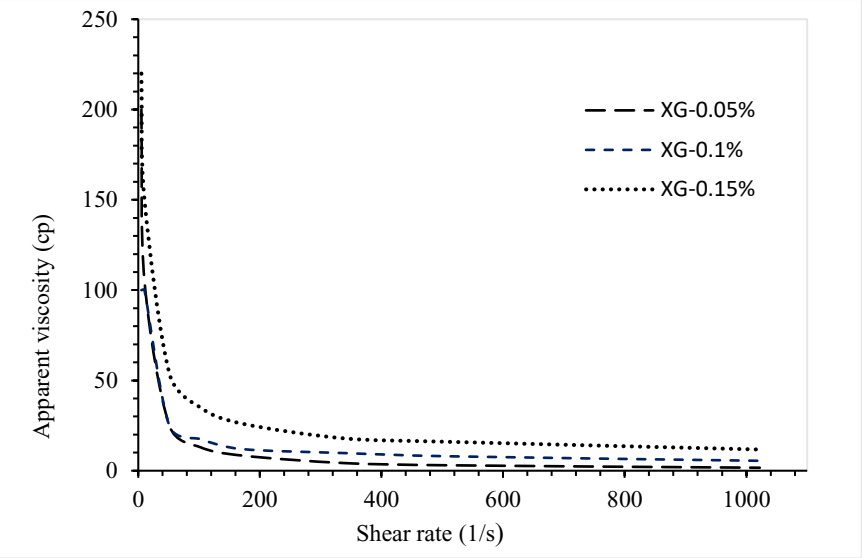

Figure 5-2. Xanthan gum apparent viscosity vs. shear rate at different concentration.

For each cell, the viscosity and density are given by continuity equation for as follows:

$$\eta = a_2\rho\eta_2 + (1 - a_2)\eta_1 \tag{5.4}$$

$$\rho = a_2\rho_2 + (1 - a_2)\rho_1 \tag{5.5}$$

For non-Newtonian fluid (YPL), the apparent viscosity calculated from equation 5-1:

A separate continuity equation for αq is consider as follows:

$$\frac{\partial a_q}{\partial x}\left(U_q.\Delta\right) = S_{\alpha q} \tag{5.6}$$

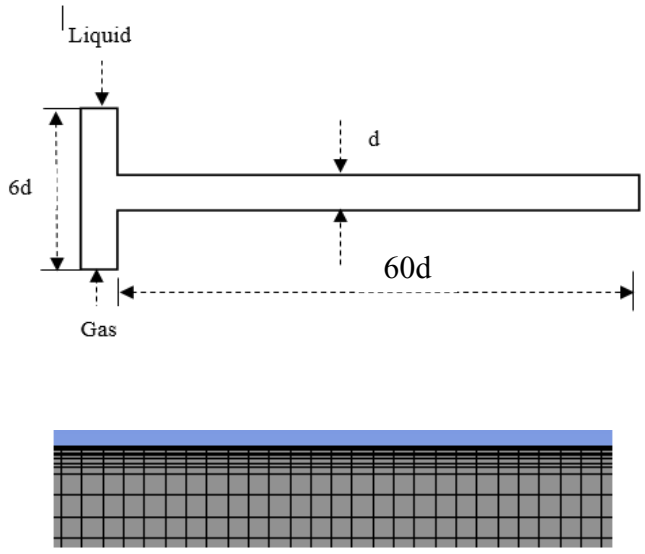

Figure 5- 3.Schematic of the 2D geometry and layers near the minichannel wall.

Where q is a liquid or gas phase, the tracking of the interfaces between the gas and liquid is calculate by solving the continuity equation of one of the phases.

$$\sum_{q=1}^{n} \alpha_q = 1 \tag{5.7}$$

For a two-phase, the void fraction field will the following three possibilities cases.

$\alpha_q = 0$ if the cell is empty.

$\alpha_q = 1$ if the cell is full.

$0 < \alpha_q < 1$ interface between the two fluids.

5.3.1 Surface Tension and Wall Adhesion

In employing the VOF approach, surface tension is included in the interface between phases. Specifically, contact angles between wall and phases have been built into the model, with the surface tension coefficient assumed as a constant. In the present study, the well-known continuum surface force (CSF) model [18] is utilized, and surface tension force (FSF) has been included in the VOF formulation as follows:

$$F_{SF} = \sigma \left(\frac{k_n \rho \nabla \alpha_1}{\frac{1}{2}(\rho_1 + \rho_2)} \right) \tag{5.8}$$

Where σ is surface tension, k_n is the radius of curvature and ρ is the volume–average density calculated using Equation 5.5.

The radius of curvature k_n is define in teams of the unit normal (m)

$$k_n = \nabla . \hat{m} = \frac{1}{|m|} \left[\left(\frac{m}{|m|} . \nabla \right) |m| - (\nabla . m) \right] \tag{5.9}$$

$$\text{Where } \hat{m} = \frac{m}{|m|} \text{ and } m = \nabla \alpha_q$$

The wall adhesion angle in conjunction with the surface tension is available in the VOF model. In case θ_w is the content angle, then the surface normal to the wall at the live call is.

$$\hat{m} = \hat{t}_w \sin \theta_w + \hat{m}_w \cos \theta_w \tag{5.10}$$

Where $\hat{t}_w$ and $\hat{m}_w$ are the tangential and vectors normal and to the wall.

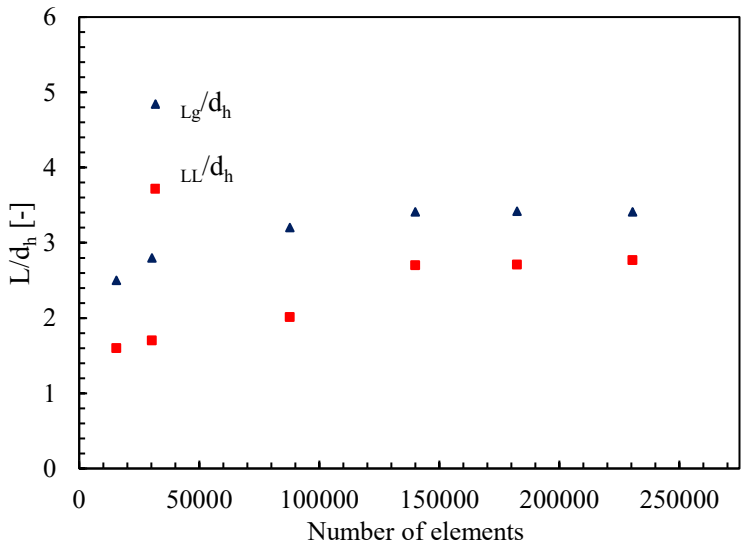

Figure 5- 4. Grid dependency of the liquid slug length and bubble length. $U_G = U_L = 0.25$ m/s.

5.3.2 Grid Independency

Outcomes for CFD computations are strongly related to the size and quality of the grid size used for performing them. For this reason, the grid size should be resolved such that it leads to a grid-independent solution. Note that a "grid independent solution" is defined as one in which the solution undergoes very little change with additional refinements of the grid. That being said, grid refinement still brings with it certain computational costs (e.g., increases in computational time) with the addition of more grid elements to the domain. In general, the course of numerical solution convergence for transient partial differential equations is dictated by the Courant Friedrich-Lewy (CFL) number. The CFL specifies convergence conditions and presents as inversely proportional to grid dimension determinants. For maintaining a low CFL ('low CFL' described here as < 0.25), suitably low time steps are required, but this increases the amount of computational time needed to arrive at a complete solution. In response to this dilemma, a balance must be found that takes into account both the computational grid size and the required accuracy. In this case, the mesh size

of 0.02 mm was mostly used in the present study. The numerical simulation was performed using a core i7 duo 3.40 GHz processor, featuring 8 GB of RAM. Figure 4 shows the grid dependence of the liquid slug length and bubble length.

5.4 Results and Discussion

5.4.1 Validation of Numerical Simulation

To examine our numerical simulation accuracy, the model is verified to a Newtonian (air-water) system first. Figure 5-5 shows a comparison between correlations of Lawal and Qian [1] and numerical simulation using the VOF method under the condition σ = 0.072 N/m, U_G = 0.05 m/s and U_L varying from 0.025m/s to 1.2 m/s.

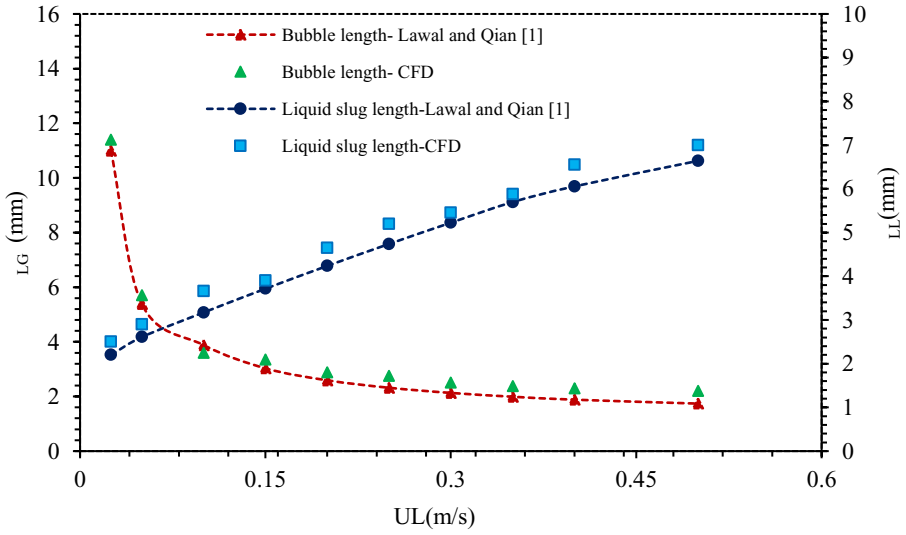

Figure 5- 5. Comparison of Taylor bubble length and liquid slug length numerical results with Lawal and Qian model in T- junction, Dh=1mm.

As shown in Figure 5-5, good agreement between the bubble length and liquid slug length is calculated by correlations and numerical simulation. Also, the model is verified with one of the

most important flow patterns in a minichannel developed by Triplett et al. [19]. As shown in Figure 5-6, the VOF method successfully predicts the slug regime at the same operation conditions (U_G=0.154 m/s and U_L= 0.213 m/s).

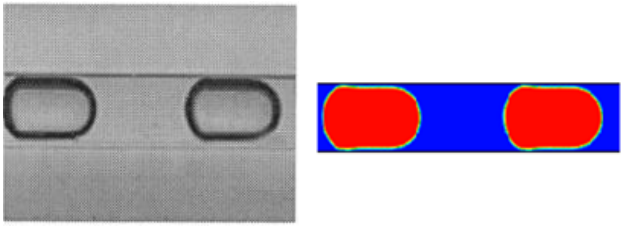

Figure 5- 6. Comparison of Taylor bubble formation between numerical simulation and Triplett et al. [19] at same operation conditions (U_G=0.154 m/s and U_L= 0.213 m/s).

5.4.2 Non-Newtonian Liquid

To obtain a deeper understanding of how Taylor bubbles might function by rheological parameters of a non-Newtonian fluid phase, three separate XG solutions are used for continuous liquid phases that present characteristics of the yield power-law. The XG concentrations, which are first prepared and then tested at the Drilling Technology Laboratory (DTL), exhibit yield power-low (shear-thinning) characteristics. Table 5.1 charts the rheological parameters of these concentrations. Chilton and Stainsby [20] presented analytical solutions to calculate the Reynolds number formulation for Herschel-Buckley (YPL) fluids in laminar flow as:

$$Re_g = \frac{\rho V D}{k \left(\frac{8V}{D}\right)^{n-1} \left(\frac{3n+1}{4n}\right)^n \left(\frac{1}{1-X}\right)\left(\frac{3n+1}{1-aX-bX^2-cX^3}\right)^n} \tag{5.11}$$

$$X = \frac{\tau_0}{\tau_w} \tag{5.12}$$

$$a = \frac{1}{(2n+1)} \; ; \; b = \frac{2n}{(n+1)(2n+1)} \; ; \; c = \frac{2n^2}{(n+1)(2n+1)} \tag{5.13}$$

For laminar flow of Herschel-Buckley (YPL) fluid in a pipe, Enfis et al. [21] presented analytical solutions to calculate the wall shear stresses as:

$$\tau_w = \tau_0 + k\left(0.693 + \frac{0.302}{n}\right)^n \left(\frac{8v}{D}\right)^n \tag{5.14}$$

Effective viscosity in laminar flows is expressed as [20]:

$$\mu^* = k\left(\frac{8V}{D}\right)^{n-1} \left(\frac{3n+1}{4n}\right)^n \left(\frac{1}{1-X}\right)\left(\frac{3n+1}{1-aX-bX^2-cX^3}\right)^n \tag{5.15}$$

5.4.3 Slug or Taylor Flow Generation

Figure 5-7 illustrates how Taylor slugs grow in concentration (XG-0.05%) during different time steps (t = 0.085 s, 0.26 s, and 2.1 s) at U_G =0.05 and U_L = 0.15 m/s. The red is gas while the blue is a liquid slug. As is shown, the slug regime includes several flow conditions of gas-non-Newtonian two-phase flows for minichannels. Bubbles develop near the inlet mixing zone and detach near the entrance to the reaction zone, after which they move toward the reaction zone. It is worth noting that after a bubble forms, there are few instances of formed bubbles either coalescing to other bubbles or moving downwards.

5.4.4 Effect of XG Concentration

To understand the different effect of concentration of XG on Taylor bubble, we first investigated the effect of the XG solutions based on modified capillary number Ca*, film thickness and effective viscosity (μ^*). For all simulations, a vertical line is drawn in the middle of the bubble to estimate liquid film thickness around the bubble and comparison with Bretherton [22], Aussillous and Quéré

[23] correlations as shown in Figure 5-8. The effective viscosity (μ^*) and generalised Reynolds number (Reg) based on yield power–law model. We observed that the correlations are in acceptable agreement with numerical results. The simulations are also used to estimate the effect of XG concentration on bubble velocity and bubble length and compared with Newtonian fluid. As shown in Figure 5-9, with increasing the XG concentration, we observed the bubble length decrease. This is a consequence of the higher viscous force and increased the effect of shear force on the gas stage. Bubble velocity also increases when the XG concentration goes up. This is likely caused by an increase in film thickness around the bubble.

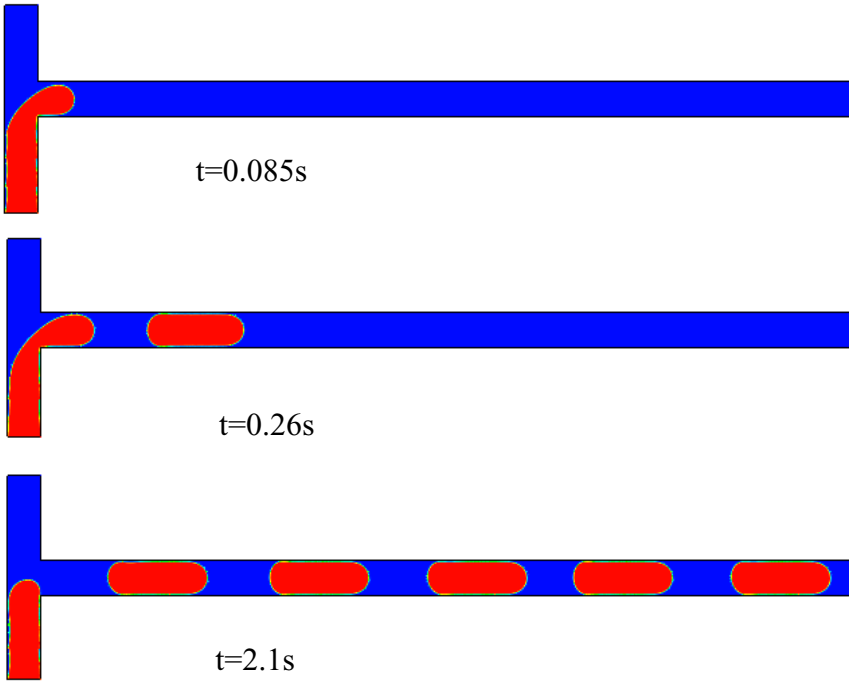

Figure 5-7. Slug flow generation in developed model.

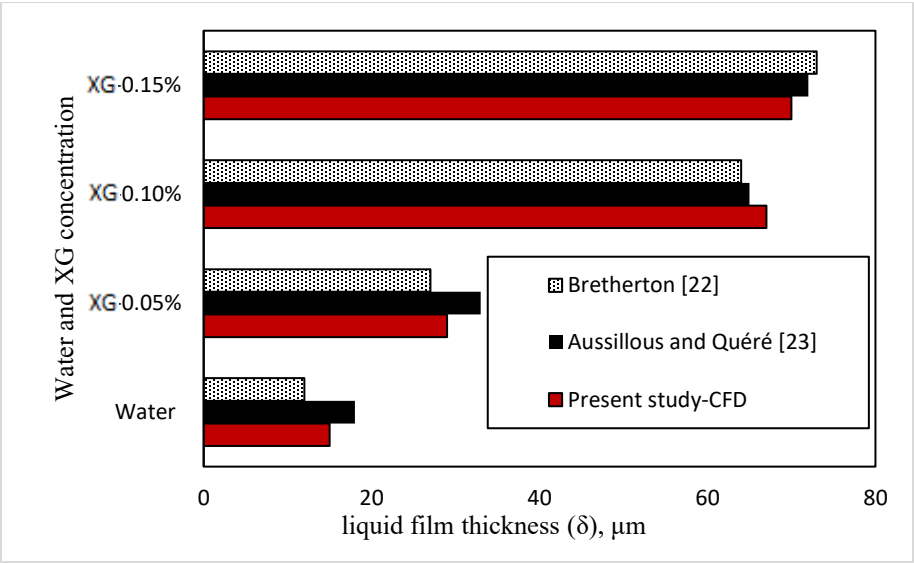

Figure 5-8. Comparison between liquid film thickness predictions from available correlations and CFD observations at U_L = 0.6 m/s and U_G = 0.4 m/s.

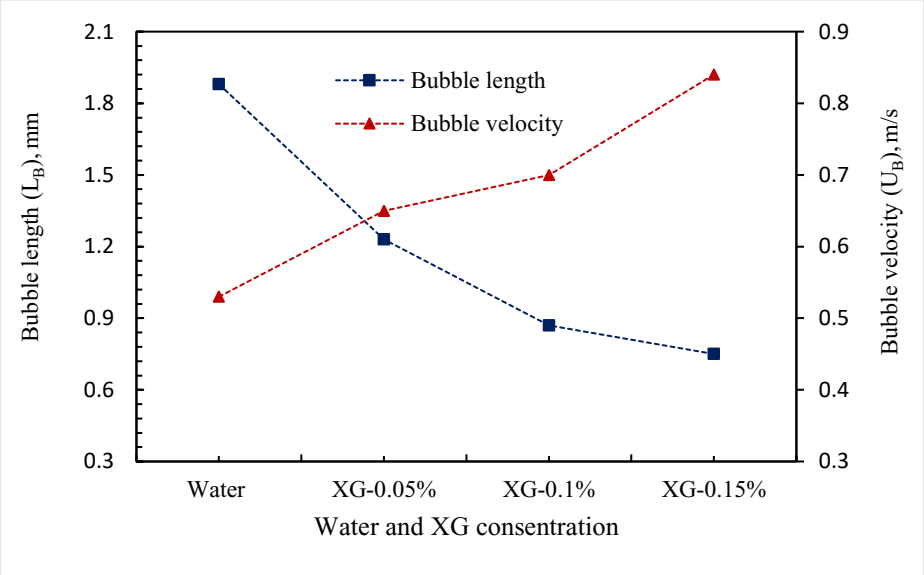

Figure 5- 9. Effect of XG concentration on bubble length and bubble velocity at $U_L = U_G$ = 0.25 m/s.

5.4.5 Effect of Liquid Inlet Velocity on Bubble Length, Bubble Velocity, and Bubble Shape

The effect of the inlet velocity of a non-Newtonian liquid on bubble velocity and bubble length is investigated and compared to a Newtonian fluid (water) as shown in Figure 5-10 and Figure 5-11. The numerical simulation was done by varying the liquid superficial velocity (U_L) and keeping the gas velocity constant at 0.4 m/s. We observed that increasing XG concentrations cause a decrease in bubble length while increasing the superficial velocity of the liquids. At the low liquid velocity, the flow is dominated by surface tension. With increasing liquid velocity, the viscous force is dominant over the surface tension. However, we observed an increase in bubble velocity and change in the shape of the bubble during the increase in liquid velocity and XG concentration. Bubble velocity increases due to a decrease in bubble shape and increased film thickness around it, which causes an increase in inertial force on the gas stage as shown in Figure 5-10.

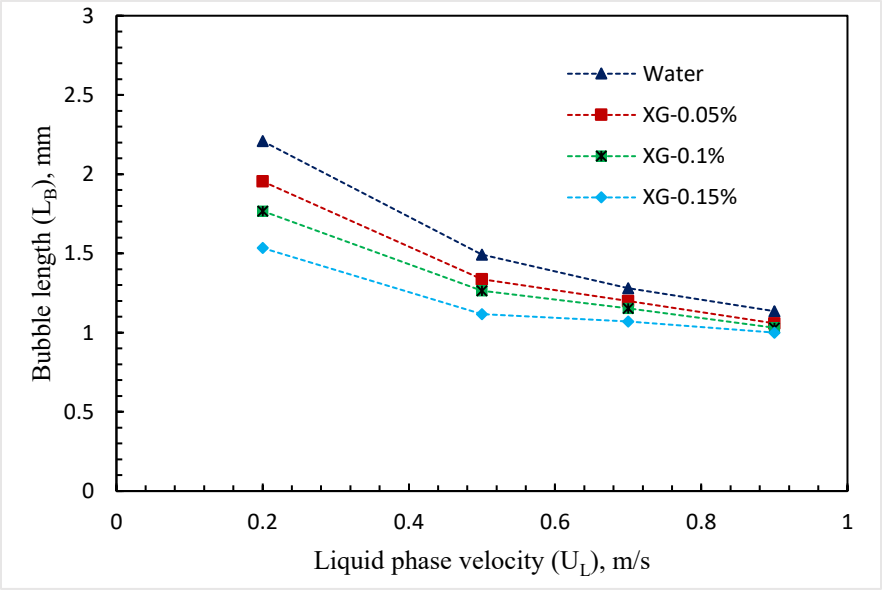

Figure 5- 10. Effect of liquid phase velocity on bubble length for water and three XG solutions at U_G = 0.05 m/s.

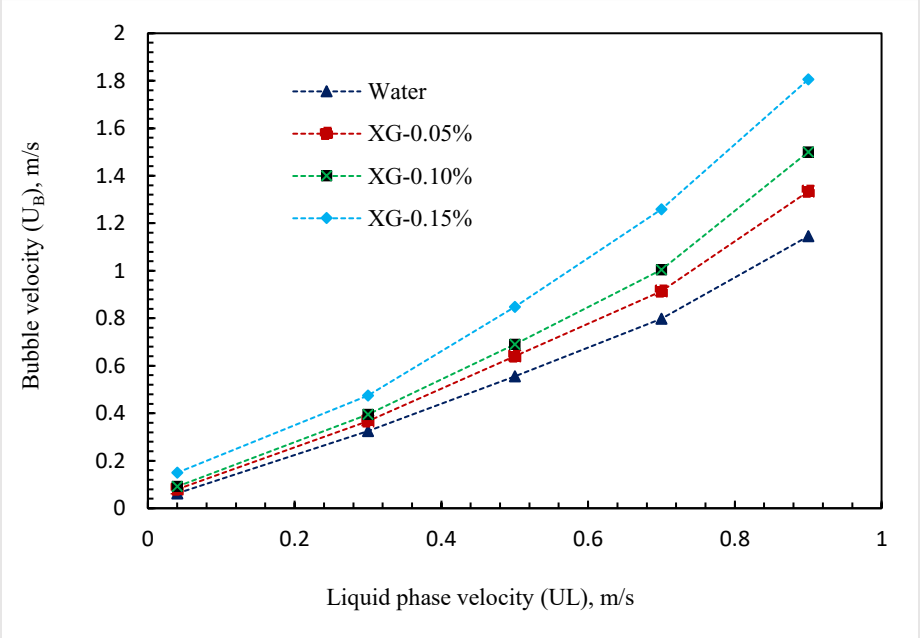

Figure 5-11. Effect of liquid phase velocity on bubble velocity for water and three XG solutions at U_G= 0.05 m/s.

The effect of the inlet velocity of non-Newtonian liquids on the bubble shape was also studied with three XG concentrations, and the results were compared to Newtonian liquids as shown in Figure 5-12. We observed that at a lower inlet velocity, an elongated shape was observed with increasing inlet velocity and XG concentration. The shape changed to a bullet-shape with increasing modified capillary number (Ca*) due to the effect of the higher shear force of the liquid phase.

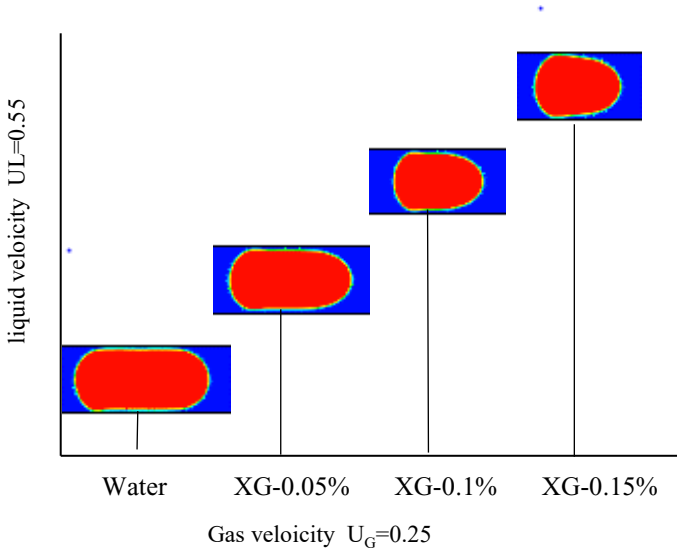

Figure 5-12. Effect of XG concentration and liquid inlet velocity on bubble shape.

5.6 Conclusion

A Computational examination of Taylor bubbles was performed for gas/non-Newtonian fluid developed in a minichannel T-junction mixer with an inner diameter of 1 mm. The investigations employed three separate aqueous Xanthan gum solutions at different concentrations of 0.05, 0.1 and 0.15 w/w, which are referred to as non-Newtonian liquids YPL models. The effect of XG solution concentrations and the superficial velocity of the inlet liquid phase on the length, velocity, and shape of the Taylor bubbles was investigated and compared against gas/Newtonian outcomes. Liquid film thickness was also presented to understand its effect on the Taylor bubbles for all the cases. The Taylor bubble velocity was found to increase with the increasing XG concentrations, particularly in solutions of higher viscosity GX 0.15%. Furthermore, bubble lengths decreased as the XG concentrations increased, but bubble shapes underwent alterations when the concentrations increased. Another interesting result of the tests shows that when liquid inlet velocity increases,

bubble lengths decrease during lower liquid superficial velocity, whereas during higher velocities, they change only slightly after increases in concentration. Finally, the liquid film thickness was created and then compared against correlations with a modified capillary number (Ca*) as non-Newtonian liquids, giving good agreement in all cases.

REFERENCES

[1] Qian, D., & Lawal, A. (2006). Numerical study on gas and liquid slugs for Taylor flow in a T-junction microchannel. *Chemical Engineering Science*, *61*(23), 7609-7625.

[2] Taha, T., & Cui, Z. F. (2006). CFD modelling of slug flow in vertical tubes. *Chemical Engineering Science*, *61*(2), 676-687.

[3] Rosengarten, G., Harvie, D. J. E., & Cooper-White, J. (2006). Contact angle effects on microdroplet deformation using CFD. *Applied Mathematical Modelling*, *30*(10), 1033-1042.

[4] Salman, W., Gavriilidis, A., & Angeli, P. (2006). On the formation of Taylor bubbles in small tubes. *Chemical Engineering Science*, *61*(20), 6653-6666.

[5] Akbar, M. K., & Ghiaasiaan, S. M. (2006). Simulation of Taylor flow in capillaries based on the volume-of-fluid technique. *Industrial & engineering chemistry research*, *45*(15), 5396-5403.

[6] Bhatelia, T., Utikar, R., Pareek, V., & Tade, M. (2009). Hydrodynamics of slug flow in capillary microchannels. *University Journal of Engineering and Technology*, *1*, 1-9.

[7] Guo, F., & Chen, B. (2009). Numerical study on Taylor bubble formation in a micro-channel T-junction using VOF method. *Microgravity Science and Technology*, *21*(1), 51-58.

[8] Chen, Y., KULenovic, R., & Mertz, R. (2007, January). Numerical study on the formation of Taylor bubbles in capillary tubes. In *ASME 2007 5th International Conference on Nanochannels, Microchannels, and Minichannels* (pp. 939-946). American Society of Mechanical Engineers.

[9] Zheng, D., He, X., & Che, D. (2007). CFD simulations of hydrodynamic characteristics in a gas-liquid vertical upward slug flow. *International Journal of Heat and Mass Transfer*, *50*(21-22), 4151-4165.

[10] Santos, R. M., & Kawaji, M. (2010). Numerical modeling and experimental investigation of gas-liquid slug formation in a microchannel T-junction. *International Journal of MULtiphase Flow*, *36*(4), 314-323.

[11] Santos, R., & Kawaji, M. (2011). Gas-liquid slug formation at a rectangular microchannel T-junction: A CFD benchmark case. *Open Engineering*, *1*(4), 341-360.

[12] Mansour, M. H., Kawahara, A., & Sadatomi, M. (2015). Experimental investigation of gas–non-Newtonian liquid two-phase flows from T-junction mixer in rectangular microchannel. *International Journal of Multiphase Flow*, *72*, 263-274.

[13] Mahjoob, M. R., Etemad, S. G., & Thibaut, J. (2009). Numerical study of non-Newtonian flow through rectangULar microchannels. *Iranian Journal of Chemical Engineering*, *6*(4), 45.

[14] Yang, Z. C., Bi, Q. C., Liu, B., & Huang, K. X. (2010). Nitrogen/non-Newtonian fluid two-phase upward flow in non-circular microchannels. *International Journal of Multiphase Flow*, *36*(1), 60-70.

[15] Fu, T., Ma, Y., Fun schilling, D., Zhu, C., & Li, H. Z. (2012). Breakup dynamics of slender bubbles in non-newtonian fluids in microfluidic flow-focusing devices. *AIChE Journal*, *58*(11), 3560-3567.

[16] Sontti, S. G., & Atta, A. (2017). CFD Analysis of Taylor Bubble in a Co-Flow Microchannel with Newtonian and Non-Newtonian Liquid. *Industrial & Engineering Chemistry Research*, *56*(25), 7401-7412.

[17] Ihmoudah, A., Rahman, M. A., & Butt, S. D. (2018, June). CFD and Experimental Studies of Yield Power-Law Fluids in Turbulent Pipe Flow. In *ASME 2018 37th International Conference on Ocean, Offshore and Arctic Engineering* (pp. V008T11A012-V008T11A012). American Society of Mechanical Engineers.

[18] Fluent, A. ANSYS Fluent 17.0 User's Guide; 2017.

[19] Triplett, K. A., Ghiaasiaan, S. M., Abdel-Khalik, S. I., & Sadowski, D. L. (1999). Gas-liquid two-phase flow in microchannels Part I: two-phase flow patterns. *International Journal of Multiphase Flow*, *25*(3), 377-394.

[20] Chilton, R. A., & Stainsby, R. (1998). Pressure loss equations for laminar and turbulent non-Newtonian pipe flow. *Journal of hydraulic engineering*, *124*(5), 522-529

[21] Enfis, M., Ahmed, R., & Osisanya, S. (2013). New hydraulic model for flow of Herschel–Buckley fluid in pipes and annuli. *Can. Energy Technol. Innov*, *1*(3), 41-47.

[22] Bretherton, F. P. (1961). The motion of long bubbles in tubes. *Journal of Fluid Mechanics*, *10*(2), 166-188.

[23] Aussillous, P., & Quéré, D. (2000). Quick deposition of a fluid on the wall of a tube. *Physics of fluids*, *12*(10), 2367-2371.

Chapter 6: Summary, Conclusions, and Future Recommendations

6.1 Introduction

The current research investigated the flow behaviour of Newtonian and non-Newtonian fluids on flow characteristics and pressure gradient as a function of single and two-phase flow rate conditions. In addition, this research aimed to provide a clear understanding of the effects of rheological models of shear-thinning fluids and their estimated parameters on the predictions of laminar, transitional, and turbulent flows in a horizontal pipe. The interactions between various parameters were investigated. The research was conducted following the objectives outlined in Chapter 1. This thesis has aimed to develop a design procedure for shear-thinning fluids in both the laminar region and transition zone into full turbulence.

6.2 Summary

The flow of Non-Newtonian fluid in pipelines has significant implications in industry and drilling operations, where the fluid rheology plays a critical role in the transportation process and efficient wellbore cleaning. This thesis investigates the flow behaviour of shear-thinning fluids in different pipe sizes and orientations. Contributions and outcomes of this research were provided in Chapters 2, 3, 4, and 5. These research areas are commented on as follows:

Chapter 2 discusses the single-phase flow of a shear-thinning fluid, with characteristics such as friction pressure gradient and translational velocity being measured using twelve explicit equations. The models are compared statistically to experimental results using two different-sized smooth pipes. Most correlations involving shear-thinning, e.g., the power law rheology model, adopt a best-fit approach for experimental results of up to around 45,000 R_{MR}. The modified model was then evaluated using laminar and transitional region experiments, as this strategy considers how the plug region impacts the flow. The evaluation shows good agreement with the Herschel–

Bulkley fluid viscosity. Slatter's modified Reynolds number for Herschel–Bulkley fluid shows the highest accuracy for critical velocity prediction. Furthermore, turbulent pipe flow estimations for Herschel–Bulkley fluid tend to be more accurate when applied within a specific rheological model, especially with cases involving high-stress yield. For Newtonian fluid turbulent flows, Chapter 2 also validates computational fluid dynamic (CFD) turbulent models related to wall functions. The k-ω models (ANSYS Fluent 19) provide accurate outcomes on power law fluid with higher behaviour index values. In contrast, the k-ε models were shown to work better when applied to fluids with behaviour index values exceeding 0.65. Moreover, when comparing the Herschel–Bulkley fluid model with the experimental results found in the present work, the percentile error increased along with the yield stress (τ_y). The novel CFD model modified for the Herschel–Bulkley viscosity was then implemented using ANSYS Fluent 19, and the experimental data were used for validation. The results were discontinuity-free and stable at vanishing shear rates numerically, particularly in transitional regions. They also show an excellent fit with low wall shear stress experimentally.

CFD and experimental studies are carried out in Chapter 3 to investigate the effect of the rheological parameters on the transition boundaries of flow regime maps for air/Newtonian and air/non-Newtonian fluids in a two-phase model. Typical slug flow characteristics, such as frequency and translational velocity, were observed in air/water and air/shear-thinning fluids. A 3-inch PVC horizontal pipe was used to monitor the flow characteristics of both water and four different shear-thinning solutions. The VOF model in ANSYS Fluent 19 was selected to detect the flow regimes and investigate the effects of rheological parameters on the flow pattern maps. This study adopted new modified flow regime maps that were evaluated based on the experimental results. Next, the maps' developed transition boundaries are compared to earlier results from

published research. For air-water flow, the bulk of the experimental testing points are well within Taitel and Dukler's and Mandhane et al.'s flow regime map boundaries. Furthermore, in observing how rheological parameters impact flow regime transition boundaries, Chhabra and Richardson's work on experimental flow regime transition is shown to nearly match the air-CMC1 and air-CMC4 power-law fluids with regard to dispersed bubbly interval flow to plug-slug flow. However, the transition from plug to slug flow was not considered in Chhabra and Richardson's regime map. Compared with Mandhane et al.'s flow map, no cases of transition were observed from plug to slug flow for air-CMC1 with a low concentration. However, for air-CMC4, there is an instance of plug-slug flow whose transition began earlier. In Mandhane et al.'s flow map, the predicted boundary considers power-law fluid viscosity, agreeing well with transition boundary experimental maps of plug-slug flow. Furthermore, the Herschel–Bulkley fluid yield stress effect on flow pattern maps is measured in two cases but shows only minor yield stress impacts (3.06 Pa) and an overall low effect (1.92 Pa). The yield stress and viscosity impacts were applied to modified X values between plug-slug flow in Mandhane et al.'s flow map boundaries for air- BXG2 and BXG4, and Herschel–Bulkley fluids were considered. The regions' plug-slug flow pattern transition lines shift to the right as the solution mass fraction increases, and the updated predicted boundary for the Mandhane et al. [7] flow map that considered the solid plug (diameter) effect from the Herschel–Bulkley fluid was found to agree well with the plug-slug flow transition lines in the experimental maps. The bubbles in the liquid plug-slug flow increase as the concentration of shear-thinning working fluids increases. These fluids were produced from the shear between the gas slug and liquid film. Because of the relative motion and viscosity, bubbles conglomerated, which then travelled underneath the large bubble. The slug velocity increased when the concentrations and flow velocity were maintained under the same operational conditions. The translational velocity of slugs is formulated based on experimental results for water as well as two shear-thinning models. In statistically

evaluating experimental results and existing correlations, the study indicates that the proposed model provides more accurate predictions of shear-thinning fluid behaviour. However, any correlations derived from the present research need to be tested in larger datasets, as the more data utilized in deriving results, the greater the predictive power for a broader range of conditions, including pipe size and fluid properties. The measurements obtained here are based only on a single pipe diameter.

In Chapter 4, the thesis conducts a numerical and experimental investigation of rheological properties in non-Newtonian fluid in two-phase flows. It compares the outcomes of these investigations with those for Newtonian fluid. The aim was to understand how rheological properties in gas/shear-thinning (Herschel–Bulkley fluid) impact slug characteristics in vertical flows. Water and three concentrations of aqueous xanthan gum (XG) (0.017 %, 0.035 %, and 0.052 %) were used as working liquids. At the same time, air was used as a gas. Pressure transducers were used to measure the response pressure, and a high-speed camera was used to observe the behaviour and effect of the non-Newtonian fluid. A VOF model in ANSYS Fluent 2019 was chosen to measure how rheology parameter characteristics affect slug flow in shear-thinning two-phase flow in a turbulent model. Comparing the empirical results from the literature to the simulated results, the slug-bubble transition flow was observed to be affected by alterations in the non-Newtonian phase rheology parameters. As the XG concentrations increase under the same operational conditions, a random, non-uniform distribution of small bubbles occurs as slug size increases, likely caused by the liquid phase's viscous force. The slug shape then morphs into a bullet shape in higher concentration due to higher shear forces in the liquid phase. Over time, gas/non-Newtonian fluid slug flows can lead to equipment loss. These flows are present in many standard industrial processes. The outcomes of the present study indicate that a VOF model in

ANSYS Fluent may be a valuable and reliable technique for predicting gas/shear-thinning fluid behaviour in a two-phase flow.

Chapter 5 provides a computational examination of Taylor bubbles in gas/non-Newtonian fluid. For the investigation, a mini-channel T-junction mixer was developed that has an inner diameter of 1 mm, and three aqueous XG solutions of 0.05, 0.1 and 0.15 w/w concentrations are used as shear-thinning liquids (Herschel–Bulkley model). The effects of the inlet liquid phase superficial velocity and XG concentration on the Taylor bubble velocity, shape, and length were examined and compared with the gas/Newtonian results. The liquid film thickness was also tested to understand better how it affects Taylor bubbles. The results show that the velocity of the Taylor bubbles increases as XG concentrations increase, especially for solutions with higher viscosity XG (0.15%). It was also discovered that bubble lengths decrease with increases in XG solution concentrations. However, when this occurs, the bubble shapes change. Moreover, when there is an increase in liquid inlet velocity, the length of the bubbles decreases under reduced liquid superficial velocity, while under higher velocities, bubble length shows only minor changes with increases in concentration. As a final test, the liquid film thickness is created and compared to correlations having a modified capillary number (Ca*) as non-Newtonian liquids. In all cases, there is good agreement.

6.3 Conclusions

- New criteria have been developed to predict Herschel-Bulkley fluid transitional flow. This model, which considered the effect of the plug region, provided good agreement with the behaviour of the Herschel-Bulkley fluid.
- The Herschel–Bulkley rheological model does not always occasionally describe the drilling fluid viscosity for low shear rate values.

- Predictions in turbulent pipe flow of Herschel–Bulkley fluid are superior with a specific rheological model. Using a different model could significantly impact predictions, particularly when the yield stress is high.
- Most turbulent models (RANS) in ANSYS Fluent associated with wall functions have been successfully validated to Newtonian fluid turbulent flows.
- More accurate results were observed with fluids with a higher behaviour index in the numerical (ANSYS Fluent) k–ω models for the power-law fluid. In contrast, k-ε was observed to work better with fluids that had a behaviour index value greater than 0.54.
- The numerical results of the Herschel–Bulkley fluid against the experimental results of this study, the percentile error was observed to increase with an increase in the yield stress (τ_y).
- In the current ANSYS Fluent 19 simulations, user-defined viscosity functions were implemented, which resulted in the best fit at the low shear rates experimentally and produced more stable and discontinuity-free results at vanishing shear rates numerically.
- For the air-water flow, most of the experimental testing points reported by Taitel and Dukler and Mandhane et al. fall within the boundaries of the corresponding flow maps.
- Chhabra and Richardson's flow map almost matched the experimental flow regime transition in the interval of dispersed bubbly flow to plug or slug flow for shear thinning fluid air-CMC1 and air-CMC4 power-law model.
- No transition cases from plug-to-slug flow for air-CMC1 with a low concentration were observed. Moreover, one case of transition delay from plug to slug flow for air-CMC4.
- The transition line of the regions' plug and slug flow patterns was found to shift to the right owing to increases in the solution mass fraction.

- The number of bubbles in the liquid plug-slug flow increases with the increasing concentration of shear-thinning working fluids, which are produced by the shear between the liquid film and the gas slug.
- The bubbles conglomerate and travel beneath the large bubble. Also, the results show that the slug velocity increases with increased concentrations and the mixture velocity of flow at the same operation conditions.
- The correlations developed in this study require further testing in a broader range of data sets to be more reliable. The more data used to derive it, the greater its predictive power over various conditions, fluid properties, and pipe sizes. As a result, our measurements were obtained with one pipe diameter.
- For slug characteristics in an upward vertical, we observed that the slug-bubble transition flow was affected by changing the rheology parameters of shear-thinning fluid at the same operations conditions.
- We observed a non-uniform and random distribution of small bubbles with an increase in slug size due to the effective viscous force of a liquid phase. Also, the shape of the slug changed to a bullet shape in higher concentration due to the influence of the higher shear force of the liquid phase.
- In the minichannel, the Taylor bubble velocity was found to increase with the higher viscosity of the shear-thinning of the fluid. Furthermore, bubble lengths decreased as shear-thinning fluid concentrations increased, but bubble shapes underwent alterations when the concentrations increased.
- Another intriguing outcome in the minichannel shows that when inlet air velocity increases, bubble lengths decrease during the lower superficial velocity of the shear-thinning fluid. In contrast, during higher velocities, they change only slightly after increases in concentration.

- There was good agreement when the liquid film thickness was modified and evaluated against correlations using the modified capillary number (Ca*) for shear-thinning liquids.

6.2 Recommendations for Future Research

The following aspects should be investigated that are not covered in this thesis:

- In this thesis only, single-phase pressure losses have been considered for two-phase flow. the pressure data collected but not published yet due to the pandemic and lack of time.
- The highest flow rates obtained for liquid and air were 0.0266 m3/s and 0.0166 m3/s, respectively, and one pipe size was obtained for two-phase flow.
- The introduction of more rheology can also be considered. Can be employed experimentally and numerically of more complex rheological problems.
- Two-phase inclined and vertical flow maps should be created and verified with the literature. In this study, only bentonite and xanthan gum have been used. For non-Newtonian fluid flow analysis, the experiments should be done with higher concentrations of different fluid rheologies.
- The effect of mud rheology on cutting movement was not considered in this study.
- A screw type progressive cavity pump would be an excellent replacement for a centrifugal water pump. This is a viscous fluid-handling screw progressive cavity pump. It is used to propel high viscosity drilling fluid.
- The work presented in this thesis may form the basis for further future research that informs important technical and environmental issues. Evidently, CFD ANSYS Fluent becoming a powerful tool applicable to a wide range of single and two-phase of non-Newtonian fluid.

Appendix A

Determination of the rheological parameters.

Appendix A

Determination of the rheological parameters.

This section includes methods were used to determine the rheological parameters of power-law and Herschel-Bulkley models.

A.1 Power-law model:

$$\tau = \tau_o + K\dot{\gamma}^n$$

$$\tau = K\dot{\gamma}^n$$

$$\log_{10}(\tau) = \log_{10} K + n \log_{10} \dot{\gamma}$$

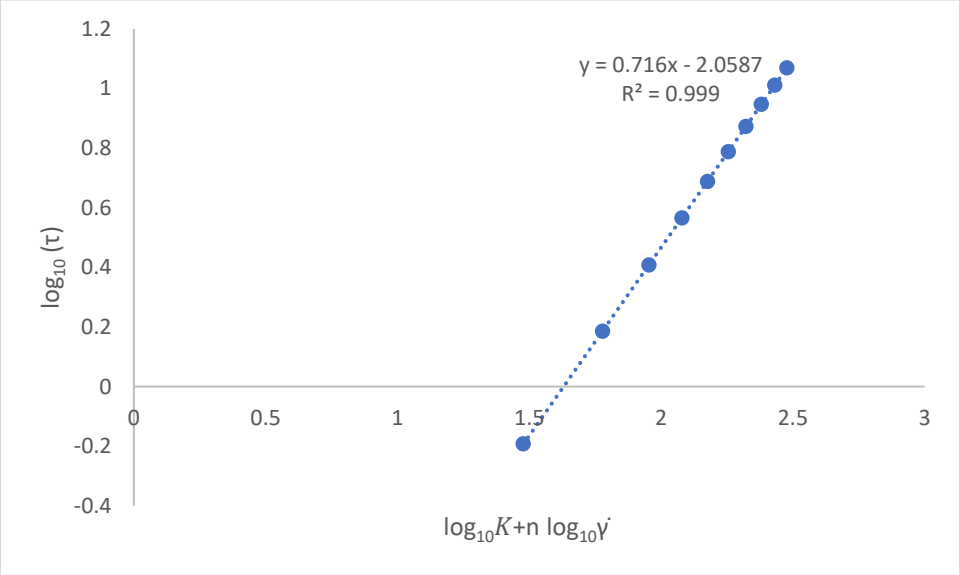

Where n = 0.716

and $K = 10^{(-2.0587)} = 0.008736$ Pa.s^n

Power-law Fluid - CMC1

τ_y (Pa)	0.00
n	0.71
K (Pa.s^n)	0.06

Flow Model

Power Law

RPM	Shear Rate (s^{-1})	Shear Stress - Calculated (Pa)
600	1022	8.2
300	511	5.0
200	341	3.8
100	170	2.3
6	10	0.3
3	5	0.2

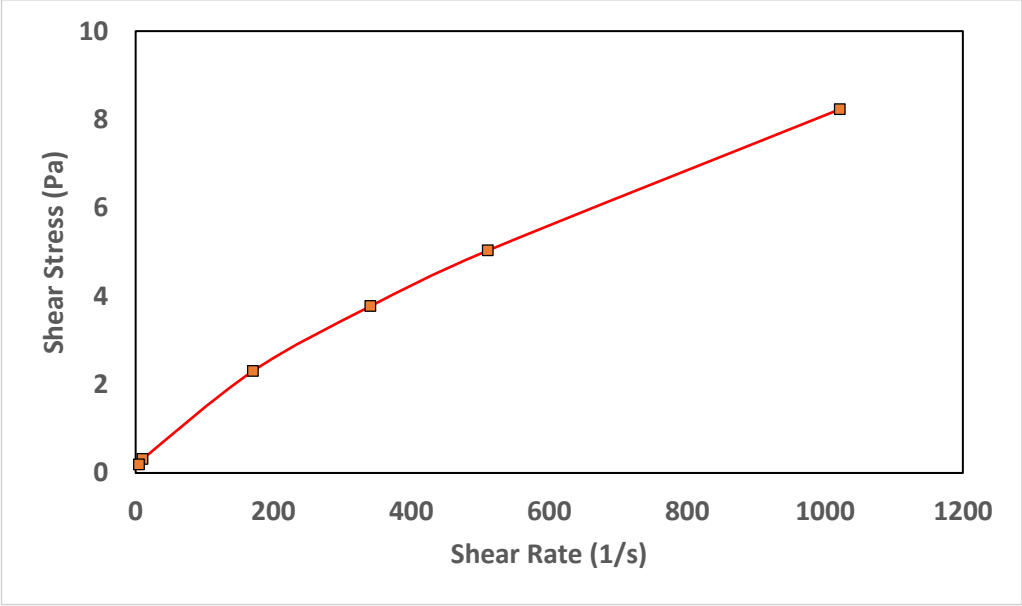

Power-law Fluid - CMC2

τ_y (Pa)	0.00
n	0.60
K (Pa.s^n)	0.23

Flow Model

Power Law

RPM	Shear Rate (1/s)	Shear Stress - Calculated (Pa)
600	1022	14.9
300	511	9.8
200	341	7.7
100	170	5.1
6	10	0.9
3	5	0.6

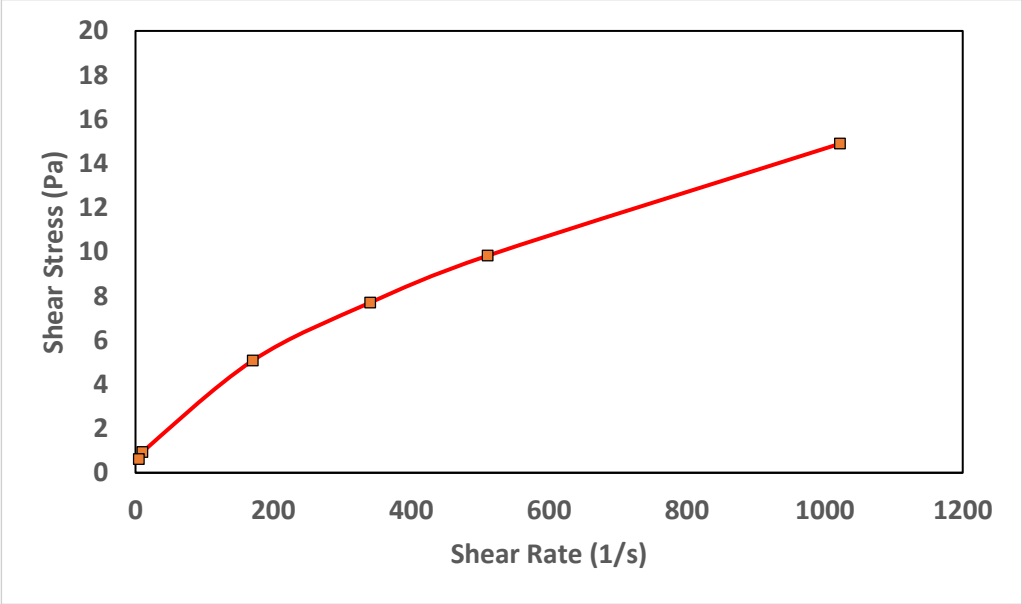

Power-law Fluid - CMC4

τ_y (Pa)	0.00
n	0.57
K (Pa.s^n)	0.41

Flow Model

Power Law

RPM	Shear Rate (1/s)	**Shear Stress - Calculated (Pa)**
600	1022	21.0
300	511	14.2
200	341	11.2
100	170	7.6
6	10	1.5
3	5	1.0

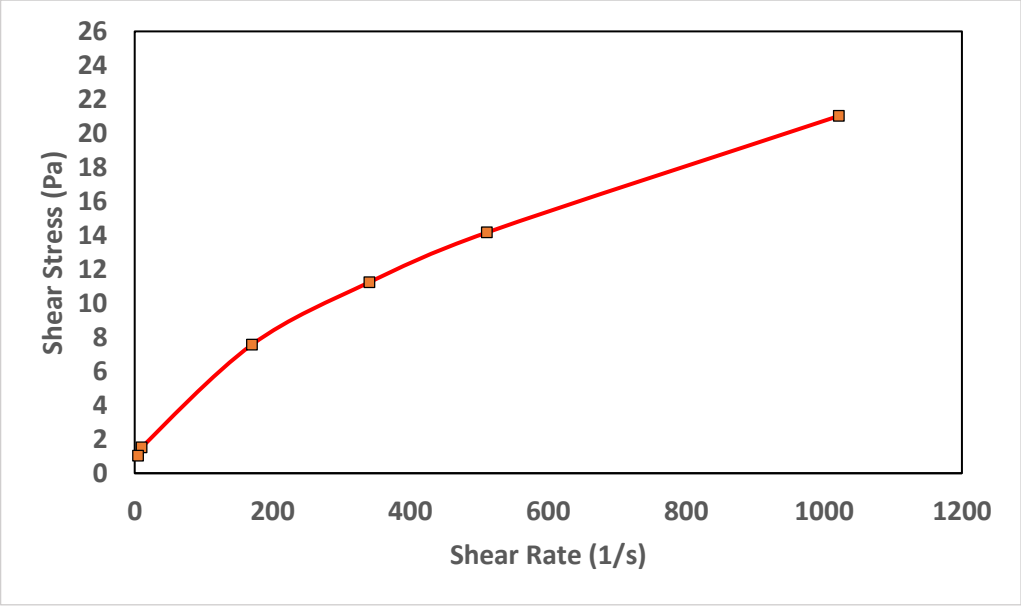

Fluid FBXG1

τ_y (Pa)	0.00
n	0.53
K (Pa.s^n)	0.22

Flow Model

Power Law

RPM	Shear Rate (1/s)	Shear Stress - Calculated (Pa)
600	1022	8.7
300	511	6.0
200	341	4.9
100	170	3.4
6	10	0.8
3	5	0.5

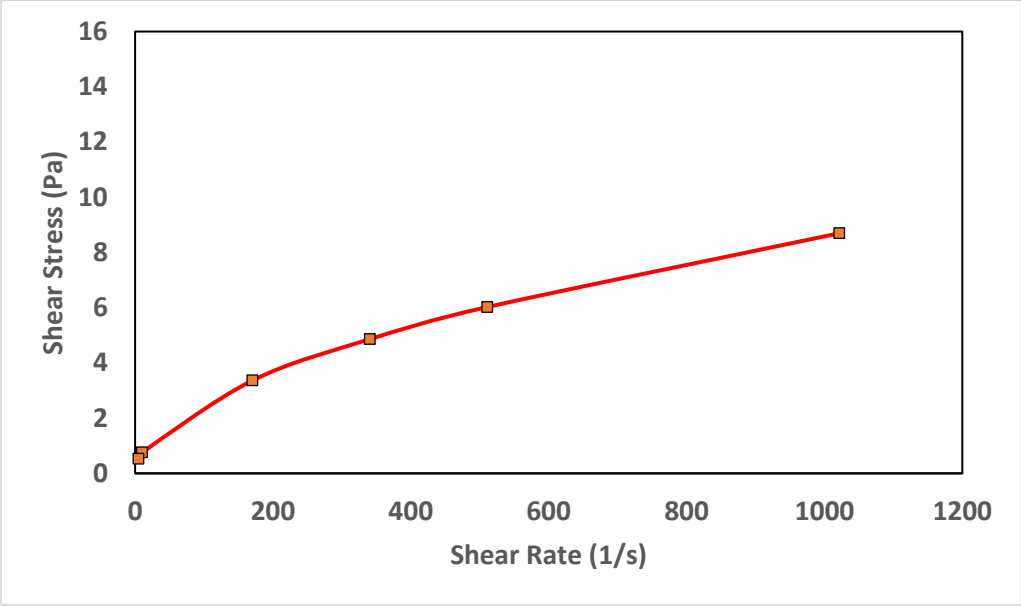

A.2 Herschel-Bulkley model:

Methods used to determine the rheological parameters of Herschel-Bulkley models.

$$\tau = \tau_o + K\dot{\gamma}^n$$

$$\tau - \tau_o = K\dot{\gamma}^n$$

$$\log_{10}(\tau - \tau_o) = \log_{10} K + n \log_{10} \dot{\gamma}$$

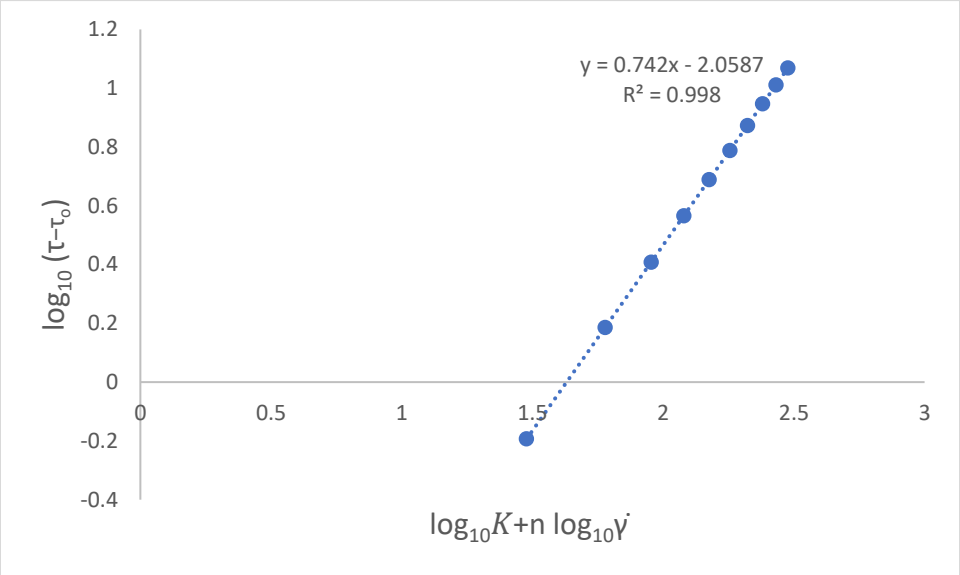

Where n = 0.742 and

and K = 10^ (-2.0587) = 0.008736 Pa.s^n

Herschel-Bulkley Fluid XG-0.05%

τ_y (Pa)	0.40
n	0.66
K (Pa.s^n)	0.037

Flow Model

Herschel-Bulkley Model

RPM	Shear Rate (1/s)	Shear Stress - Calculated (Pa)
600	1022	2.2
300	511	1.6
200	341	1.4
100	170	1.0
6	10	0.5
3	5	0.5

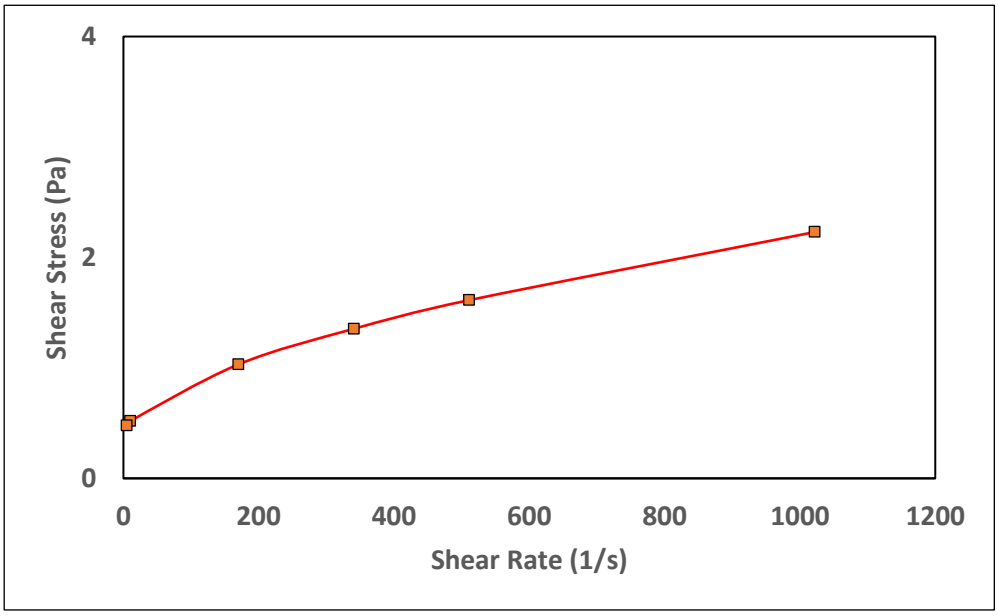

Herschel-Bulkley Fluid XG2

τ_y (Pa)	0.77
n	0.54
K (Pa.s^n)	0.13

Flow Model

Herschel-Bulkley Model

RPM	Shear Rate (1/s)	Shear Stress - Calculated (Pa)
600	1022	6.4
300	511	4.6
200	341	3.9
100	170	2.9
6	10	1.2
3	5	1.1

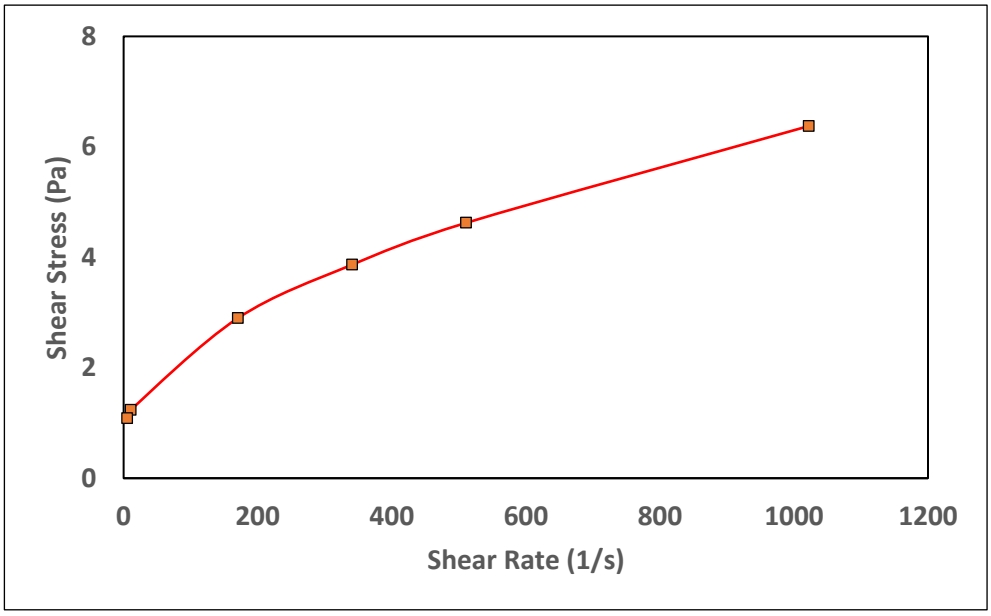

Herschel-Bulkley Fluid XG3

τ_y (Pa)	1.33
n	0.43
K (Pa.s^n)	0.35

Flow Model

Herschel-Bulkley Model

RPM	Shear Rate (1/s)	Shear Stress - Calculated (Pa)
600	1022	8.3
300	511	6.5
200	341	5.7
100	170	4.5
6	10	2.3
3	5	2.0

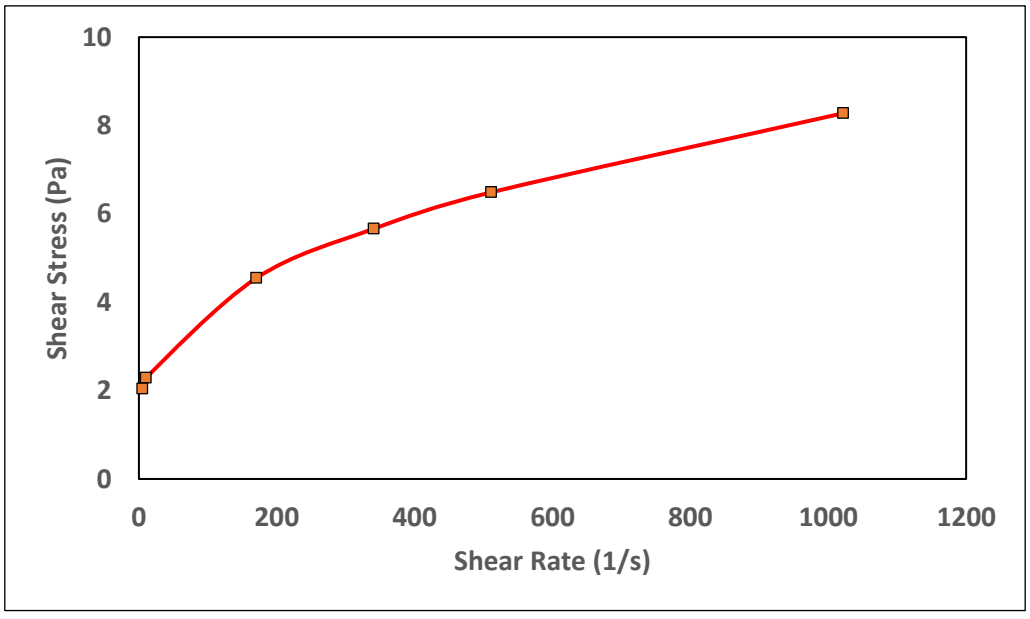

Herschel-Bulkley Fluid BXG1

τ_y (Pa)	0.76
n	0.74
K (Pa.s^n)	0.05

Flow Model

Herschel-Bulkley Model

RPM	Shear Rate (1/s)	Shear Stress - Calculated (Pa)
600	1022	9.4
300	511	5.9
200	341	4.6
100	170	3.1
6	10	1.0
3	5	0.9

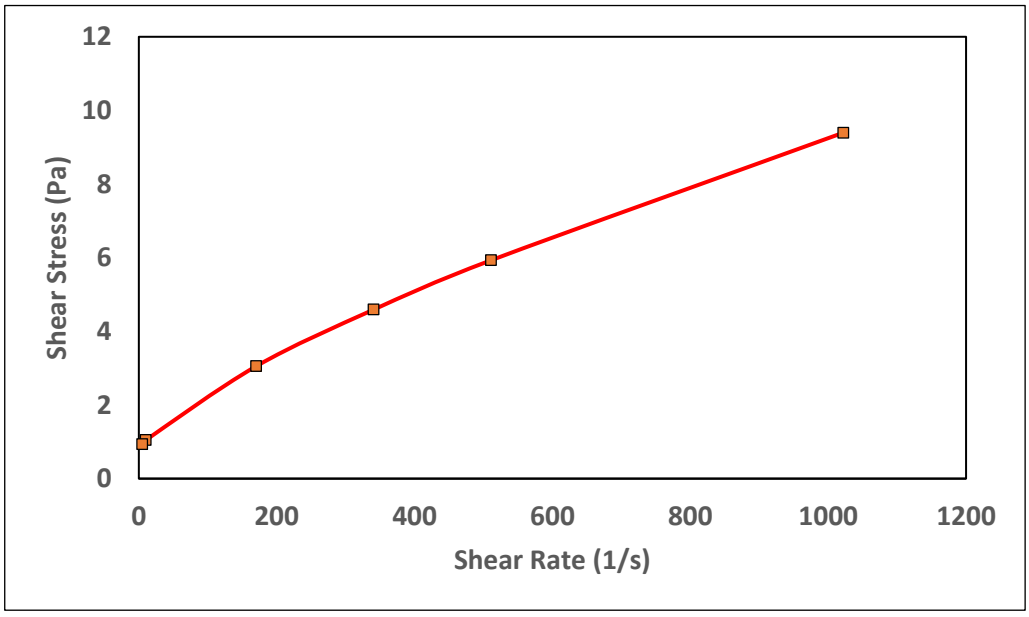

Herschel-Bulkley Fluid BXG2

τ_y (Pa)	1.92

n	0.61
K (Pa.s^n)	0.24

Flow Model
Herschel-Bulkley model

RPM	Shear Rate (1/s)	Shear Stress - Calculated (Pa)
600	1022	18.4
300	511	12.7
200	341	10.4
100	170	7.5
6	10	2.9
3	5	2.6

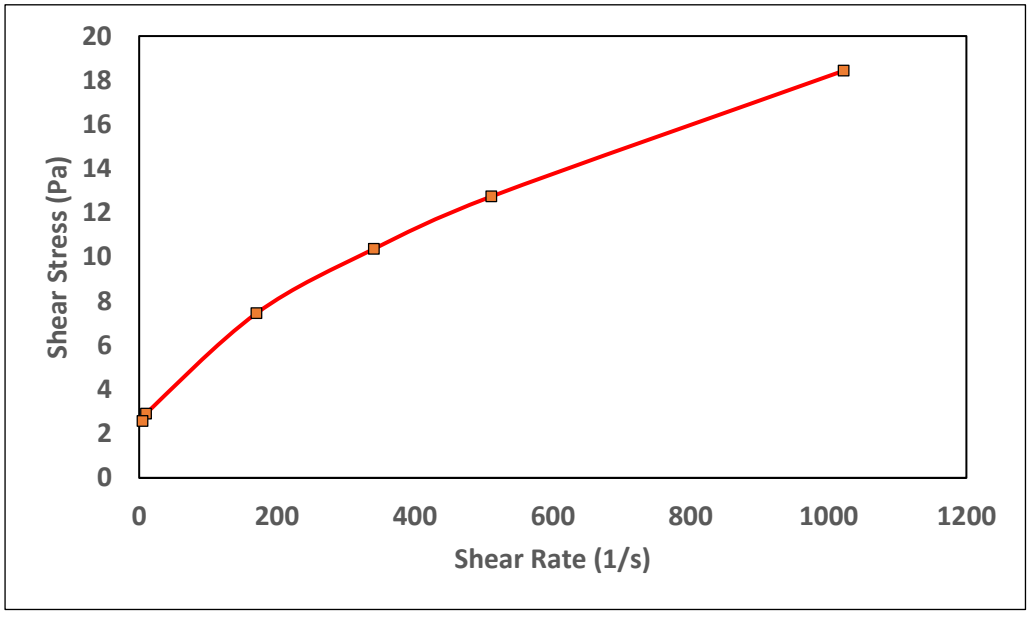

Herschel-Bulkley Fluid BXG4

τ_y (Pa)	3.06

n	0.56
K (Pa.s^n)	0.42

Flow Model

Herschel-Bulkley model

RPM	Shear Rate (1/s)	Shear Stress - Calculated (Pa)
600	1022	23.2
300	511	16.7
200	341	13.9
100	170	10.4
6	10	4.6
3	5	4.1

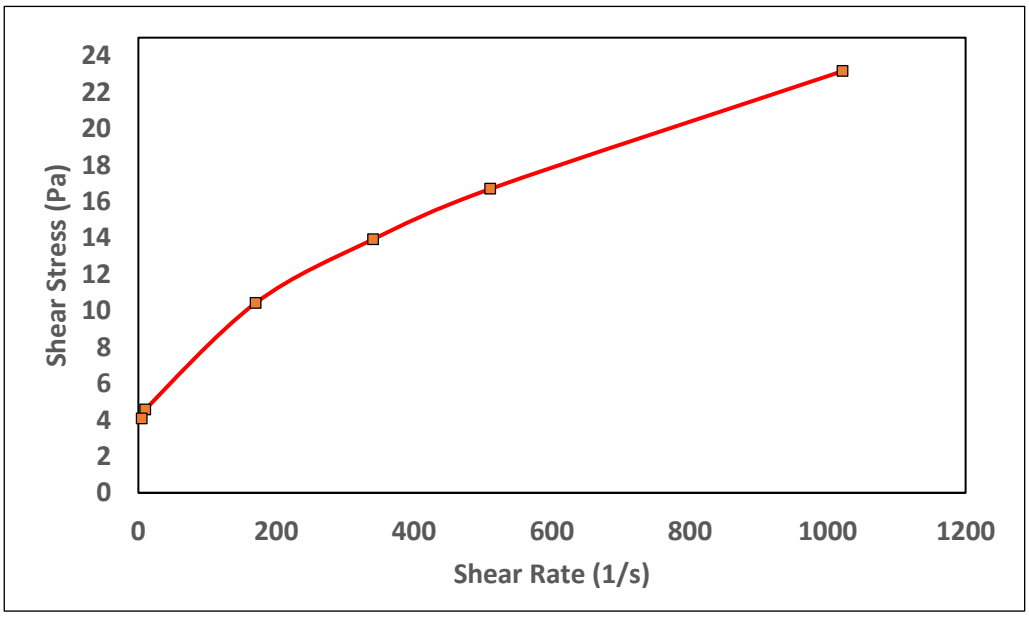

Appendix B

Experimental and Numerical Investigation of Gas/Yield Power-Law Fluids in a Horizontal Pipe

Proceedings of the ASME 2019 38th International Conference on Ocean, Offshore and Arctic Engineering
OMAE2019
June 09-14, 2019, Glasgow, Scotland, UK

OMAE2019-95219

Experimental and Numerical Investigation of Gas/Yield Power-Law Fluids in a Horizontal Pipe

Abdalsalam Ihmoudah

Faculty of Engineering & Applied Science, Memorial University of Newfoundland, St. John's, NL, Canada, A1B 3X5

aai117@mun.ca

Mohammad Azizur Rahman

Texas A&M University at Qatar, Doha, Qatar

aziz.rahman@qatar.tamu.edu

Mohamed M. Awad

Mechanical Power Engineering Department

Faculty of Engineering, Mansoura University

Mansoura, Egypt / m_m_awad@mans.edu.eg

Stephen D. Butt

Faculty of Engineering & Applied Science, Memorial University of Newfoundland, St. John's, NL, Canada, A1B 3X5

sdbutt@mun.ca

ABSTRACT

Two-phase flow of gas/yield power-law (YPL) fluids in pipes can be found in a wide range of practical and industrial applications. To improve the understanding of the effects of rheological parameters of non-Newtonian liquids in a two-phase model, experimental and Computational Fluid Dynamics (CFD) investigations of gas/yield power-law fluids in a horizontal pipe were carried out. Two Xanthan gum (XG) solutions at concentrations of (0.05% and 0.10% by weight) were used as the working liquids. The experiments were conducted in a flow loop in a 65-m open-cycle system. The horizontal test section had a diameter of 3 inches (76.2 mm). The transient calculations were conducted using a Volume of Fluid (VOF) model in ANSYS Fluent version 17.2. Slug flow characteristics were recorded and observed by a high-speed digital camera in different operating conditions. The slug velocity and slug frequency were investigated experimentally and numerically, and a comparison of results with empirical relationships found in the literature was performed. We observed that the rheological properties of non-Newtonian phase influence the flow behavior in two-phase flow with increasing XG concentrations. The results of the empirical correlation to measure the slug frequency of a gas/non-Newtonian with considered the rheology of the shear-thinning behaver gave acceptable agreement with numerical measurements at low polymer concentration. The effect of liquid superficial velocity on slug translational velocity at low gas superficial velocity was relatively high.

INTRODUCTION

In the chemical and petroleum industries, gas/non-Newtonian two-phase flows are common phenomena. The characterization of two-phase flow, especially in non-Newtonian behavior is of essential importance due to its appearance during the production and transportation of petroleum derivatives. There are essential hydrodynamic features in two-phase flow which should be considered in the determination of the flow pattern, void of the fraction and pressure drop that imply some difficulties due to the advanced flow mechanism and thus the range of parameters concerned. The majority of research thus far has examined gas-Newtonian two-phase flow, with little research being conducted on non-Newtonian liquids in two-phase flow [1-6]. Furthermore, there is minimal understanding of the rheological parameter's behavior of gas-non-Newtonian flow, especially for oil and gas applications. As a result, there is a clear need for more research into the realm of two-phase Newtonian and non-Newtonian flows on an experimental, theoretical and numerical basis. Such research could ultimately assist engineers in designing safer, more efficient and more cost-effective transport and production systems. Pipeline flows that are characterized as two-phase gas and liquid are distributed in different ways, giving rise to a variety of flow patterns. These

patterns, which are determined by different properties of the fluid as well as various operating conditions, exhibit distinct flow features. The main flow patterns in horizontal pipelines are slug flow (sometimes referred to as intermittent), dispersed bubble flow, and stratified smooth, wavy and annular flow.

Research indicates that the hydrodynamics or physical properties of gas-non-Newtonian liquid two-phase flow exhibit different behaviors compared to gas-Newtonian liquid flow. However, some research findings point to liquid properties having only a slight impact on flow patterns [7-9]. Based on these conclusions, Chhabra and Richardson [7] made a few minor alterations to Mandhane et al.'s [8] map of horizontal flow patterns while also taking into consideration Weisman et al.'s [9] work on the topic. Also, Xu et al. [10] investigated three CMC solutions by employing 0.2, 0.4 and 0.6-cm transparent tubes with a different inclination angle. Rosehart et al. [11] published their findings on the first experimental study dealing with the effect of non-Newtonian characteristics. In that study, the researchers used capacitive sensors for measuring the velocity of the slug as well as average hold-up and frequency. Otten and Fayed [12] published their experimental results, which included pressure-drop measurements for two-phase flows in air/shear thinning fluid and CarbopolR 941 solutions. For the prediction of void fraction and pressure loss of gas/non-Newtonian liquid, Farooqi and Richardson [13] adjusted the model developed by Lockhart and Martinelli [14] for predicting void fraction averages. They also investigated drag reduction for intermittent regimes. Then, based on the notion of loss coefficient, Dziubinski [15] revised the drag ratio of two-phase pressure drops that occur in intermittent flows of gas/non-Newtonian fluid. Ruiz-Viera et al. [16] investigated air-lubricating grease two-phase flow experimentally by applying various types of geometries, considering rough as well as smooth surfaces. Additionally, they developed a two-phase pressure drop empirical model that combined sigmoidal-type equations and power law. Abdalsalam et al. [17] numerically and experimentally studied rheological parameters for single-phase yield-power law in vertical and horizontal pipelines. They investigated the effect of rheological parameters of yield power-law fluids on pressure drop.

More recently, Picchi at al. [18] experimentally investigated in horizontal and inclined pipes with an inner diameter of 22.8 mm, characteristic of air-shear thinning two-phase liquid flow. They observed that flow pattern maps are affected by the inclination angle and rheology of the shear thinning fluid. Baungartner et al. [19] experimentally studied a 44.2-mm diameter horizontal pipe's influence on the rheological parameters of carboxymethylcellulose (CMC) solution and air. They found thatthe flow behavior was heavily affected by the rheological parameters of the continuous phase.

Recently, many researchers have employed computational fluid dynamics (CFD) simulation tools for examining two-phase flow hydrodynamics characteristics. However, none of these authors looked at two-phase flow yield power-law fluid. Ko et al. [20] employed a shear stress transport model for solving kinetic energy-related equations for turbulent wavy core flow. One of the main findings of these researchers was that, compared to the K-ω turbulence model, their model gave more accurate predictions for wavelength and pressure distribution. Alyaari et al. [20] applied the RNG k-ε turbulence model as a means to simulate stratified flow for horizontal pipes. Lo and Tomasello [21] utilized the volume of fluid (VOF) approach to simulate stratified Newtonian fluid flows, demonstrating how the turbulence model impacts CFD outcomes. However, their findings indicate that the *k*-ω turbulence model gave accurate results more than others model. Kroes and Henkes [22] used FLUENT (ANSYS 14) to investigate drift velocity in elongated gas bubbles in Newtonian fluid occurring in pipelines. The researchers observed good agreement in the experimental results of the analytical solution. Jia et al. [23] compared pressure gradients and drag reduction ratios in slug and stratified flow regime types. Additionally, they applied the 3D CFD process as a means to determine the friction factor of the liquid wall, which they then compared to values found for empirical standard correlations. All these studies did not consider yield-power law fluid in a two-phase flow. Sanderse et al. [24] used CFD FLUENT, based on a two-phase model, to track elongated bubbles in a channel. The primary objective of these simulations was to predict the pressure variations and drift velocity of a bubble in the channel. The outcomes of this research were then validated using a 2D CFD inviscid flow solution. Again, however, as with the earlier studies mentioned above, none of these investigations considered yield-power law fluid for two-phase flows.

Until now, very little research has been devoted to the flow of two-phase gas/non-Newtonian liquids, especially yield stress effect behavior in pipes. In the present study, we experimentally and numerically investigated the effect of the change in rheology parameters on the slug flow characteristics in a horizontal pipe. Air and two different concentrations of XG solutions are referred to as non-Newtonian (yield power-law) and as working as fluids.

FLUID CHARACTERISTICS

To achieve the goals, two different concentrations of XG according to weight (XG-0.05% and 0.10% w/w) were prepared in the Drilling Technology Laboratory (DTL) by the addition of minute amounts of polymer powders to water. The rheology and characteristics of the solutions were determined by using an 8-speed API-compliant rotational viscometer (Model 800) and 4-

scale mud balance. As shown in Figure 1, the non-Newtonian liquids refer to the shear thinning of the Herschel-Bulkley model also called the yield power-law (YPL) model, which is described with three parameters. Also, we measured the angle of contact and surface tension. Herschel and Bulkley's [25] nonlinear three-parameter pseudo plastic model has been used to express fluid rheology.

$$\tau = \tau_y + k\,\gamma^n \qquad (1)$$

Where τ shear stress, n the fluid behavior index, k the consistency index and τ_y yield stress. Table 1 shows the properties of the YPL fluid of the different XG concentration used in the experiments and simulations. The rheological behavior between shear rate and non-Newtonian liquid apparent viscosity define the fluid type. Hence, if apparent viscosity decreases with increased shear rate, it is called "shear-thinning," while if apparent viscosity increases with increasing the shear rate, it is called "shear-thickening," Figure 2 illustrates this relationship. See Ihmoudah et al. [17] for more details.

For turbulent flows, the generalized Reynolds number for YPL fluids can express as [26]:

$$R_{eg} = \frac{\rho V D}{\mu_w\left(\frac{3n+1}{4n}\right)\left(\frac{3n+1}{1-aX-bX^2-cX^3}\right)} \qquad (2)$$

Where

$$\mu_w = \frac{\tau_w}{\gamma_w} = \tau_w{}^{(n-1)/n}\left(\frac{k}{1-X}\right)^{\left(\frac{1}{n}\right)} \qquad (3)$$

And

$$a = \frac{1}{(2n+1)};\ b = \frac{2n}{(n+1)(2n+1)};\ c = \frac{2n^2}{(n+1)(2n+1)} \qquad (4)$$

$$X = \frac{\tau_0}{\tau_w} = \frac{4L\tau_0}{D\Delta P} \qquad (5)$$

For laminar of (YPL) fluid in pipe flows the Pressure loss can be expressed as:

$$\frac{\Delta p}{L} = \frac{4k}{D}\left(\frac{8V}{D}\right)^n\left(\frac{3n+1}{4n}\right)^n\left(\frac{1}{1-X}\right)\left(\frac{3n+1}{1-aX-bX^2-cX^3}\right)^n \qquad (6)$$

Then, the wall shear stress for turbulent flow can calculate by using $\frac{\Delta p}{L}$ from experimental results as:

$$\frac{\Delta p}{L} = \frac{4\tau_w}{D} \qquad (7)$$

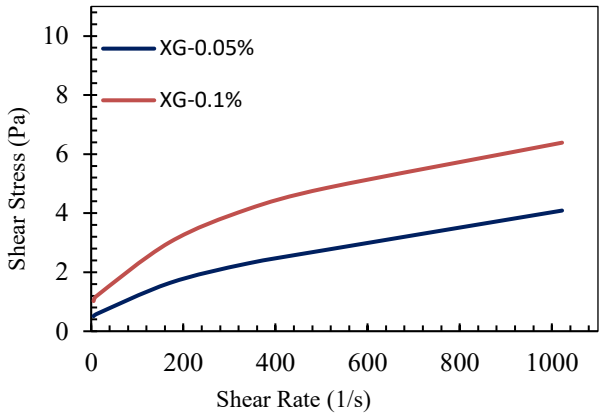

Fig. 1. The rheological behavior of xanthan solutions was at 20 °C.

Table 1. Physical properties of YPL fluids at 20 °C.

Symbol	n	k (Pa.s^n)	τ_y (Pa)
XG-0.05	0.66	0.037	0.4
XG-0.10	0.54	0.133	0.7

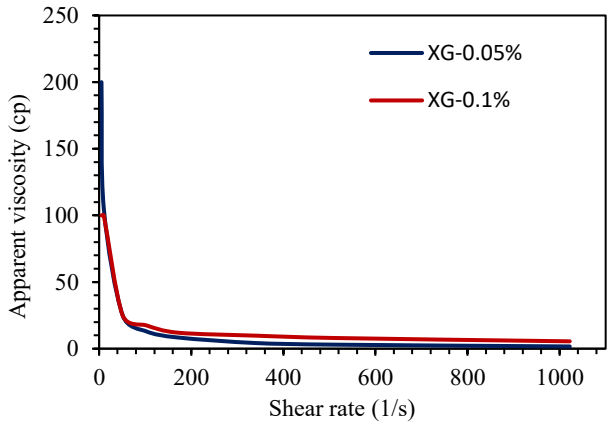

Fig. 2. The apparent viscosity of Xanthan gum solutions as a function of shear rate.

Experimental set-up

In the present work, the experiments adopted the setup illustrated in Figure 3. As can be seen, compressor pump air is channeled via an air tank and regulating valve as a means for keeping the pressure stable. Then, the centrifugal pump moves the non-Newtonian liquid phase out of the liquid phase tank to the entire system. An inverter maintains **the** rotary pump speed via changes in frequency by regulating the power. Next, the gas and non-Newtonian phases enter the pipe through a T-junction positioned ahead of the test area. The volumetric flow rates for gas and liquids can be regulated independently and are measured. To ensure that the flow rates for all of the phases are

independently regulated and measured, two Omega meters were installed. The DN 15 pipe flow meter is FLR 6715D, whose effective measures are 3.3 m³/h to 2.50 m³/h, while the DN 25 pipe flow meter is FLR 6750D, with effective measures of 9 m³/h to 85 m³/h. The non-Newtonian liquid phase was measured by an Omega FTB-730 turbine flow meter with 0.7 m³/h to 89.87 m³/h range, with an accuracy estimated at ±1.1% full scale. Also, differential and absolute pressure transducers (Omega PX603-100Q5V whose effective measures are 0–100 Psi) obtained pressure data for both liquid and gas. Four thermo-coupling Omega TC-(*)-NPT series, T-type sensors were employed. The high-speed cameras were situated at a 14-m distance from the mixing tee. The mixture moves into the test section, after which the fluid moves back to the primary storage tank and the phases separate due to gravitational effects.

EXPERIMENTAL PROCEDURE

In the present study, two different concentrations of XG solutions (XG-0.05and XG-0.10) are used as liquid phases. The low gas and liquid velocities were selected from a Mandhane et al. [8] flow pattern map to ensure the critical transition conditions between the two flow regimes in this study. For each experiment, a waiting time of 7–15 minutes was maintained to stabilize readings before recording the video. Therefore, we considered four slugs to be sufficient for each case to calculate the slug flow characteristics; moreover, the tests were repeated to ensure the positive consistency of results. Then, through the inverter frequency changes mentioned in the previous section, we initiated a liquid solution XG-0.05 introduced at low-speed $U_{SL.}$ The gas was also introduced in the system, also at low-speed U_{GS}. After the acquisition and recorded observation of data, we increased the flow rate for the new U_{SL} and U_{GS}. Such a procedure was repeated for XG-0.10 solutions. A high-speed digital camera recorded the flow patterns throughout the processes; these videos were later viewed in slow-motion.

NUMERICAL METHODOLOGY

The simulations wear carried out as 3D transient flow in a horizontal pipe. The domain was built and meshed in ANSYS FLUENT 17.2. The geometry consists of a horizontal section with an inner diameter of 76.2 mm. The gas and XG solutions were introduced into the pipe through a T- junction. The XG solutions enter into the pipe from the horizontal direction and gas from a vertical direction at diameter 25mm. Figure 4 shows the schematic of three-dimension pipe and layers near the wall. In this set-up, nine layers near the pipe wall have been utilized in order to capture both the bubble shape and film thinness.

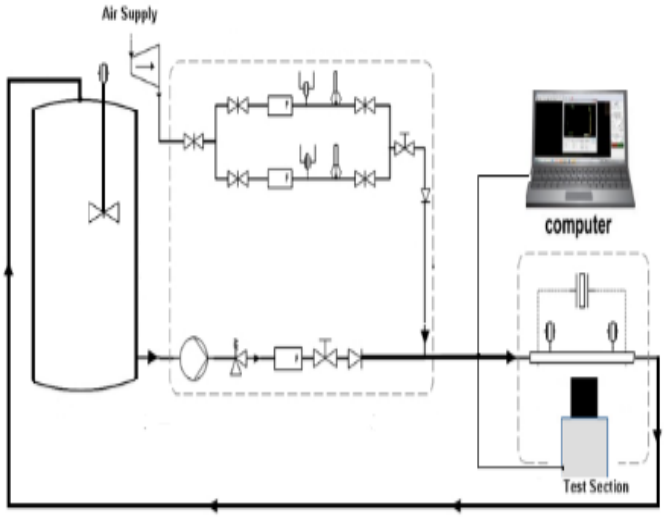

Fig. 3. Schematic of the experimental set-up.

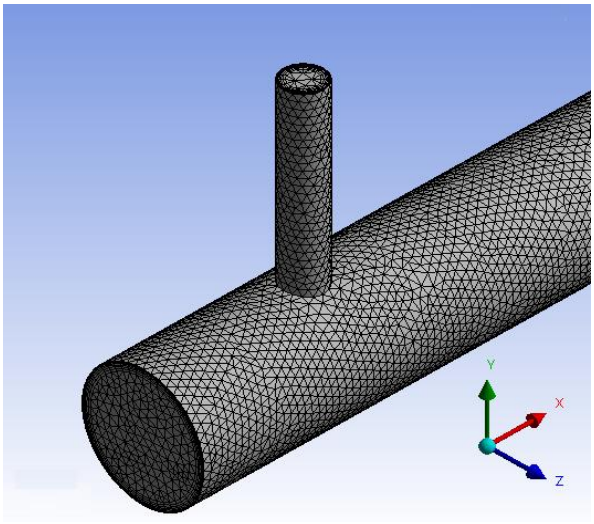

Fig. 4. 3D Mesh distribution in the pipe geometry.

NUMERICAL PROCEDURE

In this set-up, two non-Newtonian fluids working as liquids, while air was working as gas. The fluids enter the mixing area via two different inlets to the T-junction. The non-Newtonian fluid enters in a horizontal direction and gas in a vertical direction. The time step or a convergence criterion 10-4 has been employed to maintain Courant number (CLF) ≤ 0.25 with a SIMPLE scheme for pressure-velocity coupling, Geo-Reconstruct for volume fraction and second-order upwind for momentum equation.

GOVERNING EQUATION IN THE VOF MODEL

The VOF model in Fluent is a surface-tracking mechanism used to a fixed Eulerian mesh. This model selected to track the interface between the liquid and gas by determining the changing in the rate of volume fractions for an individual of fluid in the computational domain [27]. The continuity equation and the momentum equation govern fluid motion in each point in the domain as follows.

The equation of continuity:

$$\frac{\partial \rho}{\partial t} + \nabla.\left(\rho\, \vec{U}\right) = 0 \qquad (8)$$

Where, ρ, t and U are density, time and velocity, respectively.

The equation of Momentum:

$$\frac{\partial(\rho\vec{U})}{\partial \mathrm{t}} + \nabla.\left(\rho\vec{U}\vec{U}\right) = -\nabla P + \nabla.\bar{\bar{\tau}} + F_{ST} \qquad (9)$$

$$\bar{\bar{\tau}} = \eta(\nabla\vec{U} + \nabla\vec{U}^{T}) \qquad (10)$$

Where $\vec{U}$ is the velocity vector, p denoted pressure, ρ is volume-averaged density, η is dynamic viscosity, F_{SF} is surface tension force, $\bar{\bar{\tau}}$ is shear stress, respectively.

The mixture density and viscosity given by continuity equation in each cell are as follows:

$$\rho = a_2\rho_2 + (1 - a_2)\rho_1 \qquad (11)$$

$$\eta = a_2\rho\eta_2 + (1 - a_2)\eta_1 \qquad (12)$$

The continuity equation for each α_q is considered as follows:

$$\frac{\partial a_q}{\partial x}\left(U_q.\Delta\right) = S_{\alpha q} \qquad (13)$$

Where q is a liquid or gas phase, the tracking of the interfaces between the liquid phase and gas phase can calculate by solving the continuity equation of one of the phases as following.

$$\sum_{q=1}^{n} \alpha_q = 1 \qquad (14)$$

For a two-phase model, the void fraction will take the following three cases.

$\alpha_q = 0$ if the cell is empty of fluid.

$\alpha_q = 1$ if the cell is full of fluid.

$0 < \alpha_q < 1$ interface between the two fluids.

The surface tension force can be expressed as:

$$F_{SF} = \sigma\left[\frac{[k_n\rho\nabla\alpha_1]}{\frac{1}{2}(\rho_1+\rho_2)}\right] \qquad (15)$$

Where σ is surface tension, k_n is the radius of curvature.

$$\mathrm{k}_n = \nabla.\hat{m} = \frac{1}{|m|}\left[\left(\frac{m}{|m|}.\nabla\right)|m| - (\nabla.m)\right] \qquad (16)$$

Where $\hat{m} = \frac{m}{|m|}$ and $m = \nabla\alpha_q$

In the VOF model, the wall adhesion angle with the surface tension as:

$$\hat{m} = \hat{m}_w\cos\theta_w + \hat{t}_w\sin\theta_w \qquad (17)$$

Where $\hat{m}_w$ and $\hat{t}_w$ are vectors normal and the tangential to the wall.

TURBULENT MODEL

The present study, turbulent regime consider since the Reynolds numbers for the gas phase and liquid phase are in the range of turbulent flow. Several models have been developed in CFD software ANSYS FLUENT commercials such as $\kappa-\epsilon$ model, large eddy simulation (LES) and $\kappa-\omega$ model. In this study $\kappa-\omega$ approach, the classification of Reynolds-averaged Navier-Stokes (RANS) selected to solving two transport equation model are shown as:

$$\frac{\partial}{\partial t}(\rho k) + \frac{\partial}{\partial x_i}(\rho k u_i) = \frac{\partial}{\partial x_i}\left[(\mu + \frac{\mu_t}{\sigma_k})\frac{\partial k}{\partial x_i}\right] + G_k + G_b - \rho\varepsilon \qquad (17)$$

$$\frac{\partial}{\partial t}(\rho\varepsilon) + \frac{\partial}{\partial x_i}(\rho\epsilon u_i) = \frac{\partial}{\partial x_i}\left[(\mu + \frac{\mu_t}{\sigma_\varepsilon})\frac{\partial k}{\partial x_i}\right] + G_\varepsilon + G_b + \frac{\varepsilon}{k}\left(c_{1\varepsilon}G_k + {}_{3\varepsilon}c_b\rho - \varepsilon c_{2\epsilon\rho}\right) \qquad (18)$$

The turbulent viscosity is computed by ε *and* k as following:

$$\mu_t = \rho c_\mu \frac{k}{\varepsilon} \qquad (19)$$

Non-Newtonian (YPL) phase.

For non-Newtonian fluid, the shear stress can be written in term of viscosity as:

$$\tau_{ij} = \mu\left(\frac{\partial \mathrm{u}_i}{\partial x_j} + \frac{\partial \mathrm{u}_j}{\partial x_j}\right) \qquad (20)$$

The viscosity of non-Newtonian YPL in fluent expressed as:

$$\mu = \frac{\tau_0}{(\lambda\dot{\gamma})} + k(\lambda\dot{\gamma})^{n-1} \quad (21)$$

Where μ the viscosity, k is the consistency coefficient (Pa s^n), $\dot{\gamma}$ is the shear rate (s^{-1}), n the power-law index, and λ is the time constant [27].

Measurement technique and analysis

In this work, the intermittent flow model includes the plug and slug flow patterns used. In this model, the liquid slug could potentially include dispersed bubbles, while the gas bubbles sit on a layer of liquid film. A similar mechanism might manifest during low liquid rates if there is not enough liquid to form slugs. The model is developed based on momentum and mass balance, which features the total slug unit with length l, the liquid slug has length l_s, while the film zone has a length l_f. Furthermore, it is made up of a liquid film that features a stable height and is overlaid with a gas bubble, $l = l_s + l_f$. By applied mass balance in a unit of slug yielding.

$$U_{SL} = \frac{1}{l}\left[(1-\alpha_S).l_s.U_S + \int_0^{l_l} U_l.(1-\alpha_l).dx\right] \quad (22)$$

$$U_{Sg} = \frac{1}{l}\left[\alpha_S.l_s.U_S + \int_0^{l_l} U_g.\alpha_l.dx\right] \quad (23)$$

Where *S, L, Ug, U_s*, and α denotes, respectively, liquid slug zone, elongated bubble zone, gas bubble velocity, liquid slug velocity and void fraction. As proposed by Taitel and Barnea [28] the liquid slug velocity, U_s, is evaluated by

$$U_S = U_m = U_{SL} + U_{Sg} \quad (24)$$

Where U_m is the mixture velocity of liquid and gas phases.

Translational velocity

In multiphase flows, translational velocity refers to the rate of speed traveled by a slug unit, which is gas bubbles moving in conjunction with alternating liquid slugs in a typical slug flow pattern. Translational velocity can be expressed by multiplying the mixture's velocity portion with the drift velocity and distribution parameter. Nicklin et al. [29] proposed the expression of slug unit translational velocity, as shown in Eq. (24):

$$U_t = C_0.U_m + U_d \quad (25)$$

In this formulation, U_m denotes gas-liquid mixture superficial velocity, and U_d represents drift velocity. Furthermore, distribution parameter C_0 indicates an approximate ratio of a slug unit's average and maximum velocity when taking into account a fully-formed profile for slug unit velocity. In this study, we following Bendiksen [30] and Weber [31] models to obtained U_d and C_0 based on experimental data.

Slug Frequency

Slug frequency f_S, can be defined as the number of slugs moving past a particular point in the pipeline during a specific time. This type of frequency serves as a function for each slug unit's average translational velocity as well as flow rate and inclination angle. Estimating the f_S is required in some industrial processes and pipelines to precisely predict corrosion rates. Gregory and Scott [32] devised a correlation that is valid to predicting slug frequency in Newtonian fluids.

$$f_S = 0.0226\left[\frac{U_{SL}}{gD}\left(\frac{19.75}{U_m} + U_m\right)\right]^{1.2} \quad (26)$$

Then, in Picchi et al. [33], they extended the Gregory and Scott [32] model as a means to predicted slug frequency of shear-thinning fluid rheology.

$$f_S = 0.0448\left[\frac{U_{SL}}{gD}\left(\frac{32.2014}{U_m} + U_m\right)\right]^{0.88}\left(\frac{Re_p}{Re_w}\right)^{0.07}(n)^{-2.85} \quad (27)$$

Where f_S donated the slug frequency, $U_m$is the mixture velocity, n is flow behavior index, U_{SL} is the liquid velocity, g is gravity, D is the pipe diameter, Re_p is non-Newtonian Reynolds number and Re_w is Newtonian liquid Reynolds number.

Flow visualization and recording videos were achieved by using Mega Speed MS55K - High-speed camera with a full resolution of 1280x1024 and speed 2000fps. Phantom camera control (PCC) software was used to tracking slug characteristics along a horizontal pipe.

RESULTS AND DISCUSSION

Grid Independence and Validation of Numerical Simulation

The results of computational fluid dynamics (CFD) are strongly related to the quality and mesh size of the grid size. To examine the accuracy of our numerical simulation results, the results of the developed model in ANSYS Fluent are verified to our experimental results as a gas/non-Newtonian. Figure 5 shows a comparison of experimental results and numerical simulation results by using the VOF method. The results of numerical simulation CFD are affected by the size and quality of the grid size. The effect of mesh size on the numerical simulation results was investigated under operation conditions at mixture

superficial velocity, U_m =2.1 (m/s). Also, the number of elements increased from 5x10^5 to 3.8x10^6. As can be seen in Figure 5 and based on the computational time and accuracy of the results, the number of elements was 3.1x10^6 and a grid size of 0.004 was used in this study.

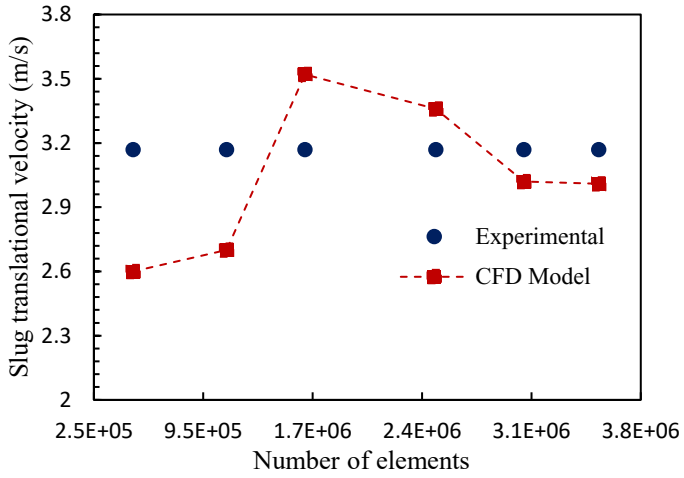

Fig. 5. Grid-independent study for XG-0.05 solution at mixture superficial velocity, U_m =2.1 (m/s).

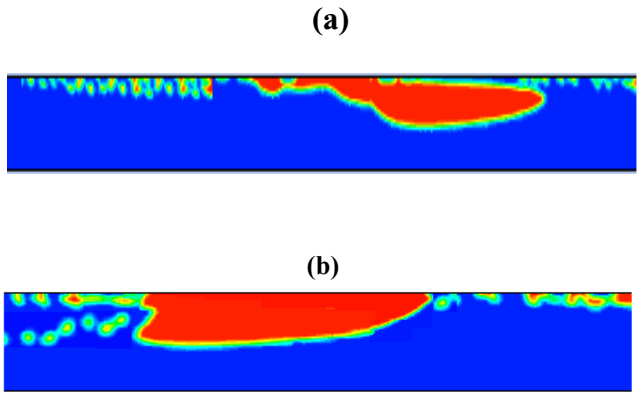

Fig. 6. Phase volume fraction contours (color red, gas; color blue, liquid) for XG-0.05 solution (a) plug, U_{SL} = 3.5 m/s, and U_{SG} = 0.7 m/s, and (d) slug, U_{SL} = 1.5 m/s, U_{SG} =2.5 m/s.

Figure 6 describes the CFD flow pattern for gas/non-Newtonian flow- XG-0.05 solution obtained from the VOF method. We followed the flow pattern classification in a horizontal pipe given by Taitel and Duckler [34]. As shown in Figure 6, the VOF method successfully to predict the slug and plug flow regimes at different phase velocities.

Slug translational velocity

Slug transitional velocity for non-Newtonian liquids flowing through horizontal pipelines was investigated experimentally by used high-speed camera and compression with numerical and empirical correlations found in the literature. In general terms, 'slug transitional velocity' refers to the interface velocity between liquid slug the gas pocket. The velocity at this interface is typically the greatest for slug units occurring in horizontal flow.

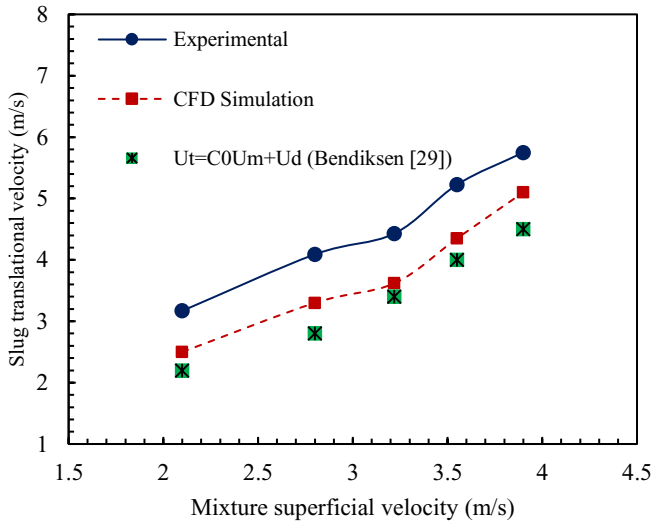

Fig. 7. Experimentally obtained mean slug velocities compared to numerically computed results and Nicklin et al. [29] correlation for XG-0.05 flow.

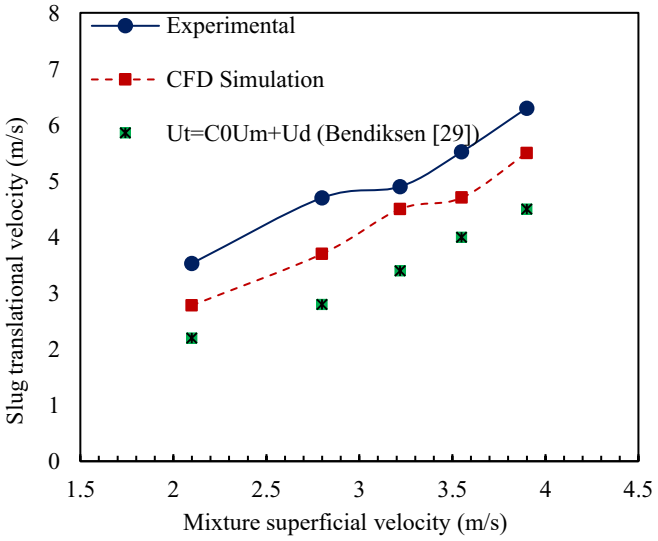

Fig. 8. Experimentally obtained slug velocities compared to numerically computed results and Nicklin et al. [29] correlation for XG-0.10 solution.

As shown in Figure 7, the comparison between predicted slug transitional velocities by Eq. (24) and the measures numerically and experimentally are presented for XG-0.05 at different gas superficial velocity. We observed that the increases in gas

superficial velocity lead to increases in slug translational velocity at a constant of liquid superficial velocity.

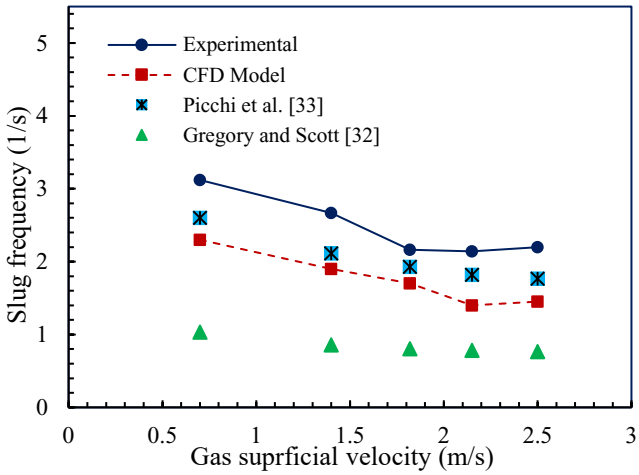

Fig. 9. Slug liquid frequency versus gas superficial velocity for XG-0.05 flow, U_{SL}=1.4 (m/s).

With increasing XG concentration we observed that the slug translation velocity increased due to dominating viscous force of the fluid phase. As a result, the data of the CFD model have an acceptable level of agreement with the correlation results with increasing the gap between. We can also observe from Figure 8 that the CFD model had the best result as compared to the correlation of Nicklin et al. [29].

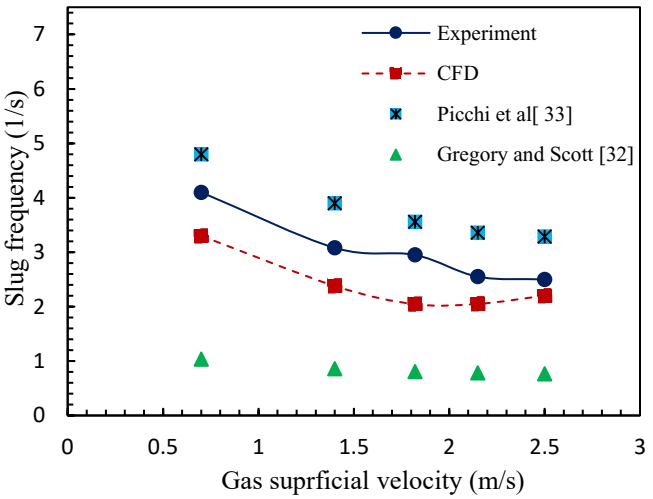

Fig. 10. Slug liquid frequency versus gas superficial velocity for XG-0.10 flow, U_{SL}=1.4 (m/s).

The drift velocity and distribution parameter C_0 values in Eq. (24) have been formulated according to operational parameters from the experiments. Hence, the values for C_0 in the XG-0.5 solution can be similar to those for air-water C_0 = 1.09, whereas, in the XG-0.10 solution, C_0 = 1.21 for turbulent cases. From this, we can see that increases in the XG concentration occur with increases in the distribution parameter C_0. In Otten and Fayed [12] a similar progression of C_0 was observed through the addition of polymer. It is worth noting how C_0 decreases with rises in surface tension, and that yield-power law characteristics lead to slug translational velocity increases. These findings also appeared in the studies of Baumgartner et al. [19] and Picchi et al. [33] with regard to non-Newtonian behavior trends.

Slug frequency

The slug frequency obtained from experimental work is compared to CFD results and empirical correlations suggested by Gregory and Scott [32] and Picchi et al. [33] as shown in Figure 9. Gregory and Scott [32] do not hold acceptable for higher rheological parameters as the same cases in this work. A similar trend was observed by Picchi et al. [33]. The frequency for the XG-0.05 solution is good predicted by the correlation Picchi et al. [33]. With increasing the rheological behavior of the XG-0.1 solution, we observed that Picchi et al. [33] gave a higher prediction from experimental and CFD models as shown in Figure 10. This relationship is valid to power-law (shear thinning fluid). Also, we notice that the yield stress may be an effect on the slug flow characteristics.

CONCLUSION

In the present study, experimental and Computational Fluid Dynamics (CFD) investigations to study the effect of rheological parameters of non-Newtonian YPL fluids in a two-phase model were presented. The experiments were performed in 3-inch PVC, a horizontal pipe, to study two different concentrations of XG solutions. A volume of fluid (VOF) model in ANSYS Fluent 17.2 was selected to analyze the characteristics of slug flow. The simulation results were compared to experimental results and empirical correlations reported in the literature. We observed that the rheological characteristics of the non-Newtonian phase had some influence on the characteristics of slug flow behavior in two-phase flow with increased XG concentrations. We observed that with increased concentrations at the same operations conditions, the translational slug velocity increased. The empirical correlation of slug frequency for a gas/non-Newtonian with considered the rheology of the shear-thinning behavior gave the acceptable agreement with experimental measurements at low polymer concentrations. With the increasing concentration of polymer, the error was increased. The distribution parameters C_0 increased with the increasing concentration of xanthan gum, and the drift velocity was calculated by considering the effect of PYL fluid parameters. Acceptable agreement between CFD results and measurements of empirical correlation was found in all cases.

NOMENCLATURE

C_o= distribution parameter or flow coefficient
D = channel diameter, m
f_S = slug frequency (1/s)
F_{SF} = surface tension force, N/m^3
k = consistency index, Pa·s^n
l = slug unit of length, m
l_l = film zone of length, m
l_s = slug zone of length, m

n = flow behavior index
P = pressure, Pa
Re_g= generalized Reynolds number
T= time, s
Δt= time step, s
U_{SG} =gas superficial velocity, m/s
U_{SL} =liquid superficial velocity, m/s
U_T = translational Velocity, m/s
U_m = Mixture superficial velocity (m/s)
Δx= grid size, m
y = distance from the wall pipe, m
y_+ = dimensionless wall distance

Greek Symbols

α = volume fraction
δ = liquid film thickness, m
$\dot{\gamma}$ = shear rate, 1/s
θ = Contact angle, (_)
λ =Time constant
η = dynamic viscosity, kg/m·s
ρ = density, kg/m^3
σ = surface tension, N/m
τ = shear stress, Pa
τ_w= wall shear stress, Pa

Glossary

CFD = Computational fluid dynamics
DTL = Drilling Technology Laboratory
HB = Herschel-Bulkley
XG = Xanthan gum
YPL =Yield power-law

ACKNOWLEDGEMENT

The authors are grateful to the Ministry of Higher Education and Scientific Research, Libya through Canadian Bureau International Education (CBIE) and Drilling Technology Laboratory (DTL) staff for their support. This publication was also made possible by the grant NPRP10-0101-170091 from Qatar National Research Fund (a member of the Qatar Foundation). Statements made herein are solely the responsibility of the authors.

REFERENCES

[1] Chhabra, R. P., Richardson, J. F. (1986). The co-current horizontal and vertical upward flow of gas and non- Newtonian liquid. Encyclopedia of Fluid Mechanics, 3, 563-609.

[2] Dziubinski, M. (1995). A General Correlation for 2-Phase Pressure-Drop in Intermittent Flow of Gas and Non- Newtonian Liquid-Mixtures in a Pipe. Chemical engineering research and design, 73(5), 528-534.

[3] Chhabra, R. P., Richardson, J. F. (1999). Non-Newtonian Flow: Fundamentals and Engineering Applications.
Elsevier.

[4] Oliver, D. R., Hoon, A. Y. (1968). 2-phase non-Newtonian flow heat transfer. Transactions of the Institution of Chemical Engineers and the Chemical Engineer, 46(4), T116.

[5] Srivastava, R. P. S., Narasimhamurty, G. S. R. (1973). Hydrodynamics of non-Newtonian two-phase flow in pipes. Chemical Engineering Science, 28(2), 553-558.

[6] Srivastava, R. P. S., Narasimhamurthy, G. S. R. (1981). Void Fraction and Flow Pattern during Two-Phase Flow of Pseudoplastic Fluids. The Chemical Engineering Journal, 21(2), 165-176.

[7] Chhabra, R. P., Richardson, J. F. (1984). Prediction of flow pattern for the co-current flow of gas and non-Newtonian liquid in horizontal pipes. The Canadian Journal of Chemical Engineering, 62(4), 449-454.

[8] Mandhane, J. M., Gregory, G. A., Aziz, K. (1974). A flow pattern map for gas-liquid flow in horizontal pipes. International Journal of Multiphase Flow, 1(4), 537-553.

[9] Weisman, J., Duncan, D. G. J. C. T., Gibson, J., Crawford, T. (1979). Effects of fluid properties and pipe diameter on two-phase flow patterns in horizontal lines. International Journal of Multiphase Flow, 5(6), 437-462.

[10] Xu, J. Y., Wu, Y. X., Shi, Z. H., Lao, L. Y., Li, D. H. (2007). Studies on two-phase co-current air/non-Newtonian shear-thinning fluid flows in inclined smooth pipes. International Journal of Multiphase Flow, 33(9), 948-969.

[11] Rosehart, R. G., Rhodes, E., Scott, D. S. (1975). Studies of gas-liquid (non-Newtonian) slug flow: void fraction meter, void fraction and slug characteristics. The Chemical Engineering Journal, 10(1), 57-64.

[12] Otten, L., Fayed, A. S. (1976). Pressure drop and drag reduction in two-phase non-Newtonian slug flow. The Canadian Journal of Chemical Engineering, 54(1-2), 111-114.

[13] Farooqi, S.I., Heywood, N.I., Richardson, J.F., 1980. Drag reduction by air injection for highly shear-thinning suspensions in horizontal pipe flow. Trans. IChemE 58, 16–27.

[14] Lockhart, R. W., Martinelli, R. C. (1949). Proposed correlation of data for isothermal two-phase, two-component flow in pipes. Chem. Eng. Prog, 45(1), 39-48.
[15] Dziubinski, M. (1996). A general correlation for two-phase pressure drop in intermittent flow of gas and non-Newtonian liquid mixtures in a pipe. International Journal of Multiphase Flow, 22(S1), 101-101.
[16] Ruiz-Viera, M. J., Delgado, M. A., Franco, J. M., Sánchez, M. C., Gallegos, C. (2006). On the drag reduction for the two-phase horizontal pipe flow of highly viscous non-Newtonian liquid/air mixtures: Case of lubricating grease. International Journal of Multiphase Flow, 32(2), 232-247.
[17] Ihmoudah, A., Rahman, M. A., Butt, S. D. (2018). CFD and Experimental Studies of Yield Power-Law Fluids in Turbulent Pipe Flow. In ASME 2018 37th International Conference on Ocean, Offshore and Arctic Engineering (pp. V008T11A012-V008T11A012). American Society of Mechanical Engineers.
[18] Picchi, D., Ullmann, A., Brauner, N. (2018). Modeling of core-annular and plug flows of Newtonian/non-Newtonian shear-thinning fluids in pipes and capillary tubes. International Journal of Multiphase Flow, 103, 43-60.
[19] Baungartner, R., J., Loureiro, G., Freire, A. (2017). Horizontal Pipe Slug Flow of Air/Shear-thinning Fluid Experiments and Modelling. Multiphase Flow Journeys, 4, 2017-0053. March 27, 2017.
[20] Ko, T., Choi, H. G., Bai, R., Joseph, D. D. (2002). Finite element method simulation of turbulent wavy core-annular flows using a k–ω turbulence model method. International Journal of Multiphase Flow, 28(7), 1205-1222
[21] Al-Yaari, M. A., Abu-Sharkh, B. F. (2011). CFD prediction of stratified oil-water flow in a horizontal pipe. Asian Transactions on Engineering, 1(5), 68-75.
[20] Lo, S., Tomasello, A. (2010). Recent progress in CFD modeling of multiphase flow in horizontal and near-horizontal pipes. In 7th North American Conference on Multiphase Technology. BHR Group.
[22] Kroes, R. F., Henkes, R. A. W. M. (2014). CFD for the motion of elongated gas bubbles in viscous liquid. In 9th North American Conference on Multiphase Technology. BHR Group.
[23] Jia, N., Gourma, M., Thompson, C. P. (2011). Non-Newtonian multi-phase flows: On drag reduction, pressure drop and liquid wall friction factor. Chemical engineering science, 66(20), 4742-4756.
[24] Sanderse, B., Haspels, M., Henkes, R. A. W. M. (2015). Simulation of Elongated Bubbles in a Channel Using the Two-Fluid Model. Journal of Dispersion Science and Technology, 36(10), 1407-1418.
[25] Herschel, V. W. H. (1926). Consistency of Measurements Rubber-Benzene Solutions. Kolloid-Zeit., 39, 291-300.
[26] Chilton, R. A., Stainsby, R. (1998). Pressure loss equations for laminar and turbulent non-Newtonian pipe flow. Journal of Hydraulic Engineering, 124(5), 522-529.
[27] Fluent, A. ANSYS Fluent 17.0 User's Guide; 2017.
[28] Taitel, Y., Barnea, D. (1990). A consistent approach for calculating pressure drop in inclined slug flow. Chemical Engineering Science, 45(5), 1199-1206.
[29] Nicklin, D. J. (1962). Two-phase flow in vertical tubes, Trans. Inst. Chem. Engr., 40(1), 61-68.
[30] Bendiksen, K. H. (1984). An experimental investigation of the motion of long bubbles in inclined tubes. International Journal of Multiphase Flow, 10(4), 467-483.
[31] Weber, M. E. (1989). Drift in intermittent two-phase flow in horizontal pipes. Can. J. Chern. Eng. 59: 398-99
[32] Gregory, G. A., Scott, D. S. (1969). Correlation of liquid slug velocity and frequency in horizontal concurrent gas-liquid slug flow. AIChE Journal, 15(6), 933-935.
[33] Picchi, D., Manerba, Y., Correra, S., Margarone, M., Poesio, P. (2015). Gas/shear-thinning liquid flows through pipes: Modeling and experiments. International Journal of Multiphase Flow, 73, 217-226.
[34] Taitel, Y., Dukler, A. E. (1976). A model for predicting flow regime transitions in horizontal and near horizontal gas-liquid flow. AIChE Journal, 22(1), 47-55.

Appendix C

A user defined function (UDF) to implement the Herschel-Bulkley-Papanastasiou model

UDF for applying the Herschel-Bulkley-Papanastasiou model - BOX1 Fluid

```
/************************************************************************

 viscosity_udf.c

 ************************************************************************/

#include "udf.h"

#define n 0.74

#define k 0.0512

#define ys 0.76

#define m  1.28

 DEFINE_PROPERTY(HB_viscosity,c,t)

 {

real mu_casson;

real gamma = C_STRAIN_RATE_MAG(c,t);

 if(gamma!=0){

 mu_HB = ((1-exp(-m*gamma))/ ys)*(ys/ gamma)+ k*pow(gamma,n-1);}

 else{
```

```
mu_HB = 0.0030;

}

return mu_HB;

}
```

Appendix D

Additional experimental images of flow patterns.

Appendix D

Additional experimental images of flow patterns.

This section includes additional images obtained from the experiment work in Chapter 3.

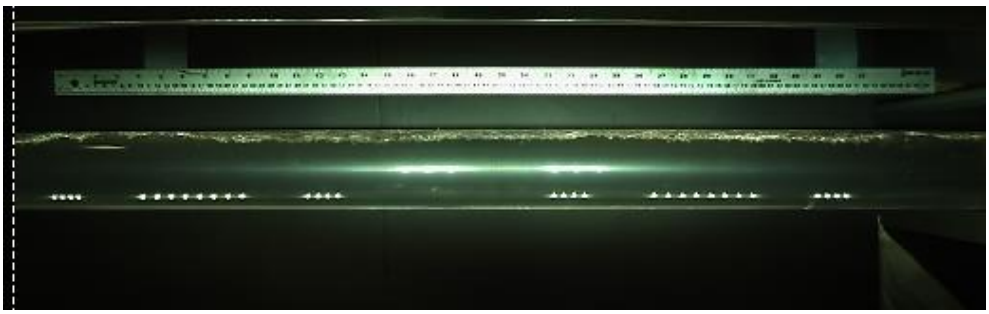

Figure C.1: Flow patterns air-water two-phase flow - dispersed bubble

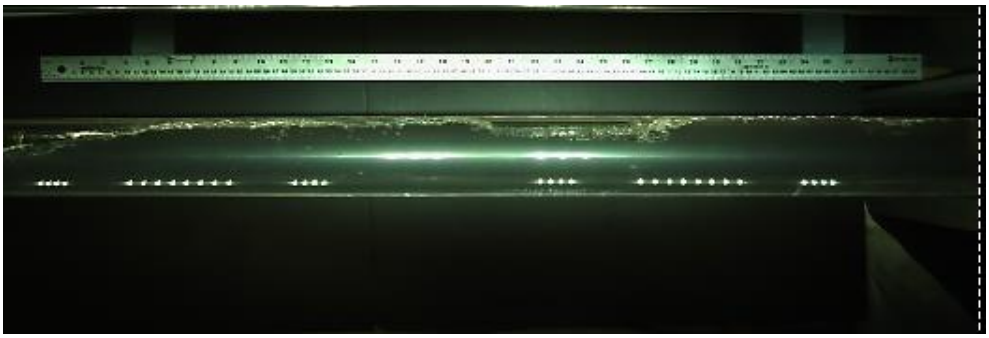

Figure C.2: Flow patterns air-water two-phase flow - dispersed bubble/ plug flow

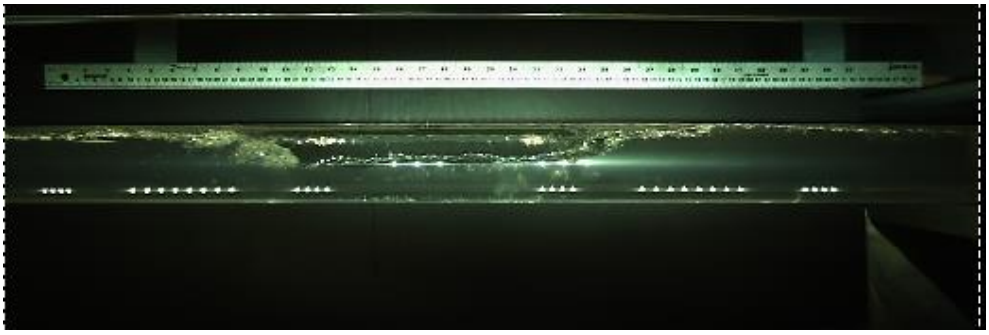

Figure C.3: Flow patterns air-water two-phase flow - plug flow

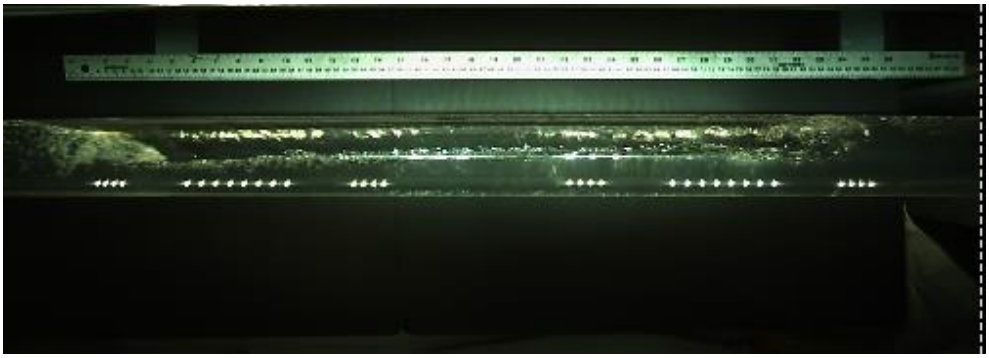

Figure C.4: Flow patterns air-water two-phase flow – slug flow

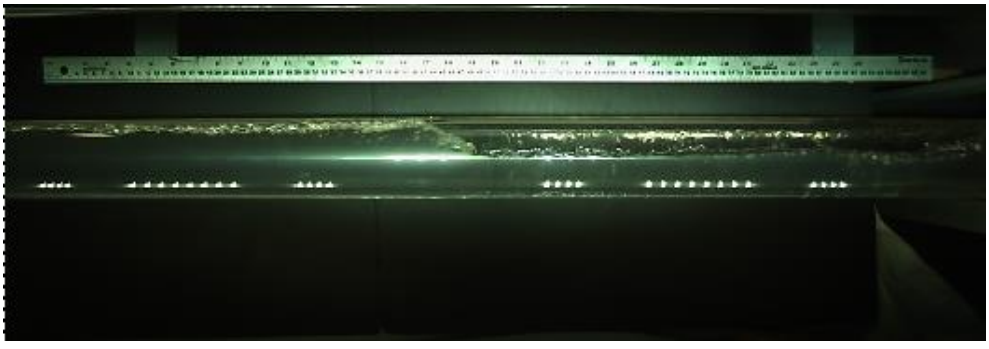

Figure C.5: Flow patterns air-water two-phase flow – tail of slug flow

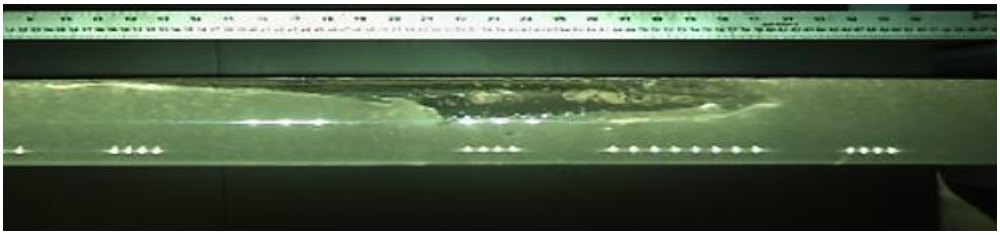

Figure C.6: Flow patterns air-CMC4 two-phase flow – Plug flow

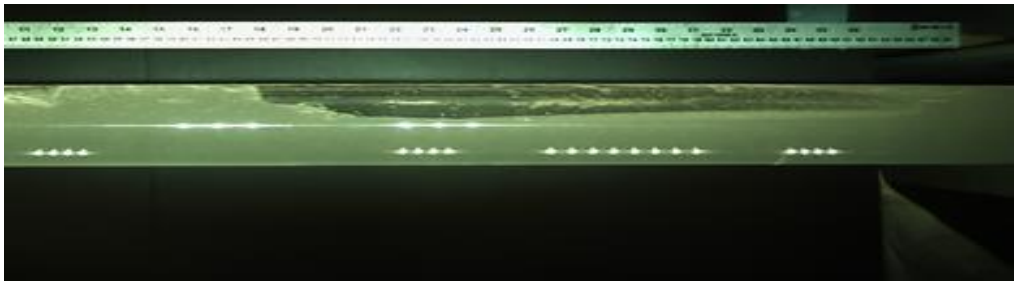

Figure C.7: Flow patterns air-CMC4 two-phase flow – Slug flow

Figure C.8: Flow patterns air-BOX4 two-phase flow – Plug flow

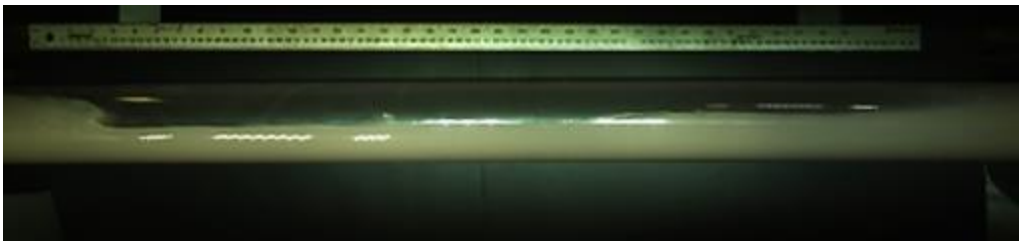

Figure C.9: Flow patterns air-BOX4 two-phase flow – Slug flow